

VALORIZATION OF MARINE PET LITTER

**From conventional methods to
chemical recycling for the
synthesis of novel polyurethanes**

**Eider Mendiburu Valor
2023**

eman ta zabal zazu



Universidad
del País Vasco

Euskal Herriko
Unibertsitatea

VALORIZATION OF MARINE PET LITTER

From conventional methods to chemical recycling for the synthesis of novel polyurethanes

PhD dissertation presented by
EIDER MENDIBURU VALOR

Supervised by
Dr. Cristina Peña Rodríguez and Dr. Arantxa Eceiza Mendiguren

Donostia-San Sebastián, June 2023

ACKNOWLEDGEMENTS

Lehenik eta behin nire tesi zuzendariak izan diren Arantxa Eceiza doktorea eta Cristina Peña doktorea biziki eskertu nahi nituzke lau urte hauetan doktore-tesi hau garatzeko eta bere taldearekin bat egiteko aukera profesionala eman izanagatik. Horrekin batera eskerrik asko Cristina gradua bukatu nuenean eta dena anbiguoaz zenean ikerketa-proiektu batean lan egiteko aukera emateagatik, gerora tesi honen garapenean bukatu dena.

Bestalde, Eusko Jaurlaritza eskertu nahi dut lan hau aurrera eraman ahal izateko emandako doktoretza-aurreko programaren diru laguntzagatik (PRE_2018_1_0014) eta nazioarteko egonaldia burutzeko dirulaguntza eman izanagatik. Horrekin batera, Politecnico di Milano-ko Materialak eta Ingeniaritza Kimikoko saila “Giulio Natta” estantzian zehar emandako laguntzagatik eskertu nahi nuke, bereziki Giovanni Dotelli eta Valeria Arosio doktoreak, eta Alessandro Salvi dokoregai, Gipuzkoako Foru Aldundiaren Ingurumen saila ere eskertu nahi nuke, doktoretza egitera bideratu ninduen ikerketa beka emanagatik.

Eskerrak eman ere Euskal Herriko Unibertsitateari (UPV/EHU) eta baita Ikerkuntzarako Zerbitzu Orokorrei (SGIker) emandako laguntza teknikoagatik. Bereziki, Makroportaera-Mesoegitura Nanoteknologia zerbitzuko Loli Martin doktorea eskertu nahiko nuke, denbora honetan nirekin izandako pazientziagatik, laguntza eta prestotasun guztiengatik.

Horrekin batera, Nerea Zaldua doktorea eskertu nahiko nuke, azken urte honetan, lanak itotzen ninduenean eskainitako etengabeko laguntza eta dedikazioagatik. Ez dut ahaztu nahi laborategian eta laborategitik kanpo gehien lagundu didan pertsona, Gurutz Mondragon doktorea. Eskerrik asko Gurutz izandako pazientziagatik eta hartu ditugun pintxo eta trago guztiengatik, plazer bat izan da hori dena zurekin partekatzea. Jarraitzeko GMT ikerketa taldeko nire lagun guztiak eskertu nahi nituzke. Aipamen berezia Tamara eta Izaskuni beti laguntzeko prest egoteagatik eta une oro pazientzia izateagatik. Raquel eta Amairi nire azken hilabeteetako galdera eta duda guztiak erantzun eta emandako animoengatik. Azkenik, nire frustrazioen, poztasunen eta bereziki momentu on guztien parte izan diren lankideak, hobe esanda lagunak, sutzuki eskertu nahi nituzke, funtsezko pilareak izan zarete, beti zuen laguntza eskainiz eta animoak ematen. Horregatik eskerrik beroena zuei, Senda, Julen, Stefano, Ane, Ander, Nagore, Sebas, Joseba, Garazi eta Laura (espero inor ahaztu ez izana).

Lanetik kanpo ere azken lau urte hauetan aguantatu nautenak eskertu nahi nituzke. Hasteko familia, aita eta ama, hona iritsi izanaren meritu handi bat zuena da, beti nigan izandako konfiantzagatik. Nire nebei, Unai eta Jon, beti hor egoteagatik eta nire lorpen bakoitzaz pozteagatik, nahiz eta uste dudan ez dakitela ondo zertan datzan lan hau. Nire iloba txikiari, Aimar, egunak alaitzeagatik eta nire koinatari ere bere animoengatik. Horiekin batera, familiako

matriarka eskertu nahiko nuke, amama, gorabehera guztien aurrean aurrera egiten irakasteagatik, nahiz eta, briskan karta txarrak egokitu.

Bukatzeko aukeratzen den familia eskertu nahiko nuke, lagunik gabe ez ginateke ezer izango. Lehenik eta behin kuadrilakoei eskerrak, behar nuen espazioa eskaintzeagatik eta animo guztiengatik, nahiz eta ikusten ninduten bakoitzean galdera berdina entzun behin eta berriz “Eider, zelan doa tesia?” Ikasia dute jada doktoregai bati hobe dela horrelakorik ez galdetzea. Eskerrik asko Iñaut, beti ni ulertzeagatik, laster tokatuko zaizu zuri tesia entregatzea, animo. Eskerrik asko Marta, beti hor egon den laguna izateagatik, ezer gutxi behar dugu elkar ulertzeko. Ane, Aziz eta Mada ere eskertu nahi nituzke, emandako momentu on guztiengatik. Horiekin batera naiz eta kuadrilakoa ez izan, oraingoz, Ana eskertu nahiko nuke beti nigatik arduratzeagatik. Beste alde batetik, tesiaren lehenengo 3 urteetan etxean aguantatu nauen lagun mina eskertu nahiko nuke. Eskerrak etxean zeundela Josu, tesia bukatzeko pieza garrantzitsu bat izan zara eta eskerrak ere bidai lagun, jaialdi lagun eta farra lagun bikaina izateagatik. Gainera, izugarri eskertu nahi nuke tesiaren gora-beherako azken urtean batez ere egon den pertsona. Mila esker Leire, ni ulertzeagatik, ni neu ulertzen ez nintzenean eta emandako animo guztiengatik eta azken urteetan ni hain ondo zaintzeagatik. Gaurko egunera heldu izanaren beste arrazoi oso garrantzitsua da zu alboan zaitudala, ezin dut imajinatu bizikide hoberik, horregatik guztiagatik, eskerrik asko bihotzez.

Urte hauetan asko lagundu didan beste gauza bat kirola da eta horretan errugbia izan dut lagungarri. Horregatik mila esker nire errugbi taldeari Bera Berako otsemeei askatasun eta barre iturri izateagatik, era berean, Milaneko estantzian besoak zabalik hartu ninduten Amantori Union taldea ere eskertu nahiko nuke.

Bukatzeko, Nietzscheren hitzak hartu nahi nituzke gogora “ La vida sin música no tiene sentido”. Horregatik, eskertu nahi nituzke alde batetik Spotify aplikazioa urte hauetan bidelagun fina izan dena eta beste alde batetik, Viña Rockeko familia, jaialdi hori zuek gabe ez litzateke berdina izango. Hiru egun horiek zail ahazten ditugu urte osoan zehar “es una fantasía”.

SUMMARY

The present work is focused on the recycling of marine poly(ethylene terephthalate) litter (PET-m), in order to give a second life to this polluting waste. The marine conditions to which marine PET litter is exposed can generate changes in the physicochemical properties of the materials due to possible degradation. Therefore, first of all, the characterization of marine PET litter has been carried out and compared with urban post-consumer PET waste (PET-u) and other two PET raw materials, a virgin PET (PET-v) and a post-condensed PET (PET-ssp), in order to evaluate potential degradation caused by marine environment on PET materials.

After characterizing both waste types and studying the effects of possible degradations on physicochemical properties, recycling was carried out by the two most common methods employed for PET waste: thermo-mechanical recycling and energy recovery. At present, due to the large volume of waste, its high efficiency and its easy transformation, PET urban waste is generally thermo-mechanically recycled. However, marine PET litter is not currently recycled in a systematic way, probably because it can negatively affect the recycling chain, due to its high degradation together with the fact that the management is also a limitation. To analyze the viability of the most conventional recycling method, a thermo-mechanical recyclability study has been carried out for PET-m and PET-u samples, and also for a PET raw material. Moreover, different processing variables were evaluated in order to optimize the thermo-mechanical recycling process of marine PET litter. The suitability of energy recovery was also evaluated by measuring the calorific value of the above mentioned PET samples.

After analyzing the critical effect of degraded PET samples on the properties of thermo-mechanically recycled materials, chemical recycling by glycolysis was studied, with the aim of designing an optimal recycling strategy for highly degraded samples such as marine PET litter. For this reason, in order to optimize the glycolysis yield and reduce the energy consumption, kinetics studies were performed with a raw PET material. Reactions were carried out at short times ranging from 10 to 180 min. In the same way, the effect of temperature was studied by performing reactions at 180, 200 and 220 °C. Finally, the effect of degradation on the depolymerization reaction was analyzed. In this context, glycolysis of different PET samples was carried out under previously optimized reaction conditions. The glycolyzed product obtained in each reaction was characterized in order to identify the effect of PET degradation on the depolymerization. In all cases, the obtained product is mainly formed by bis(2-hydroxyethyl) terephthalate (BHET) monomer.

Then thermoplastic and thermoset polyurethanes were synthesized by employing the BHET monomer obtained in the chemical recycling of PET. In this way, new, more environmentally friendly materials are obtained, reducing the consumption of fossil resources. In addition, a

biobased macrodiol was used for the synthesis of thermoplastic polyurethane samples, thus obtaining materials with more than 30 % of their components coming from renewable and recycled sources. In the same way, thermoset polyurethanes were also synthesized, using a biobased polyol derived from castor oil, thus developing materials with a renewable/recycled content higher than 40 %. The different samples synthesized for both polyurethanes were characterized, studying also their recyclability.

Finally, the environmental impacts of some of the processes developed were evaluated through Life Cycle Assessment (LCA). On the one hand, the LCA corresponding to the glycolysis reaction of marine PET litter, from collection to the obtention of the final recycled product, was carried out. On the other hand, the LCA of the synthesis of biobased thermoplastic polyurethanes, incorporating the recycled glycolyzed product, was studied and compared to that of polyurethanes synthesized from a commercial chain extender and a petrochemical polyol, respectively.

Graphical abstract

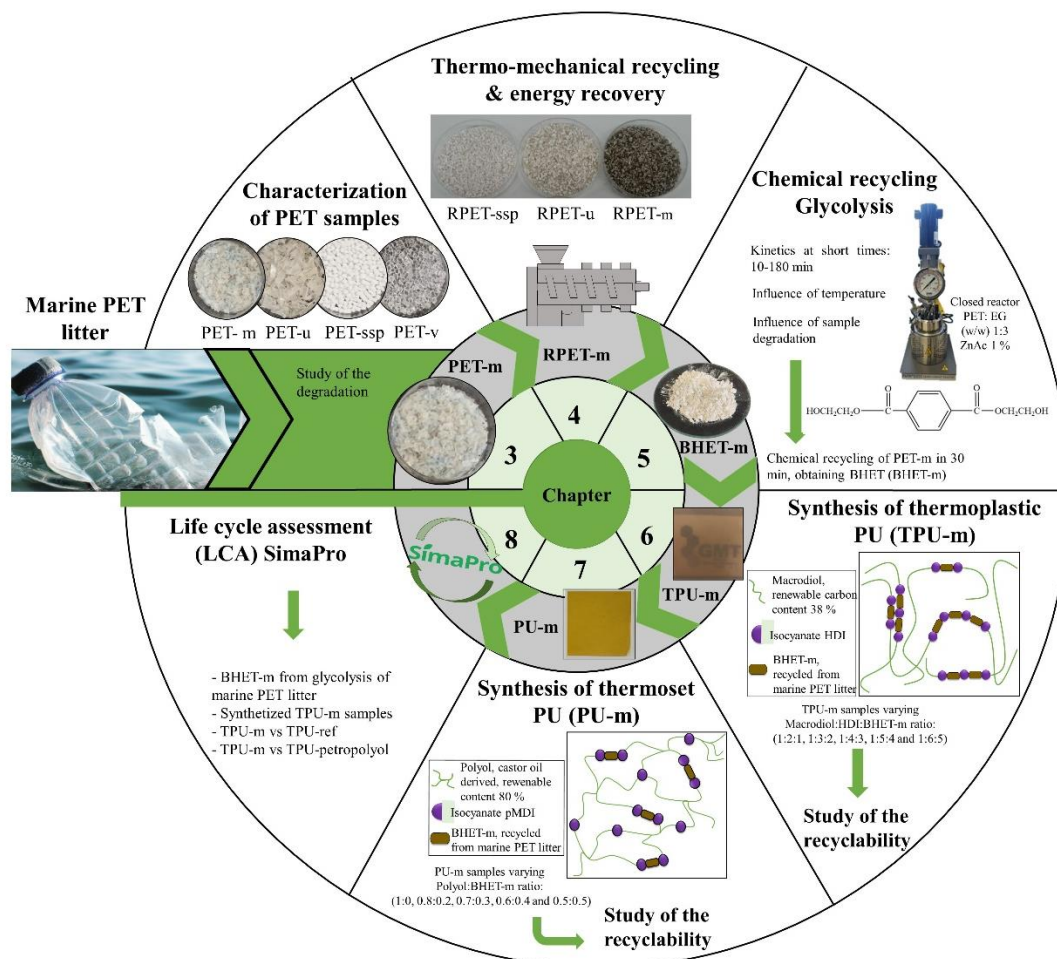


TABLE OF CONTENTS

1. INTRODUCTION.....	3
1.1. Motivation.....	3
1.2. Plastic pollution.....	4
1.3. Degradation of polymers.....	5
1.4. Circular economy.....	9
1.5. Poly(ethylene terephthalate) (PET).....	10
1.6. Recycling of PET.....	12
1.6.1. Thermo-mechanical recycling.....	12
1.6.2. Chemical recycling.....	14
1.6.2.1. Methanolysis.....	14
1.6.2.2. Glycolysis.....	14
1.6.2.3. Hydrolysis.....	17
1.6.2.4. Ammonolysis.....	18
1.6.2.5. Aminolysis.....	18
1.6.3. Energy recovery.....	19
1.7. BHET.....	20
1.7.1. BHET as raw material for PET production.....	20
1.7.2. BHET as raw material for new polymers.....	20
1.8. Polyurethanes.....	22
1.8.1. Reagents.....	22
1.8.1.1. Polyols.....	22
1.8.1.2. Isocyanates.....	23
1.8.1.3. Chain extender.....	23
1.8.2. Thermoplastic polyurethanes (TPU).....	24
1.8.3. Thermoset polyurethanes (thermoset PU).....	25
1.9. General objectives.....	26
1.10. References.....	27

2. MATERIALS AND METHODS.....	47
2.1 Content	47
2.2 Materials.....	47
2.2.1. PET samples.....	47
2.2.2. Materials for the chemical recycling	48
2.2.3. Materials for the synthesis of TPUs	48
2.2.4. Materials for the synthesis of thermoset PUs	49
2.3 Physicochemical characterization	50
2.3.1. Fourier transform infrared spectroscopy (FTIR).....	50
2.3.2. Gel permeation chromatography (GPC).....	50
2.3.3. Elemental analysis (EA).....	50
2.3.4. Proton nuclear magnetic resonance (¹ H NMR).....	50
2.3.5. I _{OH}	51
2.3.6. pH.....	51
2.4 Thermal characterization.....	51
2.4.1. Differential scanning calorimetry (DSC)	51
2.4.2. Thermogravimetric analysis (TGA)	52
2.4.3. Dynamic mechanical analysis (DMA)	52
2.4.4. Calorimetry.....	53
2.4.5. Ashes percentages	53
2.5 Mechanical characterization.....	53
2.5.1. Tensile tests.....	53
2.5.2. Flexural tests	53
2.6 Rheological characterization: melt flow index (MFI), intrinsic viscosity (IV) and molar mass	54
2.7 Morphological characterization.....	54
2.8 Surface hydrophilicity	54
2.9 Spectrophotometry	55
2.10 Life Cycle Assessment (LCA)	55

2.11	References	61
3.	CHARACTERIZATION OF POLY(ETHYLENE TEREPHTHALATE) SAMPLES FROM DIFFERENT SOURCES.....	65
3.1.	Aim of the chapter.....	65
3.2.	Characterization of PET samples from different sources.....	65
3.2.1.	Determination of viscosity, molar mass and ash percentages	65
3.2.2.	Physicochemical characterization	67
3.2.3.	Thermal characterization.....	70
3.2.4.	Surface characterization	73
3.3.	Conclusions	75
3.4.	References	75
4.	STUDY OF THE VALORIZATION OF MARINE PET LITTER BY CONVENTIONAL METHODS	81
4.1.	Aim of the chapter.....	81
4.2.	Thermo-mechanical recycling of PET samples.....	81
4.3.	Characterization of recycled PET samples.....	83
4.3.1.	Spectrophotometry	83
4.3.2.	MFI, IV and molar mass	83
4.3.3.	FTIR	84
4.3.4.	DSC.....	86
4.3.5.	TGA.....	88
4.3.6.	WCA	89
4.4.	Optimization of thermo-mechanical recycling.....	90
4.4.1.	Temperature control	90
4.4.2.	Recycling by extrusion of PET-u/PET-m blends	92
4.5.	Energy recovery	94
4.6.	Conclusion.....	95
4.7.	References	96

5. CHEMICAL RECYCLING	103
5.1. Aim of the chapter.....	103
5.2. Glycolysis reaction.....	103
5.2.1. Characterization of depolymerized BHET	105
5.3. Reaction kinetics	106
5.3.1. Effect of reaction time on glycolysis.....	106
5.3.2. Effect of temperature on the glycolysis reaction.....	112
5.4. Influence of PET sample degradation on glycolysis	114
5.4.1. Characterization of the glycolyzed product obtained from different PET samples	114
5.5. Comparing commercial BHET and recycled BHET from marine PET litter.....	118
5.6. Conclusions	121
5.7. References	122
6. SYNTHESIS OF NEW THERMOPLASTIC POLYURETHANES BASED ON RECYCLED BHET	127
6.1. Aim of the chapter.....	127
6.2. Reactants and synthesis of TPUs	127
6.3. Characterization of synthesized TPUs	128
6.3.1. Spectrophotometry	128
6.3.2. FTIR	129
6.3.3. DSC	131
6.3.4. AFM	132
6.3.5. TGA.....	133
6.3.6. DMA	135
6.3.7. Mechanical properties	136
6.3.8. WCA	137
6.4. Recycling of synthesized TPUs	137
6.4.1. Thermo-mechanical recycling of synthesized TPUs	137
6.4.2. Chemical recycling of synthesized low molar mass TPUs by glycolysis.....	140

6.5.	Conclusions	146
6.6.	References	147
7.	SYNTHESIS OF NEW THERMOSET POLYURETHANES BASED ON RECYCLED BHET	153
7.1.	Aim of the chapter.....	153
7.2.	Reactants and synthesis of thermoset PUs	153
7.3.	Characterization of synthesized thermoset PUs	154
7.3.1.	DSC	154
7.3.2.	Spectrophotometry	156
7.3.3.	FTIR	156
7.3.4.	TGA.....	157
7.3.5.	DMA	158
7.3.6.	Mechanical properties	160
7.3.7.	WCA	161
7.4.	Chemical recycling of synthesized thermoset PUs.....	161
7.4.1.	GPC	162
7.4.2.	FTIR	164
7.4.3.	DSC	165
7.4.4.	TGA.....	165
7.5.	Conclusions	166
7.6.	References	167
8.	LIFE CYCLE ASSESSMENT OF THE DIFFERENT PROCESSES AND MATERIALS DEVELOPED.....	173
8.1.	Aim of the chapter.....	173
8.2.	Life Cycle Assessment for the chemical recycling of marine PET litter	173
8.3.	LCA of synthesized TPUs	180
8.3.1.	Comparative of LCA between TPU-m and TPU-ref.....	186

8.3.2. Comparative analysis between TPU-m and a TPU synthesized with a commercial polyol	191
8.4. Conclusions.....	193
8.5. References.....	194
9. GENERAL CONCLUSIONS, FUTURE WORKS AND PUBLICATIONS	199
9.1. General conclusions	199
9.2. Future works.....	200
9.3. List of publications and communications.....	201
9.3.1. List of publications.....	201
9.3.2. Conferences.....	203
9.3.3. Diffusion.....	205
9.3.4. Predoctoral Stay	206
ANNEXE I- List of tables	209
ANNEXE II- List of figures.....	213
ANNEXE III- List of abbreviations.....	219
ANNEXE IV- List of symbols	221

Chapter 1

INTRODUCTION

1. INTRODUCTION

1.1. Motivation

Nowadays, we are immersed in a climate emergency related to CO₂ emissions, resource depletion, waste management, pollution, deforestation, loss of biodiversity and fertile soils, among others, which has been increasing over the last decade. In addition, the global health crisis due to COVID-19 has aggravated the situation and there is a need to act quickly with a policy for reducing the impact of the climate emergency [1,2]. Therefore, environmentally friendly materials, together with an adequate waste treatment system, are needed to move from a linear economy system to a circular one [3].

Plastics are one of the most abundant materials used worldwide, and their production is growing steadily. As an example, the global production of plastics is estimated to be of around 360 million tons per year, Europe producing around 57.9 million tons of plastic in 2019 [4]. This high production of plastics leads to the generation of a large amount of wastes. As plastics usually present high physical and chemical stability, their natural degradation can last for thousands of years [5]. A large amount of plastic waste ends up in the sea, with the consequent danger to the marine environment, resulting in one of the biggest environmental problems. It is estimated that 12.7 million tons of plastics per year end up in the sea.

Poly(ethylene terephthalate) (PET) is one of the most consumed plastics in the world, being therefore very common to find it in the sea or in the ocean [6]. This plastic is a petroleum-derived polymer used for bottling water and carbonated beverages, among other applications [7].

Recycling of urban PET waste is very common, nowadays implemented at industrial scale. It can be recycled by thermo-mechanical recycling for PET remanufacturing, by chemical recycling to obtain a monomer that can be used for PET synthesis or for the production of other materials and, finally, by energy valorization [8]. However, the incorporation of marine PET litter in the recycling chain of industries is not widely explored, since the difficulty in managing marine litter and the effect of marine degradation could affect the recycling process.

Therefore, it is necessary to evaluate the physicochemical characteristics of marine PET litter and compare them with those of a virgin material, in order to determine the degree of degradation and design a recycling system that would give added value to these wastes, by incorporating them into the circular economy as raw materials. This would be a step towards a more sustainable and environmentally friendly world, reducing the extraction of raw materials, impacts and waste generated.

1.2. Plastic pollution

Global plastics production is estimated as 360 million tons per year and continues exponentially increasing each year [9]. The unstoppable production and massive use of plastic materials have created one of the biggest pollution problems worldwide, creating significant amounts of plastic waste that accumulate in landfills and natural environments, including marine and terrestrial ecosystems [10]. It is estimated that 33 billion tons of plastic waste will accumulate on Earth by 2050 [10]. Moreover, with the health crisis caused by COVID-19, the consumption of single-use plastic, plastic-packaged food and personal protective equipment has grown considerably, which may lead to a new environmental crisis [1,2]. In the same way, it is estimated that around one million of plastic bottles become waste every minute, being the trend to double in the next 20 years [11].

It has been reported that the main global plastic productions corresponds to high and low density polyethylene (HDPE and LDPE respectively), polypropylene (PP), polyvinyl chloride (PVC), poly(ethylene terephthalate) (PET), polyurethanes (PU) and polystyrene (PS) [12,13]. The percentages of the annual global demand for plastics are shown in Figure 1.1 [14,15]. However, PET is the most abundant plastic in textile and packaging industry [9], making it one of the most wasteful plastics [11,16].

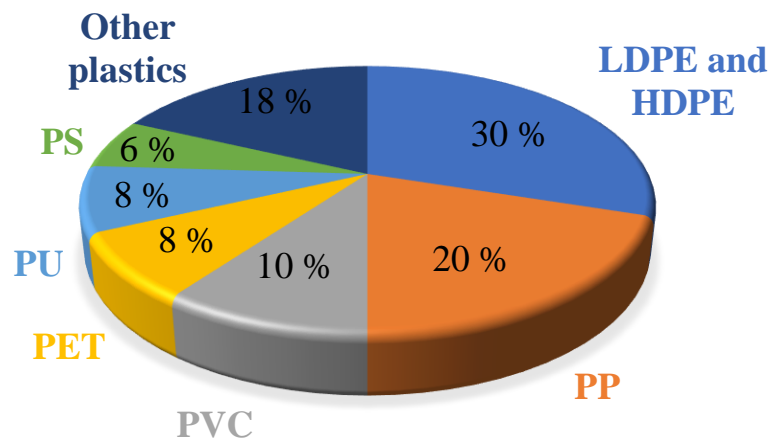


Figure 1.1. Global plastic demand.

According to United Nations Environment Programme (UNEP) statistics, although the proportion of recycling depends on the country, the overall proportion is very low: only the 9 % of plastic production is recycled, while the 12 % is burnt for energy recovery and around the 79 % is disposed of in landfills and natural environments [17,18], with an estimated 66 % accumulating in landfills [19]. Due to the large amount of non-recycled plastic waste, it is estimated that a large amount of this waste ends up in the sea, generating one of the biggest environmental problems. Currently, the dumping of non-biodegradable fossil plastics in marine ecosystems, leading to the

formation of floating islands, as well as the production of plastic debris and fragments such as microplastics, which affect water and biota, is becoming the main environmental concern that deserves international interest and a fast solution [20].

It is estimated that between 4.8-2.7 million tons per year are dumped in the oceans [21,22]. In addition, 80-85 % of marine litter is composed of plastic [23]. A higher amount of plastics than fishes (in weight ratio) is predicted to be found for 2050 in the oceans [24], accumulating 3.5 trillion tons of macro plastics and 2.5 million tons of microplastics in the marine environment [16]. Depending on the size, plastic debris are classified into three groups: macro plastics (≥ 2.5 cm), mesoplastics (2.5 cm - 5 mm) and microplastics (≤ 5 mm) [25]. The most common plastic wastes in marine environment are PP, PE and PET [6]. The composition of the main plastics found in the oceans is: bottles, containers and packaging straps from HDPE and PET, plastic bags from PE and PP and fibers from nylon or PET of textile industry, among other materials [26].

Plastics need long degradation times, due to their stability and high durability, tending to accumulate in the environment and becoming a huge problem [27]. It is therefore necessary to collect and treat for reuse, recycle or burn for energy recovery. Treatment techniques for marine litter are similar to those for urban waste, but for the marine environment solar radiation, sea salinity, atmospheric oxygen, temperature changes, and friction with waves and other elements such as rocks must be taken into account, which could lead to the degradation of plastics [26,28].

1.3. Degradation of polymers

Degradation is defined as the partial or complete breakdown of a polymer chain [28]. This occurs due to several environmental factors such as temperature, humidity, radiation, enzymatic, organisms and mechanical stress, among others [20,29]. As a result, the modification of chemical structures, the decrease in molar mass with the consequent reduction in mechanical properties, thermal stability and morphological alteration can occur[29,30].

Thus, in extreme conditions such as those of marine environment, plastics undergo greater degradation compared to those from urban wastes. As mentioned above, ultraviolet (UV) radiation, temperature, oxygen and mechanical friction affect plastic degradation. Five types of degradation processes can occur in the marine environment: hydrolytic, thermo-oxidative, mechanical, biological and photodegradation [28].

Structural and crystallinity or chain conformation changes occur in PET due to the degradation caused by the marine environment [31–34]. These changes could be related to hydrolytic degradation, since polyesters such as PET are sensitive to moisture. This reaction is influenced by the permeability of water molecules. This degradation is the reverse reaction of PET esterification [27]. Hydrolytic degradation acts on the ester bond of the amorphous region

inducing the formation of acidic and alcoholic functional groups and the cleavage of the ester bond, together with a decrease in molar mass [20,27], as shown in Figure 1.2. When carboxylic end groups are formed, the hydrolysis of PET becomes an autocatalytic reaction [27].

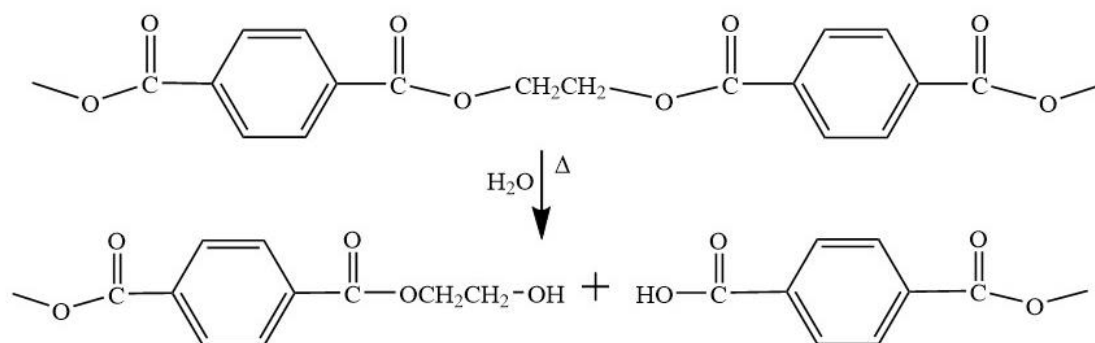


Figure 1.2. PET hydrolytic degradation.

Another degradation occurring in the marine environment is the thermo-oxidative one in the presence of oxygen, which is explained as the Bolland mechanism [20]. This degradation is initiated by the extraction of hydrogen by oxygen molecules in the methylene group of the diester linkage of the main chain, resulting in the formation of hydroperoxide groups [20,29], as shown in Figure 1.3.

Even if the mechanism is not fully understood, it is thought to begin with the cleavage of these hydroperoxides with formation of macroradicals on the main chain and the formation of other oxygen-containing species through other radical reactions [20]. The consequences of this degradation are an increase in carboxylic amount and a decrease in molar mass [27].

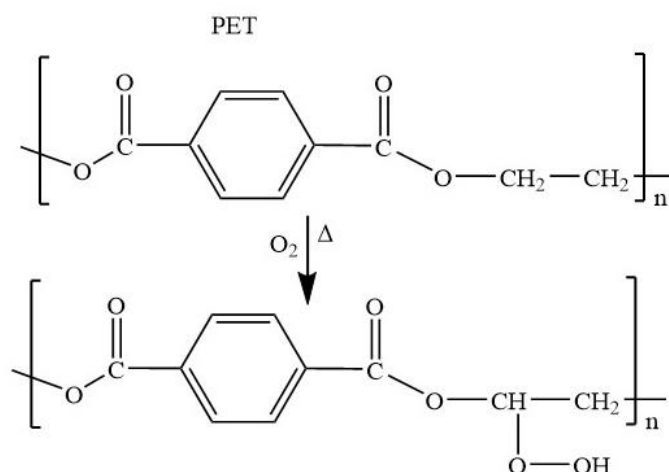


Figure 1.3. Formation of hydroperoxide groups.

Another relevant degradation pathway of PET under marine environmental conditions is the photodegradation [27]. In this case, the radiation source is UV light, and the literature suggests the occurrence of Norrish I, Norrish II and photo-fries reactions [20,35]. UV light rapidly

degrades PET materials, with chain cleavage and subsequent formation of carbonyl end-groups (Norrish II) and cross-linking points (Norrish I) [20,36]. The proposed photodegradation mechanism is shown in Figure 1.4.

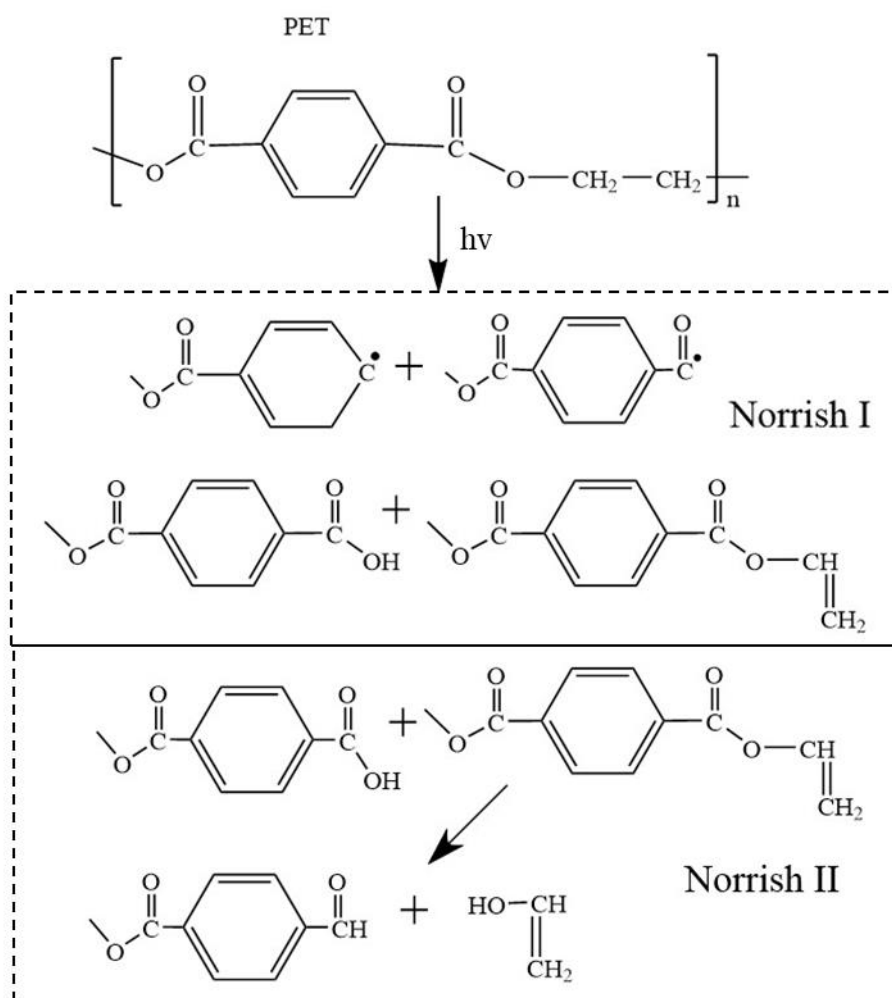


Figure 1.4. PET photodegradation scheme.

In the same way, photodegradation leads to the formation of vinyl esters that could also act as cross-links with the formation of polyenes and other conjugated colored species [20,27]. The polymers become brittle, yellowish and also develop cracked surfaces [27,29]. Therefore, as the main products of photodegradation are the hydroxyl and carboxyl end groups, together with carbon dioxide and carbon monoxide, changes in the materials can be observed by Fourier transform infrared spectroscopy (FTIR), analyzing the hydroxyl and carboxyl regions [29,36].

The other two degradation processes that can occur in the marine environment are the biodegradation and the mechanical degradation, even if they are not as common as those cited above. PET, like most plastics, is very resistant to biodegradation and takes several years to complete degradation [20]. This polyester can remain robust in the marine environment for about fifteen years [37]. After that there is a decrease in functional ester groups, but in general plastics

can last in the sea for hundreds or even thousands of years [28,37], thus increasing the risk of hydrosphere accumulation of marine debris [38]. However, during the last decade, the possibility of PET and other plastics biodegradation by some specific microorganisms is being studied [39]. Besides, polyesters can also undergo a stress-induced degradation reaction when exposed to mechanical stress, wave and tidal action and abrasion. This results in mechanical degradation leading to various changes, such as reduction in molar mass, discoloration, increased polarity, or cross-linking, among others [28,29].

Finally, another important degradation process for plastics, especially for PET, is the thermo-mechanical or thermal one. This occurs at high temperatures between 250-350 °C, and is mainly related to the degradation in thermo-mechanical recycling process [20]. Thermal degradation consists on the random cleavage of the ester groups of the main chain, resulting in the formation of vinyl esters and carboxylic end-groups. Vinyl alcohol is then obtained by transesterification of the vinyl ester, which is immediately transformed into acetaldehyde by tautomerization [20,29]. The scheme is shown in Figure 1.5. This is a critical issue in the bottled water industry, as the release of acetaldehyde can alter the taste of the water [40]. However, thermal degradation results in other degradation products, such as ethylene, cyclic aromatic oligomer, benzene, carbon dioxide and carbon monoxide, among others [41]. Thus, in addition to the increase in chain end groups, such as carboxyl groups, a decrease in molar mass and discoloration can also occur during heat treatment at high temperatures [29]. Several degradations processes can also occur together, as in thermo-mechanical processing, where increasing the concentration of the carboxyl end-group also increases the rate of hydrolysis, thus turning the hydrolysis degradation of PET into an autocatalytic reaction [42].

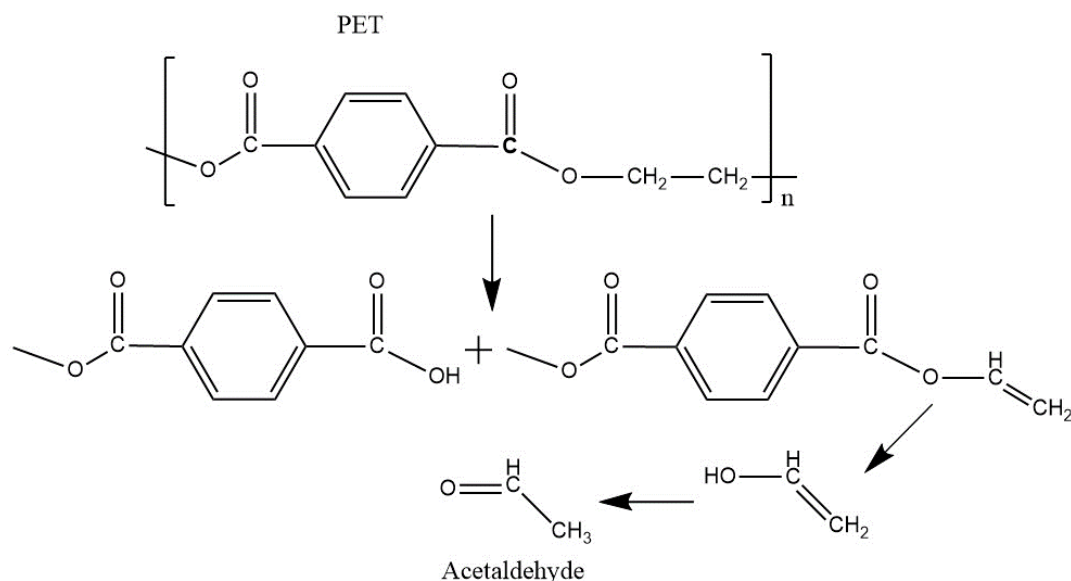


Figure 1.5. Thermal degradation of PET.

1.4. Circular economy

Single-use and disposable plastics are the main reason for the increase in plastics production. It is based on a linear economy, in which plastics are produced, used and discarded, as shown in Figure 1.6 [43].

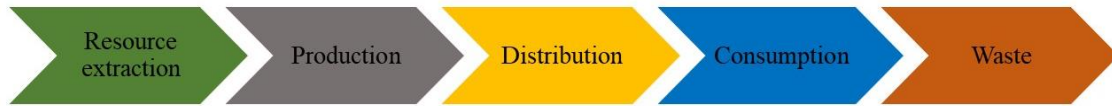


Figure 1.6. Linear economy flow diagram.

Plastics production consumes the 4-8 % of the global crude oil annual extraction, so if plastics are discarded instead of recycled, those resources are lost [44]. Thus, the best solution to tackle plastic pollution is the transition to a circular economy [3]. In the circular economy, it is essential to increase resource efficiency and decrease environmental impacts along value chains. This can be achieved by applying one or more of the following nine circular economy strategies or principles defined as 9R's: Refuse, Rethink, Reduce, Reuse, Repair, Refurbish, Remanufacture, Repurpose and Recycle (Figure 1.7) [45,46].

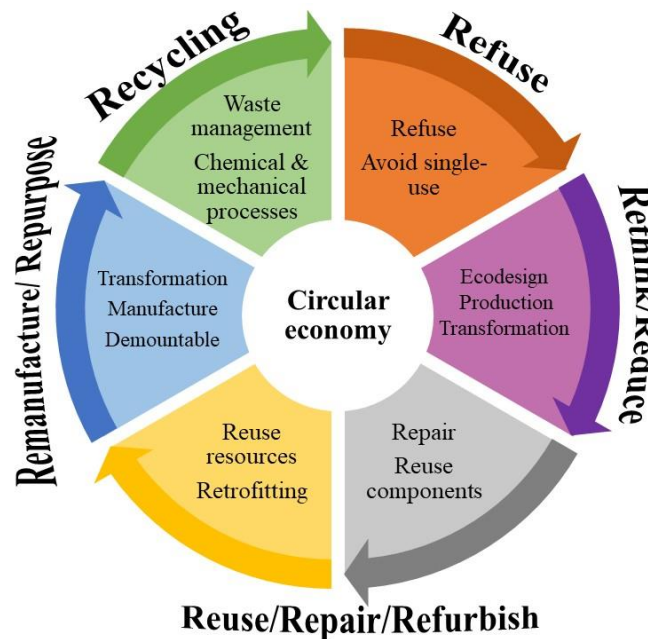


Figure 1.7. Circular economy strategies.

Current societal knowledge tends to focus research work on the end-of-life phase designed for the recovery and recycling of plastic waste [47]. However, the transition to a closed circular economy cannot be achieved by changing waste treatment alone, but must be a combination with other parts of the value chain, such as the design, production and use phases [48]. Indeed, the EU

Strategy for Plastics in the Circular Economy indicates that it is necessary to increase the uptake of recycled plastics and contribute to the more sustainable use of plastics [49]. This highlights a global need to develop scientific knowledge to improve the transition to a circular economy, including recycling as one aspect of an overall strategy among others [48,50].

1.5. Poly(ethylene terephthalate) (PET)

Poly(ethylene terephthalate) (PET) is a semi-crystalline thermoplastic polymer, classified as aromatic-aliphatic, with an empirical formula of $(C_{10}H_8O_4)_n$ and a molar mass of 192 g/mol per repeating unit [51,52]. The chemical structure is shown in Figure 1.8.

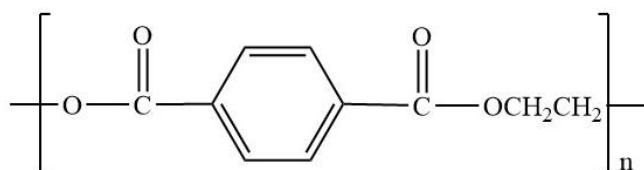


Figure 1.8. Chemical structure of PET.

Presents a density of 1.38 g/cm³ and an intrinsic viscosity (IV) ranging from 0.4 to 0.9 dl/g, depending on the type of application (Table 1.1) [53,54]. The glass transition temperature (T_g) of PET is around 70-80 °C and the melting temperature is of about 250-260 °C [10,53]. The percentage of carbon, oxygen, and hydrogen is of about 60, 30, and 4 % by weight, respectively, with a negligible amount of ashes [55].

PET type	IV (dl/g)
Textil	0.4-0.7
Film grade	0.6-0.7
Water bottles	0.7-0.8
Carbonated soft drink grade	0.8-0.9

Table 1.1. Intrinsic viscosity range depending on PET type and application.

The production of this polyester is usually performed in two steps; first the prepolymer synthesis, mainly bis(2-hydroxyethyl) terephthalate (BHET), followed by a polycondensation step [56]. The first synthesis dates back to 1941, in which during a study about phthalic acid, Whinfield J.R. and Dickson J.T. obtained the PET [57,58]. Originally, the prepolymer synthesis was a transesterification of dimethyl terephthalate (DMT) and ethylene glycol (EG) in a ratio of 1:2.4 at 200-290 °C, distilling methanol as the synthesis progressed [56,59]. However, in 1960, pure terephthalic acid (TA) with excess EG at 250 °C began to be [59]. Currently, both methods are used, direct esterification with TA and the transesterification reaction with DMT, which

transforms one ester into another [55,56,59–61]. Those synthesis reactions are shown in Figure 1.9 and Figure 1.10, respectively [20,52].

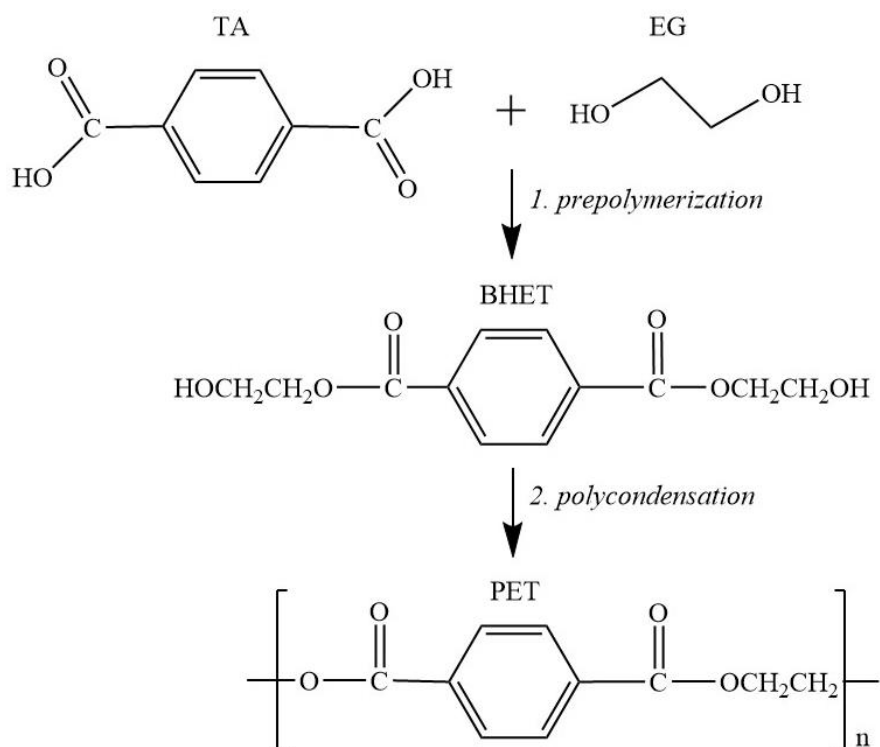


Figure 1.9. Direct esterification between TA and EG for the synthesis of PET.

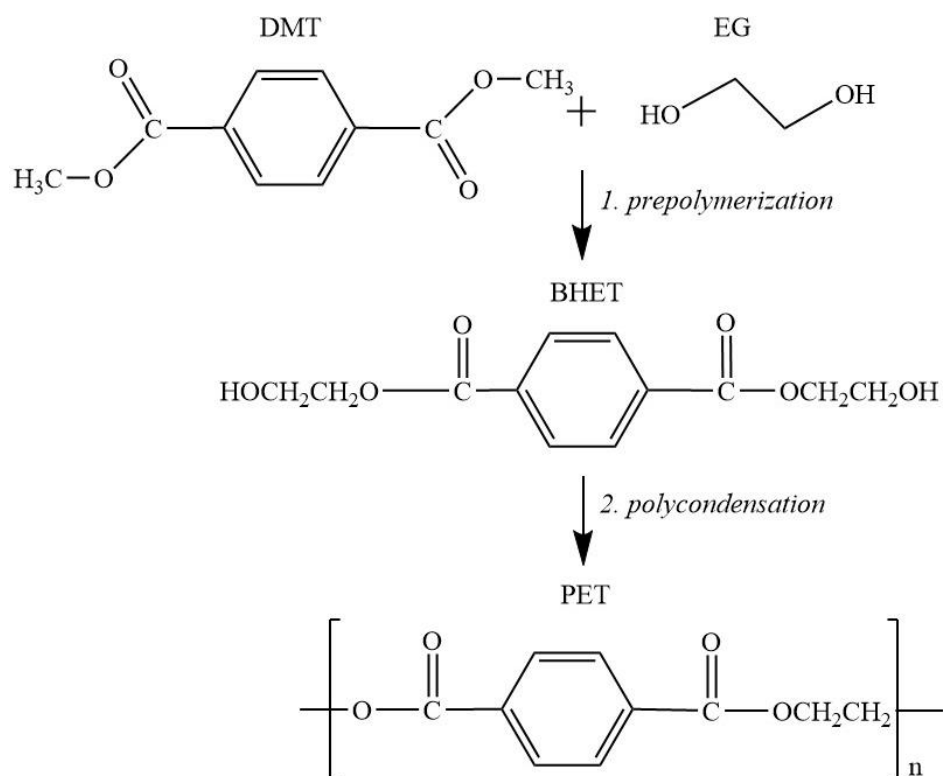


Figure 1.10. Transesterification reaction between DMT and EG for the synthesis of PET.

PET is the fifth most produced plastic in the world, with a production of 70 million tons per year [10,14]. This polyester is used in the manufacture of several products such as films, multilayer materials and plastic reinforcements [62]. The most common application for PET is the manufacture of bottles (51 %) followed by sheets and films (13.8 %), food packaging (9.1 %) and also non-food products (6.1 %). In the last two decades PET has been considered as one of the most important engineering polymers in the world [63,64], due to the physicochemical stability, good mechanical and barrier properties and low gas permeability [62,65–67]. Moreover, the low density and high flexibility, together with the low cost, make this polyester as a very attractive material for industries [68], nowadays this polyester being the main packaging material for mineral water, beverages and oils [65].

Therefore, PET plastic production has grown exponentially in recent years. In 2000, the global demand for this material was of about 6.4 million tons, and in 2010 it almost doubled reaching around 12.6 million tons, being currently at 33 million tons per year and expected to increase up to around 35.5 million tons by 2024 [55,69]. As a consequence of this high production the volume of PET waste is continuously increasing. According to a study conducted by Plastic Recyclers Europe, Petcore Europe and European Federation of Bottled Waters, 4.3 million tons of PET waste were generated in 2018 in Europe, but only the 45 % (1.9 million tons) were collected [70], a high amount of PET ending up in the sea. However, the recycling and management of marine debris is more complicated than those for urban waste. Firstly, the collection of these materials is laborious, becoming a serious problem for oceans and seas. In addition, due to the higher degradation suffered in the marine environment, the quality of the material to be recycled is poor, and in some cases not suitable for the most used recycling procedures.

1.6. Recycling of PET

Under normal conditions, PET is a non-degradable plastic, with a slow natural decomposition rate, since no known organism consumes its relatively large molecule [54]. Therefore, for waste disposal, recycling processes are the way to reduce PET waste [71]. Currently, three are the most widespread processes for the recovery or recycling of PET waste: thermo-mechanical recycling [72], chemical recycling [73] and energy recovery [74].

1.6.1. Thermo-mechanical recycling

Thermo-mechanical recycling is nowadays the most widely employed method for PET waste, due to its simplicity and low cost. This method was implemented in 1977 [54]. The process starts with the separation, washing, drying, and cutting of the residue, essential steps to obtain a high-quality end product [75,76]. The PET flakes thus prepared are then melted at high temperature (250-260 °C) and mixed in an extruder to obtain a homogeneous material, which is finally granulated.

Obtained pellets are then used as a raw material for other plastic products. Figure 1.11 shows a scheme of the thermo-mechanical process [76,77].

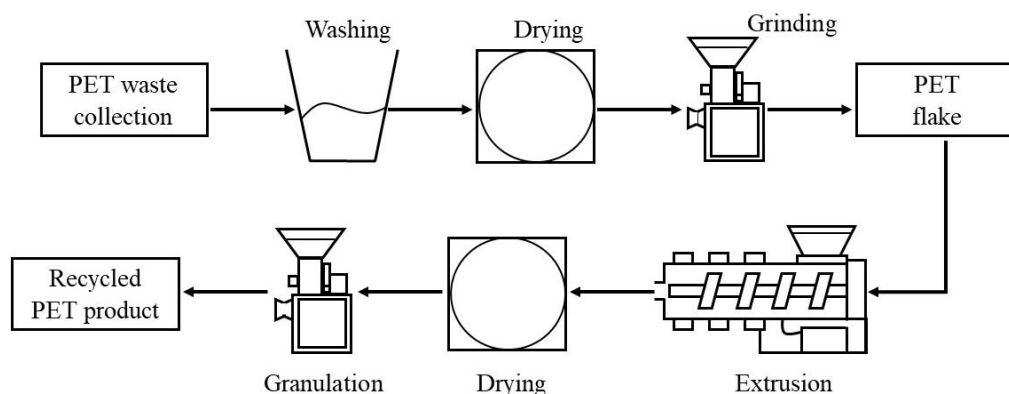


Figure 1.11. Scheme of the thermo-mechanical recycling process.

As it has been reported, PET is one of the most favorable packaging polymers for bottle-to-bottle recycling because it is easy to separate from other materials and does not need additives, among other reasons [78]. Nowadays, several companies around the world recycle post-consumer PET, mainly bottles, through thermo-mechanical processing to produce packaging laminates or fibers [79]. Among the fibers, the most interesting are those with a diameter between 5 and 150 μm (staple grades), while the larger ones are used for stuffing anoraks, sleeping bags and stuffed toys. Recycled PET is also used to spin smaller diameter fibers, which are then woven into the "fleece" fabric used for sweatshirts, jackets and scarves [79]. Urban PET waste presents rheological, and physicochemical properties very close to those of virgin material, which allows a successfully as thermo-mechanical process [80].

However, as in this process the thermoplastic is exposed to high temperatures, pressures and shearing conditions, undesired coloration and various degradations types can occur[81]. In reprocessing, the degradation during recycling is the most important problem. The degradation processes that occur in thermo-mechanical recycling are thermal, thermo-oxidative, hydrolysis and mechanical degradations [82]. As a consequence of degradation, a reduction in viscosity, molar mass, mechanical and thermal properties, and coloration, among many other changes, are reported [62,76,83,84].

The constant processing of the material at high temperatures causes degradation, resulting in lower quality products. In addition, it should be noted that the complexity and contamination of PET waste makes thermo-mechanical recycling difficult [75]. Thus, the purity and quality of the waste to be recycled are important factors to take into account. Therefore, it can be concluded that thermo-mechanical recycling of PET is a good recycling system but presenting limitations. Thermo-mechanical recycling is suitable for low degraded, high purity materials, while for lower

purity materials, chemical recycling and energy recovery are recommended [85].

1.6.2. Chemical recycling

Another alternative for the recycling of PET materials is chemical recycling, which allows the incorporation of PET with lower purity into materials cycle through depolymerization with high successful results [81,85]. However, this alternative needs high temperatures and equipment's that consumes high energy and also the employment of solvents and degrading agents [87]. Historically, the methods of chemical recycling of PET are generally classified into glycolysis [87-89], methanolysis [90], hydrolysis [91], ammonolysis [92,93] and aminolysis [92,93].

1.6.2.1. Methanolysis

Methanolysis is one of the most widely applied method on a commercial scale, being one of the former methods [82,87]. Consists on the decomposition of the thermoplastic by means of methanol under high temperature (180-200 °C) and pressure (20-40 atm) conditions. This leads to high purity DMT and EG, which are also the raw materials for PET synthesis [90,94]. Figure 1.12 depicts the scheme of the methanolysis process. In addition, methanolysis has a relatively high tolerance to contaminants allowing the treatment of low-quality raw materials [95].

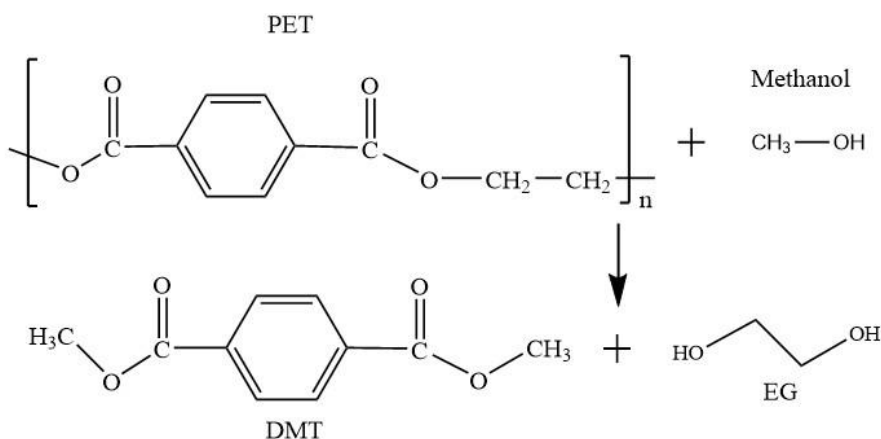


Figure 1.12. Methanolysis of PET.

1.6.2.2. Glycolysis

Glycolysis has been reported as the oldest method for chemical recycling of polymeric wastes [96]. Due to the simplicity and versatility, it is the most established and popular chemical recycling method for PET [97,98]. In addition, the lower cost of this method compared to methanolysis makes it the most widely employed system for the depolymerization of polymers such as polyurethanes and PET [99].

Glycolysis is a solvolytic degradation of PET that reacts with glycols such as EG, diethylene glycol (DEG) or propylene glycol (PG), among others, breaking the ester bonds of the polymer

chain and replacing them with hydroxyl groups, obtaining different oligomers, dimer and bis(2-hydroxyethyl) terephthalate BHET monomer [96,98,100]. Glycolysis is carried out at 180-250 °C in the presence of catalyst for 3-8 h depending on the glycol used [80]. Figure 1.13 shows a scheme of PET glycolysis with EG [101]. The obtained BHET monomer can be used in the production of PET or for the synthesis of polymers such as unsaturated polyesters, polyurethanes, vinyl esters or epoxy resins, among others [89,102].

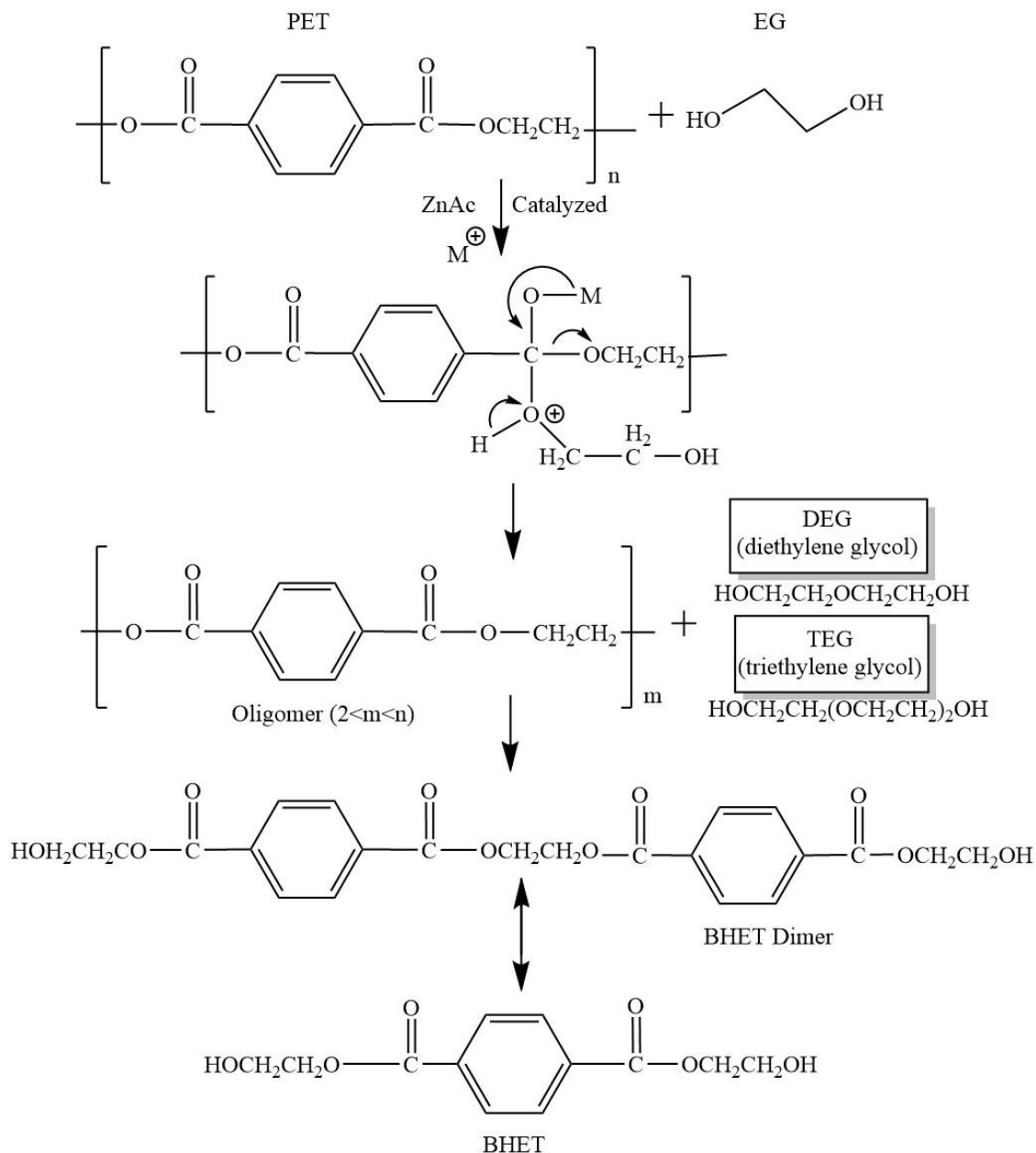


Figure 1.13. Glycolysis of PET [101].

In order to optimize the reaction rate and yield of BHET monomer production, several authors developed different glycolysis processes as shown in Table 1.2

Conditions	Time (h)	Temperature (°C)	Pressure (atm)	Catalyst	Ratio PET:EG Molar ratio	Yield (%)
Xylene medium [103]	1–3	170–245	-	-	1:0.5–1:3	20
Microwave irradiation [51]	0.5	180–190	-	ZnAc 0.5 %	1:2,1:4, 1:6	40
Ionic liquids [104]	5–10	160–195	1	Ionic liquids 1–4 L	1:4 (w/w)	78
Pressure reactor [105]		235–275	High pressure	ZnAc	1:1.3 (w/w)	-
Autoclave [106]	1	260	5	ZnMn ₂ O ₄ 1 %	5:86 Molar ratio	92.2
Atmospheric pressure [107]	1–2	196	1	ZnAc 1 % or Na ₂ CO ₃ 1%	1:7.6 Molar ratio	70
Potassium nitrate bath [108]	8	190	-	ZnAc % 0.5 CoAc % 0.5 MnAc % 0.5	1:4 Molar ratio	-
Atmospheric pressure [109]	1–4	180–190	1	ZnAc 2.35 %	1:4 (w/w)	91.6
Under pressure [110]	0.5–3	190–240	1–6	-	1:1–1:4 Molar ratio	-
Atmospheric pressure [111]	2–10	190	1	ZnAc 0.25–0.75 %	1:4 Molar ratio	-
Supercritical [112]	0.5	450	69–148	-	-	93.5

Table 1.2. Glycolysis procedures reported in the literature.

A solvent-assisted glycolysis, in which an organic solvent such as xylene is employed as reaction medium [103], supercritical glycolysis at 450 °C and 7–15 MPa pressure [112]; microwave-assisted glycolysis in which a significantly shorter reaction time (30 min) is enough to achieve the maximum yield of BHET compared to the conventional heating method of 8–9 h [51]; and finally, catalytic glycolysis with ionic liquids as reaction medium in which reaction takes around 5–10 h at 165–190 °C [104], can be mentioned. Among the advantages of mentioned glycolysis methods, several works have reported the zinc derivative catalyzed method as the most efficient [105–108]. López-Fonseca et al. obtained a yield of 70 % working with a PET:EG molar ratio of 1:7.6 in a three-neck glass reactor under atmospheric pressure at 196 °C for 1 h [107]. However, it is reported that with reaction times ranging from 1 to 4 h, nearly the 100 % conversion can be

achieved [109]. Chen et al. [110,111] analyzed the effect of temperature, PET:EG ratio and pressure (between 1~6 atm) on glycolysis. They confirmed that depolymerization of PET materials is temperature and PET:EG ratio dependent, occurring faster under pressure than at atmospheric pressure. Besides, Campanelli et al. [113] studied depolymerization in a pressure reactor at temperatures above 245 °C, using a PET:EG molar ratio of 1:2, also concluding that reaction occurs faster under pressure. Hence, it can be concluded that pressure enhances the depolymerization process of PET leading to higher amounts of BHET. Therefore, in order to obtain a high yield, several parameters can be modulated, and also the composition of the reaction products should be analyzed to define the most useful application or the most suitable polymer into which they will be transformed, using optimized reagents and conditions.

1.6.2.3. Hydrolysis

Hydrolysis of PET consist on the chain cleavage, obtaining TA and EG. Depolymerization can be promoted by acid catalysts such as sulfuric [91] or nitric acid [114], by alkaline catalysts such as sodium hydroxide [115] and by at neutral pH hydrolysis [116]. Each bond cleavage in the polymer chain during hydrolysis consumes one molecule of water to form carboxyl and hydroxyl functional groups. The reaction is carried out at elevated temperature and pressure, values with reaction times usually lower than 30 min, producing TA or disodium terephthalate together with EG, depending on the pH. Figure 1.14 shows the different PET hydrolysis processes [80].

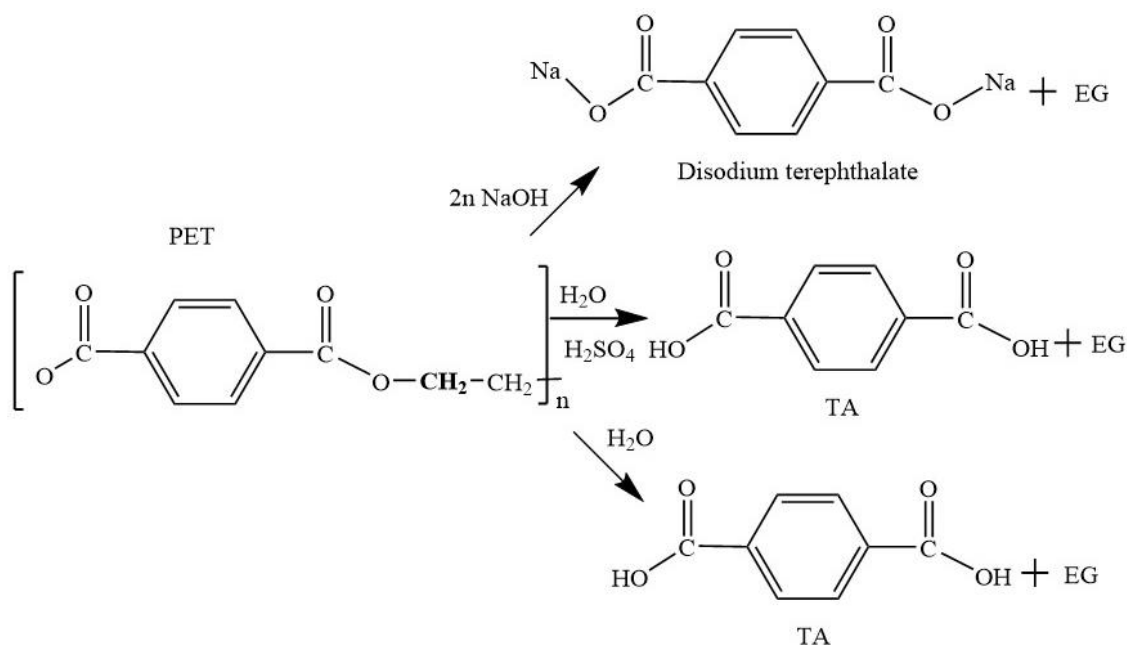


Figure 1.14. PET hydrolysis processes.

The alkaline and acidic reaction conditions provide hydronium ions that thermodynamically favor ester hydrolysis, by donating protons to the nucleophilic center of the ester group, thus reducing the activation energy for water-mediated cleavage [117,118]. However, the use of high

concentrations of acidic or basic media present serious problems in terms of high corrosiveness and the generation of high amount of strongly acidic/basic wastewater [118]. Moreover, the alkaline and acid catalysts used in these reactions are difficult to recover and reuse, increasing the cost of production [118,119]. Thus, in recent decades, hydrolysis at neutral pH is gaining interest [116]. Compared to glycolysis and methanolysis, this process has not been widely employed in the industry due to the high cost of TA purification. However, due to its commercial availability, most industries use monomeric TA as a feedstock for PET synthesis. Therefore, hydrolysis is becoming an important recycling process [80,116,120].

1.6.2.4. Ammonolysis

Anhydrous ammonia is also used to depolymerize PET to form terephthalamide [92,93]. This could be converted to terephthalonitrile and subsequently to para-xylene diamine or 1,4-bis(aminomethyl) cyclohexane [121]. The depolymerization scheme is shown in Figure 1.15. The reaction is usually carried out at 120-180 °C for 1-7 h, under a pressure of about 1 MPa. After the reaction, the mixture is filtered, rinsed with water and dried at 80 °C to collect the amide. Very good results have been reported in the literature, with a purity of 99 % and a yield of over 90 % [122]. A method of low-pressure depolymerization with ammonia in EG medium at 70 °C with a PET:NH₃ ratio of 1:6 was also reported, thus obtaining terephthalamide with a yield of 87 % [122].

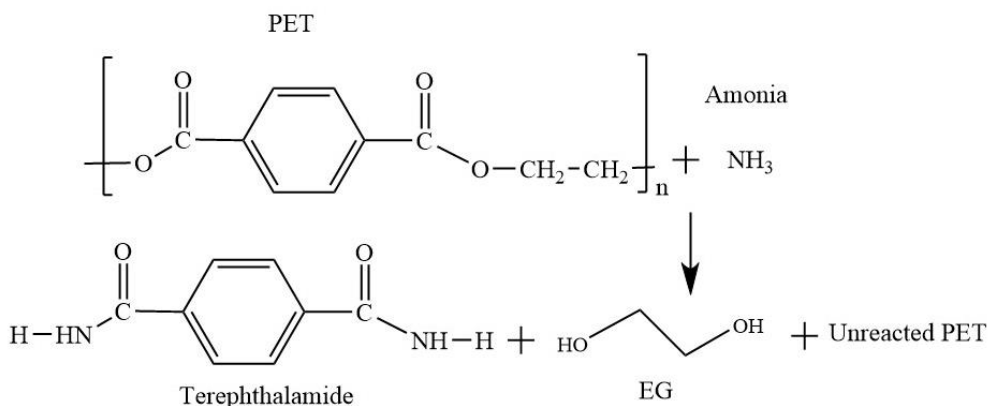


Figure. 1.15. PET ammonolysis scheme.

1.6.2.5. Aminolysis

Finally, the aminolysis process uses primary amines such as methylamine, ethylamine and ethanolamine, among others, in the aqueous phase, for the depolymerization of PET, leading to the formation of diamides of TA and EG [92]. The formation of N, N'-dimethyl terephthalamide is reported by the degradation of PET waste through aminolysis using aqueous methylamine [93], as shown in Figure 1.16. An excess of methylamine is used with a 10:1 methylamine:PET ratio at 40 °C with constant stirring for various reaction times ranking between 3-45 days, obtaining an

amine value of about 17 % [93,123]. Although aminolysis could be defined as a green reaction, it is not often used on an industrial scale. In most aminolysis processes PET was in the form of powder or fiber [112,123].

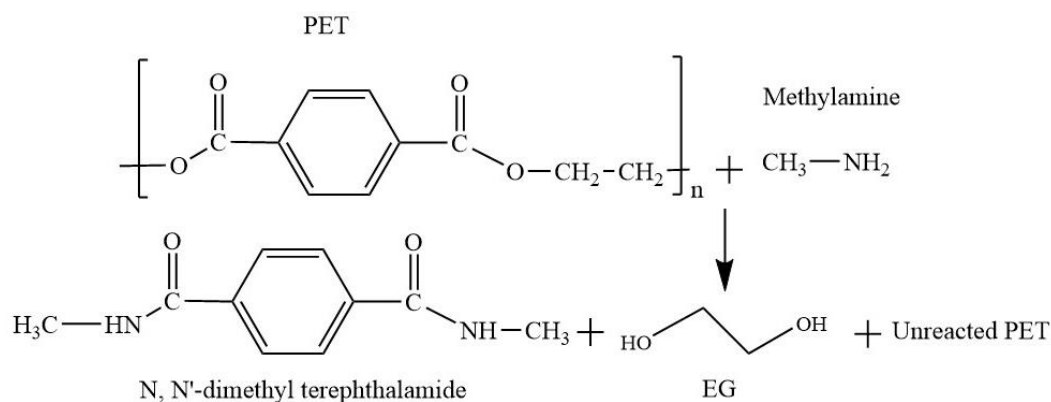


Figure 1.16. PET aminolysis scheme.

Among all cited chemical recycling processes, only methanolysis and glycolysis are used in a commercial scale, although recently hydrolysis has also been incorporated. This thesis, is focused in optimization of PET glycolysis [124,125].

1.6.3. Energy recovery

The third recycling method, energy recovery, is recommended for low purity plastics, such as highly degraded PET recovered from marine environment. This method consists on the incineration of PET to take benefit from the heat released during combustion [81]. In this way, PET is used as a fuel and burned, taking advantage of its hydrocarbonated nature, obtaining carbon dioxide and water, releasing energy in the process [26]. The main advantage of this method is the absence of restrictions in PET composition or quality, to be energetically recovered [126]. In the literature, lower heating values (LHV) of around 21.9-24.0 MJ/kg are reported for PET materials [127–129].

However, this recovery method involves atmospheric emissions, of carbon monoxide, acid gases and particles, which are not environmentally favorable. Most of the emissions from this recycling method are related to the incinerator combustion. However, it should be noted that waste collection is the main source of volatile organic compounds due to the transport, and also to the fact that the production of reagents for acid gas scrubbing is the main source of heavy metals, particulates and HCl [126]. Therefore, when analyzing the environmental impact, all processes must be taken into account, not only combustion emissions. Therefore, energy recovery should be the alternative for highly degraded plastics when other recycling methods are not suitable, becoming the third and last alternative for PET recycling.

1.7. BHET

BHET is the monomer obtained after depolymerization of PET through glycolysis or, in other words, it is the ester of terephthalic acid and ethylene glycol, the intermediate monomer in the production of PET [96]. The molecular formula of BHET is $C_{12}H_{14}O_6$ with a molar mass of 254 g/mol [51,130]. The chemical structure can be seen in Figure 1. 17.

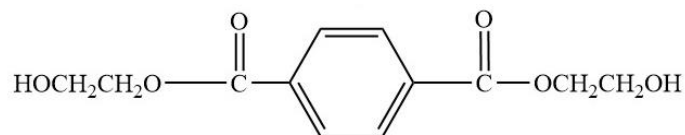


Figure 1.17. Chemical structure of BHET.

This monomer could be used in the synthesis of various polymers, obtaining a wide range of materials with very different properties.

1.7.1. BHET as raw material for PET production

It is common to use recycled BHET from PET depolymerization for PET production, so it can be considered as a reversible reaction. The synthesis of PET using BHET obtained from urban PET waste by glycolysis has been reported in the literature [131]. The BHET obtained by glycolysis and EG are added to a batch polycondensation reactor, at 230 °C for 2 h. Then it is heated to 260-280 °C at a pressure of 100 Pa and with a stirring of 10 rpm, in order to start the polycondensation reaction. When the reaction stops, N_2 gas at 230 °C is used to remove the excess of EG, and thereafter the regenerated PET is dried for 24 h in an oven at 90 °C.

1.7.2. BHET as raw material for new polymers

The BHET molecule has also been used in the production of new polymers [98], such as, unsaturated polyesters [132], vinyl esters [133], epoxy resins [134] and polyurethanes [135], among others.

In recent years, several studies employed PET glycolysis products as raw material for the synthesis of unsaturated polyester (UP) [136]. UPs are obtained by polyesterification of the glycolyzed PET product with unsaturated diacids and the subsequent cross-linking of this polyester with styrene monomer [132]. Physicochemical properties, such as gel time and degree of polymerization, can be controlled by changing the nature of the polyester chain and the styrene-polyester ratio [136]. Duque-Ingunza et al. have synthesized a UP using BHET obtained from the glycolysis of PET as raw material for the synthesis of an unsaturated diacid with maleic anhydride (MA), at a constant molar ratio BHET (-OH groups):MA (-COOH groups) of 1.1:1.0 [132]. Several polyesterification reactions were performed by changing the temperature (135, 150 and

180 °C) and time (1, 4, 6 and 8 h), concluding that the viscosity of the synthesized UPs is proportional to the temperature and time, becoming higher at long times and at high temperatures.

Besides, Atta et al. have worked on the synthesis of epoxy resin and vinyl ester using glycolyzed PET products [137]. The epoxy resin was prepared by reacting epichlorohydrin and with glycolysis products of PET. For the reaction, 0.17 mol of depolymerized PET were placed in the reactor at 40 °C and 0.7 mol of epichlorohydrin were added gradually over 2 h. After complete addition of epichlorohydrin, temperature was increased to 60 °C from 30 min and 0.35 mol NaOH were added. Then, the synthesized epoxy was used for the production of vinyl esters. The epoxy resin containing terminal epoxy groups was reacted with acrylic or methacrylic acid. In this way, ester resins with acrylic or methacrylic groups at chain ends were prepared, which were subsequently used to synthesize UPs [98].

Finally, several works related to the synthesis of polyurethanes (PU) using BHET, either commercial or produced by different recycling routes, are reported in the literature. Mafi et al. synthesized thermoplastic PUs using commercial BHET and polycaprolactone (PCL) as diols in various ratios, to which BHET was added up to a 20 wt.% [135], becoming a potential raw material for PU synthesis. In recent years, BHET recovered from municipal PET waste has been widely used to develop PUs for various applications. For example, Cevher and Sürdem [138] synthesized cross-linked PU adhesives using BHET recovered from PET bottle waste by glycolysis together with castor oil and commercial aromatic methylene diphenyl diisocyanate (MDI), in different ratios.

The best adhesion performance was obtained with a formulation containing approximately 20 wt % of BHET and 40 wt % of castor oil. Jamdar et al. [139] synthesized an environmentally friendly polyol based on linseed oil and BHET derived from recycled PET by electron beam irradiation, and then reacted with various polyisocyanate cross-linkers to produce thermoset PU coatings with good performance. In addition, Li et al. [140] synthesized a water-based PU using BHET recovered from PET waste by alcoholysis as a chain extender, with significantly improved mechanical properties, adhesive properties and thermal stability, and reduced water absorption. BHET recycled from textile waste by glycolysis has also been used to synthesize PU rigid foams using polymeric methylene diphenyl diisocyanate (pMDI) [141].

On the other hand, the use of recycled BHET from municipal PET waste as a diol for the synthesis of PU-alginate nanoparticles was reported in several works by Bhattacharyya et al. [142,143], which were employed for the encapsulation and delivery of insulin [144].

Therefore, the incorporation of glycolyzed PET monomer or BHET for the synthesis of various materials is confirmed. Among them, PU production is the most interesting and widespread, since due to its versatility different types of material can be obtained. Nevertheless, despite the intensive

research on the incorporation of recycled BHET in the chemistry of PUs, to the best of our knowledge, there are no research studies in which BHET obtained from the chemical recycling of marine PET litter has been used to synthesize PUs.

1.8. Polyurethanes

Polyurethanes (PU) are one of the most abundant plastics in the world, ranking, with a global production of 27 million tons per year, [16] seventh in the world in terms of production [14]. Due to the wide range of reagents available for their synthesis, materials with very different structures and properties can be synthesized [145–147]. PU can thus be used in a wide variety of applications, such as biomedicine, packaging, construction, textiles, automotive, thermal and acoustic insulation [148–151]. In addition, PUs can be chemically recycled into their monomers or segments, or into new ones, which can then be used for the synthesis of new polymers [152–155]. Moreover, reprocessing is also possible for thermoplastic PUs.

PUs are characterized by urethane functional group formed from the addition reaction between an isocyanate and a hydroxyl group, as shown in Figure 1.18a. Typically, polyols are used as hydroxyl groups supplier. In the case of PU-ureas, in addition to urethane group, urea group formed by the reaction of isocyanate and amine groups is also present, as shown in Figure 1.18b.

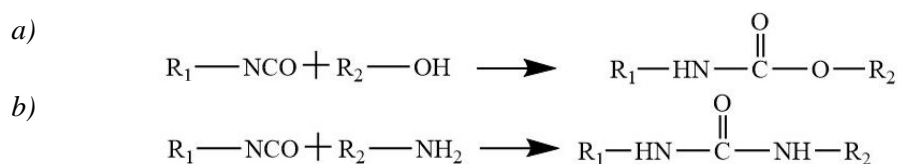


Figure 1.18. Addition reaction for **a)** urethane and **b)** urea groups formation.

Different reagents can be used in the synthesis of PU, differing in chemical structure, thus resulting in different properties.

1.8.1. Reagents

The main reagents used for the synthesis of PUs are polyol, isocyanate and chain extender.

1.8.1.1. Polyols

Polyols are low molar mass components containing hydroxyl functional groups. For PU synthesis the most common polyols are polyester and polyether. They present a molar mass between 500–8000 g/mol and a functionality of 2–8. The diverse choice of polyols allows the synthesis of PUs with different characteristics, since molar mass, structure, crystallinity and functionality have an important impact on the final PU. Using a bifunctional polyol, thermoplastic PUs with a high molar mass and linear structure can be synthesized. By increasing the functionality to 3, a network with few cross-links will be formed, producing flexible polyurethane elastomers. In contrast,

using low molar mass polyols of 400-1000 g/mol and functionality between 3-8, thermoset PUs are synthesized, presenting a highly cross-linked network [156]. Figure 1.19 shows the different polymer structures.

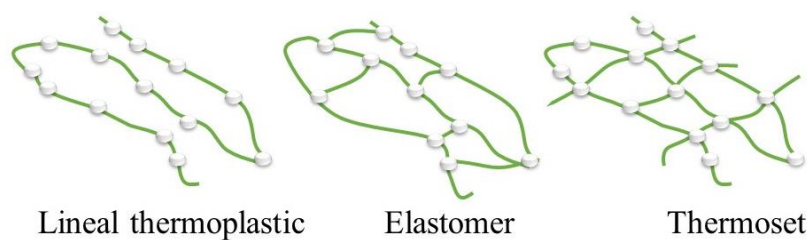


Figure 1.19. Molecular structure of thermoplastic, elastomer and thermoset PUs [157].

In recent years, due to the environmental concern, there has been a growing interest in the use of polyols from renewable sources, such as soybean oil, castor oil and other vegetable oils [156,158–160]. Analyzing the Life Cycle Assessment, replacing conventional polyols with polyols obtained from vegetable oils is an economic and environmentally friendly option [161].

1.8.1.2. Isocyanates

The selection of the isocyanate among many types available in the market, will depend on the final properties expected [148,162]. For the synthesis of thermoplastic PU and elastomers with low cross-linking, aromatic diisocyanates are popular, the most commonly used being methylene diphenyl diisocyanate (MDI) and toluene diisocyanate (TDI). However, aliphatic diisocyanates such as HDI are also being used for the synthesis of PUs [143,144], as they present higher biocompatibility, higher hydrolytic and thermal stability, and, above all, lower toxicity compared to aromatics [163,164].

Besides, the functionality of the isocyanate also influences the cross-linking of PUs. Thus, to obtain a thermoplastic PU it is necessary to employ a diisocyanate, while polymeric isocyanates can be employed for thermoset PUs. Similarly, the nature of the isocyanate is also related to the material stiffness, since when isocyanates with high aromaticity are used, the stiffness of the material increases due to the steric hindrance and mobility restrictions of the polymeric chain.

1.8.1.3. Chain extender

The chain extenders most employed for the synthesis of thermoplastic PUs or elastomers are low molar mass diols that react with the isocyanate terminated prepolymer and the isocyanate in excess to extend the polymer chain through urethane groups [165]. In this way, segments with high urethane density are formed, which constitute the hard segment of the polymer chain. Moreover, urethane groups of adjacent chains can interact by hydrogen bonding interactions leading to the formation of high melting temperature crystalline domains (Figure 1.20). Although

chain extenders are added in small amounts, they have a strong impact on the final properties of the polyurethanes [166].

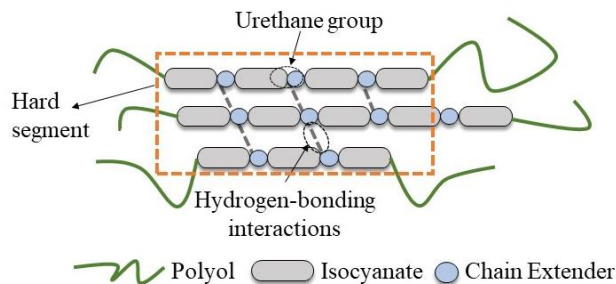


Figure 1.20. Hard segment and hydrogen bonding interactions between urethane groups in a PU.

1.8.2. Thermoplastic polyurethanes (TPU)

TPUs are very versatile block copolymers composed of soft (SS) and hard segments (HS). As explained above, the HS is generated by the reaction of the isocyanate and the chain extender, although the SS consists of a high molar mass macrodiol. At low temperatures, the properties are controlled by the soft segment while at high temperatures by the hard segment. The synthesis of TPUs can be performed in one or two-step. The general scheme of a two steps reaction is shown in Figure 1.21.

In the first step, the macrodiol is usually reacted with an excess of isocyanate, obtaining a prepolymer with isocyanate groups at the end of the chain. In the second step, the chain extender is added to the homogeneous prepolymer mixture. In this way, the chain extender reacts with the isocyanate groups left in the previous step, joining the prepolymer chains and obtaining a high molar mass polymer.

TPU usually shows a phase-separated microstructure with SS-rich and HS-rich domains. This separation depends on several factors such as reagent structure, segment length, segment affinity, crystallinity and hydrogen bonding [168].

The hard domain acts as physical cross-linking, and are generated by hydrogen bonding interactions between the N-H and C=O groups of adjacent chains, as shown in Figure 1.20. Thus, HS can arrange in semicrystalline structures acting as reinforcement.

On the other hand, the SS is responsible for extensibility, ductility and recovery [168]. SS can be amorphous or semicrystalline. Figure 1.22. shows a scheme of the phase separated hard and soft segments and domains formation.

degree of cross-linking of PUs depends on the reagents; higher cross-linking density is obtained by using high functionality polyols and/or polymeric isocyanates such as pMDI [170]. The cross-linking density can also be enhanced by using additional materials such as cross-linkers, which are short molecules with more than two hydroxyl groups, such as glycerol or triethanolamine [171]. The general scheme of the structure of a thermoset is shown in Figure 1.23.

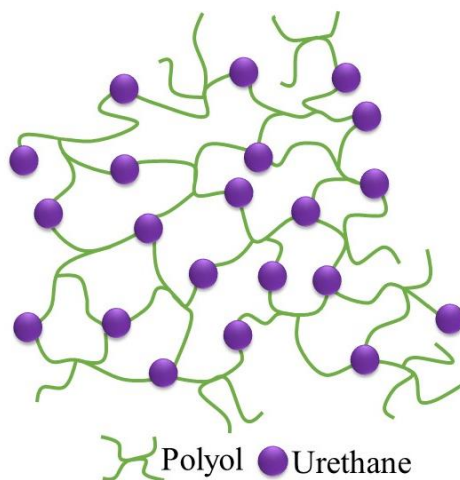


Figure 1.23. Overall molecular structure of thermoset PU.

1.9. General objectives

The main objective of this work has been the valorization of marine PET litter, a waste that nowadays is not systematically recycled in the industry. Several recycling methods and valorization strategies have been studied for the production of new, more environmentally friendly materials, with the aim of reducing impacts and raw materials, supporting the circular economy.

After the introduction in Chapter 1 and the presentation of materials and methods used in Chapter 2, this thesis is divided into the following chapters:

- In Chapter 3, different PET samples, such as virgin and post-condensed PET raw materials and post-consumer urban PET waste and marine PET litter have been studied. The effect of degradation on waste has been analyzed by an extensive characterization of the materials.
- In Chapter 4, the valorization of marine PET litter has been carried out using the most conventional methods: thermo-mechanical recycling and energy recovery. The degradations that occur during thermo-mechanical recycling were also studied.
- In Chapter 5, the chemical recycling of marine PET litter has been studied as the best

alternative for highly degraded PET, such as that found in the marine environment. In order to carry out the chemical recycling, the glycolysis reaction was optimized first in a closed reactor, obtaining great yields for a very low reaction times. After the chemical recycling of the marine PET litter, obtained product has been characterized.

- In Chapter 6, the synthesis of different biobased/recycled TPU has been carried out using a biobased macrodiol, the recycled BHET obtained in Chapter 5 and HDI. The characterization of the synthesized PUs has been performed comparing them with PUs synthesized using commercial BHET. Finally, a preliminary study of both thermo-mechanical and chemical recyclability, of the synthesized TPUs has also been conducted.
- In Chapter 7, thermoset biobased/recycled PUs have been synthesized using different ratios of a polyol derived from castor oil, the recycled BHET obtained in Chapter 5 and a pMDI. The objective of this chapter is to synthesize thermoset PUs with a high percentage of renewable/recycled componets, giving added value to the recycled BHET obtained from marine PET litter. Likewise, the characterization of the synthesized thermoset PUs has been carried out, together with a preliminary study of their chemical recyclability.
- In Chapter 8, a quantitative analysis of some processes of this thesis has been performed by a Life Cycle Assessment study. The impact of chemical recycling of marine PET litter for the recovery of BHET in Chapter 5 has been analyzed. In addition, the impacts of one of the PUs synthesized in this thesis, specifically of the TPUs synthesized in Chapter 6, have been studied by comparing them with PUs synthesized with commercial BHET and a petrochemical-based TPU.
- In Chapter 9, the general conclusions, publications and future works related with this thesis are presented.

1.10. References

- [1] J. Jiang, K. Shi, X. Zhang, K. Yu, H. Zhang, J. He, Y. Ju, J. Liu, From plastic waste to wealth using chemical recycling: A review, *J Environ Chem Eng.* 10 (2022) 106867–106877. <https://doi.org/10.1016/j.jece.2021.106867>.
- [2] K.R. Vanapalli, H.B. Sharma, V.P. Ranjan, B. Samal, J. Bhattacharya, B.K. Dubey, S. Goel, Challenges and strategies for effective plastic waste management during and post COVID-19 pandemic, *Sci Total Environ.* 750 (2021) 141514–141555. <https://doi.org/10.1016/j.scitotenv.2020.141514>.

- [3] K. Syberg, M.B. Nielsen, L.P. Westergaard Clausen, G. van Calster, A. van Wezel, C. Rochman, A.A. Koelmans, R. Cronin, S. Pahl, S.F. Hansen, Regulation of plastic from a circular economy perspective, *Curr Opin Green Sustain Chem.* 29 (2021) 100462–100469. <https://doi.org/10.1016/j.cogsc.2021.100462>.
- [4] PlasticsEurope, *Plastics—the Facts 2020*, (2020). <https://plasticseurope.org/knowledge-hub/plastics-the-facts-2020/> (accessed December 15, 2019).
- [5] D.K.A. Barnes, F. Galgani, R.C. Thompson, M. Barlaz, Accumulation and fragmentation of plastic debris in global environments, *Phil Trans R Soc B.* 364 (2009) 1985–1998. <https://doi.org/10.1098/rstb.2008.0205>.
- [6] M.E. Iñiguez, J.A. Conesa, A. Soler, Effect of marine ambient in the production of pollutants from the pyrolysis and combustion of a mixture of plastic materials, *Mar Pollut Bull.* 130 (2018) 249–257. <https://doi.org/10.1016/J.MARPOLBUL.2018.03.040>.
- [7] P. Benyathiar, P. Kumar, G. Carpenter, J. Brace, D.K. Mishra, Polyethylene terephthalate (PET) bottle-to-bottle recycling for the beverage industry: A review, *Polymers* (2022) 2366–2395. <https://doi.org/10.3390/polym14122366>.
- [8] N.A.S. Suhaimi, F. Muhamad, N.A. Abd Razak, E. Zeimaran, Recycling of polyethylene terephthalate wastes: A review of technologies, routes, and applications, *Polym Eng Sci.* 62 (2022) 2355–2375. <https://doi.org/10.1002/pen.26017>.
- [9] V. Tournier, C.M. Topham, A. Gilles, B. David, C. Folgoas, E. Moya-Leclair, E. Kamionka, M.L. Desrousseaux, H. Texier, S. Gavalda, M. Cot, E. Guémard, M. Dalibey, J. Nomme, G. Cioci, S. Barbe, M. Chateau, I. André, S. Duquesne, A. Marty, An engineered PET depolymerase to break down and recycle plastic bottles, *Nature.* 580 (2020) 216–219. <https://doi.org/10.1038/s41586-020-2149-4>.
- [10] R.R. Pasula, S. Lim, F.J. Ghadessy, B. Sana, The influences of substrates' physical properties on enzymatic PET hydrolysis: Implications for PET hydrolase engineering, *Eng Biol.* 6 (2022) 17–22. <https://doi.org/10.1049/enb2.12018>.
- [11] B. Sadeghi, Y. Marfavi, R. AliAkbari, E. Kowsari, F. Borbor Ajdari, S. Ramakrishna, Recent studies on recycled PET fibers: production and applications: a review, *Mater Circ Econ.* 3 (2021) 1–18. <https://doi.org/10.1007/s42824-020-00014-y>.
- [12] D. Lithner, Å. Larsson, G. Dave, Environmental and health hazard ranking and assessment of plastic polymers based on chemical composition, *Sci of The Total Environ.* 409 (2011) 3309–3324. <https://doi.org/10.1016/j.scitotenv.2011.04.038>.

- [13] R. Geyer, J.R. Jambeck, K.L. Law, Production, use, and fate of all plastics ever made, *Sci Adv.* 3 (2017) 170078–170084. <https://doi.org/10.1126/sciadv.1700782>.
- [14] PlasticsEurope, *Plastics—the Facts 2021*, (2021). <https://plasticseurope.org/knowledge-hub/plastics-the-facts-2021/> (accessed June 10, 2022).
- [15] Hisham A. Maddah, Polypropylene as a promising plastic: a review, *Am J Polym Sci.* 6 (2016) 1–11. [https://doi.org/DOI: 10.5923/j.ajps.20160601.01](https://doi.org/DOI:10.5923/j.ajps.20160601.01).
- [16] Z. Yuan, R. Nag, E. Cummins, Ranking of potential hazards from microplastics polymers in the marine environment, *J Hazard Mater.* 429 (2022) 128399–128418. <https://doi.org/10.1016/j.jhazmat.2022.128399>.
- [17] United Nations Environment Programme, *Single-use plastics: A roadmap for sustainability*, (2018). <https://www.unep.org/resources/report/single-use-plastics-roadmap-sustainability> (accessed September 10, 2022).
- [18] H.L. Chen, T.K. Nath, S. Chong, V. Foo, C. Gibbins, A.M. Lechner, The plastic waste problem in Malaysia: management, recycling and disposal of local and global plastic waste, *SN Appl Sci.* 3 (2021) 1–15. <https://doi.org/10.1007/s42452-021-04234-y>.
- [19] L.D. Ellis, N.A. Rorrer, K.P. Sullivan, M. Otto, J.E. McGeehan, Y. Román-Leshkov, N. Wierckx, G.T. Beckham, Chemical and biological catalysis for plastics recycling and upcycling, *Nat Catal.* 4 (2021) 539–556. <https://doi.org/10.1038/s41929-021-00648-4>.
- [20] R. Nisticò, Polyethylene terephthalate (PET) in the packaging industry, *Polym Test.* 90 (2020) 106707–106741. <https://doi.org/10.1016/j.polymertesting.2020.106707>.
- [21] L. Roager, E.C. Sonnenschein, Bacterial candidates for colonization and degradation of marine plastic debris, *Enviro Sci Technol* (2019) 11636–11643. <https://doi.org/10.1021/acs.est.9b02212>.
- [22] L.C.M. Lebreton, J. van der Zwet, J.W. Damsteeg, B. Slat, A. Andrady, J. Reisser, River plastic emissions to the world’s oceans, *Nat Commun.* 8 (2017) 15611–15621. <https://doi.org/10.1038/ncomms15611>.
- [23] H.S. Auta, C.U. Emenike, S.H. Fauziah, Distribution and importance of microplastics in the marine environment A review of the sources, fate, effects, and potential solutions, *Environ Int.* 102 (2017) 165–176. <https://doi.org/10.1016/j.envint.2017.02.013>.
- [24] L. Magnier, R. Mugge, J. Schoormans, Turning ocean garbage into products – Consumers’ evaluations of products made of recycled ocean plastic, *J Clean Prod.* 215 (2019) 84–98. <https://doi.org/10.1016/J.JCLEPRO.2018.12.246>.

- [25] L. Sherry, S. Opfer, A. Courtney, Marine debris monitoring and assessment: recommendations for monitoring debris trends in the marine environment, 2013. URL: <https://repository.library.noaa.gov/view/noaa/268>
- [26] C. Peña-Rodríguez, G. Mondragon, A. Mendoza, E. Mendiburu-Valor, A. Eceiza, G. Kortaberria, Recycling of marine plastic debris, in: *Recent Developments in Plastic Recycling*, Springer (2021) 121–141. https://doi.org/10.1007/978-981-16-3627-1_6.
- [27] B. Gewert, M.M. Plassmann, M. Macleod, Pathways for degradation of plastic polymers floating in the marine environment, *Environ Sci Process Impacts*. 17 (2015) 1513–1521. <https://doi.org/10.1039/c5em00207a>.
- [28] M.E. Iñiguez, J.A. Conesa, A. Fullana, Recyclability of four types of plastics exposed to UV irradiation in a marine environment, *Waste Manage*. 79 (2018) 339–345. <https://doi.org/10.1016/J.WASMAN.2018.08.006>.
- [29] S. Venkatachalam, G. Shilpa, V. Jayprakash, R. Prashant, Rao. Krishna, K. Anil, Degradation and recyclability of poly (ethylene terephthalate), in: *Polyester*, InTech, 2012: pp. 75–98. <https://doi.org/10.5772/48612>.
- [30] A. Frache, G. Camino, *Degradazione, stabilizzazione e ritardo alla fiamma di Polimeri*, Nuova Cultura, Edizioni Nuova Cultura, Roma (Italy), 2012.
- [31] F. Dubelley, E. Planes, C. Bas, E. Pons, B. Yrieix, L. Flandin, The hydrothermal degradation of PET in laminated multilayer, *Eur Polym J*. 87 (2017) 1–13. <https://doi.org/10.1016/J.EURPOLYMJ.2016.12.004>.
- [32] C. Sammon, J. Yarwood, N. Everall, An FT–IR study of the effect of hydrolytic degradation on the structure of thin PET films, *Polym Degrad Stab*. 67 (2000) 149–158. [https://doi.org/10.1016/S0141-3910\(99\)00104-4](https://doi.org/10.1016/S0141-3910(99)00104-4).
- [33] B.J. Holland, J.N. Hay, The thermal degradation of PET and analogous polyesters measured by thermal analysis–Fourier transform infrared spectroscopy, *Polymer (Guildf)*. 43 (2002) 1835–1847. [https://doi.org/10.1016/S0032-3861\(01\)00775-3](https://doi.org/10.1016/S0032-3861(01)00775-3).
- [34] E. Pirzadeh, A. Zadhoush, M. Haghghat, Hydrolytic and thermal degradation of PET fibers and PET granule: The effects of crystallization, temperature, and humidity, *J Appl Polym Sci*. 106 (2007) 1544–1549. <https://doi.org/10.1002/app.26788>.
- [35] B.D. Dean, M. Matzner, J.M. Tibbitt, Polyarylates, in: *Comprehensive Polymer Science and Supplements*, Oxford (1989) 317–329.

- [36] M. Day, D.M. Wiles, Photochemical degradation of poly(ethylene terephthalate). III. determination of decomposition products and reaction mechanism, *J Appl Polym Sci.* 16 (1972) 203–215. <https://doi.org/10.1002/app.1972.070160118>.
- [37] C. Ioakeimidis, K.N. Fotopoulou, H.K. Karapanagioti, M. Geraga, C. Zeri, E. Papathanassiou, F. Galgani, G. Papatheodorou, The degradation potential of PET bottles in the marine environment: An ATR-FTIR based approach, *Sci Rep.* 6 (2016) 1–8. <https://doi.org/10.1038/srep23501>.
- [38] A. Ganesh Kumar, K. Anjana, M. Hinduja, K. Sujitha, G. Dharani, Review on plastic wastes in marine environment – Biodegradation and biotechnological solutions, *Mar Pollut Bull.* 150 (2020) 110733–110741. <https://doi.org/10.1016/j.marpolbul.2019.110733>.
- [39] S. Yoshida, K. Hiraga, T. Takehana, I. Taniguchi, H. Yamaji, Y. Maeda, K. Toyohara, K. Miyamoto, Y. Kimura, K. Oda, A bacterium that degrades and assimilates poly(ethylene terephthalate), *Science.* 2016 1–5. <https://doi.org/DOI:10.1126/science.aad6359>.
- [40] M. Mutsuga, T. Tojima, Y. Kawamura, K. Tanamoto, Survey of formaldehyde, acetaldehyde and oligomers in polyethylene terephthalate food-packaging materials, *Food Addit Contam.* 22 (2005) 783–789. <https://doi.org/10.1080/02652030500157593>.
- [41] P. Das, P. Tiwari, Thermal degradation study of waste polyethylene terephthalate (PET) under inert and oxidative environments, *Thermochim Acta.* 679 (2019) 178340–178347. <https://doi.org/10.1016/j.tca.2019.178340>.
- [42] E.G. El'darov, F.V. Mamedov, V.M. Gol'dberg, G.E. Zaikov, A kinetic model of polymer degradation during extrusion, *Polym Degrad Stab.* 51 (1996) 271–279. [https://doi.org/10.1016/0141-3910\(95\)00160-3](https://doi.org/10.1016/0141-3910(95)00160-3).
- [43] J. Payne, P. McKeown, M.D. Jones, A circular economy approach to plastic waste, *Polym Degrad Stab.* 165 (2019) 170–181. <https://doi.org/10.1016/j.polymdegradstab.2019.05.014>.
- [44] S. Huysman, J. de Schaepmeester, K. Ragaert, J. Dewulf, S. de Meester, Performance indicators for a circular economy: A case study on post-industrial plastic waste, *Resour Conserv Recycl.* 120 (2017) 46–54. <https://doi.org/10.1016/j.resconrec.2017.01.013>.
- [45] T. Bauwens, R. Mees, M. Gerardts, J.V. Dune, H. Friedel, C.V. Daniels, C. Teurlings, M. Brasz, M. Henry, M. Hekkert, J. Kirchherr, How circular startups can accelerate the circular economy transition, (2019).

- https://assets.change.inc/downloads/DISRUPTORS_CIRCULAR-START-UPS_UU_E-VERSION.pdf (accessed September 26, 2022).
- [46] European Commission, Directorate-General for Research and Innovation, C. Schempp, P. Hirsch, *Categorisation system for the circular economy: a sector-agnostic categorisation system for activities substantially contributing to the circular economy*, Publications Office, 2020. <https://doi.org/doi/10.2777/172128>.
- [47] T.D. Nielsen, J. Hasselbalch, K. Holmberg, J. Stripple, *Politics and the plastic crisis: A review throughout the plastic life cycle*, *Wiley Interdiscip Rev Energy Environ.* 9 (2020) 360–368. <https://doi.org/10.1002/wene.360>.
- [48] M.R. Johansen, T.B. Christensen, T.M. Ramos, K. Syberg, *A review of the plastic value chain from a circular economy perspective*, *J Environ Manage.* 302 (2022) 113975–113964. <https://doi.org/10.1016/j.jenvman.2021.113975>.
- [49] European Commission, *A new circular economy action plan for a cleaner and more competitive Europe*, (2020). <https://eur-lex.europa.eu/legal-content/EN/TXT/?qid=1583933814386&uri=COM:2020:98:FIN> (accessed December 11, 2022).
- [50] J. Kirchherr, D. Reike, M. Hekkert, *Conceptualizing the circular economy: An analysis of 114 definitions*, *Resour Conserv Recycl.* 127 (2017) 221–232. <https://doi.org/10.1016/j.resconrec.2017.09.005>.
- [51] S. Chaudhary, P. Surekha, D. Kumar, C. Rajagopal, P.K. Roy, *Microwave assisted glycolysis of poly(ethylene terephthalate) for preparation of polyester polyols*, *J Appl Polym Sci.* 129 (2013) 2779–2788. <https://doi.org/10.1002/app.38970>.
- [52] V.G. Mihucz, G. Záray, *Occurrence of antimony and phthalate esters in polyethylene terephthalate bottled drinking water*, *Appl Spectrosc Rev.* 51 (2016) 163–189. <https://doi.org/10.1080/05704928.2015.1105243>.
- [53] S. Farah, K.R. Kunduru, A. Basu, A.J. Domb, *Molecular weight determination of polyethylene terephthalate*, in: *Poly(Ethylene Terephthalate) Based Blends, Composites and Nanocomposites*, Elsevier Inc., 2015: pp 143–165. <https://doi.org/10.1016/B978-0-323-31306-3.00008-7>.
- [54] F. Awaja, D. Pavel, *Recycling of PET*, *Eur Polym J.* 41 (2005) 1453–1477. <https://doi.org/10.1016/J.EURPOLYMJ.2005.02.005>.

- [55] S. Sharifian, N. Asasian-Kolur, Polyethylene terephthalate (PET) waste to carbon materials: Theory, methods and applications, *J Anal Appl Pyrolysis*. 163 (2022) 105496 – 105517. <https://doi.org/10.1016/j.jaap.2022.105496>.
- [56] M. di Serio, R. Tesser, A. Ferrara, E. Santacesaria, Heterogeneous basic catalysts for the transesterification and the polycondensation reactions in PET production from DMT, *J Mol Catal A Chem*. 212 (2004) 251–257. <https://doi.org/10.1016/j.molcata.2003.10.032>.
- [57] J.R. Whinfield, J.T. Dickson, UK Patent No. 578079., 578079, 1946.
- [58] J. Pang, M. Zheng, R. Sun, A. Wang, X. Wang, T. Zhang, Synthesis of ethylene glycol and terephthalic acid from biomass for producing PET, *Green Chem*. 18 (2016) 342–359. <https://doi.org/10.1039/c5gc01771h>.
- [59] P.J. Chenier, *Survey of Industrial Chemistry*, Springer US, Boston, MA, 2002. <https://doi.org/10.1007/978-1-4615-0603-4>.
- [60] T. Yamada, Y. Imamura, Simulation of continuous direct esterification process between terephthalic acid and ethylene glycol, *Polym Plast Technol Eng*. 28 (1989) 811–876. <https://doi.org/10.1080/03602558908049829>.
- [61] K. Dutt, R.K. Soni, A review on synthesis of value added products from polyethylene terephthalate (PET) waste, *Polym Sci Ser B Polym Chem. B*. 55 (2013) 430–452. <https://doi.org/10.1134/S1560090413070075>.
- [62] M. del Mar Castro López, A.I. Ares Pernas, M.J. Abad López, A.L. Latorre, J.M. López Vilariño, M.V. González Rodríguez, Assessing changes on poly(ethylene terephthalate) properties after recycling: Mechanical recycling in laboratory versus postconsumer recycled material, *Mater Chem Phys*. 147 (2014) 884–894. <https://doi.org/10.1016/J.MATCHEMPHYS.2014.06.034>.
- [63] S. Ubeda, M. Aznar, C. Nerín, Determination of oligomers in virgin and recycled polyethylene terephthalate (PET) samples by UPLC-MS-QTOF, *Anal Bioanal Chem*. 410 (2018) 2377–2384. <https://doi.org/10.1007/s00216-018-0902-4>.
- [64] T.H. Begley, J.E. Biles, C. Cunningham, O. Piringer, Migration of a UV stabilizer from polyethylene terephthalate (PET) into food simulants, *Food Addit Contam*. 21 (2004) 1007–1014. <https://doi.org/10.1080/02652030400010447>.
- [65] B. Li, Z.-W. Wang, Q.-B. Lin, C.-Y. Hu, Study of the migration of stabilizer and plasticizer from polyethylene terephthalate into food simulants, *J Chromatogr Sci*. 54 (2016) 939–951. <https://doi.org/10.1093/chromsci/bmw025>.

- [66] C.A. Chapa-Martínez, L. Hinojosa-Reyes, A. Hernández-Ramírez, E. Ruiz-Ruiz, L. Maya-Treviño, J.L. Guzmán-Mar, An evaluation of the migration of antimony from polyethylene terephthalate (PET) plastic used for bottled drinking water, *Sci Total Environ.* 565 (2016) 511–518. <https://doi.org/10.1016/J.SCITOTENV.2016.04.184>.
- [67] Y.S. Hu, V. Prattipati, S. Mehta, D.A. Schiraldi, A. Hiltner, E. Baer, Improving gas barrier of PET by blending with aromatic polyamides, *Polymer (Guildf)*. 46 (2005) 2685–2698. <https://doi.org/10.1016/J.POLYMER.2005.01.056>.
- [68] H. sen Wei, K.T. Liu, Y.C. Chang, C.H. Chan, C.C. Lee, C.C. Kuo, Superior mechanical properties of hybrid organic-inorganic superhydrophilic thin film on plastic substrate, *Surf Coat Technol.* 320 (2017) 377–382. <https://doi.org/10.1016/J.SURFCOAT.2016.12.025>.
- [69] Chemie, Polyethylene terephthalate (PET) Global market to 2020 - Increasing demand from carbonated soft drinks, (2020). <http://www.chemie.de/marktstudien/10877/polyethylene-terephthalate-pet-global-market-to-2020-increasing-demand-from-carbonated-soft-drinks-food-and-beer-packaging-in-bric-nations-driving-growth.html> (accessed December 20, 2019).
- [70] Plastics Recyclers Europe, Natural Mineral Waters Europe, PETCORE Europe, UNESDA Soft Drinks Europe, PET Market in Europe state of play 2022, collection and recycling, (2022). <https://www.plasticsrecyclers.eu/plastics-recyclers-publications> (accessed April 20, 2022).
- [71] M.S. Farahat, A.-A.A. Abdel-Azim, M.E. Abdel-Raowf, Modified unsaturated polyester resins synthesized from poly(ethylene terephthalate) waste, 1 Synthesis and curing characteristics, *Macromol Mater Eng.* 283 (2000) 1–6. [https://doi.org/1438-7492/2000/0111-0001\\$17.50+.50/0](https://doi.org/1438-7492/2000/0111-0001$17.50+.50/0).
- [72] L.K. Nait-Ali, X. Colin, A. Bergeret, Kinetic analysis and modelling of PET macromolecular changes during its mechanical recycling by extrusion, *Polym Degrad Stab.* 96 (2011) 236–246. <https://doi.org/10.1016/j.polymdegradstab.2010.11.004>.
- [73] D.E. Nikles, M.S. Farahat, New motivation for the depolymerization products derived from poly(ethylene terephthalate) (PET) waste: a review, *Macromol Mater Eng.* 290 (2005) 13–30. <https://doi.org/10.1002/mame.200400186>.
- [74] R.M.S. Radin Mohamed, A.A. Wurochekke, G. Sanusi Misbah, A.H. bin Mohd. Kassim, Energy recovery from polyethylene terephthalate(PET) recycling process, *GSTF J of Eng Technol.* 2 (2014) 39–44. https://doi.org/10.5176/2251-3701_2.4.98.

- [75] S.M. Al-Salem, P. Lettieri, J. Baeyens, Recycling and recovery routes of plastic solid waste (PSW): A review, *Waste Manage.* 29 (2009) 2625–2643. <https://doi.org/10.1016/j.wasman.2009.06.004>.
- [76] H.J. Koo, G.S. Chang, S.H. Kim, W.G. Hahm, S.Y. Park, Effects of recycling processes on physical, mechanical and degradation properties of PET yarns, *Fibers Polym.* 14 (2013) 2083–2087. <https://doi.org/10.1007/s12221-013-2083-2>.
- [77] M.P. Aznar, M.A. Caballero, J.A. Sancho, E. Francés, Plastic waste elimination by co-gasification with coal and biomass in fluidized bed with air in pilot plant, *Fuel Process Technol.* 87 (2006) 409–420. <https://doi.org/10.1016/j.fuproc.2005.09.006>.
- [78] F. Welle, Twenty years of PET bottle to bottle recycling - An overview, *Resour Conserv Recycl.* 55 (2011) 865–875. <https://doi.org/10.1016/j.resconrec.2011.04.009>.
- [79] Petcore Europe, Recycled Products, (2020). <https://www.petcore-europe.org/recycled-products.html> (accessed September 14, 2020).
- [80] K. Vinnakota, A. Bryant-Friedrich, Chemical recycling of poly (ethylene terephthalate) and its co-polyesters with 2, 5-furandicarboxylic acid using alkaline hydrolysis, 2018 1–115.
- [81] B. Geyer, G. Lorenz, A. Kandelbauer, Recycling of poly(ethylene terephthalate) – A review focusing on chemical methods, *Express Polym Lett.* 10 (2016) 559–586. <https://doi.org/10.3144/expresspolymlett.2016.53>.
- [82] S. Altun, Y. Ulcay, Improvement of waste recycling in PET fiber production, *Express Polym Lett.* 10 (2016) 559–586. <https://doi.org/DOI:10.3144/expresspolymlett.2016.53>.
- [83] R. Assadi, X. Colin, J. Verdu, Irreversible structural changes during PET recycling by extrusion, *Polymer (Guildf)*. 45 (2004) 4403–4412. <https://doi.org/10.1016/j.polymer.2004.04.029>.
- [84] J.D. Badia, E. Strömberg, S. Karlsson, A. Ribes-Greus, The role of crystalline, mobile amorphous and rigid amorphous fractions in the performance of recycled poly (ethylene terephthalate) (PET), *Polym Degrad Stab.* 97 (2012) 98–107. <https://doi.org/10.1016/j.polymdegradstab.2011.10.008>.
- [85] Petcore Europe, Processing, (2020). <https://www.petcore-europe.org/processing.html> (accessed September 18, 2020).

- [86] B. Geyer, S. Röhrner, G. Lorenz, A. Kandelbauer, Designing oligomeric ethylene terephthalate building blocks by chemical recycling of polyethylene terephthalate, *J Appl Polym Sci.* 131 (2014) 39786–39798. <https://doi.org/10.1002/app.39786>.
- [87] D. Paszun, T. Szychaj, Chemical recycling of poly(ethylene terephthalate), *Ind Eng Chem. Res* (1997) 1373–1383. <https://pubs.acs.org/sharingguidelines>.
- [88] A. Ghaderian, A.H. Haghighi, F.A. Taromi, Z. Abdeen, A. Boroomand, S.M.-R. Taheri, Characterization of rigid polyurethane foam prepared from recycling of PET waste, *Period Polytech-Chem.* 59 (2015) 296–305. <https://doi.org/10.3311/PPch.7801>.
- [89] M.Y. Abdelaal, T.R. Sobahi, M.S.I. Makki, Chemical transformation of pet waste through glycolysis, *Constr Build Mater.* 25 (2011) 3267–3271. <https://doi.org/10.1016/J.CONBUILDMAT.2011.03.013>.
- [90] Z.T. Laldinpui, V. Khiangte, S. Lalmangaihzuola, C. Lalmuanpuia, Z. Pachuau, C. Lalhriatpuia, K. Vanlaldinpuia, Methanolysis of PET waste using heterogeneous catalyst of bio-waste origin, *J Polym Environ.* 30 (2022) 1600–1614. <https://doi.org/10.1007/s10924-021-02305-0>.
- [91] T. Yoshioka, T. Motoki, A. Okuwaki, Kinetics of hydrolysis of poly(ethylene terephthalate) powder in sulfuric acid by a modified shrinking-core model, *Ind Eng Chem Res.* 40 (2001) 75–79. <https://doi.org/10.1021/ie000592u>.
- [92] P. Gupta, S. Bhandari, Chemical depolymerization of PET bottles via ammonolysis and aminolysis, in: *Recycling of Polyethylene Terephthalate Bottles*, Elsevier, 2019: pp. 109–134. <https://doi.org/10.1016/b978-0-12-811361-5.00006-7>.
- [93] A. Mittal, R.K. Soni, K. Dutt, S. Singh, Scanning electron microscopic study of hazardous waste flakes of polyethylene terephthalate (PET) by aminolysis and ammonolysis, *J Hazard Mater.* 178 (2010) 390–396. <https://doi.org/10.1016/j.jhazmat.2010.01.092>.
- [94] V. Jankauskaitė, G. Macijauskas, R. Lygaitis, Polyethylene terephthalate waste recycling and application possibilities: a review, *Mater Sci (Medžiagotyra)*. 14 (2008) 119–127.
- [95] M. Han, Depolymerization of PET bottle via methanolysis and hydrolysis, in: *Recycling of Polyethylene Terephthalate Bottles*, Elsevier, 2019: pp. 85–108. <https://doi.org/10.1016/b978-0-12-811361-5.00005-5>.
- [96] B. Shojaei, M. Abtahi, M. Najafi, Chemical recycling of PET: A stepping-stone toward sustainability, *Polym Adv Technol.* 31 (2020) 2912–2938. <https://doi.org/10.1002/pat.5023>.

- [97] L. Bartolome, M. Imran, K.G. Lee, A. Sangalang, J.K. Ahn, D.H. Kim, Superparamagnetic γ -Fe₂O₃ nanoparticles as an easily recoverable catalyst for the chemical recycling of PET, *Green Chem.* 16 (2014) 279–286. <https://doi.org/10.1039/c3gc41834k>.
- [98] N. George, T. Kurian, Recent developments in the chemical recycling of postconsumer poly(ethylene terephthalate) waste, *Ind Eng Chem Res.* (2014) 14185–17198. <https://doi.org/10.1021/ie501995m>.
- [99] X. Wang, H. Chen, C. Chen, H. Li, Chemical degradation of thermoplastic polyurethane for recycling polyether polyol, *Fibers Polym.* 12 (2011) 857–863. <https://doi.org/10.1007/s12221-011-0857-y>.
- [100] A.B. Raheem, Z.Z. Noor, A. Hassan, M.K. Abd Hamid, S.A. Samsudin, A.H. Sabeen, Current developments in chemical recycling of post-consumer polyethylene terephthalate wastes for new materials production: A review, *J Clean Prod.* 225 (2019) 1052–1064. <https://doi.org/10.1016/J.JCLEPRO.2019.04.019>.
- [101] M. Imran, B.K. Kim, M. Han, B.G. Cho, D.H. Kim, Sub- and supercritical glycolysis of polyethylene terephthalate (PET) into the monomer bis(2-hydroxyethyl) terephthalate (BHET), *Polym Degrad Stab.* 95 (2010) 1686–1693. <https://doi.org/10.1016/J.POLYMDEGRADSTAB.2010.05.026>.
- [102] D.E. Nikles, M.S. Farahat, New motivation for the depolymerization products derived from poly(ethylene terephthalate) (PET) waste: a review, *Macromol Mater Eng.* 290 (2005) 13–30. <https://doi.org/10.1002/mame.200400186>.
- [103] G. Güçlü, A. Kasgöz, S. Özbudak, S. Özgümüş, M. Orbay, Glycolysis of poly(ethylene terephthalate) wastes in xylene, *J Appl Polym Sci.* 69 (1998) 2311–2319. [https://doi.org/10.1002/\(SICI\)1097-4628\(19980919\)69:12<2311::AID-APP2>3.0.CO;2-B](https://doi.org/10.1002/(SICI)1097-4628(19980919)69:12<2311::AID-APP2>3.0.CO;2-B).
- [104] H. Wang, Y. Liu, Z. Li, X. Zhang, S. Zhang, Y. Zhang, Glycolysis of poly(ethylene terephthalate) catalyzed by ionic liquids, *Eur Polym J.* 45 (2009) 1535–1544. <https://doi.org/10.1016/j.eurpolymj.2009.01.025>.
- [105] J.-W. Chen, L.-W. Chen, W.-H. Cheng, Kinetics of glycolysis of polyethylene terephthalate with zinc catalyst, *Polym Int.* 48 (1999) 885–888. [https://doi.org/10.1002/\(SICI\)1097-0126\(199909\)48:9<885::AID-PI216>3.0.CO;2-T](https://doi.org/10.1002/(SICI)1097-0126(199909)48:9<885::AID-PI216>3.0.CO;2-T).
- [106] M. Imran, D.H. Kim, W.A. Al-Masry, A. Mahmood, A. Hassan, S. Haider, S.M. Ramay, Manganese-, cobalt-, and zinc-based mixed-oxide spinels as novel catalysts for the

- chemical recycling of poly(ethylene terephthalate) via glycolysis, *Polym Degrad Stab.* 98 (2013) 904–915. <https://doi.org/10.1016/j.polymdegradstab.2013.01.007>.
- [107] R. López-Fonseca, I. Duque-Ingunza, B. de Rivas, S. Arnaiz, J.I. Gutiérrez-Ortiz, Chemical recycling of post-consumer PET wastes by glycolysis in the presence of metal salts, *Polym Degrad Stab.* 95 (2010) 1022–1028. <https://doi.org/10.1016/j.polymdegradstab.2010.03.007>.
- [108] S. Baliga, W.T. Wong, Depolymerization of poly(ethylene terephthalate) recycled from post-consumer soft-drink bottles, *J Polym Sci A Polym Chem.* 27 (1989) 2071–2082. <https://doi.org/10.1002/pola.1989.080270625>.
- [109] M.E. Viana, A. Riul, G.M. Carvalho, A.F. Rubira, E.C. Muniz, Chemical recycling of PET by catalyzed glycolysis: Kinetics of the heterogeneous reaction, *Chem Eng J.* 173 (2011) 210–219. <https://doi.org/10.1016/j.cej.2011.07.031>.
- [110] J.Y. Chen, C.F. Ou, Y.C. Hu, C.C. Lin, Depolymerization of poly(ethylene terephthalate) resin under pressure, *J Appl Polym Sci.* 42 (1991) 1501–1507. <https://doi.org/10.1002/app.1991.070420603>.
- [111] J.-W. Chen, L.-W. Chen, The glycolysis of poly(ethylene terephthalate), *J Appl Polym Sci.* 73 (1999) 35–40. [https://doi.org/10.1002/\(SICI\)1097-4628\(19990705\)73:1<35::AID-APP4>3.0.CO;2-W](https://doi.org/10.1002/(SICI)1097-4628(19990705)73:1<35::AID-APP4>3.0.CO;2-W).
- [112] A.M. Al-Sabagh, F.Z. Yehia, Gh. Eshaq, A.M. Rabie, A.E. ElMetwally, Greener routes for recycling of polyethylene terephthalate, *Egyp J Pet.* 25 (2016) 53–64. <https://doi.org/10.1016/j.ejpe.2015.03.001>.
- [113] J.R. Campanelli, M.R. Kamal, D.G. Cooper, Kinetics of glycolysis of poly(ethylene terephthalate) melts, *J Appl Polym Sci.* 54 (1994) 1731–1740. <https://doi.org/10.1002/app.1994.070541115>.
- [114] T. Yoshioka, N. Okayama, A. Okuwaki, Kinetics of hydrolysis of PET powder in nitric acid by a modified shrinking-core model, *Ind Eng Chem Res.* (1998) 336–340. <https://doi.org/https://doi.org/10.1021/ie970459a>.
- [115] G.P. Karayannidis, A.P. Chatziavgoustis, D.S. Achilias, Poly(ethylene terephthalate) recycling and recovery of pure terephthalic acid by alkaline hydrolysis, *Adv Polym Techn.* 21 (2002) 250–259. <https://doi.org/10.1002/adv.10029>.
- [116] M. Čolnik, Ž. Knez, M. Škerget, Sub- and supercritical water for chemical recycling of polyethylene terephthalate waste, *Chem Eng Sci.* 233 (2021) 116389–116401. <https://doi.org/10.1016/j.ces.2020.116389>.

- [117] Keith. Yates, R.A. McClelland, Mechanisms of ester hydrolysis in aqueous sulfuric acids, *J Am Chem Soc.* 89 (1967) 2686–2692. <https://doi.org/10.1021/ja00987a033>.
- [118] M.J. Kang, H.J. Yu, J. Jegal, H.S. Kim, H.G. Cha, Depolymerization of PET into terephthalic acid in neutral media catalyzed by the ZSM-5 acidic catalyst, *Chem Eng J.* 398 (2020) 125655–125691. <https://doi.org/10.1016/j.cej.2020.125655>.
- [119] W. Yang, R. Liu, C. Li, Y. Song, C. Hu, Hydrolysis of waste polyethylene terephthalate catalyzed by easily recyclable terephthalic acid, *Waste Manage.* 135 (2021) 267–274. <https://doi.org/10.1016/j.wasman.2021.09.009>.
- [120] J.J.R. Arias, W. Thielemans, Instantaneous hydrolysis of PET bottles: an efficient pathway for the chemical recycling of condensation polymers, *Green Chem.* (2021) 9945–9956. <https://doi.org/10.1039/d1gc02896k>.
- [121] T. Szychaj, Chemical recycling of PET: methods and products, in: *Handbook of Thermoplastic Polyesters*, Wiley, 2002: pp. 1252–1290. <https://doi.org/10.1002/3527601961.ch27>.
- [122] K.P. Blackmon, D.W. Fox, S.J. Shafer, Process for converting PET scrap, U.S. Patent No 4,973,746, 1990.
- [123] R.K. Soni, S. Singh, Synthesis and characterization of terephthalamides from poly(ethylene terephthalate) waste, *J Appl Polym Sci.* 96 (2005) 1515–1528. <https://doi.org/10.1002/app.21502>.
- [124] E. Mendiburu-Valor, G. Mondragon, N. González, G. Kortaberria, A. Eceiza, C. Peña-Rodríguez, Improving the efficiency for the production of bis-(2-hydroxyethyl) terephthalate (BHET) from the glycolysis reaction of poly(ethylene terephthalate) (PET) in a pressure reactor, *Polymers (Basel).* 13 (2021) 1461–1474. <https://doi.org/10.3390/polym13091461>.
- [125] E. Mendiburu-Valor, G. Mondragon, N. González, G. Kortaberria, L. Martín, A. Eceiza, C. Peña-Rodríguez, Valorization of urban and marine PET waste by optimized chemical recycling, *Resour Conserv Recycl.* 184 (2022) 106413–106423. <https://doi.org/10.1016/j.resconrec.2022.106413>.
- [126] T. Chilton, S. Burnley, S. Nesaratnam, A life cycle assessment of the closed-loop recycling and thermal recovery of post-consumer PET, *Resour Conserv Recycl.* 54 (2010) 1241–1249. <https://doi.org/10.1016/j.resconrec.2010.04.002>.

- [127] L. Zhao, A. Giannis, W.Y. Lam, S.X. Lin, K. Yin, G.A. Yuan, J.Y. Wang, Characterization of Singapore RDF resources and analysis of their heating value, *Sustainable Environ Res.* 26 (2016) 51–54. <https://doi.org/10.1016/j.serj.2015.09.003>.
- [128] J. Chattopadhyay, T.S. Pathak, R. Srivastava, A.C. Singh, Catalytic co-pyrolysis of paper biomass and plastic mixtures HDPE (high density polyethylene), PP (polypropylene) and PET (polyethylene terephthalate) and product analysis, *Energy*. 103 (2016) 513–521. <https://doi.org/10.1016/j.energy.2016.03.015>.
- [129] P. Kannan, A. al Shoaibi, C. Srinivasakannan, Energy recovery from co-gasification of waste polyethylene and polyethylene terephthalate blends, *Comput Fluids*. 88 (2013) 38–42. <https://doi.org/10.1016/j.compfluid.2013.09.004>.
- [130] R. López-Fonseca, I. Duque-Ingunza, B. de Rivas, S. Arnaiz, J.I. Gutiérrez-Ortiz, Chemical recycling of post-consumer PET wastes by glycolysis in the presence of metal salts, *Polym Degrad Stab.* 95 (2010) 1022–1028. <https://doi.org/10.1016/j.polymdegradstab.2010.03.007>.
- [131] Y. Hu, Y. Wang, X. Zhang, J. Qian, X. Xing, X. Wang, Synthesis of poly(ethylene terephthalate) based on glycolysis of waste PET fiber, *J Macromol Sci, Part A*. 57 (2020) 430–438. <https://doi.org/10.1080/10601325.2019.1709498>.
- [132] I. Duque-Ingunza, R. López-Fonseca, B. de Rivas, J.I. Gutiérrez-Ortiz, Synthesis of unsaturated polyester resin from glycolysed postconsumer PET wastes, *J Mater Cycles Waste Manag.* 15 (2013) 256–263. <https://doi.org/10.1007/s10163-013-0117-x>.
- [133] A.M. Atta, M.E. Abdel-Raouf, S.M. Elsaed, A.A.A. Abdel-Azim, Curable resins based on recycled poly(ethylene terephthalate) for coating applications, *Prog Org Coat.* 55 (2006) 50–59. <https://doi.org/10.1016/j.porgcoat.2005.11.004>.
- [134] A.M. Atta, A.F. El-Kafrawy, M.H. Aly, A.A.A. Abdel-Azim, New epoxy resins based on recycled poly(ethylene terephthalate) as organic coatings, *Prog Org Coat.* 58 (2007) 13–22. <https://doi.org/10.1016/j.porgcoat.2006.11.001>.
- [135] E.M. Maafi, F. Malek, L. Tighzert, Synthesis and characterization of new polyurethane based on polycaprolactone, *J Appl Polym Sci.* 115 (2010) 3651–3658. <https://doi.org/10.1002/app.31448>.
- [136] D.J. Suh, O.O. Park, K.H. Yoon, The properties of unsaturated polyester based on the glycolyzed poly(ethylene terephthalate) with various glycol compositions, *Polymer*, 41(2) (2000) 461–466. [https://doi.org/10.1016/S0032-3861\(99\)00168-8](https://doi.org/10.1016/S0032-3861(99)00168-8).

- [137] A.M. Atta, Epoxy resin based on poly(ethylene terephthalate) waste: Synthesis and characterization, *Prog Rubber Plast Recycl.* 19 (2003) 17–40. <https://doi.org/10.1177/147776060301900102>.
- [138] D. Cevher, S. Sürdem, Polyurethane adhesive based on polyol monomers BHET and BHETA depolymerised from PET waste, *Int J Adhes Adhes.* 105 (2021) 102799–102906. <https://doi.org/10.1016/j.ijadhadh.2020.102799>.
- [139] V. Jamdar, M. Kathalewar, K.A. Dubey, A. Sabnis, Recycling of PET wastes using Electron beam radiations and preparation of polyurethane coatings using recycled material, *Prog Org Coat.* 107 (2017) 54–63. <https://doi.org/10.1016/j.porgcoat.2017.02.007>.
- [140] Q. Li, H. He, C. Zhang, X. Liang, Y. Shen, Research on synthesis of polyurethane based on a new chain extender obtained from waste polyethylene terephthalate, *J Appl Polym Sci.* 139 (2022) 52402–52414. <https://doi.org/10.1002/app.52402>.
- [141] M. Li, J. Luo, Y. Huang, X. Li, T. Yu, M. Ge, Recycling of waste poly(ethylene terephthalate) into flame-retardant rigid polyurethane foams, *J Appl Polym Sci.* 131 (2014) 40857–40863. <https://doi.org/10.1002/app.40857>.
- [142] A. Bhattacharyya, D. Mukherjee, R. Mishra, P.P. Kundu, Development of pH sensitive polyurethane–alginate nanoparticles for safe and efficient oral insulin delivery in animal models, *RSC Adv.* 6 (2016) 41835–41846. <https://doi.org/10.1039/C6RA06749B>.
- [143] A. Bhattacharyya, D. Mukherjee, R. Mishra, P.P. Kundu, Preparation of polyurethane–alginate/chitosan core shell nanoparticles for the purpose of oral insulin delivery, *Eur Polym J.* 92 (2017) 294–313. <https://doi.org/10.1016/j.eurpolymj.2017.05.015>.
- [144] A. Bhattacharyya, P. Mukhopadhyay, P.P. Kundu, Synthesis of a novel pH-sensitive polyurethane-alginate blend with poly(ethylene terephthalate) waste for the oral delivery of protein, *J Appl Polym Sci.* 131 (2014) 40650–40661. <https://doi.org/10.1002/app.40650>.
- [145] B. Wang, S. Ma, X. Xu, Q. Li, T. Yu, S. Wang, S. Yan, Y. Liu, J. Zhu, High-performance, biobased, degradable polyurethane thermoset and its application in readily recyclable carbon fiber composites, *ACS Sustain Chem Eng.* 8 (2020) 11162–11170. https://doi.org/10.1021/ACSSUSCHEMENG.0C02330/SUPPL_FILE/SC0C02330_SI_001.PDF.
- [146] H. Bergmeister, N. Seyidova, C. Schreiber, M. Strobl, C. Grasl, I. Walter, B. Messner, S. Baudis, S. Fröhlich, M. Marchetti-Deschmann, M. Griesser, M. di Franco, M. Krssak, R.

- Liska, H. Schima, Biodegradable, thermoplastic polyurethane grafts for small diameter vascular replacements, *Acta Biomater.* 11 (2015) 104–113. <https://doi.org/10.1016/j.actbio.2014.09.003>.
- [147] M.A. Munir, K.H. Badri, L.Y. Heng, A. Inayatullah, H.A. Badrul, E. Emelda, E. Dwinta, N. Kusumawardani, A.S. Wulandari, V. Aprilia, R.B.Y. Supriyono, Design and synthesis of conducting polymer bio-based polyurethane produced from palm kernel oil, *Int J Polym Sci.* (2022) 1–13. <https://doi.org/10.1155/2022/6815187>.
- [148] P. Singhal, W. Small, E. Cosgriff-Hernandez, D.J. Maitland, T.S. Wilson, Low density biodegradable shape memory polyurethane foams for embolic biomedical applications, *Acta Biomater.* 10 (2014) 67–76. <https://doi.org/10.1016/j.actbio.2013.09.027>.
- [149] P.M. Kapatel, R.H. Patel, Green approach for the development of novel flame retardant waterborne polyurethanes: Synthesis and its characterizations, *Mater Today Proc.* 23 (2020) 389–399. <https://doi.org/https://doi.org/10.1016/j.matpr.2020.02.058>.
- [150] H. Hao, J. Shao, Y. Deng, S. He, F. Luo, Y. Wu, J. Li, H. Tan, J. Li, Q. Fu, Synthesis and characterization of biodegradable lysine-based waterborne polyurethane for soft tissue engineering applications, *Biomater Sci.* 4 (2016) 1682–1690. <https://doi.org/10.1039/c6bm00588h>.
- [151] H. Honarkar, Waterborne polyurethanes: A review, *J Dispers Sci Technol.* 39 (2018) 507–516. <https://doi.org/10.1080/01932691.2017.1327818>.
- [152] P. Koczczyńska, T. Calvo-Correas, A. Eceiza, J. Datta, Synthesis and characterisation of polyurethane elastomers with semi-products obtained from polyurethane recycling, *Eur Polym J.* 85 (2016) 26–37. <https://doi.org/10.1016/j.eurpolymj.2016.09.063>.
- [153] D. Simón, A.M. Borreguero, A. de Lucas, J.F. Rodríguez, Recycling of polyurethanes from laboratory to industry, a journey towards the sustainability, *Waste Manage.* 76 (2018) 147–171. <https://doi.org/10.1016/j.wasman.2018.03.041>.
- [154] G. Kiss, G. Rusu, F. Peter, I. Tănase, G. Bandur, Recovery of flexible polyurethane foam waste for efficient reuse in industrial formulations, *Polymers (Basel).* 12 (2020) 1533–1547. <https://doi.org/10.3390/polym12071533>.
- [155] L. Gausas, S.K. Kristensen, H. Sun, A. Ahrens, B.S. Donslund, A.T. Lindhardt, T. Skrydstrup, Catalytic hydrogenation of polyurethanes to base chemicals: from model systems to commercial and end-of-life polyurethane materials, *JACS Au.* 1 (2021) 517–524. <https://doi.org/10.1021/jacsau.1c00050>.

- [156] A. Zlatanovic, C. Lava, W. Zhang, Z.S. Petrovic, Effect of structure on properties of polyols and polyurethanes based on different vegetable oils, *J Polym Sci B Polym Phys.* 42 (2004) 809–819. <https://doi.org/10.1002/polb.10737>.
- [157] A. Vashchuk, A.M. Fainleib, O. Starostenko, D. Grande, Application of ionic liquids in thermosetting polymers: Epoxy and cyanate ester resins, *Express Polym Lett.* 12 (2018) 898–917. <https://doi.org/10.3144/expresspolymlett.2018.77>.
- [158] Z.S. Petrovic, Polyurethanes from vegetable oils, *Polym Rev.* 48 (2008) 109–155. <https://doi.org/10.1080/15583720701834224>.
- [159] C. Sharma, S. Kumar, A.R. Unni, V.K. Aswal, S.K. Rath, G. Harikrishnan, Foam stability and polymer phase morphology of flexible polyurethane foams synthesized from castor oil, *J Appl Polym Sci.* 131 (2014) 8420–8427. <https://doi.org/10.1002/app.40668>.
- [160] L. Maisonneuve, G. Chollet, E. Grau, H. Cramail, Vegetable oils: A source of polyols for polyurethane materials, *OCL - Oilseeds Fats Crops Lipids.* 23 (2016) D508 –D518. <https://doi.org/10.1051/ocl/2016031>.
- [161] A. Fridrihsone, F. Romagnoli, V. Kirsanovs, U. Cabulis, Life Cycle Assessment of vegetable oil based polyols for polyurethane production, *J Clean Prod.* 266 (2020) 121403 –12431. <https://doi.org/10.1016/j.jclepro.2020.121403>.
- [162] M.A. Corcuera, L. Rueda, A. Saralegui, M.D. Martín, B. Fernández-D’arlas, I. Aki Mondragon, A. Eceiza, Effect of diisocyanate structure on the properties and microstructure of polyurethanes based on polyols derived from renewable resources, *J Appl Polym Sci.* 122 (2011) 3677–3685. <https://doi.org/10.1002/app.34781>.
- [163] H. Stripple, R. Westman, D. Holm, Development and environmental improvements of plastics for hydrophilic catheters in medical care: an environmental evaluation, *J Clean Prod.* 16 (2008) 1764–1776. <https://doi.org/10.1016/j.jclepro.2007.12.006>.
- [164] B. Fernández-D’Arlas, A. Alonso-Varona, T. Palomares, M.A. Corcuera, A. Eceiza, Studies on the morphology, properties and biocompatibility of aliphatic diisocyanate-polycarbonate polyurethanes, *Polym Degrad Stab.* 122 (2015) 153–160. <https://doi.org/10.1016/j.polymdegradstab.2015.10.023>.
- [165] L. Lei, L. Zhong, X. Lin, Y. Li, Z. Xia, Synthesis and characterization of waterborne polyurethane dispersions with different chain extenders for potential application in waterborne ink, *Chem Eng J.* 253 (2014) 518–525. <https://doi.org/10.1016/j.cej.2014.05.044>.

- [166] Yu.V. Savelyev, E.R. Akhranovich, A.P. Grekov, E.G. Privalko, V.V. Korskanov, V.I. Shtompel, V.P. Privalko, P. Pissis, A. Kanapitsas, Influence of chain extenders and chain end groups on properties of segmented polyurethanes. I. Phase morphology, *Polymer (Guildf)*. 39 (1998) 3425–3429. [https://doi.org/10.1016/S0032-3861\(97\)10101-X](https://doi.org/10.1016/S0032-3861(97)10101-X).
- [167] K. Bagdi, K. Molnár, M. Kállay, P. Schön, J.G. Vancsó, B. Pukánszky, Quantitative estimation of the strength of specific interactions in polyurethane elastomers, and their effect on structure and properties, *Eur Polym J*. 48 (2012) 1854–1865. <https://doi.org/10.1016/j.eurpolymj.2012.07.016>.
- [168] K. Bagdi, K. Molnár, A. Wacha, A. Bóta, B. Pukánszky, Hierarchical structure of phase-separated segmented polyurethane elastomers and its effect on properties, *Polym Int*. 60 (2011) 529–536. <https://doi.org/10.1002/pi.3003>.
- [169] D.E. Heath, S.A. Guelcher, S.L. Cooper, Polyurethanes, in: *Biomater Sci*, Elsevier, 2020: pp. 103–107. <https://doi.org/10.1016/B978-0-12-816137-1.00010-6>.
- [170] H. Ulrich, Polyurethanes, in: *Encyclopedia of Polymer Science and Technology*, John Wiley & Sons, Inc., Hoboken, NJ, USA, 2001. <https://doi.org/10.1002/0471440264.pst295>.
- [171] M. Chen, L.R. Dalton, L.P. Yu, Y.Q. Shi, W.H. Steier, Thermosetting polyurethanes with stable and large second-order optical nonlinearity, *Macromolecules*. 25 (1992) 4032–

Chapter 2

MATERIALS AND METHODS

2. MATERIALS AND METHODS

2.1 Content

This chapter introduces the different PET samples studied in the thesis, as well as the materials used for their characterization and chemical recycling. The materials for the synthesis of PUs, both thermoplastics and thermosets, are also described. This chapter also describes the characterization techniques and conditions used for the analysis of physicochemical, thermal, mechanical, morphological and surface properties.

In addition, for Life Cycle Assessment (LCA), certain criteria were assumed. Therefore, the inputs not available in the database of Ecoinvent v3.5 of the SimaPro program were also modeled, explaining their scheme with all inputs and outputs. Similarly, the inputs/outputs inventory was also represented.

2.2 Materials

2.2.1. PET samples

In this work, four different PET samples were used and characterized. Virgin PET pellets (PET-v) supplied by Plastiverd (Barcelona, Spain), a transparent and amorphous PET with a viscosity of 0.58 ± 0.04 dl/g. Post-condensed PET pellets (PET-ssp) supplied by Indorama (Cádiz, Spain), a commercial post-condensed virgin PET, an opaque crystalline sample with a viscosity of 0.78 ± 0.05 dl/g from the supplier. Since for bottle production PET should present viscosity values between 0.78-0.80 dl/g, virgin PET is post-condensed. Urban post-consumer PET waste (PET-u) provided by Eko-Rec company (Andoain, Spain), obtained from beverage bottles recovered from municipal wastes and milled into flakes. For comparative purposes, commercial PET bottles were used (PET-bottle) provided by Nestlé, Aquarel. PET-v and PET-ssp pellets and PET-u flakes were used as received. Marine post-consumer PET litter (PET-m) was directly collected from the coast of the Basque Country, in the flysch zone between Deba and Zumaia (Gipuzkoa, Spain). Collected bottle (shown in Figure 2.1) were washed with tap water, dried for 3 h at 60 °C in a vacuum oven and milled into flakes in a grinder for obtaining 1-1.5 cm size pellets. It is important to point out that both urban flakes and marine bottles showed a wide variety of colors.

Since humidity can interfere in the characterization or could also provoke hydrolytic degradation during thermo-mechanical processing [1], all samples were conditioned for 1 h at 65 °C in a vacuum oven before any characterization or treatment. Figure 2.2 shows different PET materials studied in this work.



Figure 2.1. PET bottles recovered from the sea.

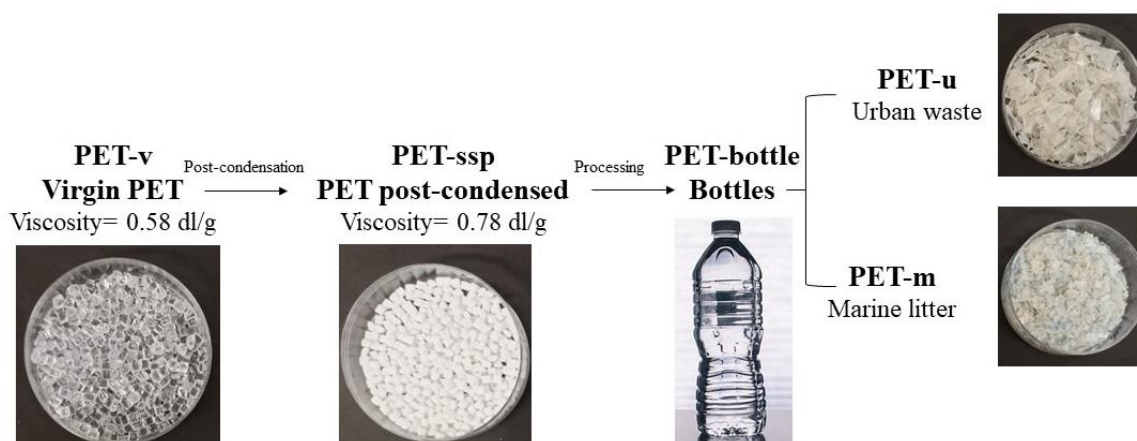
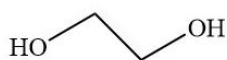


Figure 2.2. Digital images of different PET materials analyzed.

2.2.2. Materials for the chemical recycling

For the glycolysis process of PET and also for the chemical recycling of thermoplastic and thermoset PUs, employed materials were the same. In the depolymerization reactions carried out in a closed reactor, EG was used as reagent and chemically pure zinc acetate as catalyst, both supplied by Sigma-Aldrich (USA). The structure of reagents used in all depolymerization reactions is shown in Figure 2.3.

Ethylene glycol: EG



Zinc acetate: ZnAc

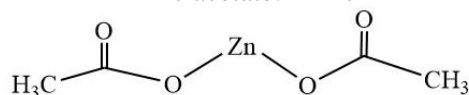


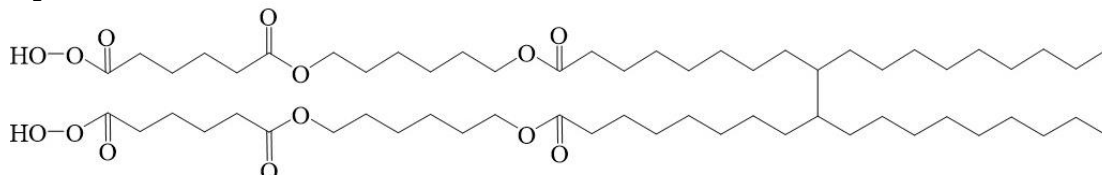
Figure 2.3. Structure of reagents used in the chemical recycling reactions.

2.2.3. Materials for the synthesis of TPUs

In the synthesis of thermoplastic polyurethanes (TPU), a macrodiol coming from renewable sources with 38 % of renewable carbon content, Priplast 3192[®] (M_w 2000 g/mol) purchased from Croda (Snaith, UK), was used as SS. On the other hand, hexamethylene diisocyanate (HDI, Desmodur H) from Covestro (Germany) was used as component of the HS. The macrodiol was

dried under vacuum at 65 °C for 4 h before use. In the Figure 2.4 the chemical structure of the reagents employed are represented. BHET obtained in Chapter 5 from the glycolysis of marine PET litter was used as chain extender and component of the HS as well. In addition, for comparison purposes, TPUs have also been synthesized using a commercial BHET from Sigma-Aldrich (San Luis, Missouri, USA).

Priplast 3192®: macrodiol



Hexamethylene diisocyanate: HDI

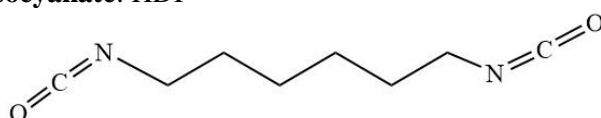


Figure 2.4. Structure of reagents used in the synthesis of TPUs.

2.2.4. Materials for the synthesis of thermoset PUs

For the synthesis of thermoset polyurethanes (PU), a castor oil derived polyol with an 80 % of renewable carbon content purchased from Vertellus (Denham Springs, USA) (Polycin 12, functionality = 4, hydroxyl index (I_{OH}) = 330 mg KOH/g and viscosity = 300 mPa s), was used. The I_{OH} value was determined according to the procedure explained at section 2.3.5. On the other hand, as isocyanate a commercial aromatic polymeric pMDI supplied by Covestro (Germany) (Desmodur 44 V, NCO equivalent weight = 131.3 g/eq and viscosity = 160-240 mPa s) was used (Figure 2.5). The polyol was dried under vacuum at 65 °C for 4 h before used. The BHET obtained from the chemical recycling of marine PET litter in Chapter 5 was employed to partially replace the biobased polyol.

Polymeric methylene diphenyl diisocyanate: pMDI

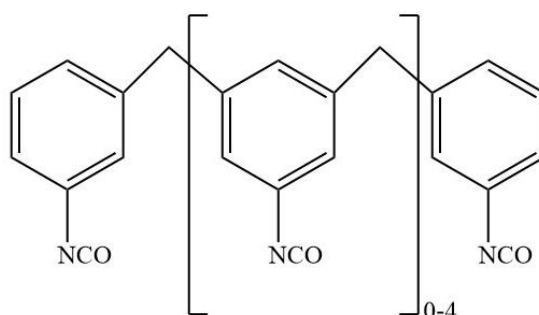


Figure 2.5. Structure of isocyanate used in the synthesis of thermoset PUs.

2.3 Physicochemical characterization

2.3.1. Fourier transform infrared spectroscopy (FTIR)

The infrared spectra of samples were obtained by Fourier transform infrared spectroscopy using a Nicolet Nexus spectrometer (Thermo Fisher Scientific, Waltham, Massachusetts, USA) provided with a MKII Golden Gate accessory (Specac) with a diamond crystal with a nominal incidence angle of 45° and ZnSe lens. Spectra were recorded in attenuated total reflection (ATR) mode between 4000 and 650 cm^{-1} , performing 64 scans with a resolution of 8 cm^{-1} . In this technique, the sample is irradiated by an infrared light source of different frequencies and the amount absorbed by each beam is measured.

2.3.2. Gel permeation chromatography (GPC)

The weight and number average molar masses, M_w and M_n , respectively, were determined by gel permeation chromatography (GPC) using a Thermo Scientific chromatograph (Thermo Fisher Scientific, Waltham, Massachusetts, USA) equipped with an isocratic Dionex UltiMate 3000 pump and a RefractoMax 521 refractive index detector. The separation was carried out at 30 °C within four Phenogel GPC columns from Phenomenex with 5 μm particle size and porosities of 10⁵, 10³, 100, and 50 Å, located in an UltiMate 3000 thermostated column compartment. Tetrahydrofuran (THF) was used as mobile phase at a flow rate of 1 mL/min. Samples were prepared solving the materials into THF at 1 wt.% and filtering with 2 μm pore size nylon filters. M_w and M_n were reported as weight average based on the calibration curve with monodisperse polystyrene standards. THF used in this technique was provided by Macron Fine Chemicals™ (Avantor, Gliwice, Poland).

2.3.3. Elemental analysis (EA)

EA was performed in order to determine the changes in composition of the PET samples. Euro EA3000 Elemental Analyzer (EuroVector S.p.A., Milan, Italy) was used to determine the percentage of C, N, O and S elements. In this technique, the sample is combusted and the resultant products are analyzed in a chromatographic column, where a thermal conductivity detector provides a signal of each element.

2.3.4. Proton nuclear magnetic resonance (¹H NMR)

¹H NMR spectra of the glycolyzed BHET samples were recorded on an Avance Bruker 500 (Billerica, Massachusetts, USA) spectrometer equipped with a Z axis gradient BBO probe. The ¹H NMR spectra were recorded using sequence *zg* from Bruker's library at 500.13 MHz a time domain of 64k, and a spectral width of 10000 Hz. The number of scans was 16, with a delay of 1

s and an acquisition time of 3.2 s. Samples were solved in deuterated dimethyl sulfoxide (DMSO-d6) from measurements.

2.3.5. I_{OH}

The hydroxyl value of the glycolized samples was determined by titration according to ASTM D 4274-05 [2]. The hydroxyl index was calculated following the Equation 2.1.

$$I_{OH} = \frac{(V_B - V_M) \cdot N_{NaOH} \cdot 56,1^g/eq}{m_M} \quad (\text{Equation 2.1})$$

V_B and V_M are the volume in mL of NaOH required for titration of the blank and for the sample, respectively. N_{NaOH} is the normality of NaOH and m_M refers to the mass of the sample.

Therefore, the polymer equivalent weight (M_{eq}) was calculated using the Equation 2.2

$$M_{eq} = \frac{56,1^g/eq}{I_{OH}} \cdot 1000 \quad (\text{Equation 2.2})$$

The molar mass of obtained BHET-m was determined as 248 g/mol considering its functionality 2.

2.3.6. pH

The pH of the glycolized polyol from the synthesized thermoplastic and thermoset PUs was measured using a pH meter pH8 +DHS of LabProcess, which was calibrated with pH 4.00 and 7.00 buffer solution standards.

2.4 Thermal characterization

2.4.1. Differential scanning calorimetry (DSC)

Thermal properties of the different samples were determined by DSC using a Mettler Toledo DSC3+ equipment (Columbus, Ohio, USA) provided with a robotic arm and an electric intracooler as refrigerator unit.

Between 5 and 10 mg of sample were encapsulated in aluminum pans. The analysis was carried out under nitrogen atmosphere with heating and cooling rates of 10 °C/min.

In this way, from the obtained thermograms, glass transition (T_g), crystallization (T_c) and melting (T_m) temperatures were determined. The T_g was ascribed to the inflexion point of the heat capacity. The exothermic peak minimum and endothermic peak maximum were taken as T_c and T_m , respectively. The area of each peak was considered as the crystallization and melting enthalpy, ΔH_c and ΔH_m , respectively.

Thermal properties of PET samples were analyzed from three consecutive scans: a first heating scan from 25 °C up to 300 °C, followed by a cooling scan from 300 to 25 °C and a second heating scan up to 300 °C. The degree of crystallinity (X_c) was calculated by the following Equation 2.3 [3].

$$X_c = \left[\frac{\Delta H_m - \Delta H_c}{\Delta H_0} \right] \cdot 100 \quad (\text{Equation 2.3})$$

Where term ΔH_0 is a reference value corresponding to the melting enthalpy of a 100 % crystalline PET (135.8 J/g) [4]. Taking into account the sample variability among PET-u and PET-m, three samples were analyzed for each of them, estimating the mean value and the standard deviation.

However, for the analysis of the thermal properties of glycolyzed products and synthesized PUs, both thermoplastics and thermosets, only one scan was performed. In the case of glycolyzed product, the sample was subjected to a heating scan from 25 °C to 170 °C, while the PUs were subjected to a heating scan from -85 °C to 200 °C.

2.4.2. Thermogravimetric analysis (TGA)

The thermal stability of PET samples, glycolyzed samples and synthesized polyurethanes was analyzed by TGA using a TGA/SDTA851 Mettler Toledo (Columbus, Ohio, USA) equipment. Samples were heated from room temperature to 800 °C at a heating rate of 10 °C/min under nitrogen atmosphere.

From the weight evolution and its first derivative curves the different degradation temperatures, weight loss percentage and the final residue were determined. For the test, samples of 5-10 mg were employed.

2.4.3. Dynamic mechanical analysis (DMA)

The dynamic mechanical behavior of TPUs was analyzed by DMA in tensile mode on an Eplexor Gabo 100 N analyzer from Netzsch (Selb, Bavaria, Germany), using a static strain of 0.50 %, a contact force of 0.5 N and a fixed operating frequency of 1 Hz. The temperature was varied from -85 to 175 °C at a heating rate of 2 °C/min. Samples were cut into strips of 25 mm x 5 mm x 1.5 mm (length x width x thickness).

However, the dynamic mechanical behavior of the thermoset PUs was analyzed in bending mode using the same analyzer. A contact force of 0.8 N, a bending distance of 20 mm and a frequency of 1 Hz were used. The temperature was varied between -80 °C and 200 °C at a heating rate of 2 °C/min. For thermoset PUs, the cross-linking density was calculated from the value of storage modulus in the rubbery region according to de Equation 2.4 [5].

$$v(\text{mol}/\text{m}^3) = \frac{E'_{T_{\alpha}+50}}{3 R (T_{\alpha}+50)} \quad (\text{Equation 2.4})$$

Where $E'_{T_{\alpha}+50}$ is the storage modulus in the rubbery region (taken at $T_{\alpha} + 50$ °C), R is the universal constant of gases (8.314 J/mol · K) and T_{α} is the T_g in Kelvin taken as the maximum of $\tan \delta$.

2.4.4. Calorimetry

To measure the heat capacity of PET samples during the combustion, the energy value was measured using an IKA C 200 calorimeter. The measurement was performed following the ISO 1815:2018 standard [6]. For each test, 1 ± 0.01 g of PET sample was used, repeating measurements three times to obtain average values. The results obtained from the equipment refer to the higher heating value (HHV). The lower heating value (LHV) was determined according to Equation 2.5 [7].

$$LHV = HHV - 24.54(W + 9H) \quad (\text{Equation 2.5})$$

Where W is the moisture content of the sample determined by weight difference before and after drying the samples at 60 °C for 3 h under vacuum, and H is the hydrogen content analyzed in the EA.

2.4.5. Ashes percentages

The ash study was carried out for different PET samples. For this purpose, about 2 g of PET were placed in a crucible and introduced in an oven at 420 °C for 5 h to perform the combustion, then leaving the samples to cool to room temperature. After cooling, the crucibles were weighed and the ash percentage was determined by weight difference.

2.5 Mechanical characterization

2.5.1. Tensile tests

Mechanical tensile testing was carried out at room temperature using an Instron 5697 equipment (Instron, Norwood, MA, USA) provided by a load cell of 500 N. Samples were cut into 25 mm long, 5 mm wide and 1.5 mm thickness specimens and tested at a crosshead speed of 20 mm/min with a distance between clamps of 16 mm. Tensile modulus (E), stress at yield (σ_y), stress at break (σ_b) and elongation at break (ϵ_b) were averaged from stress-strain curves of five specimens of each serie.

2.5.2. Flexural tests

Mechanical flexural testing was carried out at room temperature using an Instron 5697 equipment (Instron, Norwood, MA, USA) provided by a load cell of 30 kN. Samples were cut into 30 mm long, 10 mm wide and 1.5 mm thickness specimens and tested at 3 point bending device with a separation between supports of 20 mm. Flexural modulus (E), flexural strength (σ) and strain (ϵ)

were determined from stress-strain curves. In order to determine an average value, five different tests were carried out for each sample.

2.6 Rheological characterization: melt flow index (MFI), intrinsic viscosity (IV) and molar mass

MFI value of PET and thermo-mechanically recycled PET (RPET) samples was measured by using the HAAKE Meltflow^{LT} analyzer (Thermo Fisher Scientific, Waltham, Massachusetts, USA). In this technique, the sample is placed in the barrel previously heated at 280 °C. According to DIN ISO 1133 standard, 7 g of sample were placed in the analyzer, measuring the time taken by the sample for falling between the established scales, weighting the mass that flew in that time. The MFI value was determined by averaging the values obtained in five tests. As reported, there is a relationship between intrinsic viscosity (IV) and MFI value [8]. Therefore, to determinate the IV values of PET samples, a calibration straight was created from MFI and IV values, using different standard samples, obtaining the following relationship (Equation 2.6).

$$[IV] = 1.7956 \cdot MFI^{-0.245} \quad (\text{Equation 2.6})$$

Moreover, weight and number average molar mass values, M_w and M_n , were calculated from IV values, from the following Equations 2.7 and 2.8 [8].

$$[IV] = 3.72 \cdot 10^{-4} \cdot M_n^{0.73} \quad (\text{Equation 2.7})$$

$$[IV] = 4.68 \cdot 10^{-4} \cdot M_w^{0.68} \quad (\text{Equation 2.8})$$

2.7 Morphological characterization

The morphology of the synthesized TPUs was analyzed by atomic force microscopy (AFM) using a Bruker Dimension ICON scanning probe microscope equipped with a Nanoscope V controller. To that end TESP-V2 type silicon tips having a nominal resonance frequency of 320 kHz and a cantilever spring constant of 42 N/m were employed.

2.8 Surface hydrophilicity

The surface hydrophilicity of samples was measured at room temperature by static water contact angle (WCA) using the SEO Phoenix Series P-300 equipment (Kromtek Sdn Bhd, Selangor, Malaysia). In this technique, a deionized water drop is deposited on the sample surface to measure the value of the contact angle formed by the water drop, which depends on the chemical interactions between water and the surface. In the case of hydrophilic materials, the contact angle is low, increasing with hydrophobicity. For this purpose, a water drop of 2 μ L was deposited on

the surface of the material using a 0.4 mm diameter syringe. The contact angle was measured ten seconds after drop deposition. For original PET samples and thermo-mechanically recycled PET samples, prior to the measurements, pellets and flakes were compressed using a Santec 30 hydraulic press at 58 bar and 270 °C for 10 minutes, obtaining a plaque. WCA values of five drops of water deposited on the plaque were averaged for each sample.

2.9 Spectrophotometry

The color parameters of different samples such as recycled PET and synthesized thermoplastic and thermoset PUs were measured by X-rite 962 spectrophotometer (Grand Rapids, Michigan, USA). L^* (lightness-darkness), a^* (red-green), b^* (yellow-blue) were calculated as an average of five different tests. Materials were placed on white standard to perform the measurement. The color differences between samples and white standard (ΔE^*) and also whiteness index (WI) were calculated following the Equations 2.9 and 2.10 [9].

$$\Delta E^* = \sqrt{(\Delta L^*)^2 + (\Delta a^*)^2 + (\Delta b^*)^2} \quad (\text{Equation 2.9})$$

$$WI = 100 - \sqrt{(100 - L^*)^2 + a^{*2} + b^{*2}} \quad (\text{Equation 2.10})$$

2.10 Life Cycle Assessment (LCA)

Life Cycle Assessment was performed following the ISO 14040 and ISO 14044 guidelines. For the study, the SimaPro 9.0 developed by Ecoinvent v3.5 software was used to create LCA model and perform the impact assessment calculations.

For the analysis, the ReCiPe 2016 Midpoint (H) method was used, because in the analysis of a biobased polyester the midpoint is a significant category to be analyzed [10,11]. The LCA studies are conducted with a special focus on the global warming potential, also called climate footprint or climate change [12]. In this case, the “cut-off” rule was followed, which distinguishes the first life and the second life as separate systems [13].

The energy consumption for each step depends on the time, so the energy was estimated by the following equation (Equation 2.11), where Q is the energy consumption in kWh, P is the power of the machinery and t is the time spend.

$$Q(\text{kWh}) = P \cdot t \quad (\text{Equation 2.11})$$

For the recollection of marine PET litter, PET kilograms (30 kg) and the distance from the recollection point to the laboratory (31.3 km) were taken into account. Transport was carried out with a lorry and the tkm (weight per distance) of the transport was calculated.

The zinc acetate catalyst is not found in the Ecoinvent v3.5 databased, so it was modeled considering the reaction shown in Figure 2.6 [11]. The schema of the modeled ZnAc is shown in Figure 2.7 and the corresponding inventory in Table 2.1. The column entitled Remarks refers to the name that the SimaPro program gives to the input used.

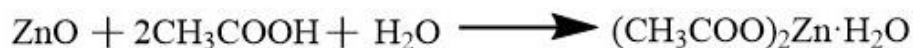


Figure 2.6. Zinc acetate synthesis reaction.

Zinc acetate: ZnAc			
Inputs	Amount	Unit	Remarks
Zinc oxide	1.3	kg	Zinc oxide {GLO} market for APOS, U
Acetic acid	1.9	kg	Acetic acid, without water, in 98% solution state {GLO} market for APOS, U
Water	250	mL	Water, deionized {Europe without Switzerland} market for water, deionized APOS, U
Outputs	Amount	Unit	Remarks
ZnAc	3.2	kg	

Table 2.1. Inventory of modeled zinc acetate.

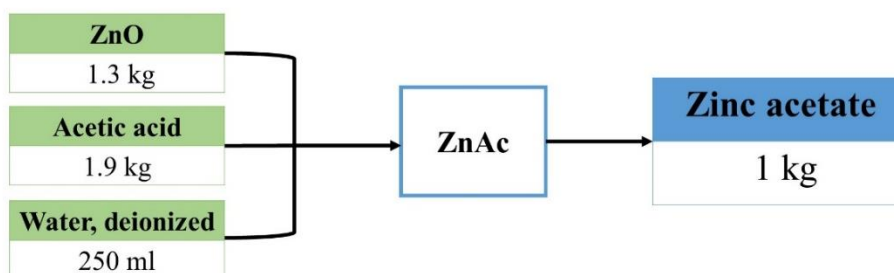


Figure 2.7. Scheme of the modeled zinc acetate.

Similarly, commercial BHET (BHET-ref) is not found in the Ecoinvent v3.5 databased, so it was also modeled using the PET depolymerization reaction, whose inventory is shown in Table 2.2 for BHET-ref. The modeling was carried out based on several models reported in the literature [14,15]. The recovery of EG [13] and a yield of 80 % [16] was assumed.

For the synthesis of TPUs all inputs were taken from Ecoinvent v3.5, except for the cases in which the inputs are not included, so they were modeled separately. This is the case of the macrodiol, Priplast 3192, used for the synthesis, which is not in data and the suppliers do not give enough information to model it from the beginning.

Therefore, taking into account that Priplast is a biobased polyol, with a renewable content of 38 %, with a footprint about 3.5 kg CO₂ eq, an estimation of this bio-polyol was done based on the

model of Fridrihsone et al. [11]. The modeled macrodiol was named as bio-polyol and the scheme for LCA is depicted in Figure 2.8.

BHET-ref: commercial BHET			
Inputs	Amount	Unit	Remarks
Ethylene glycol	3.75	kg	Ethylene glycol {GLO} market APOS, U
Poly(ethylene terephthalate)	1.25	kg	Polyethylene terephthalate, granulate, amorphous {Europe without Switzerland} polyethylene terephthalate, granulate, amorphous, recycled to generic market for amorphous PET granulate APOS, U
Zinc acetate*	50	g	Modeled*
Electricity	73.1	kWh	Electricity, medium voltage {ES} market for APOS, U
Outputs	Amount	Unit	Remarks
BHET	1	kg	
Recovered Ethylene glycol	2	kg	
Solvent waste	3.2	kg	Spent solvent mixture {CH} market for spent solvent mixture APOS, U
Wastewater	0.1524	L	Wastewater, average {Europe without Switzerland} market for wastewater, average APOS, U

Table 2.2. Inventory of modeled commercial BHET.

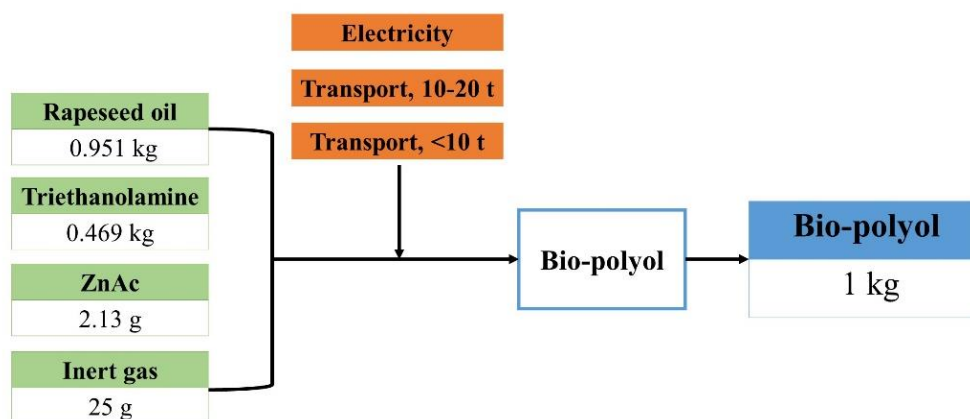


Figure 2.8. Scheme of the modeled bio-polyol.

The inventory table with all the inputs and outputs for the production of 1 kg of bio-polyol is summarized in Table 2.3. Neither HDI is included in the Ecoinvent v3.5 database. HDI is produced by the reaction of hexamethylenediamine (HMDA) and phosgene giving rise to HDI

and hydrochloric acid as by-product, resulting in the reaction shown in Figure 2.9.

However, as HMDA is not included in the database, it was also modeled from a previous work of Dros et al [17]. The model is more complex than the previous ones, the HMDA inventory table and the subsequent HDI are shown in Tables 2.4 and 2.5, respectively, and the scheme in Figure 2.10, the acronym ADN referring to adiponitrile.

Bio-polyol			
Inputs	Amount	Unit	Remarks
Rapessed oil	0.951	kg	Rape oil, crude {RoW} rape oil mill operation APOS, U
Triethanolamine	0.469	kg	Triethanolamine {GLO} market for APOS, U
<i>Zinc acetate*</i>	2.13	g	<i>Modeled*</i>
Inert gas	25	g	Nitrogen, liquid {RER} market for APOS, U
Electricity	0.682	kWh	Electricity, medium voltage {GLO} market group for APOS, U
Transport 20 t, truck	0.781	kWh	Transport, truck 10-20t, EURO5, 100%LF, default/GLO Mass
Transport 3.5-7.5 t, truck	0.0469	tkm	Transport, truck <10t, EURO4, 100%LF, default/GLO Mass
Outputs	Amount	Unit	Remarks
Bio-polyol	1	kg	

Table 2.3. Inventory of modeled bio-polyol.

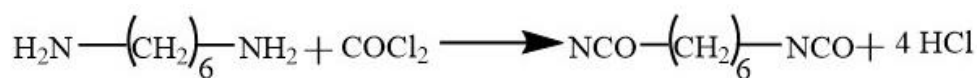


Figure 2.9. HDI synthesis reaction.

Hexamethylenediamine: HMDA			
Inputs	Amount	Unit	Remarks
Natural gas, fuel	8.86	kWh	Heat, district or industrial, natural gas {RER} market group for APOS, U
Ammonia	0.409	Kg	Ammonia E
Electricity	0.46	kWh	Electricity, medium voltage {GLO} market group for APOS, U
Steam	8.99	kg	Steam, in chemical industry {RER} market for steam, in chemical industry APOS, U
Phosphoric acid	5	g	Phosphoric acid, industrial grade, without water, in 85% solution state {GLO} market for APOS, U
Cooling water	0.67	m ³	Water, decarbonised {RoW} market for water, decarbonised APOS, U
Process water	1.44	L	Water, deionised {RoW} market for water, deionised APOS, U
Natural gas, fuel	0.05	kWh	Heat, district or industrial, natural gas {RER} market group for APOS, U
Inert gas	0.01	L	Carbon dioxide, in chemical industry {GLO} market for carbon dioxide, in chemical industry APOS, U
Hydrogen	0.067	kg	Hydrogen, gaseous {GLO} market for hydrogen, gaseous APOS, U
Sodium hydrogen sulfite	0.109	kg	Sodium hydrogen sulfite {GLO} market for APOS, U
Sodium sulfite	0.067	kg	Sodium sulfite {GLO} market for APOS, U
Butadiene	0.545	kg	Butadiene {RER} market for butadiene APOS, U
Fe-cat	6	g	Iron pellet {GLO} market for APOS, U
By-products	Amount	Unit	Remarks
Amine	0.013	kg	
Imine	0.004	kg	
Outputs	Amount	Unit	Remarks
HMDA	1	kg	
Carbon dioxide, waste fossil	0.616	kg	Carbon dioxide, fossil

Table 2.4. Inventory of modeled HMDA.

Hexamethylene diisocyanate: HDI			
Inputs	Amount	Unit	Remarks
<i>HMDA*</i>	690.8	g	<i>Modeled*</i>
Phosgene	588.6	g	Phosgene {GLO} market for APOS, U
Electricity	0.1999	kWh	Electricity, medium voltage {RER} market group for APOS, U
Heat, steam	3.149	MJ	Heat, from steam, in chemical industry {RER} market for heat, from steam, in chemical industry APOS, U
By-products	Amount	Unit	Remarks
Hydrochloric acid	0.868	kg	
Outputs	Amount	Unit	Remarks
HDI	1	kg	

Table 2.5. Inventory of modeled HDI.

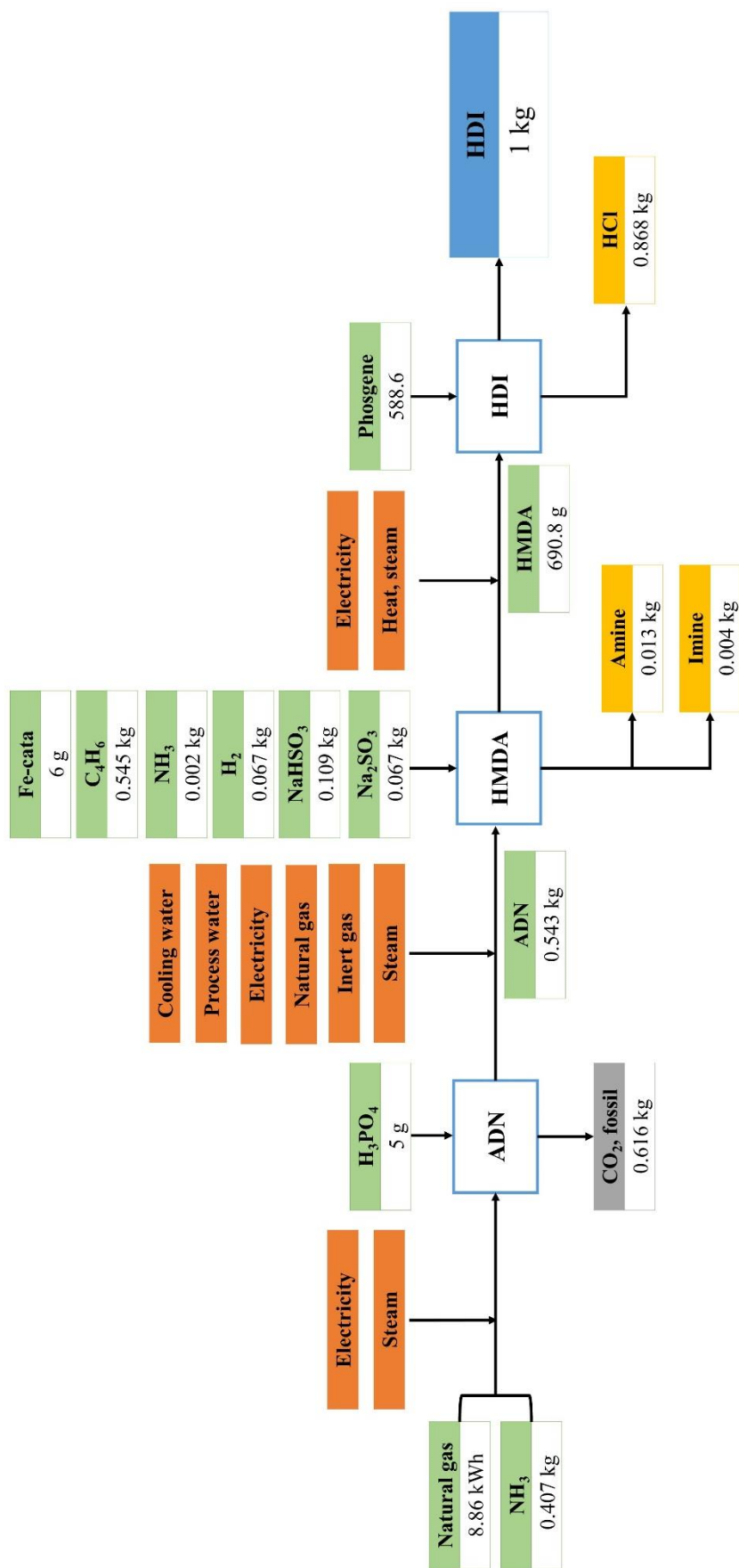


Figure 2.10. Scheme of the modeled HDI.

2.11 References

- [1] M. Abbasi, M.R.M. Mojtahedi, A. Khosroshahi, Effect of spinning speed on the structure and physical properties of filament yarns produced from used PET bottles, *J Appl Polym Sci.* 103 (2007) 3972–3975. <https://doi.org/10.1002/app.25369>.
- [2] International ASTM 4274-05, Standard test methods for testing polyurethane raw materials: determination of hydroxyl numbers of polyols, 1999.
- [3] M. Ahani, M. Khatibzadeh, M. Mohseni, Preparation and characterization of poly(ethylene terephthalate)/hyperbranched polymer nanocomposites by melt blending, *Nanocomposites.* 2 (2016) 29–36 <https://doi.org/10.1080/20550324.2016.1187966>.
- [4] H.W. Starkweather, P. Zoller, G.A. Jones, The heat of fusion of poly(ethylene terephthalate), *J Polym Sci B Polym Phys.* 21 (1983) 295–299. <https://doi.org/10.1002/pol.1983.180210211>.
- [5] J. Seo, N. Yui, J.H. Seo, Development of a supramolecular accelerator simultaneously to increase the cross-linking density and ductility of an epoxy resin, *Chem Eng J.* 356 (2019) 303–311. <https://doi.org/10.1016/j.cej.2018.09.020>.
- [6] Biocombustibles sólidos. Determinación del poder calorífico. UNE-EN ISO 18125:2018, (2018). <https://tienda.aenor.com/norma-une-en-iso-18125-2018-n0060319> (accessed August 10, 2022).
- [7] U.S. Environmental Protection Agency, Methodology for thermal efficiency and energy input calculations and analysis of biomass cogeneration unit characteristics, (2007). https://www3.epa.gov/ttn/atw/utility/fnl_biomass_cogen_TSD_04_19_07.pdf (accessed June 30, 2022).
- [8] N.B. Sanches, M.L. Dias, E.B.A.V. Pacheco, Comparative techniques for molecular weight evaluation of poly (ethylene terephthalate) (PET), *Polym Test.* 24 (2005) 688–693. <https://doi.org/10.1016/J.POLYMERTESTING.2005.05.006>.
- [9] J. Gomez-Hermoso-De-Mendoza, J. Gutierrez, A. Tercjak, Transparent and flexible cellulose triacetate-TiO₂ nanoparticles with conductive and UV-shielding properties, *J Phys Chem.* 124 (2020) 4242–4251. <https://doi.org/10.1021/acs.jpcc.9b11298>.
- [10] S. Tortoioli, L. Paolotti, F. Romagnoli, A. Boggia, L. Rocchi, Environmental assessment of bio-oil transformation from thistle in the Italian context: an LCA study, *Enviro Clim Technol.* 24 (2020) 430–446. <https://doi.org/10.2478/rtuect-2020-0114>.

- [11] A. Fridrihsone, F. Romagnoli, V. Kirsanovs, U. Cabulis, Life Cycle Assessment of vegetable oil based polyols for polyurethane production, *J Clean Prod.* 266 (2020) 121403–121431. <https://doi.org/10.1016/j.jclepro.2020.121403>.
- [12] I. Deviatkin, M. Khan, E. Ernst, M. Horttanainen, Wooden and plastic pallets: A review of life cycle assessment (LCA) studies, *Sustainability.* 11 (2019) 5750–5767. <https://doi.org/10.3390/su11205750>.
- [13] L. Shen, E. Worrell, M.K. Patel, Open-loop recycling: A LCA case study of PET bottle-to-fibre recycling, *Resour Conserv Recycl.* 55 (2010) 34–52. <https://doi.org/10.1016/j.resconrec.2010.06.014>.
- [14] H. Sugiyama, M. Hirao, R. Mendivil, U. Fischer, K. Hungerbühler, A hierarchical activity model of chemical process design based on life cycle assessment, *Process Saf Environ Prot.* 84 (2006) 63–74. <https://doi.org/10.1205/PSEP.04142>.
- [15] E.S. Barboza, D.R. Lopez, S.C. Amico, C.A. Ferreira, Determination of a recyclability index for the PET glycolysis, *Resour Conserv Recycl.* 53 (2009) 122–128. <https://doi.org/10.1016/j.resconrec.2008.10.002>.
- [16] C.E. Komly, C. Azzaro-Pantel, A. Hubert, L. Pibouleau, V. Archambault, Multiobjective waste management optimization strategy coupling life cycle assessment and genetic algorithms: Application to PET bottles, *Resour Conserv Recycl.* 69 (2012) 66–81. <https://doi.org/10.1016/j.resconrec.2012.08.008>.
- [17] A.B. Dros, O. Larue, A. Reimond, F. de Campo, M. Pera-Titus, Hexamethylenediamine (HMDA) from fossil- vs. bio-based routes: an economic and life cycle assessment comparative study, *Green Chem.* 17 (2015) 4760–4772. <https://doi.org/10.1039/c5gc01549a>.

Chapter 3

CHARACTERIZATION OF POLY(ETHYLENE
TEREPHTHALATE) SAMPLES FROM DIFFERENT
SOURCES

3. CHARACTERIZATION OF POLY(ETHYLENE TEREPHTHALATE) SAMPLES FROM DIFFERENT SOURCES

3.1. Aim of the chapter

In this chapter, PET samples of different origins are chemically and physically characterized to assess the effect of degradation on PET waste. For this purpose, four samples of pellets and bottles were used. Two of them were raw materials and the other two post-consumer PET. Degradation due to the environmental conditions such as the marine environment to which PET has been exposed could affect the physicochemical properties of PET waste.

In order to analyze the properties of mentioned PET materials, both raw and wastes, different characterization techniques were employed, such as FTIR, DSC, TGA, viscosity and molar mass determination, among others.

3.2. Characterization of PET samples from different sources

In this work four different PET samples were selected: virgin PET pellets (PET-v), post-condensed PET pellets (PET-ssp), post-consumer urban PET waste (PET-u) and post-consumer marine PET litter (PET-m). Samples were characterized in order to study the effect of the degradation on urban waste and marine litter.

3.2.1. Determination of viscosity, molar mass and ash percentages

As the viscosity of PET products is a key parameter for their processing, the IV of samples was determined according to the method explained in Chapter 2, using the MFI values. The MFI values, the corresponding IV and the M_n and M_w values are summarized in Table 3.1. PET-u and PET-m have shown higher MFI values comparing to the starting PET-ssp and, therefore, they present lower viscosity and molar mass values.

The experimentally obtained results for PET-v and PET-ssp were in the range of those provided by the supplier. The IV value decreased considerably for PET-m compared to starting PET-ssp, as can be seen in Table 3.1. Moreover, M_n and M_w values determined according to equations 2.7 and 2.8 confirmed that PET residues showed a lower molar mass. As can be seen, PET-ssp has higher viscosity and molar mass when compared to PET-v, due to the post-condensation process performed during industrial production.

Regarding MFI values, it is well known that high values could be related with some degradation [1]. As PET-m sample has shown the highest value, it seems to be the most degraded sample, as

will be later confirmed.

Samples	MFI (g/10 min)	IV (dl/g)	M_n (g/mol)	M_w (g/mol)
PET-v	97 ± 32	0.60 ± 0.05	28228 ± 3998	37281 ± 6444
PET-ssp	39 ± 13	0.74 ± 0.08	33116 ± 6912	50833 ± 11377
PET-u	89 ± 14	0.60 ± 0.02	24780 ± 1600	37206 ± 2578
PET-m	126 ± 15	0.55 ± 0.02	21997 ± 1549	32740 ± 2475

Table 3.1. Measured MFI values, together with the corresponding IV and M_n and M_w values for different PET samples.

On the other hand, the ashes of the different PET samples were also determined. The ashes obtained after the calcination are shown in Figure 3.1. As it can be seen, for PET-v and PET-ssp raw samples no ashes were observed.

The ash content values are summarized in the Table 3.2, confirming that more degraded samples, PET-u and PET-m, showed a higher ash percentage of ashes, attributed to impurities in the case of marine PET litter.



Figure 3.1. Ashes for PET-v, PET-ssp, PET-bottle, PET-m and PET-u from left to right.

Samples	Ashes (%)
PET-v	0.00
PET-ssp	0.00
PET-bottle	0.02
PET-u	0.05
PET-m	0.15

Table 3.2. Ash content values of the different PET samples.

3.2.2. Physicochemical characterization

The functional groups of PET samples were analyzed through FTIR, a very sensitive technique to identify structural changes [2]. Changes in crystallinity or chain conformation in PET samples due to environmental degradation were extensively studied in several works [2–4].

The main bands of PET samples can be seen in the spectra of Figure 3.2a, normalized with respect to the in-plane C-H bending band of the benzene ring at 1410 cm^{-1} , since this band was reported as insensitive to conformational changes [5,6]. The band around 1712 cm^{-1} , attributed to the C=O stretching vibration, and those around 1240 and 1090 cm^{-1} , corresponding to the asymmetric and symmetric C-O stretching vibrations, respectively, confirmed the presence of the ester group [7]. Moreover, the band around 1500 cm^{-1} , attributed to the C=C stretching vibration in aromatic rings and those at 870 and 720 cm^{-1} , both attributed to the out-of plane C-H bending in benzene ring, confirmed the presence of the *para*-substituted aromatic structure of PET [2,4].

Regarding to PET-*v* and PET-*ssp* raw materials, the observed differences may come from their different molar mass and crystallinity. It is well known that PET should present a minimal viscosity, melt resistance, and proper mechanical properties for being injection processed for bottle production. For this reason, PET-*v* is post-condensed into PET-*ssp*, in order to increase the molar mass and achieve the rheological properties required for injection, resulting into crystallinity differences between them [8]. FTIR spectra of amorphous and semicrystalline PET show differences at the -CH₂- wagging region, in which bands around 1370 and 1340 cm^{-1} , associated with *gauche* (amorphous) and *trans* (crystalline) conformations, respectively, can be seen [9]. Figure 3.2b shows the FTIR spectra of PET-*v* and PET-*ssp* at the 1450 - 1300 cm^{-1} interval, for a better visualization.

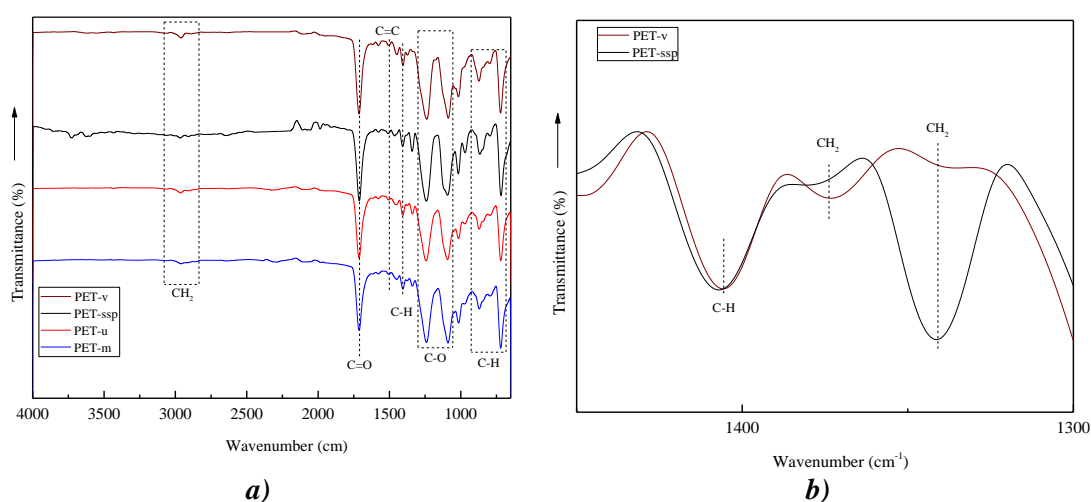


Figure 3.2. FTIR spectra of: **a)** PET-*v*, PET-*ssp*, PET-*u* and PET-*m* samples and **b)** PET-*v* and PET-*ssp* at the 1450 - 1300 cm^{-1} interval.

As can be observed in the PET-v spectrum, the band related with the amorphous structure prevails, whereas for PET-ssp the most intense band is the related to the crystalline structure.

Comparing the spectra of PET-m and PET-u wastes with that of PET-ssp (used for beverage bottle fabrication), changes related with hydrolytic degradation could be expected, since hydrolysis is the main process occurring at low temperatures [10]. Hydrolysis is a breakdown of water-activated ester bonds with the formation of carboxylic and hydroxyl end groups [3,4], which causes the cleavage of polymer chains, decreasing the molar mass. Furthermore, under marine environmental conditions, in addition to hydrolytic degradation, UV-induced photo-oxidation is also a relevant degradation pathway [11]. In fact, the ester groups in terephthalate moiety as well as $-\text{CH}_2-$ groups are strongly involved in the photodegradation of PET [12]. Photodegradation leads to the cleavage of the ester bond forming as a result carboxylic acid end groups [11,13]. As it has been reported several times in the literature, the hydrolysis and photo-oxidative degradations have similar degradation pathways [11,12]. Therefore, both photo-oxidative and hydrolysis can cause changes in the FTIR spectrum at the vibration stretching intervals of $-\text{OH}$ and $\text{C}=\text{O}$ groups, together with those of $\text{C}-\text{O}$ of ester group and $-\text{CH}_2-$ (Figure 3.3).

At the interval where the stretching vibration of hydroxyl group can be observed (Figure 3.3a), in addition to the band at around 3450 cm^{-1} related with $-\text{OH}$ stretching vibration of ethylene glycol end groups [4], PET-m showed a broad band around 3260 cm^{-1} associated to hydrogen-bonded $-\text{OH}$ groups from carboxylic and alcoholic end groups [3]. As it has been reported in the literature, this band broadens with degradation suggesting the presence of carboxylic acids [14]. Among PET wastes, the intensity of this band is higher for PET-m sample, suggesting that this sample could be more degraded due to the higher hydrolytic and photodegradation aggressiveness of marine environment. At this interval, some other bands related with aromatic and aliphatic $\text{C}-\text{H}$ stretching vibrations around 3060 cm^{-1} and 2970 cm^{-1} wavenumbers, respectively, can be observed. At the interval corresponding to the stretching vibration of carbonyl groups (Figure 3.3b), the intensity of the carbonyl band of the ester group at 1712 cm^{-1} decreased in PET-u and PET-m samples compared to that of PET-ssp. Furthermore, this band widens towards lower wavenumbers, which is usually attributed to the stretching vibration of the carbonyl group of the carboxylic acid [2]. At the third interval (Figure 3.3c), the intensity of the ester group $\text{C}-\text{O}$ band at 1240 cm^{-1} decreased in PET-u and PET-ssp. PET-ssp sample shows a shoulder at 1120 cm^{-1} , which has been attributed to *trans* (crystalline) ethylene glycol [2,15]. This shoulder is missing for PET-u and PET-m, agreeing with their lower crystallinity when compared to PET-ssp. Moreover, the band attributed to the in plane bending of $\text{C}-\text{H}$ in benzene ring at 1015 cm^{-1} , which was found to increase with crystallinity as consequence of annealing or drawing [5,15], decreased in PET-u and PET-m samples.

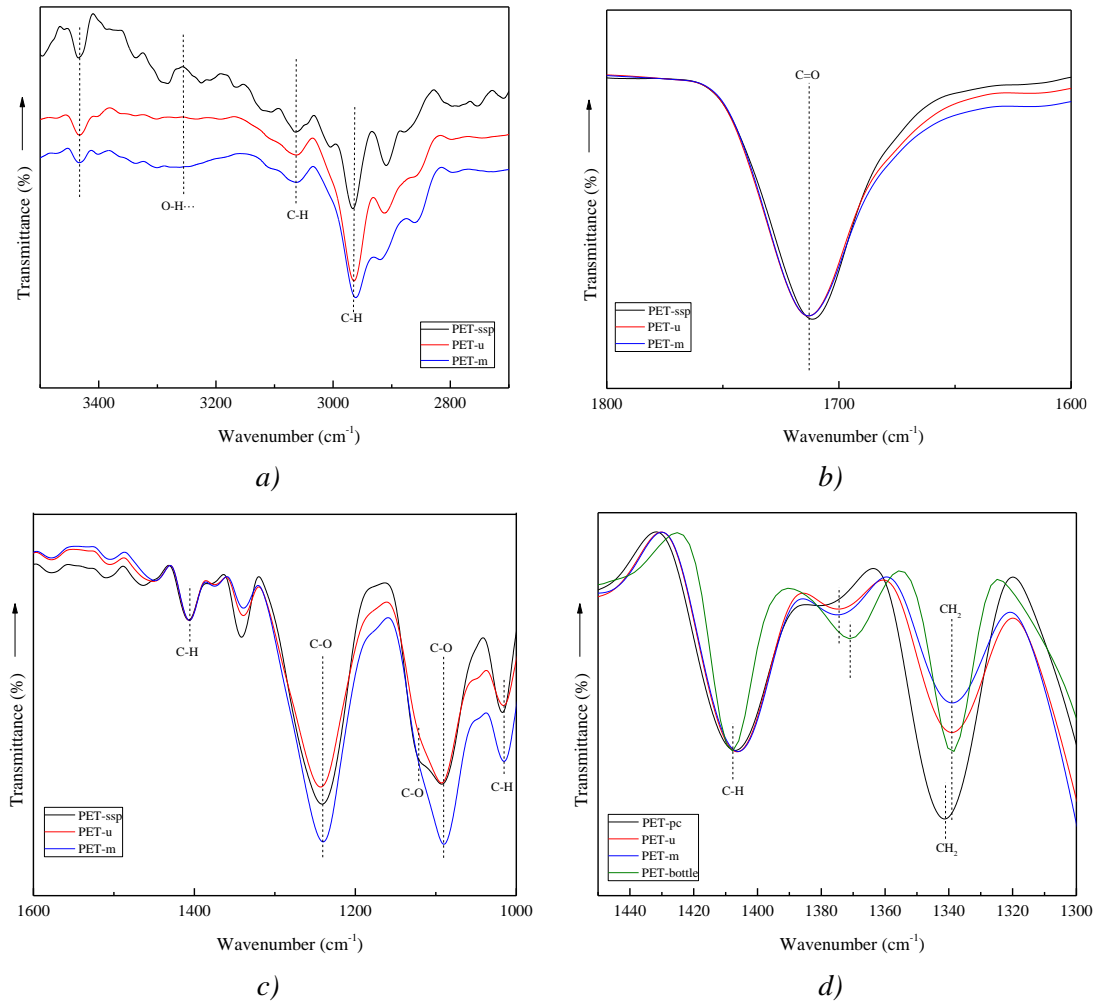


Figure 3.3. FTIR spectra of PET-ssp, PET-u and PET-m at different intervals: **a)** 3500-2700 cm^{-1} , **b)** 1800-1600 cm^{-1} , **c)** 1600-1000 cm^{-1} , and **d)** spectra of PET-ssp, PET-u and PET-m samples and PET-bottle for comparison, at the interval corresponding to the -CH₂- wagging region (1450-1300 cm^{-1}).

As it was previously discussed, the -CH₂- wagging region is useful to analyze PET crystallinity. As can be seen in FTIR spectra of Figure 3.3d, corresponding to that region, the ratio between intensities of the *trans* (crystalline) band around 1340 cm^{-1} and the band at 1410 cm^{-1} taken as reference, I_{1340}/I_{1410} , decreased for both PET-u and PET-m, in agreement with previous results. Despite the bands related with hydroxyl, carboxylic acid and ester carbonyls suggested that higher chain excision occurred in PET-m, its crystallinity seems to be lower than that of PET-u. However, it should be taken into account that after the fabrication of beverage bottles by injection molding from PET-ssp, the fast-cooling process applied results into lower crystallinity. Figure 3.3d also shows the FTIR spectra of a piece taken from a bottle of PET (PET-bottle) for comparative purposes. As can be observed the I_{1340}/I_{1410} ratio of PET-bottle is considerably lower than that of PET-ssp. Therefore, the lower I_{1340}/I_{1410} ratio observed in PET-u and PET-m residues coming from bottles comparing to PET-ssp can be mainly related to the processing.

So, it can be deduced that more degraded PET-u and PET-m samples showed lower crystallinity than PET-ssp, but quite similar to PET-bottle, as it was shown by FTIR analysis. On the other hand, EA of the PET samples was performed (Table 3.3). The results, in agreement to those reported in the literature [16], indicated that the carbon content decreased slightly in the processed and waste samples. However, the sulfur content increased considerably in PET-u (300 %) and PET-m (150 %) compared to PET-v, probably due to the impurities present in these samples.

Samples	N %	C %	H %	O %	S %
PET-v	<0.1	67.4	4.2	33.2	0.2
PET-bottle	<0.1	62.5	4.2	33.5	0.0
PET-u	<0.1	62.8	4.3	33.0	0.8
PET-m	<0.1	62.5	4.3	33.0	0.5

Table 3.3. EA results of PET samples from different sources.

3.2.3. Thermal characterization

Thermal properties of post-consumer urban PET waste and marine PET litter may change when compared to those of PET-ssp and PET-v, due to hydrolytic degradation [17–20]. Figure 3.4 shows the most representative DSC thermograms of different PET samples, corresponding to the first heating, cooling and second heating scans. The thermal properties obtained from them are summarized in Table 3.4. The results for PET residues (PET-u and PET-m) correspond to the mean obtained from 3 different samples, due to the heterogeneity of the residues.

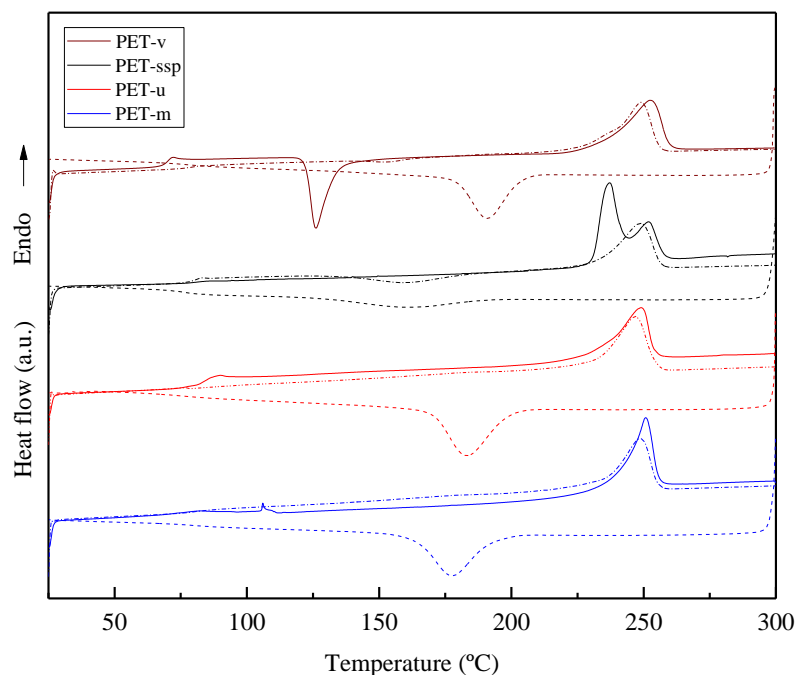


Figure 3.4. DSC thermograms of the different PET samples. First heating scan (—), cooling scan (-----) and second heating scan (-·-·-·-·).

		PET-v	PET-ssp	PET-u	PET-m	PET-bottle
1 st heating scan	T _g (°C)	70	81	82 ± 3	77 ± 3	80
	T _c (°C)	126	-	-	-	99
	ΔH _c (J/g)	25	-	-	-	1
	T _m (°C)	253	237, 252	250 ± 2	250 ± 1	247
	ΔH _m (J/g)	36	46	37 ± 6	39 ± 4	37
	X _c (%)	8	34	27 ± 7	29 ± 4	27
Cooling scan	T _g (°C)	-	76	-	-	-
	T _c (°C)	191	161	188 ± 13	185 ± 12	178
	ΔH _c (J/g)	30	13	38 ± 3	38 ± 4	9
	X _c (%)	22	10	28 ± 3	28 ± 4	7
2 nd heating scan	T _g (°C)	75	81	80 ± 1	80 ± 1	80
	T _c (°C)	153	160	-	-	-
	ΔH _c (J/g)	1	10	-	-	-
	T _m (°C)	249	248	248 ± 1	248 ± 0	243
	ΔH _m (J/g)	34	31	35 ± 4	34 ± 5	30
	X _c (%)	24	23	26 ± 4	25 ± 6	22

Table 3.4. Main thermal parameters obtained from DSC thermograms of PET-v, PET-ssp, PET-u, PET-m, and PET-bottle during the 1st heating scan, cooling and 2nd heating scan.

During the first heating scan, a T_g at 70 °C, an exothermic crystallization peak (T_c) at 126 °C and an endothermic melting peak (T_m) at 252 °C were detected for PET-v sample, whereas for PET-ssp one no exothermic crystallization peak was observed, thus confirming full crystallization after post-condensation [21]. These results agree with those observed by FTIR analysis. Moreover, PET-ssp shows a T_g at 81 °C, slightly higher than that observed for PET-v, due to the mobility restrictions imposed by the higher crystallinity. The two melting peaks observed in PET-ssp at 237 and 252 °C, suggest different crystalline structures, probably formed during post-condensation [22–24]. Even if PET-v can crystallize during heating, the melting enthalpy value is lower than that of PET-ssp, which confirmed the higher crystallinity.

PET-u and PET-m showed a T_g at 82 and 77 °C, respectively, in the range of that observed for PET-ssp, as well as the absence of any exothermic crystallization. Regarding the crystallinity of both PET-u and PET-m, they presented lower melting enthalpy than PET-ssp, and therefore a

slight lower crystallinity degree comparing with PET-ssp, in agreement with FTIR results. Moreover, both have shown a single melting peak at higher temperature, suggesting a different polymer chain arrangement. In the same way than for FTIR analysis, a piece taken from a PET bottle was analyzed by DSC for comparative purposes. Thermal transition values are summarized in Table 3.4. Results have confirmed that the differences in crystallinity among PET-u and PET-m and PET-ssp, in addition to hydrolytic degradation, would also be influenced by processing.

In the cooling scan, all PET samples, with the exception of PET-ssp, showed a pronounced sharp exothermic peak attributed to the crystallization process of PET. Comparing non degraded PET-v and PET-ssp, the higher crystallization temperature and exothermic enthalpy values observed for PET-v, suggests a faster crystallization kinetics, which could be attributed to its lower molar mass. Regarding cooling thermograms of PET-u and PET-m wastes, both crystallization temperature and crystallization enthalpy are higher than those for PET-ssp, being also higher than PET-bottle, due to the higher mobility of chains that favored the crystallization process. Moreover, only PET-ssp has shown a clear T_g around 76 °C, related to the presence of amorphous fractions of PET due to its slower crystallization kinetics.

Finally, comparing the second heating scans with the first ones, the main difference was found for PET-v and PET-ssp samples. The crystallization peak observed in the first scan for PET-v is hardly appreciated in the second one, suggesting that PET-v almost fully crystallized during the cooling scan, while in the case of PET-ssp a crystallization peak is observed at 160 °C, absent in the first scan, thus corroborating its semicrystalline state.

Besides, the PET-ssp sample showed a single melting peak, because, neither in the cooling scan nor during the second heating scan, the sample was not able to develop the same crystalline structure achieved in the post-condensation process. PET-bottle also showed slightly lower crystallinity in the second scan. However, comparing the melting enthalpies and crystallization degrees of PET-u and PET-m with those of PET-bottle, slightly higher values were measured for PET-u and PET-m once the thermal history was erased.

The thermal stability of different PET samples was also studied. Weight evolution curves obtained from TGA are presented in Figure 3.5. The main parameters are summarized in Table 3.5. A single weight loss around 438 °C (T_d) was observed for all samples, with a loss of around 80 %. This weight loss can be attributed to PET polymer degradation, in which the scission of ester links in the main chain could be done resulting in the formation of different oligomers [25]. Figure 3.5 shows that the onset of the weight loss of PET-m sample starts at a slightly lower temperature than that observed for the PET-u. As verified by MFI and confirmed by FTIR and DSC results, the PET-m sample seems to present shorter polymer chains due to degradation [26]. The percentage of final char is around 19 % for all samples.

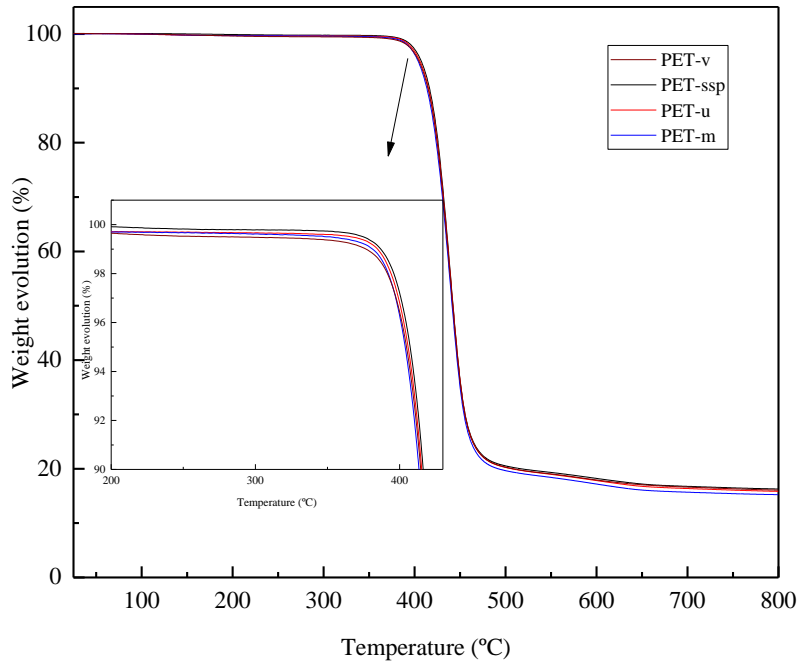


Figure 3.5. Weight evolution curves of PET-ssp, PET-v, PET-u and PET-m samples.

Samples	T _d (°C)	Residue (%)
PET-v	438	16
PET-ssp	438	16
PET-u	438	16
PET-m	438	15

Table 3.5. TGA results of the different PET samples.

3.2.4. Surface characterization

The surface properties of the different materials were evaluated on plaques obtained by thermal compression processing (Figure 3.6). As can be observed, PET-u and PET-m presented a different appearance compared to PET-v and PET-ssp. Moreover, PET-m showed an intense brown color, suggesting severe thermo-oxidative degradation during compression [18]. The yellowing or discoloration of PET samples is attributed in the literature to several degradation processes including thermo-oxidation [27], hydrolytic degradation [11] and photo-oxidation [11,28]. According to Gewert et al. [11] photodegradation leads to the cleavage of the ester bond forming a carboxylic acid end group and a vinyl end group directly, or radicals, which finally lead to the formation of a carboxylic acid end group. These act as promoter of thermo-oxidative degradation, as occurred in PET-m sample. Then, the higher degradation of PET-m sample is confirmed, in good agreement with FTIR analysis.



Figure 3.6. Images of PET samples obtained by compression molding. From left to right: PET-ssp, PET-v, PET-u and PET-m.

The influence of degradation on the surface hydrophilicity was analyzed by WCA. Obtained values, together with the images corresponding to the water drop over samples are shown in Table 3.6. A contact angle of 72° was obtained for PET-v, while PET-ssp one presented a value of 77° . The post-condensation process increases the molar mass, thus decreasing hydrophilicity and resulting in a higher WCA [29].

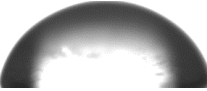
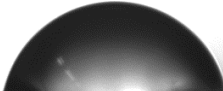
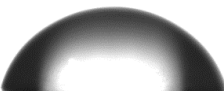
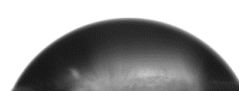
PET-v	PET-ssp	PET-u	PET-m
Water contact angle ($^\circ$)			
72 ± 3	77 ± 3	71 ± 2	66 ± 3
			

Table 3.6. Contact angle values for different PET samples, together with the corresponding image of water drop over each sample.

Regarding PET wastes, it can be observed that the higher the degradation of PET, the lower the contact angle, especially for PET-m, showing higher hydrophilicity. This observation is in agreement with the conclusions about degradation obtained from FTIR analysis.

In fact, hydrolytic and photo-oxidative degradation, as well thermo-oxidative degradation that compression molded samples could suffered, resulted into the breaking of chains, thus increasing the content of hydrophilic -COOH and -OH groups. As WCA results suggest, those functional groups could also be present at the surface and, consequently, interact with water decreasing the contact angle values.

FTIR, DSC, WCA, and MFI results could suggest that PET-u and PET-m samples have undergone some degradation producing chain cleavage, increasing crystallinity and hydrophilicity, and decreasing IV and the molar mass. Therefore, PET-u and PET-m samples analyzed could not present suitable properties to be used as raw material in common PET applications.

3.3. Conclusions

Different PET samples were characterized in order to evaluate the effect of degradation on their physicochemical properties. The photodegradation and hydrolysis seem to be the main degradation processes suffered by samples, causing the cleavage of the ester group at the polymer chain, leading to the formation of chain end groups, as corroborated by FTIR analysis. It was confirmed by FTIR and DSC that the crystallinity was similar for wastes and PET-bottle samples. In contrast, post-condensed PET sample presented a higher degree of crystallinity, also shown a double melting peak at the DSC thermogram due to different crystal structures.

The MFI values showed that the more degraded PET-m and PET-u samples presented higher MFI values and, therefore, lower viscosity and molar mass values compared to PET-ssp and PET-v. TGA also confirmed the higher degradation level for PET-m sample, since, due to the shorter polymer chains present, it started to degrade at a slightly lower temperature than the rest of samples.

The results confirm that the more aggressive environmental conditions of the marine environment cause a more severe degradation in marine PET than in urban PET waste. Once the level of degradation of different PET samples is analyzed, recycling strategies for marine PET are studied in the following chapters.

3.4. References

- [1] R.P. de Oliveira Santos, D.O. Castro, A.C. Ruvolo-Filho, E. Frollini, Processing and thermal properties of composites based on recycled PET, sisal fibers, and renewable plasticizers, *J Appl Polym Sci.* 131 (2014) 40386–40399. <https://doi.org/10.1002/app.40386>.
- [2] F. Dubelley, E. Planes, C. Bas, E. Pons, B. Yrieix, L. Flandin, The hygrothermal degradation of PET in laminated multilayer, *Eur Polym J.* 87 (2017) 1–13. <https://doi.org/10.1016/J.EURPOLYMJ.2016.12.004>.
- [3] C. Sammon, J. Yarwood, N. Everall, An FT–IR study of the effect of hydrolytic degradation on the structure of thin PET films, *Polym Degrad Stab.* 67 (2000) 149–158. [https://doi.org/10.1016/S0141-3910\(99\)00104-4](https://doi.org/10.1016/S0141-3910(99)00104-4).
- [4] B.J. Holland, J.N. Hay, The thermal degradation of PET and analogous polyesters measured by thermal analysis–Fourier transform infrared spectroscopy, *Polymer (Guildf).* 43 (2002) 1835–1847. [https://doi.org/10.1016/S0032-3861\(01\)00775-3](https://doi.org/10.1016/S0032-3861(01)00775-3).
- [5] M. Bertoldo, M. Labardi, C. Rotella, S. Capaccioli, Enhanced crystallization kinetics in

- poly(ethylene terephthalate) thin films evidenced by infrared spectroscopy, *Polymer (Guildf)*. 51 (2010) 3660–3668. <https://doi.org/10.1016/J.POLYMER.2010.05.040>.
- [6] X. Zhou, C. Wang, C. Fang, R. Yu, Y. Li, W. Lei, Structure and thermal properties of various alcoholysis products from waste poly(ethylene terephthalate), *Waste Manage*. 85 (2019) 164–174. <https://doi.org/10.1016/J.WASMAN.2018.12.032>.
- [7] S. Umamaheswari, M. Murali, FTIR spectroscopic study of fungal degradation of poly(ethylene terephthalate) and polystyrene foam Plastic biodegradation by Bacteria View project, *Elixir Chem Eng*. 64 (2013) 19159–19164. <https://www.researchgate.net/publication/258316463>.
- [8] B. Gantillon, R. Spitz, T.F. McKenna, The solid state postcondensation of PET, *Macromol Mater Eng*. 289 (2004) 88–105. <https://doi.org/10.1002/mame.200300289>.
- [9] F. Dieval, F. Khoffi, R. Mir, W. Chaouch, D. le Nouen, N. Chakfe, B. Durand, Long-Term Biostability of Pet vascular prostheses, *Int J Polym Sci*. 2012 (2012) 1–14. <https://doi.org/10.1155/2012/646578>.
- [10] E. Pirzadeh, A. Zadhoush, M. Haghghat, Hydrolytic and thermal degradation of PET fibers and PET granule: The effects of crystallization, temperature, and humidity, *J Appl Polym Sci*. 106 (2007) 1544–1549. <https://doi.org/10.1002/app.26788>.
- [11] B. Gewert, M.M. Plassmann, M. Macleod, Pathways for degradation of plastic polymers floating in the marine environment, *Environ Sci Process Impacts*. 17 (2015) 1513–1521. <https://doi.org/10.1039/c5em00207a>.
- [12] K.N. Fotopoulou, H.K. Karapanagiotti, Degradation of various plastics in the environment, in: *Handbook of Environmental Chemistry*, Springer Verlag, 2019: pp. 71–92. https://doi.org/10.1007/698_2017_11.
- [13] S. Venkatachalam, G. Shilpa, V. Jayprakash, R. Prashant, Rao. Krishna, K. Anil, Degradation and recyclability of poly (ethylene terephthalate), in: *Polyester*, InTech, 2012: pp. 75–98. <https://doi.org/10.5772/48612>.
- [14] M. Edge, R. Wiles, N.S. Allen, W.A. McDonald, S.V. Mortlock, Characterisation of the species responsible for yellowing in melt degraded aromatic polyesters—I: Yellowing of poly(ethylene terephthalate), *Polym Degrad Stab*. 53 (1996) 141–151. [https://doi.org/10.1016/0141-3910\(96\)00081-X](https://doi.org/10.1016/0141-3910(96)00081-X).
- [15] K.C. Cole, A. Ajji, É. Pellerin, New insights into the development of ordered structure in poly(ethylene terephthalate). Results from external reflection infrared spectroscopy, *Macromolecules*. 35 (2002) 770–784. <https://doi.org/10.1021/ma011492i>.

- [16] S.D. Mancini, J.A.S. Schwartzman, A.R. Nogueira, D.A. Kagohara, M. Zanin, Additional steps in mechanical recycling of PET, *J Clean Prod.* 18 (2010) 92–100. <https://doi.org/10.1016/j.jclepro.2009.09.004>.
- [17] M. Abbasi, M.R.M. Mojtahedi, A. Khosroshahi, Effect of spinning speed on the structure and physical properties of filament yarns produced from used PET bottles, *J Appl Polym Sci.* 103 (2007) 3972–3975. <https://doi.org/10.1002/app.25369>.
- [18] F. Masmoudi, F. Fenouillot, A. Mehri, M. Jaziri, E. Ammar, Characterization and quality assessment of recycled post-consumption poly(ethylene terephthalate) (PET), *Environ Sci Pollut Res.* 25 (2018) 23307–23314. <https://doi.org/10.1007/s11356-018-2390-7>.
- [19] Y. Qin, M. Qu, J. Kaschta, D.W. Schubert, Comparing recycled and virgin poly (ethylene terephthalate) melt-spun fibres, *Polym Test.* 72 (2018) 364–371. <https://doi.org/10.1016/j.polymertesting.2018.10.028>.
- [20] A. Pegoretti, A. Penati, Effects of hygrothermal aging on the molar mass and thermal properties of recycled poly(ethylene terephthalate) and its short glass fibre composites, *Polym Degrad Stab.* 86 (2004) 233–243. <https://doi.org/10.1016/J.POLYMDEGRADSTAB.2004.05.002>.
- [21] A. Bartolotta, G. di Marco, F. Farsaci, M. Lanza, M. Pieruccini, DSC and DMTA study of annealed cold-drawn PET: a three phase model interpretation, *Polymer (Guildf).* 44 (2003) 5771–5777. [https://doi.org/10.1016/S0032-3861\(03\)00589-5](https://doi.org/10.1016/S0032-3861(03)00589-5).
- [22] F. Awaja, D. Pavel, Recycling of PET, *Eur Polym J.* 41 (2005) 1453–1477. <https://doi.org/10.1016/J.EURPOLYMJ.2005.02.005>.
- [23] S. Rajendran, S.P. Mishra, Chemical, structural and thermal changes in PET caused by solvent induced polymer crystallisation, *Polym Polym Compos.* 15 (2007) 103–110. <https://doi.org/10.1177/096739110701500203>.
- [24] S. Tan, A. Su, W. Li, E. Zhou, New insight into melting and crystallization behavior in semicrystalline poly(ethylene terephthalate), *J Polym Sci B Polym Phys.* 38 (2000) 53–60. [https://doi.org/10.1002/\(SICI\)1099-0488\(20000101\)38:1<53::AID-POLB6>3.0.CO;2-G](https://doi.org/10.1002/(SICI)1099-0488(20000101)38:1<53::AID-POLB6>3.0.CO;2-G).
- [25] N. Dimitrov, L. Kratofil Krehula, A. Ptiček Siročić, Z. Hrnjak-Murgić, Analysis of recycled PET bottles products by pyrolysis-gas chromatography, *Polym Degrad Stab.* 98 (2013) 972–979. <https://doi.org/10.1016/j.polymdegradstab.2013.02.013>.
- [26] E.J. Velásquez, L. Garrido, A. Guarda, M.J. Galotto, C. López de Dicastillo, Increasing the incorporation of recycled PET on polymeric blends through the reinforcement with

- commercial nanoclays, *Appl Clay Sci.* 180 (2019) 105185–105193. <https://doi.org/10.1016/j.clay.2019.105185>.
- [27] D. Berg, K. Schaefer, A. Koerner, R. Kaufmann, W. Tillmann, M. Moeller, Reasons for the discoloration of postconsumer poly(ethylene terephthalate) during reprocessing, *Macromol Mater Eng.* 301 (2016) 1454–1467. <https://doi.org/10.1002/mame.201600313>.
- [28] D.E. Duvall, Environmental degradation of pet and its potential effect on long-term mechanical properties of oriented pet products, *Polym Plast Technol Eng.* 34 (1995) 227–242. <https://doi.org/10.1080/03602559508015825>.
- [29] G.P. Karayannidis, D.E. Kokkalas, D.N. Bikiaris, Solid-state polycondensation of poly(ethylene terephthalate) recycled from postconsumer soft-drink bottles, *J Appl Polym Sci.* 50 (1993) 2135–2142. <https://doi.org/10.1002/app.1993.070501213>.

Chapter 4

STUDY OF THE VALORIZATION OF MARINE PET
LITTER BY CONVENTIONAL METHODS

4. STUDY OF THE VALORIZATION OF MARINE PET LITTER BY CONVENTIONAL METHODS

4.1. Aim of the chapter

Municipal PET waste is industrially recycled through a thermo-mechanical process due to the high residue volume, and to the high efficiency and easy transformation of the recycling process. However, marine PET litter is not currently being systematically recycled. This could be due to the difficulty in managing marine litter. In addition, further degradation could have a negative impact on the industrial recycling chain. Therefore, the usual end for this waste is landfill or incineration. However, these methods are not environmentally friendly processes, so it is necessary to evaluate recycling alternatives for marine litter.

The aim of this chapter was to analyze, the suitability of two most conventional PET waste valorization processes in the industry, that is thermo-mechanical recycling and energy recovery by incineration, for marine PET litter recycling, comparing to those for urban PET waste and post-condensed PET.

For thermo-mechanical recycling, three different PET samples were used: urban PET waste and marine PET litter, PET-u and PET-m, respectively, and the virgin pellets used for the manufacture of PET bottles (PET-ssp), for comparative purposes. As it was already studied in the previous chapter, PET-m especially showed some signs of degradation, so in this chapter, the effect of this degradation on the quality of the recycled product was evaluated. Moreover, different processing variables were evaluated in order to optimize the thermo-mechanical recycling process.

Finally, the suitability of energy recovery was evaluated measuring the calorific value obtained.

4.2. Thermo-mechanical recycling of PET samples

Thermo-mechanical recycling is the most common and widespread method to recycle PET materials. In this work, it was carried out for PET-u and PET-m in a twin-screw extruder (Haake PolyLab QC model, Thermo Scientific). For comparative purposes, PET-ssp material was also extruded. In order to ensure a good mixing in the extruder, PET samples from marine environment were flaked in a shredder into pellets of 1-1.5 cm in size, prior to recycling. After size conditioning of samples, materials were dried at 65 °C in a vacuum oven for 1 h. All samples were then kept at room temperature in a vacuum desiccator to prevent moisture absorption prior to extrusion. Figure. 4.1 shows the PET samples used.

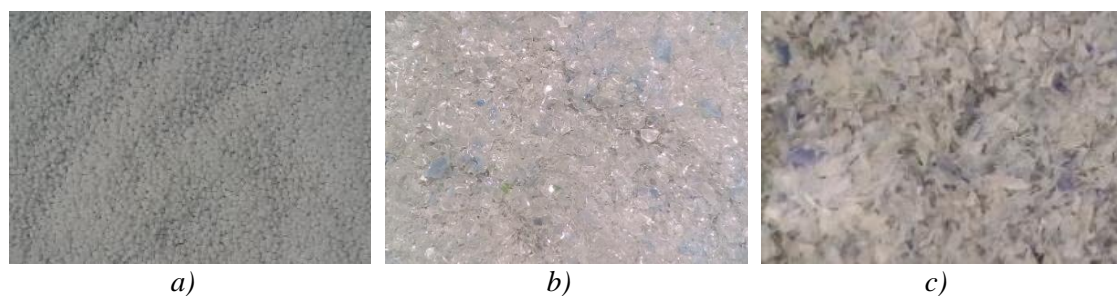


Figure 4.1. Digital images of conditioned samples before the thermo-mechanical recycling, *a) PET-ssp, b) PET-u and c) PET-m* samples.

The melting point of PET materials, as studied in Chapter 3, is around 250 °C. Therefore, the selected extrusion temperature profile was 255, 260, 265 and 270 °C, from feed to nozzle. For sample extrusion, intensive mixing screws were used, with a maximum torque of 10 Nm and a screw speed of 60-75 rpm. The thermo-mechanically recycled PET (RPET) was cooled to room temperature and subsequently shredded and sieved using a 0.4 mm light sieve. RPET-ssp, RPET-u and RPET-m samples are shown in the Figure 4.2.



Figure 4.2. Samples shredded after thermo-mechanical recycling from left to right: *RPET-ssp, RPET-u and RPET-m*.

As it can be seen, RPET-m sample shows a brownish color, probably related to the thermo-oxidative degradation that occurs during the thermo-mechanical recycling process [1]. This degradation pathway has been pointed out as the main cause for the discoloration of melt-processed PET [2].

However, despite of the fact that all three samples were subjected to the same thermo-mechanical recycling, the discoloration is only noticeable for RPET-m sample. As reported in the literature, contamination, impurities and previous degradations in PET samples can also contribute to further degradations and coloration [3,4]. Thus, the previous degradation of original PET-m sample together with the exposure to high temperatures in thermo-mechanical recycling could be the trigger for the brown color of RPET-m sample.

4.3. Characterization of recycled PET samples

4.3.1. Spectrophotometry

For a more accurate color analysis, samples were analyzed by a spectrophotometer. Results are summarized in Table 4.1. Regarding the light-darkness (L^*) values, a significant decrease is observed for the RPET-m sample, attributed to the degradation suffered [5,6]. Similarly, the increase observed for b^* parameter can also be attributed to thermal degradation [6]. The color differences (ΔE^*) between investigated materials and the white standard ($L^* = 90.18$, $a^* = -0.45$ and $b^* = 1.56$), as well as the whiteness index (WI), were calculated by Equations 2.9 and 2.10 from Chapter 2. A gradual increase in ΔE^* is observed as the degradation of PET samples increases, being considerably higher for RPET-m sample. As mentioned before, the darker color is an indicator of degradation, probably due to thermo-oxidative degradation during processing or to previous degradation of samples [1,3].

Samples	L^*	a^*	b^*	ΔE^*	WI
RPET-ssp	77.3	0.1	4.7	13.3	76.8
RPET-u	77.5	0.1	7.7	14.2	76.2
RPET-m	52.5	1.8	10.2	38.7	51.4

Table 4.1. Values of different color parameters for RPET samples.

4.3.2. MFI, IV and molar mass

Intrinsic viscosity is a critical parameter when considering thermo-mechanical recycling of PET, as a minimum viscosity is required for the manufacture of new PET material [7]. The MFI values obtained for RPET samples were measured and the corresponding viscosity calculated as explained in Chapter 2 (Equation 2.6). Moreover, M_w and M_n , respectively, were calculated from IV values with Equation 2.7 and 2.8 as described in Chapter 2. Obtained values are summarized in Table 4.2, together with those obtained for raw PET samples (Chapter 3). As it can be seen, the viscosity and molar masses decrease considerably for recycled samples comparing with those of raw PET ones.

As reported in the literature, thermo-mechanical recycling leads to a high predominance of chain scission in the process, resulting in an increase of the MFI and in the consequent decrease of the intrinsic viscosity and M_w and M_n values [8]. Chain scission usually generates polymeric radicals with hydroxyl and carboxyl end groups [1] that convert PET degradation into an autocatalytic reaction [9–11].

Samples	MFI (g/10min)	IV (dl/g)	M_n (g/mol)	M_w (g/mol)
PET-ssp	39 ± 13	0.74 ± 0.08	33116 ± 6912	50833 ± 11377
PET-u	89 ± 14	0.60 ± 0.02	24780 ± 1600	37206 ± 2578
PET-m	126 ± 15	0.55 ± 0.02	21997 ± 1549	32740 ± 2475
RPET-ssp	119 ± 7	0.56 ± 0.01	22396 ± 662	33376 ± 1059
RPET-u	133 ± 12	0.54 ± 0.02	21589 ± 939	32086 ± 1499
RPET-m	178 ± 12	0.50 ± 0.01	19567 ± 606	28872 ± 960

Table 4.2. MFI, IV, M_n and M_w values of raw PET and recycled RPET samples.

As it can be seen, recycled samples do not present the viscosity needed for the manufacture of bottles, being lower for RPET-u and RPET-m samples, obtained from the most degraded PET-u and PET-m samples.

4.3.3. FTIR

FTIR spectra of three recycled RPET samples are shown in Figure 4.3. The spectra were normalized with respect to the benzene ring band at 1410 cm^{-1} [12,13]. In Figure 4.3a the spectra of RPET samples can be seen, showing the main characteristic bands of PET described in Chapter 3.

The major difference between the spectra of raw (Figure 3.2a of Chapter 3) and the recycled PET samples is observed in the stretching vibration of the hydroxyl group (Figure 4.3b). As observed, the intensity of the band around 3430 cm^{-1} related to the -OH stretching vibration of the ethylene glycol end groups [14,15] is higher for RPET-m sample compared to the RPET-ssp and RPET-u ones, which are quite similar among them. Analyzing the absorption band at 1712 cm^{-1} related with ester carbonyl group (Figure 4.3c), RPET-m sample shows an increased intensity. In Chapter 3, nevertheless, a reduction in the intensity of this peak was observed for PET-m, related to the breakdown of the ester group. However, in thermo-mechanically recycled PET samples the intensity of the C=O band depends on both the disappearance of the ester group and the formation of acid groups. These two factors cause opposite effects, but in RPET-m the process is accelerated and the formation of acid groups could prevail over the broken esters, so there is an increase in intensity for recycled samples, related to the thermo-oxidative degradation [16].

The bands related to C-O ester group at 1238 cm^{-1} and 1091 cm^{-1} [17] increased for RPET-u and RPET-m samples, as is observed in Figure 4.3d. However, a shoulder at 1120 cm^{-1} is clearly shown for RPET-m sample, attributed to *trans* (crystalline) ethylene glycol [18,19]. This shoulder is barely observed for RPET-u and RPET-ssp, so it can be deduced that RPET-m presents the

highest crystallinity, since chains have higher mobility to generate crystalline structures due to the breakage formed during degradation.

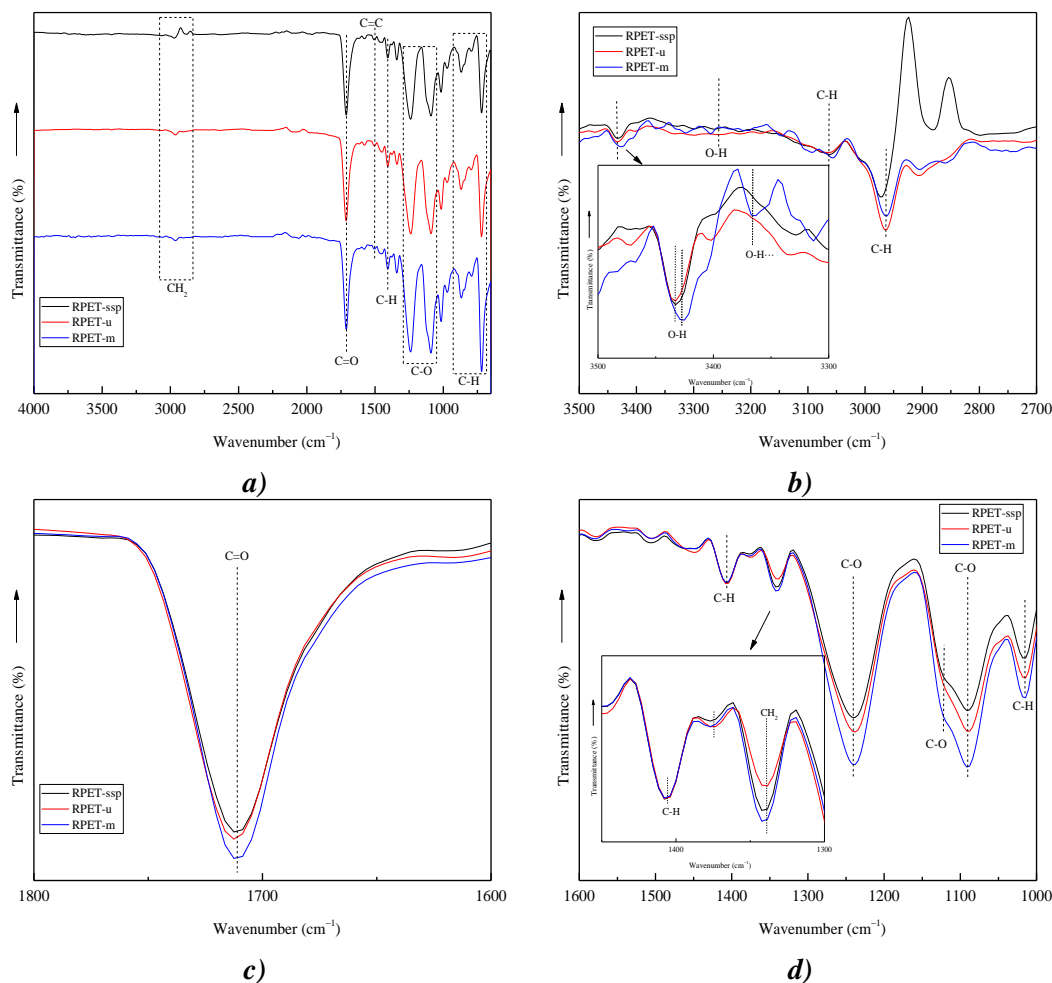


Figure 4.3. FTIR spectra of RPET samples at different intervals: **a)** 4000-700 cm^{-1} , **b)** 3500-2700 cm^{-1} , **c)** 1800-1600 cm^{-1} and **d)** 1600-1000 cm^{-1} .

The band attributed to bending in the C-H plane in the benzene ring at 1015 cm^{-1} to increases with crystallinity [19,20]. As observed in Figure 4.3d, this band slightly increased for RPET-u and RPET-m samples comparing with RPET-ssp one. In addition, the bands in the -CH₂- wagging region, around 1370 and 1340 cm^{-1} , are associated with *gauche* (amorphous) and *trans* (crystalline) conformations, respectively [21]. The intensity of the *trans* (crystalline) band was measured by the ratio between the band at 1340 cm^{-1} and the reference band at 1410 cm^{-1} , I_{1340}/I_{1410} [12]. This ratio increased considerably for RPET-m sample compared to other two samples, because the degradation of PET can favor the ordering of the molecular structure leading to a higher crystallinity [22].

Therefore, a higher amount of carboxyl and hydroxyl groups is observed for RPET-m sample comparing with RPET-u and RPET-ssp ones. Thus, it is suggested that the carboxyl and hydroxyl groups of degraded PET could act as catalysts to promote further degradation, such as the thermo-

oxidative degradation that the samples undergo when are subjected to high temperatures in thermo-mechanical recycling [1,23,24].

Finally, the FTIR spectra of raw and recycled PET waste samples were analyzed together, Figure 4.4a. As can be seen in the stretching vibration interval of the hydroxyl band, Figure 4.4b, the intensity of the band at 3430 cm^{-1} increases for RPET-m sample with respect to PET-m one, while in the case of the PET-u and RPET-u samples it appears very similar.

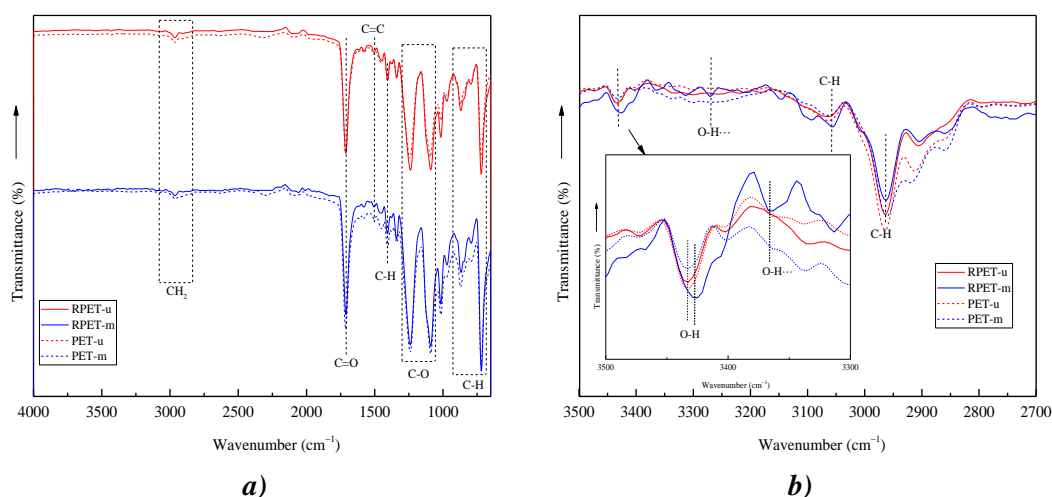


Figure 4.4. Comparative FTIR spectra of original samples before (PET) and after thermo-mechanical recycling (RPET) at: **a)** $4000\text{-}700\text{ cm}^{-1}$ and **b)** $3500\text{-}2700\text{ cm}^{-1}$ intervals.

In addition, RPET-m sample shows a clear peak at 3270 cm^{-1} , which can be related to the formed -OH end groups, indicating a higher degradation degree [25]. Therefore, thermo-oxidative degradation during the recycling process and its consequent transformation into hydroxyl and carboxyl groups only occurs for the PET-m sample and not for the RPET-u sample. This fact is related to the catalytic reactions of the degraded marine PET litter sample.

The PET-m sample, therefore, seemed to be sensitive to degradation during thermo-mechanical processing. Under temperature and torque conditions generated in the extrusion, chain scission resulted in polymer radicals with hydroxyl and carboxyl groups [1]. In the same way, as observed by FTIR, crystallinity increases for degraded samples, as chain cleavage seems to favor the ordering of the molecular structure [22].

4.3.4. DSC

The thermal behavior of the recycled PET samples was studied by DSC, evaluating transition temperatures (T_g , T_m) and the degree of crystallinity. Figure 4.5 shows the thermograms for all samples.

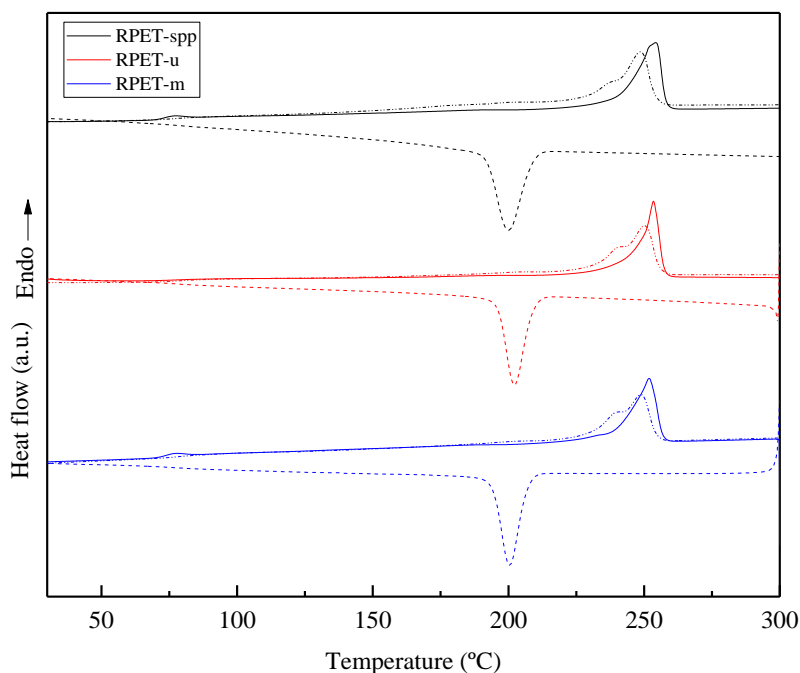


Figure 4.5. DSC thermograms of RPET-ssp, RPET-u and RPET-m samples. First heating scan (—), cooling scan (-----) and second heating scan (-----).

The values obtained from DSC analysis are summarized in Table 4.3. As it can be seen in the first heating scan, the T_m for RPET-ssp and RPET-u samples is around 254 °C, while for RPET-m is slightly lower. In general, as the viscosity and molar mass decrease due to chain scission, the T_m decreases [26].

		RPET-ssp	RPET-u	RPET-m
1 st heating scan	T_g (°C)	73	82	73
	T_m (°C)	254	254	252
	ΔH_m (J/g)	42	37	39
	X_c (%)	31	27	29
Cooling scan	T_c (°C)	200	203	201
	ΔH_c (J/g)	50	39	53
	X_c (%)	37	29	39
2 nd heating scan	T_g (°C)	78	79	78
	T_m (°C)	248	250	249
	ΔH_m (J/g)	38	36	46
	X_c (%)	28	26	34

Table 4.3. DSC results of RPET samples.

On the other hand, analyzing crystallinity values, RPET-m sample shows slightly higher crystallinity than RPET-u, but lower than RPET-ssp sample. More degraded PET samples may

present a higher crystallinity, as the thermal process provokes chain excision and increases crystallinity [27], so degraded samples may have a faster crystallization rate and a more perfect crystalline structure [26].

Furthermore, comparing cooling and second heating scans with the first one, an increase in the crystallinity value of RPET-m is observed, while the other two samples show lower value. As mentioned above, this could be related to the faster autocatalytic degradation of the marine sample occurring during DSC analysis study [1,9,11]. As the samples are subjected to elevated temperatures, degradation of materials may occur, generating a greater chain scission, which will increase their mobility and therefore, crystallinity [16].

So, it was confirmed that the degradation occurring during the thermo-mechanical processing and during DSC analysis also affected the crystallinity, since due to the chain scission the mobility is higher, leading to a faster rearrangement that increases the crystalline fraction [16,28].

4.3.5. TGA

The thermal stability of recycled samples was also analyzed. Figure 4.6 shows the weight evolution with temperature and DTG curves. A main weigh loss attributed to the degradation of PET polymer, that can be seen at the minimum of the peak (T_d), is observed at 434 °C for all samples, with a 76 % loss [29].

As shown in Figure 4.6b, RPET-m samples started to degrade at a slightly lower temperature. Therefore, the lower thermal stability observed for RPET-m could be attributed to the shorter polymeric chains created by degradation [30]. Moreover, a small second weight loss, of less than 5 %, is observed for all the samples and could be related to the decomposition of unstable char [31].

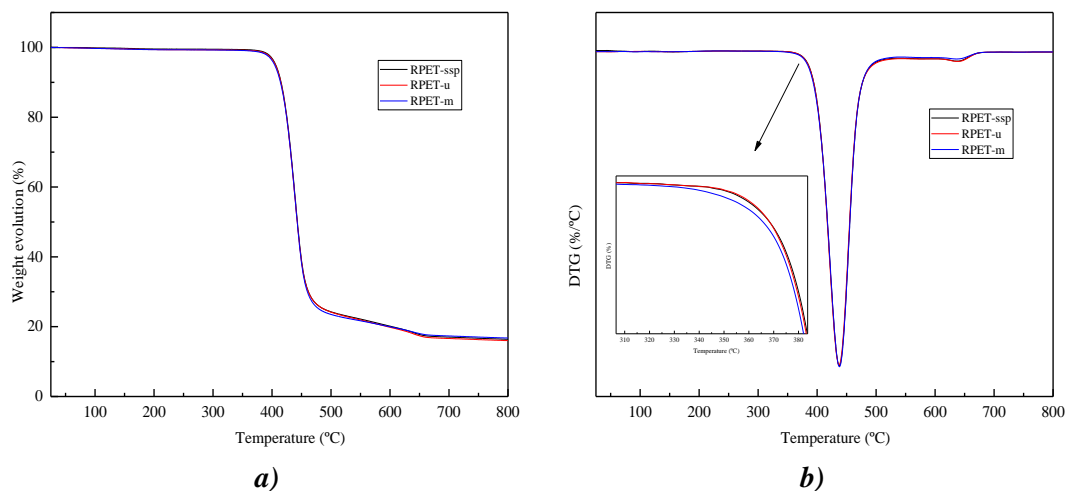


Figure 4.6. Weight evolution **a)** and DTG **b)** curves for RPET samples.

4.3.6. WCA

WCA values are related with the hydrophilicity of a sample, and can be useful in the study of sample degradation during thermo-mechanical recycling. To perform this analysis, each sample was compressed with a Santec 30 hydraulic press at 58 bar and 270 °C for 10 min. Figure 4.7 shows digital images of the thermo-mechanically recycled samples together with the samples obtained after compression. As it can be seen, RPET-m samples, both pellets and compressed, show a browner color compared to the other two samples. Yellowing is also shown for RPET-u samples. This could be related to the thermo-oxidative degradation that samples may have undergone during compression at 270 °C [1], as this degradation pathway is the main responsible for the discoloration during melt-processing [2]. As concluded in Chapter 3, PET-m and PET-u samples are more degraded than PET-ssp samples, making them proner to degradation due to catalytic reaction [1,23,24].



Figure 4.7. From left to right digital images of the compressed (at the top) and thermo-mechanically processed RPET-ssp, RPET-u and RPET-m samples.

The WCA values obtained, together with the images corresponding to the water drop on the samples, are shown in Table 4.4. Similar values were measured for RPET-ssp and RPET-u, 72 ° and 71 °, respectively. However, RPET-m sample shows a significantly lower WCA value of 56 °. Comparing with that of PET-m shown in Chapter 3, the WCA value of RPET-m is 10 ° lower. As previously discussed, the -OH and -COOH groups generated during degradation increased the hydrophilicity, decreasing the contact angle [32]. Therefore, the lower value measured for RPET-m samples corroborated the higher degradation that marine PET litter suffered during the thermo-mechanical processing, in agreement with previous FTIR and DSC results.


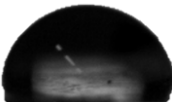
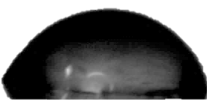
RPET-ssp	RPET-u	RPET-m
Water contact angle (°)		
72 ± 2	71 ± 2	56 ± 3
		

Table 4.4. Water contact angle values for the different RPET samples, together with the corresponding images of water drop over the samples.

Therefore, the characterization performed on the RPET samples confirmed that PET wastes underwent some degradation during the thermo-mechanical processing, especially the PET-m. The higher degradation observed in RPET-m sample is attributed to the chain end groups present at PET-m catalyzing the degradation reactions during processing. Therefore, the obtained RPET-m recycled material obtained presents low quality to be used at industrial level in the manufacture of new PET products.

4.4. Optimization of thermo-mechanical recycling

As it has been observed, RPET-u and RPET-m samples are degraded during the thermo-mechanical processing, specially RPET-m one. However, RPET-u still shows IV values suitable for some application such as textile. For this reason, some parameters or alternatives, such as the temperature control and the development of extrusion of PET-u/PET-m blends have been analyzed, for the valorization of PET-m.

4.4.1. Temperature control

High temperature is a critical parameter for thermal degradation [1,33], so the effect of temperature on the degradation of PET-ssp, PET-u and PET-m samples was studied. Thus, according to the extrusion temperature profile of 255/260/265/270 °C employed, samples were maintained at 250, 260 and 270 °C for 10 and 20 minutes in an oven. Samples were characterized from the viscosity evolution point of view according to values obtained from MFI measurements. Figure 4.8 shows the viscosity determined at different temperatures and times.

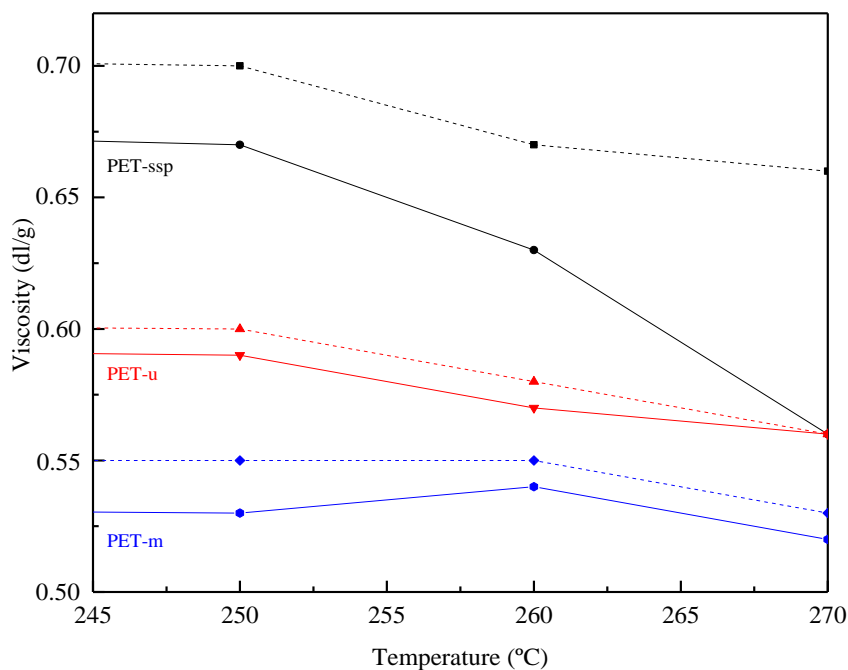


Figure 4.8. Viscosity evolution for PET-ssp, PET-u and PET-m samples with temperature after maintaining 10 (-----) and 20 (——) minutes at each ones.

As it can be seen, viscosity decreased with temperature. In addition, the viscosity decreased more as the exposure time increased. Therefore, the observed decrease in viscosity, confirmed further degradation of the sample as the temperature and exposure time increased [34].

Since in thermo-mechanical processing the degradation rate increases with temperature [35], the samples were processed at the lowest temperature that ensures melting in the extrusion. According to the melting temperatures determined in Chapter 3, a constant temperature of 255 °C was selected. The RPTE samples obtained were characterized, being results summarized in Table 4.5. No significant variations were observed when compared to values reported in Table 4.2. The slight increase in viscosity observed cannot be considered significant.

Samples	MFI (g/10min)	IV (dl/g)	M_n (g/mol)	M_w (g/mol)
RPET-u	101	0.58	23649	35383
RPET-m	146	0.53	20902	30990

Table 4.5. MFI, IV and M_n and M_w values of RPET samples processed at a constant temperature of 255 °C.

Therefore, even if temperature may be a key factor in PET degradation, it does not seem enough to adjust the processing temperature to reduce the thermal degradation and obtain suitable viscosities.

4.4.2. Recycling by extrusion of PET-u/PET-m blends

Blends with different compositions of PET-u and PET-m were prepared: 90u/10m, 80u/20m and 70u/30m (u refers to PET-u and m to PET-m) at 255 °C. The aim is to process as much PET-m as possible in the blends, for obtaining a material that fulfills industrial requirements. Figure 4.9 shows different recycled RPET formulations.



Figure 4.9. RPET blends with different compositions, from left to right 90u/10m, 80u/20m and 70u/30m.

As it can be seen, the color of samples becomes browner as PET-m content increases. As PET-m is the most degraded waste, during processing is further degraded, coloring the recycled sample as mentioned above [1,3], and as confirmed by spectrophotometry analysis. Table 4.6 summarizes the obtained color parameters. As it can be seen, the L^* (light-darkness) value decreases as the marine PET litter content in the extruded samples increases. The color differences (ΔE^*) and whiteness index (WI) increase and decrease, respectively, for samples with higher PET-m content.

Samples	L^*	a^*	b^*	ΔE^*	WI
90u/10m	69.2	1.5	11.5	23.3	67.1
RPET 80u/20m	64.0	1.8	11.7	28.2	62.1
70u/30m	58.6	1.5	15.5	34.6	55.8

Table 4.6. Color parameter values of RPET blends with different compositions.

The MFI and intrinsic viscosity values obtained along with M_n and M_w ones are summarized in Table 4.7. It is observed that the incorporation of PET-m to the blend decreases considerably the viscosity value for all samples when compared to RPET-u one in Table 4.5, and, as it was previously reported, could be attributed to the autocatalytic degradation of PET-m sample [23,24]. However, unexpectedly, a higher viscosity is observed for RPET 80u/20m sample compared to the rest. Comparing with the results for RPET-u and RPET-m in Table 4.5, a considerable decrease is observed for blend samples, due to the incorporation of a more degraded PET-m.

Samples	MFI	IV	M_n	M_w
	(g/10min)	(dl/g)	(g/mol)	(g/mol)
90u/10m	163 ± 12	0.52 ± 0.01	20139 ± 722	29779 ± 1146
80u/20m	130 ± 13	0.55 ± 0.02	21779 ± 1013	32389 ± 1617
70u/30m	176 ± 6	0.51 ± 0.01	19602 ± 338	28927 ± 535

Table 4.7. MFI, IV, M_n and M_w values of RPET blends with different compositions.

Similarly, the FTIR study shows that the intensity of -OH groups is higher for RPET 70u/30m sample (Figure 4.10a), attributed to the chain scission caused by the thermo-oxidative degradation.

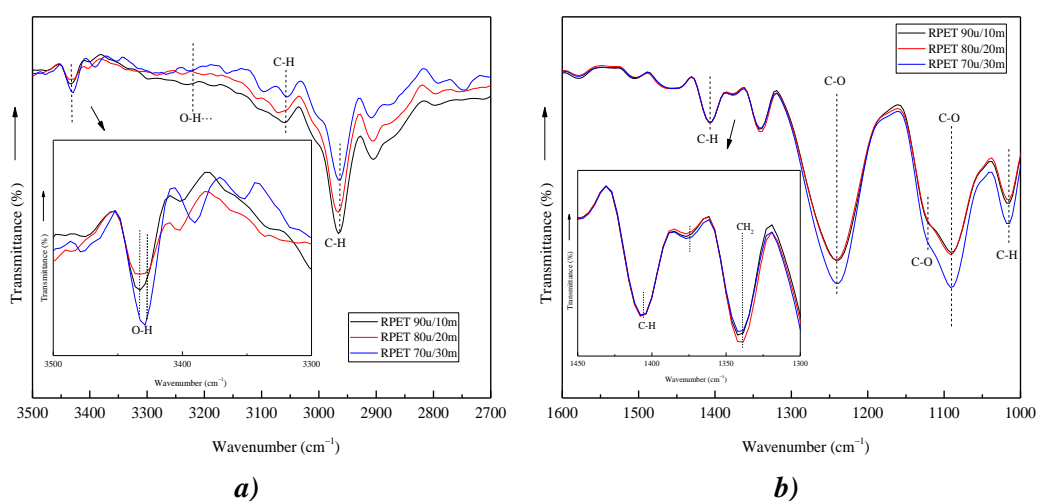


Figure 4.10. FTIR spectra for different formulations of RPET blends with different intervals: **a)** $3500\text{-}270\text{ cm}^{-1}$ and **b)** $1600\text{-}1000\text{ cm}^{-1}$.

Finally, in Figure 4.10.b can be seen that bands at 1238 cm^{-1} and 1091 cm^{-1} related to ester C-O considerably increased for the sample with highest PET-m content, RPET 70u/30m. However, all RPET samples show a shoulder at 1120 cm^{-1} , which was attributed to *trans* (crystalline) EG [18,19]. This shoulder appeared after PET-m recycling as already seen in Figure 4.3d, so it seems reasonable to appear in extruded samples with different composition of marine and urban samples. In addition, the band attributed to in-plane bending of C-H bond in the benzene ring at 1015 cm^{-1} , increases slightly for RPET 70u/30m comparing with the other two blends. This band was found to increase with crystallinity [19,20], so it can be deduced that the sample with the highest content of marine PET litter is the most degraded one, due the shorter chains of PET-m that favor the ordering of the molecular structure [22].

Finally, degradation and formation of -OH and -COOH groups were confirmed by surface hydrophilicity. For this purpose, plaques of the samples were prepared as described at 4.3.6 section and the contact angle was measured at several points. According to the previous results,

WCA values decrease with degradation, the angle decreasing with PET-m content, as it can be seen in Table 4.8. The higher the content of -OH and -COOH groups, the lower the contact angle, as the sample becomes more hydrophilic [32]. Comparing the results of WCA value of the blend with those of RPET-u and RPET-m samples in Table 4.4, a drastic reduction is observed. Only with 10 % of PET-m the WCA decreases from 71° (RPET-u) to 64°, as -OH and -COOH groups acted as catalyst promoting further degradations [23,24].



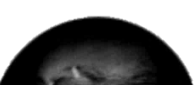
90u/10m	80u/20m	70u/30m
Water contact angle (°)		
64±4	58±3	54±3
		

Table 4.8. WCA results of RPET blends with different compositions.

Thermo-mechanical recycling through extrusion induces thermo-oxidative degradation with chain scission, increasing fluidity and reducing viscosity and molar mass drastically. In addition, highly degraded materials present faster crystallization rate and higher crystallinity, because chain mobility could promote chain ordering [27,28]. In the same way, the functional groups generated by chain scission, -OH and -COOH, increase the hydrophilicity of samples. Moreover, the presence of these functional groups is the cause of the autocatalytic degradation of PET, i.e., the samples degrade more easily in the presence of PET-m because it presents a higher amount of -OH and -COOH groups, as discussed previously in Chapter 3 [23,24]. Therefore, it can be concluded that thermo-mechanical recycling is not a viable option for highly degraded materials as PET-m.

4.5. Energy recovery

Once thermo-mechanical treatment of marine PET litter was discarded, the alternative conventional recycling method for highly degraded and low purity samples is energy recovery [36]. Energy generation by combustion is carried out with PET as fuel, taking advantage of its hydrocarbonated nature, obtaining carbon dioxide and water as products, releasing energy in the process [37]. The main advantage of this method is the absence of compositional or quality restrictions of the employed PET [38].

To determine the energy that PET samples can release, it was measured using calorimetry and higher heating values (HHV) are obtained. To determine the lower heating value (LHV), Equation 4.1 was used, based on the literature [39]. The HHV and LHV values are summarized in Table 4.9, along with the weight percent moisture (W) and weight of hydrogen in the samples (H),

employed in Equation 4.1. In the literature, LHV values around 22.1 MJ/kg are reported for commercial PET in agreement with the values obtained for PET-ssp samples [40]. As it can be concluded, all samples present similar calorific values. Therefore, it cannot be confirmed that degradation affects the energy obtained from the combustion of the PET samples. All LHV values are in the range of values found in the literature [41,42].

$$LHV = HHV - 24.54(W + 9H) \quad \text{(Equation 4.1)}$$

Samples	HHV (MJ/kg)	W (%)	H (%)	LHV (MJ/kg)
PET-ssp	23.1 ± 0.4	1.03	4.2	22.2 ± 0.5
PET-u	22.9 ± 0.1	1.05	4.3	21.9 ± 0.2
PET-m	22.8 ± 0.0	1.08	4.3	21.8 ± 0.1

Table 4.9. Values of heat combustion of PET samples.

Therefore, it could be concluded that energy recovery could be an alternative way for highly degraded PET samples such as marine PET litter.

4.6. Conclusion

It has been found that thermo-mechanical recycling is not suitable for degraded samples such as PET-m. The high extrusion temperature leads to a faster degradation of the material, due to the autocatalytic reactions occurring during processing of PET-m [23,24]. It was seen that the extruded PET-m samples underwent some degradation during processing as a browner color related to thermo-oxidative degradation was appreciated. This color difference was analyzed with spectrophotometry, confirming that L* and WI parameters, related with lightness-darkness and whiteness index respectively, decreased significantly, making these samples less reflective and darker. The molar mass and viscosity values obtained for the RPET-m samples are not enough for using as raw material in industry. In addition, it was confirmed by FTIR that during thermo-mechanical recycling the RPET-m sample suffered degradation, as the band of the stretching vibration attributed to -OH groups increased, indicating that chain scission occurred and a higher amount of end groups were formed due to degradation [14,25]. Furthermore, the presence of -COOH and -OH end groups was also confirmed by the WCA, as marine samples present higher hydrophilicity as a result of these functional groups, considerably reducing the WCA.

Besides, FTIR and DSC confirmed that degradation also affected the crystallinity, as due to chain scission the mobility is higher, leading to a chain rearrangement that increases the crystalline fraction in RPET-m samples [12,16,28]. Moreover, the shorter polymer chain of the degraded

samples is confirmed by TGA, where the weight loss started at lower temperatures for the RPET-m samples [30].

Taking into account that temperature affects the degradation of the product, the extrusion temperature was lowered. However, no significant differences were observed. Although different PET-u/PET-m blends were studied for thermo-mechanical recycling, the desired results were not obtained. It was clearly observed that as PET-m content increases in blends, the product darkened considerably due to thermo-oxidative degradation [1,2]. The presence of -COOH and -OH groups in the RPTE samples obtained from PET-u and PET-m blend was also confirmed by both FTIR and WCA, corroborating the autocatalytic reactions of samples in the presence of PET-m.

Once thermo-mechanical recycling was ruled out for the highly degraded samples, the other conventional valorization method of energy recovery was analyzed. Obtained values are in the range of those found in the literature, so this method could be suitable for PET-m sample. Even so, combustion of PET seems not to be the best option from an environmental and ecological point of view, so a more environmentally friendly recycling route, chemical recycling, is studied in the next chapter.

4.7. References

- [1] F. Masmoudi, F. Fenouillot, A. Mehri, M. Jaziri, E. Ammar, Characterization and quality assessment of recycled post-consumption poly(ethylene terephthalate) (PET), *Environ Sci Pollut Res.* 25 (2018) 23307–23314. <https://doi.org/10.1007/s11356-018-2390-7>.
- [2] C.F.L. Ciolacu, N. Roy Choudhury, N.K. Dutta, Colour formation in poly(ethylene terephthalate) during melt processing, *Polym Degrad Stab.* 91 (2006) 875–885. <https://doi.org/10.1016/j.polymdegradstab.2005.06.021>.
- [3] D. Berg, K. Schaefer, A. Koerner, R. Kaufmann, W. Tillmann, M. Moeller, Reasons for the discoloration of postconsumer poly(ethylene terephthalate) during reprocessing, *Macromol Mater Eng.* 301 (2016) 1454–1467. <https://doi.org/10.1002/mame.201600313>.
- [4] T.E. Long, J. Scheirs, *Modern polyesters: chemistry and technology of polyesters and copolyesters*, John Wiley & Sons., 2005.
- [5] U.K. Thiele, The current status of catalysis and catalyst development for the industrial process of poly(ethylene terephthalate) polycondensation, *Int J Polym Mater.* 50 (2001) 387–394. <https://doi.org/10.1080/00914030108035115>.
- [6] S. Altun, Y. Ulcay, Improvement of waste recycling in PET fiber production, *Express Polym Lett.* 10 (2016) 559–586. <https://doi.org/DOI: 10.3144/expresspolymlett.2016.53>.

- [7] F. Welle, Twenty years of PET bottle to bottle recycling - An overview, *Resour Conserv Recycl.* 55 (2011) 865–875. <https://doi.org/10.1016/j.resconrec.2011.04.009>.
- [8] L.K. Nait-Ali, X. Colin, A. Bergeret, Kinetic analysis and modelling of PET macromolecular changes during its mechanical recycling by extrusion, *Polym Degrad Stab.* 96 (2011) 236–246. <https://doi.org/10.1016/j.polymdegradstab.2010.11.004>.
- [9] H. Zimmerman, N.T. Kim, Investigations on thermal and hydrolytic degradation of poly(ethyleneterephthalate), *Polym Eng Sci.* 20 (1980) 680–683. <https://doi.org/10.1002/pen.760201008>
- [10] B. Gewert, M.M. Plassmann, M. Macleod, Pathways for degradation of plastic polymers floating in the marine environment, *Environ Sci Process Impacts.* 17 (2015) 1513–1521. <https://doi.org/10.1039/c5em00207a>.
- [11] H. Zhang, I.M. Ward, Kinetics of hydrolytic degradation of poly(ethylene naphthalene-2,6-dicarboxylate), *Macromolecules.* 28 (1995) 7622–7629. <https://doi.org/10.1021/ma00127a006>
- [12] I. Donelli, P. Taddei, P.F. Smet, D. Poelman, V.A. Nierstrasz, G. Freddi, Enzymatic surface modification and functionalization of PET: A water contact angle, FTIR, and fluorescence spectroscopy study, *Biotechnol Bioeng.* 103 (2009) 845–856. <https://doi.org/10.1002/bit.22316>.
- [13] K.C. Cole, J. Guevremont, A. Aji, M.M. Dumoulin, Characterization of surface orientation in poly(ethylene terephthalate) by front-surface reflection infrared spectroscopy, *Appl Spectrosc.* 48 (1994) 1513–1521. <https://doi.org/0003-7028/94/4812-151352.0>.
- [14] B.J. Holland, J.N. Hay, The thermal degradation of PET and analogous polyesters measured by thermal analysis–Fourier transform infrared spectroscopy, *Polymer (Guildf).* 43 (2002) 1835–1847. [https://doi.org/10.1016/S0032-3861\(01\)00775-3](https://doi.org/10.1016/S0032-3861(01)00775-3).
- [15] M. Edge, R. Wiles, N.S. Allen, W.A. McDonald, S. v Mortlock, Characterisation of the species responsible for yellowing in melt degraded aromatic polyesters—I: Yellowing of poly(ethylene terephthalate), *Polym Degrad Stab.* 53 (1996) 141–151.
- [16] A. Ruvolo-Filho, P.S. Curti, PET recycled and processed from flakes with different amount of water uptake: characterization by DSC, TG, and FTIR-ATR, *J Mater Sci.* 43 (2008) 1406–1420. <https://doi.org/10.1007/s10853-007-2282-6>.
- [17] C. Ioakeimidis, K.N. Fotopoulou, H.K. Karapanagioti, M. Geraga, C. Zeri, E. Papatheodorou, F. Galgani, G. Papatheodorou, The degradation potential of PET bottles

- in the marine environment: An ATR-FTIR based approach, *Sci Rep.* 6 (2016) 1–8. <https://doi.org/10.1038/srep23501>.
- [18] F. Dubelley, E. Planes, C. Bas, E. Pons, B. Yrieix, L. Flandin, The hygrothermal degradation of PET in laminated multilayer, *Eur Polym J.* 87 (2017) 1–13. <https://doi.org/10.1016/J.EURPOLYMJ.2016.12.004>.
- [19] K.C. Cole, A. Ajji, É. Pellerin, New insights into the development of ordered structure in poly(ethylene terephthalate). Results from external reflection infrared spectroscopy, *Macromolecules.* 35 (2002) 770–784. <https://doi.org/10.1021/ma011492i>.
- [20] M. Bertoldo, M. Labardi, C. Rotella, S. Capaccioli, Enhanced crystallization kinetics in poly(ethylene terephthalate) thin films evidenced by infrared spectroscopy, *Polymer (Guildf).* 51 (2010) 3660–3668. <https://doi.org/10.1016/J.POLYMER.2010.05.040>.
- [21] F. Dieval, F. Khoffi, R. Mir, W. Chaouch, D. le Nouen, N. Chakfe, B. Durand, Long-term biostability of PET vascular prostheses, *Int J Polym Sci.* 2012 (2012) 1–14. <https://doi.org/10.1155/2012/646578>.
- [22] M. Abbasi, M.R.M. Mojtahedi, A. Khosroshahi, Effect of spinning speed on the structure and physical properties of filament yarns produced from used PET bottles, *J Appl Polym Sci.* 103 (2007) 3972–3975. <https://doi.org/10.1002/app.25369>.
- [23] H. Fashandi, A. Zadhoush, M. Haghghat, Effect of orientation and crystallinity on the photodegradation of poly(ethylene terephthalate) fibers, *Polym Eng Sci.* 48 (2008) 949–956. <https://doi.org/10.1002/pen.21043>.
- [24] G.J.M. Fechine, M.S. Rabello, R.M. Souto Maior, L.H. Catalani, Surface characterization of photodegraded poly(ethylene terephthalate). The effect of ultraviolet absorbers, *Polymer (Guildf).* 45 (2004) 2303–2308. <https://doi.org/10.1016/j.polymer.2004.02.003>.
- [25] C. Sammon, J. Yarwood, N. Everall, An FT-IR study of the effect of hydrolytic degradation on the structure of thin PET films, *Polym Degrad Stab.* 67 (2000) 149–158. [https://doi.org/10.1016/S0141-3910\(99\)00104-4](https://doi.org/10.1016/S0141-3910(99)00104-4).
- [26] F. Awaja, D. Pavel, Recycling of PET, *Eur Polym J.* 41 (2005) 1453–1477. <https://doi.org/10.1016/j.eurpolymj.2005.02.005>.
- [27] A. Oromiehie, A. Mamizadeh, Recycling PET beverage bottles and improving properties, *Polym Int.* 53 (2004) 728–732. <https://doi.org/10.1002/pi.1389>.
- [28] D.-M. Fann, S.K. Huanc, J.-Y. Lee, Kinetics and thermal crystallinity of recycled PET. II. topographic study on thermal crystallinity of the injection-molded recycled PET, *J Appl*

- Polym Sci. 61 (1996) 261–271. [https://doi.org/https://doi.org/10.1002/\(SICI\)1097-4628\(19960711\)61:2<261::AID-APP8>3.0.CO;2-N](https://doi.org/https://doi.org/10.1002/(SICI)1097-4628(19960711)61:2<261::AID-APP8>3.0.CO;2-N).
- [29] N. Dimitrov, L. Kratofil Krehula, A. Ptiček Siročić, Z. Hrnjak-Murđić, Analysis of recycled PET bottles products by pyrolysis-gas chromatography, *Polym Degrad Stab.* 98 (2013) 972–979. <https://doi.org/10.1016/j.polymdegradstab.2013.02.013>.
- [30] E.J. Velásquez, L. Garrido, A. Guarda, M.J. Galotto, C. López de Dicastillo, Increasing the incorporation of recycled PET on polymeric blends through the reinforcement with commercial nanoclays, *Appl Clay Sci.* 180 (2019) 105185–10593. <https://doi.org/10.1016/j.clay.2019.105185>.
- [31] Y. Fang, X. Liu, X. Tao, Intumescent flame retardant and anti-dripping of PET fabrics through layer-by-layer assembly of chitosan and ammonium polyphosphate, *Prog Org Coat.* 134 (2019) 162–168. <https://doi.org/10.1016/j.porgcoat.2019.05.010>.
- [32] H.R. Kim, W.S. Song, Lipase treatment of polyester fabrics, *Fibers Polym.* 7 (2006) 339–343. <https://doi.org/10.1007/BF02875764>.
- [33] M. Dzie, J. Trzeszczyn, Studies of temperature influence on volatile thermal degradation products of poly(ethylene terephthalate), *J Appl Polym Sci.* 69 (1998), 2377–2381. [https://doi.org/10.1002/\(SICI\)1097-4628\(19980919\)69:12<2377::AID-APP9>3.0.CO;2-5](https://doi.org/10.1002/(SICI)1097-4628(19980919)69:12<2377::AID-APP9>3.0.CO;2-5).
- [34] S. Tate, H. Narusawa, Thermal degradation and melt viscosity of ultra-high-molecular-weight poly(ethylene terephthalate), 1996.
- [35] E. Pirzadeh, A. Zadhoush, M. Haghghat, Hydrolytic and thermal degradation of PET fibers and PET granule: The effects of crystallization, temperature, and humidity, *J Appl Polym Sci.* 106 (2007) 1544–1549. <https://doi.org/10.1002/app.26788>.
- [36] R. Nisticò, Polyethylene terephthalate (PET) in the packaging industry, *Polym Test.* 90 (2020) 106707–10625. <https://doi.org/10.1016/j.polymertesting.2020.106707>.
- [37] C. Peña-Rodríguez, G. Mondragon, A. Mendoza, E. Mendiburu-Valor, A. Eceiza, G. Kortaberria, Recycling of marine plastic debris, in: *Recent Developments in Plastic Recycling*. Springer, 2021: pp. 121–141. https://doi.org/10.1007/978-981-16-3627-1_6.
- [38] T. Chilton, S. Burnley, S. Nesaratnam, A life cycle assessment of the closed-loop recycling and thermal recovery of post-consumer PET, *Resour Conserv Recycl.* 54 (2010) 1241–1249. <https://doi.org/10.1016/j.resconrec.2010.04.002>.

- [39] U.S. Environmental Protection Agency, Methodology for thermal efficiency and energy input calculations and analysis of biomass cogeneration unit characteristics, (2007). https://www3.epa.gov/ttn/atw/utility/fnl_biomass_cogen_TSD_04_19_07.pdf (accessed June 30, 2022).
- [40] P. Kannan, A. al Shoaibi, C. Srinivasakannan, Energy recovery from co-gasification of waste polyethylene and polyethylene terephthalate blends, *Comput Fluids*. 88 (2013) 38–42. <https://doi.org/10.1016/j.compfluid.2013.09.004>.
- [41] L. Zhao, A. Giannis, W.Y. Lam, S.X. Lin, K. Yin, G.A. Yuan, J.Y. Wang, Characterization of Singapore RDF resources and analysis of their heating value, *Sustainable Environ Res*. 26 (2016) 51–54. <https://doi.org/10.1016/j.serj.2015.09.003>.
- [42] J. Chattopadhyay, T.S. Pathak, R. Srivastava, A.C. Singh, Catalytic co-pyrolysis of paper biomass and plastic mixtures HDPE (high density polyethylene), PP (polypropylene) and PET (polyethylene terephthalate) and product analysis, *Energy*. 103 (2016) 513–521. <https://doi.org/10.1016/j.energy.2016.03.015>.

Chapter 5

CHEMICAL RECYCLING

5. CHEMICAL RECYCLING

5.1. Aim of the chapter

The critical effect of waste degradation on the properties of materials recycled by thermo-mechanical processing was discussed in Chapter 4. In the present chapter, the chemical recycling of PET samples by glycolysis is evaluated, as it could be a good alternative for recycling degraded PET waste, such as marine litter.

For this study, virgin PET (PET-v) was employed as reference sample in the glycolysis reaction using EG as a reagent in a PET:EG ratio of 1:3. The glycolysis reaction was carried out at 220 °C for 3 h and the final product was characterized by different techniques such as FTIR, DSC, TGA and GPC. In addition, in order to optimize the glycolysis yield and to reduce the energy consumption of the process, kinetics studies were performed. The glycolyzed product obtained at different reaction times of 10, 20, 30, 40, 50, 60, 90 and 180 min was characterized.

Similarly, the effect of the glycolysis reaction temperature was analyzed. For this purpose, the glycolysis was carried out in a closed reactor at different temperatures (180, 220 and 220 °C) and times (30, 60, 90 and 180 min). The glycolyzed product obtained in each reaction was characterized by FTIR, DSC, TGA and GPC.

Finally, the effect of raw PET degradation on the depolymerization reaction was analyzed. In this context, glycolysis of different PET samples was carried out under the previously optimized reaction conditions. Concretely, the commercial PET-v and PET-ssp virgin samples and the municipal PET waste, PET-u, and marine PET litter, PET-m, characterized in Chapter 3 were selected. The composition of glycolyzed products obtained after each reaction was characterized in order to identify the effect of PET degradation on the depolymerization reaction.

5.2. Glycolysis reaction

The glycolysis reactions were carried out in a closed mini reactor (Parr 5500 HPCL reactor) equipped with a thermometer, a manometer and a mechanical stirrer, at 220 °C. Mechanical stirring was kept constant at 1000-1200 rpm. A PET:EG weight ratio of 1:3 (40 g PET, 120 g EG) was used, with 1% mass of zinc acetate as catalyst. The working volume was approximately of 160 mL. The pre-heating time was variable between 30-45 min, and after that the reaction was carried out for 3 h. During reaction, a pressure of 3 bar was kept inside the reactor. The reactor used in this work is shown in Figure 5.1.



Figure 5.1. Closed mini reactor used for the glycolysis.

At the end of each reaction, the obtained liquid mixture was identified as the glycolysis reaction product (GRP). The unreacted PET and high molar mass oligomers are insoluble in THF (insoluble fraction, IF) and were separated from THF soluble BHET monomer, dimers or low molar mass oligomers of BHET and glycols by filtration in THF. On the other hand, the glycolyzed product (G) was also recovered by filtration. For this purpose, an excess of hot water (heated in a microwave) was added to GRP to solve BHET monomer, dimer and oligomers [1]. Then samples were cooled to room temperature and left for 24 h, for being then stored in a refrigerator for 15 min at 4 °C to induce the precipitation of white crystals of BHET monomer and other oligomeric fractions [2]. Both the insoluble fraction (IF) and the glycolyzed fractions (G) were isolated by vacuum filtration using glass micro-fiber filters with pore diameters of 0.7 and 1.2 μm , respectively. Finally, filtered products were dried under vacuum at 50 °C for 24 h. The process is summarized in Figure 5.2, with two distinct steps, glycolysis and purification.

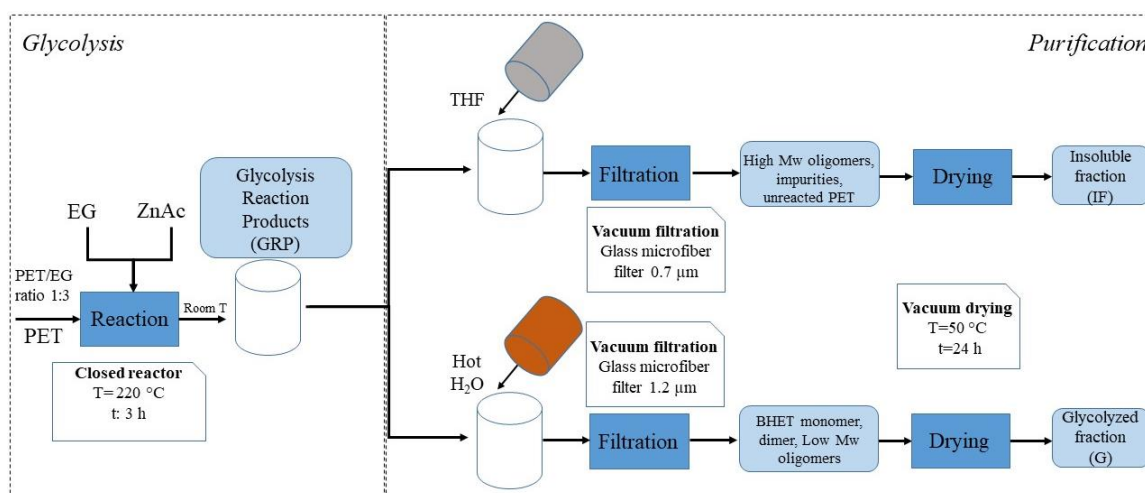


Figure 5.2. PET glycolysis reaction and products purification before characterization.

The yield (η) for BHET was calculated by weight difference, as shown in the following equation:

$$\eta(\%) = \frac{W_{\text{BHET},f}/M_{\text{W}_{\text{BHET}}}}{W_{\text{PET},0}/M_{\text{W}_{\text{PET}}}} \times 100 \quad (\text{Equation 5.1})$$

where $W_{\text{PET},0}$ refers to the initial PET weight and $W_{\text{BHET},f}$ to the BHET weight obtained at the end of the process. $M_{\text{W}_{\text{BHET}}}$ and $M_{\text{W}_{\text{PET}}}$ are the molar mass of BHET (254 g/mol) and PET (192 g/mol) repeating units, respectively [1,3].

5.2.1. Characterization of depolymerized BHET

Depolymerization of PET by glycolysis is the reverse of the polycondensation reaction for PET synthesis shown in Chapter 1, Figure 1.13. As a result, the product of glycolysis is a heterogeneous mixture of BHET, dimers and other oligomers. The insoluble fraction (IF) and yield (η) for the PET depolymerization reaction at 220 °C for 3 h were of about 6 and 58 %, respectively. Obtained BHET fraction was characterized by FTIR and GPC (Figure 5.3.).

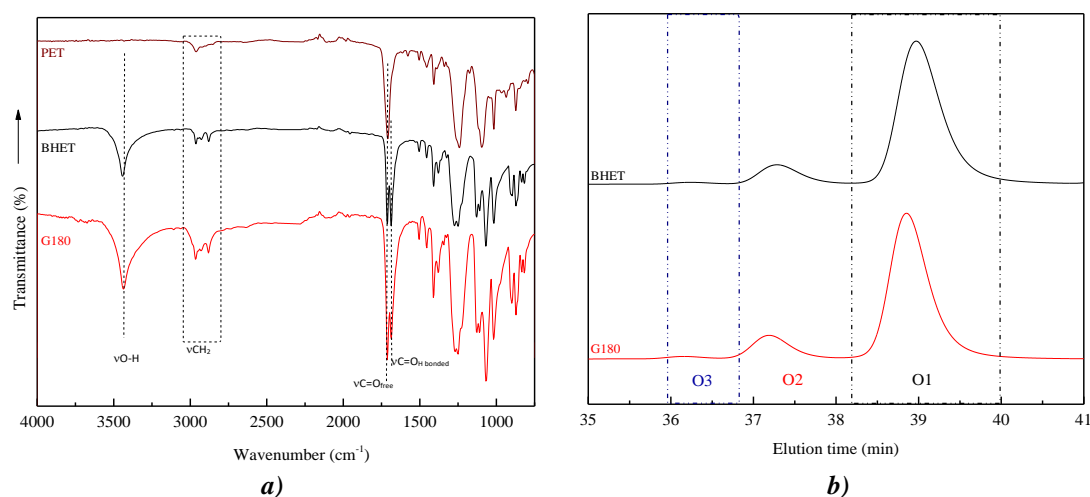


Figure 5.3. **a)** FTIR spectra of G180, commercial BHET and PET and **b)** GPC traces of G180 and commercial BHET.

In Figure 5.3a the FTIR spectra of obtained G180 sample, commercial PET and commercial BHET are compared. As can be seen, the spectrum of G180 sample matches with that of BHET. In both spectra, at the 3600-3200 cm⁻¹ interval, a clear absorption band related to the formation of hydroxyl groups is observed. In addition, the absorption band corresponding to the stretching vibration of ester carbonyl group at 1712 cm⁻¹ shows a double peak in both G180 and BHET samples, while PET sample shows a single peak. On the other hand, the study performed by GPC clearly indicates that G180 sample is mostly BHET monomer.

GPC traces of G180 and commercial BHET show three peaks. The main peak observed, O1, presents a elution time of 39 min, corresponding to a molar mass of 160-171 g/mol (M_w), and is related to BHET monomer [4,5]. O2 and O3 are smaller peaks appearing around 36-38 min, related to BHET oligomers with 2-3 repeating units. O2 fraction corresponds to a molar mass of

362-384 g/mol (M_w), while O3 corresponds to a molar mass of 559-600 g/mol (M_w) [4,5]. Molar mass values are referred to polystyrene standards. Table 5.1 summarizes the content of each fraction. Thus, it can be deduced that after glycolysis reaction and purification the product obtained is almost BHET.

	O1	O2	O3
Samples	$M_n = 155-167$ g/mol	$M_n = 358-379$ g/mol	$M_n = 556-595$ g/mol
	$M_w = 160-171$ g/mol	$M_w = 362-384$ g/mol	$M_w = 559-600$ g/mol
	(%)	(%)	(%)
BHET	87	12	1
G180	86	13	1

Table 5.1. GPC results of commercial BHET and G180.

After confirming that after 3 h of reaction the glycolyzed product obtained is BHET, the reaction kinetics was analyzed by modifying the reaction time and temperature. The objective is to reduce the energy consumption of the process, in order to obtain a more environmentally sustainable process.

5.3. Reaction kinetics

5.3.1. Effect of reaction time on glycolysis

The kinetics of the glycolysis reaction at 220 °C was studied. The reaction products obtained at 8 different reaction times ranging from 10 to 180 min (10, 20, 30, 40, 50, 60, 90 and 180 min) were characterized, following the procedure explained in section 5.2.

Firstly, reagents were added in the reactor in 1:3 ratio (PET:EG) and heated up to the specific temperature, and thereafter the reaction time was quantified. For each reaction time, the reaction was carried out in duplicate and three samples of each reaction product were taken. The insoluble fraction and the average value of the yield were determined and summarized in Table 5.2.

As it can be seen, the obtained IF and yield values do not follow a regular pattern. Similar values were obtained for all reaction times. However, it is worth to note that after only 10 min BHET with a yield of 55 % is obtained. The yield increases during 30 min, obtaining an average yield of 68 %, then decreasing and increasing up to maximum yield at 90 minutes of reaction.

Final product composition was determined by FTIR, DSC, GPC and TGA. Figure 5.4 shows the FTIR spectra of glycolyzed products (G fraction) obtained at different reaction times, as well as those for reference PET and BHET.

Samples	IF (%)	η (%)
G10	5.8	55 \pm 10
G20	8.0	60 \pm 14
G30	7.4	68 \pm 9
G40	5.1	58 \pm 4
650	5.5	63 \pm 6
G60	5.9	63 \pm 3
690	4.0	71 \pm 9
G180	6.4	58 \pm 6

Table 5.2. Insoluble fraction and yield values obtained at 220 °C for different reaction times.

As it can be seen in Figure 5.4a, spectra obtained for different glycolysis times agree with that of BHET. PET depolymerization leads to the formation of -OH groups, as shown in the 3600–3200 cm^{-1} interval, in which a band is also observed for commercial BHET [6]. No significant changes are observed between different materials, inferring that for all reaction times the final product obtained is mainly BHET.

From FTIR spectra at higher magnification, the most representative bands related to the characteristic functional groups are shown (Figure 5.4b). In the 3100-2800 cm^{-1} range, two peaks corresponding to aliphatic (-CH₂-) are found for the G samples, whereas only a single peak is detected at PET spectrum. The presence of the double peak is related to the BHET monomer, while the single peak is related to the presence of BHET oligomers [5], only present for PET samples.

In the same way, the band related to the ester carbonyl group at 1712 cm^{-1} is found for PET as a single peak, while a double peak is detected for the rest of the samples (Figure 5.4c). This second peak is observed at lower wavenumbers and is related to the BHET monomer moiety, while the peak at a higher wavenumbers is related to the oligomers [7]. For this reason, the single peak only appears in PET samples.

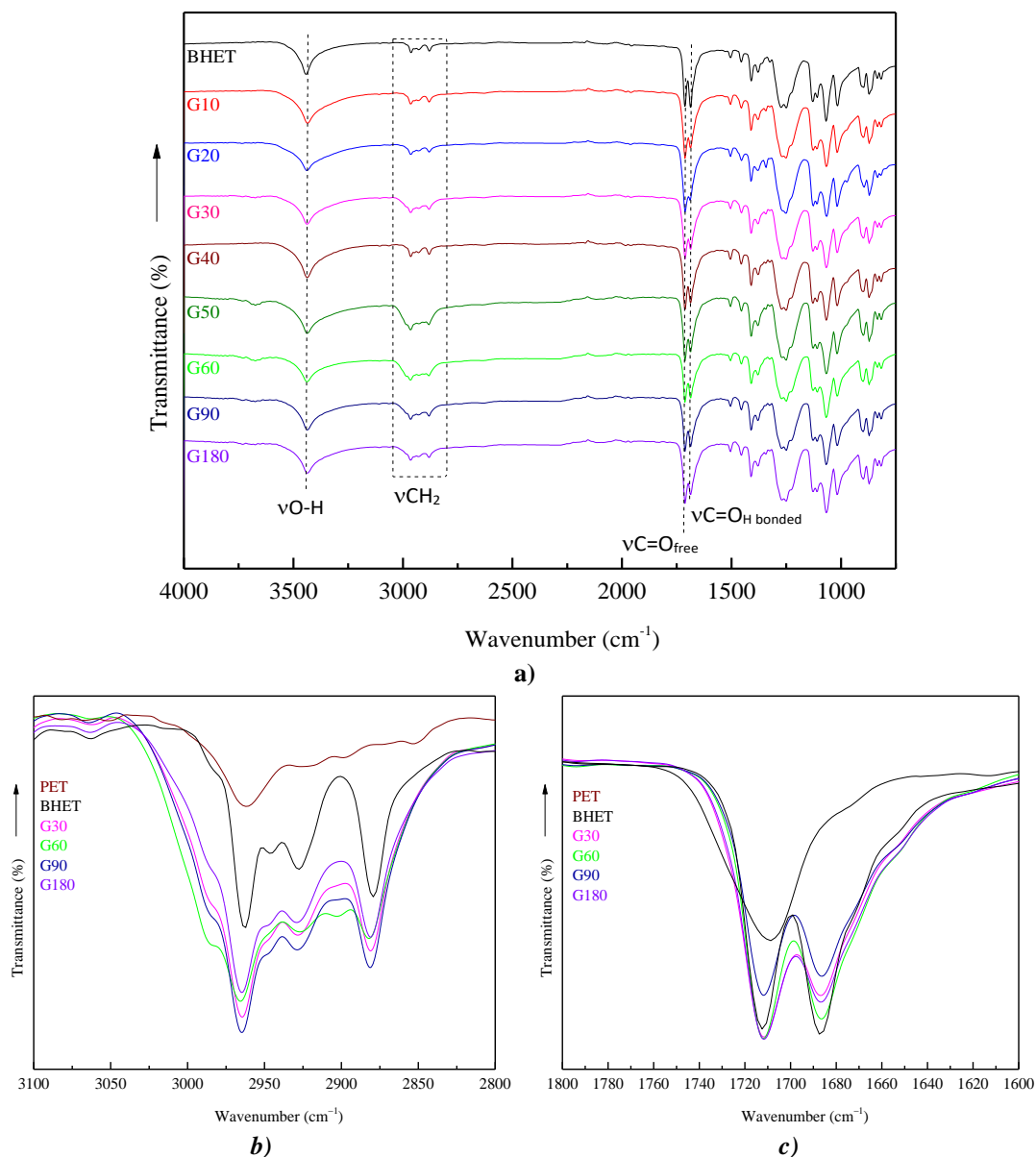


Figure 5.4. FTIR spectra of PET and glycolysis reaction products: **a)** FTIR spectra of products obtained at different reaction times together with that of the reference BHET; **b)** PET, BHET and G products spectra at 3100-2800 cm^{-1} ; **c)** PET, BHET and G products spectra at 1800-1600 cm^{-1} .

The thermal behavior of G samples was studied by DSC. The thermograms of the products obtained at different reaction times can be seen in Figure 5.5, corresponding to a heating scan from 25 to 170 $^{\circ}\text{C}$ at a heating rate of 10 $^{\circ}\text{C}/\text{min}$.

All thermograms show the maximum of the peak corresponding to the melting temperature at around 100-110 $^{\circ}\text{C}$, agreeing with that found for BHET in the literature [4], thus meaning that the product obtained for all reaction times is mainly BHET.

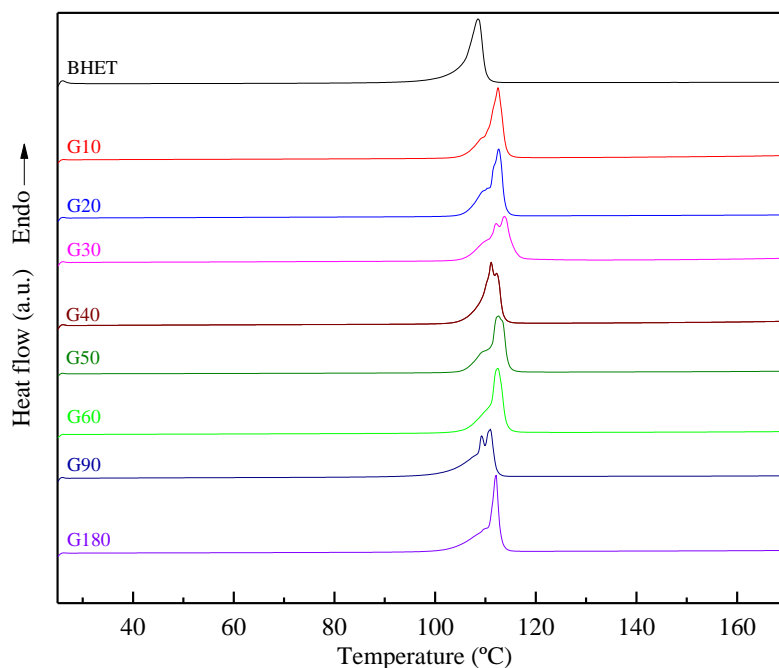


Figure 5.5. DSC thermograms corresponding to the products obtained at different reaction times, together with that of BHET-ref.

The molar mass values for obtained products were measured by GPC. Figure 5.6 shows the GPC traces obtained at different reaction times, together with that corresponding to BHET.

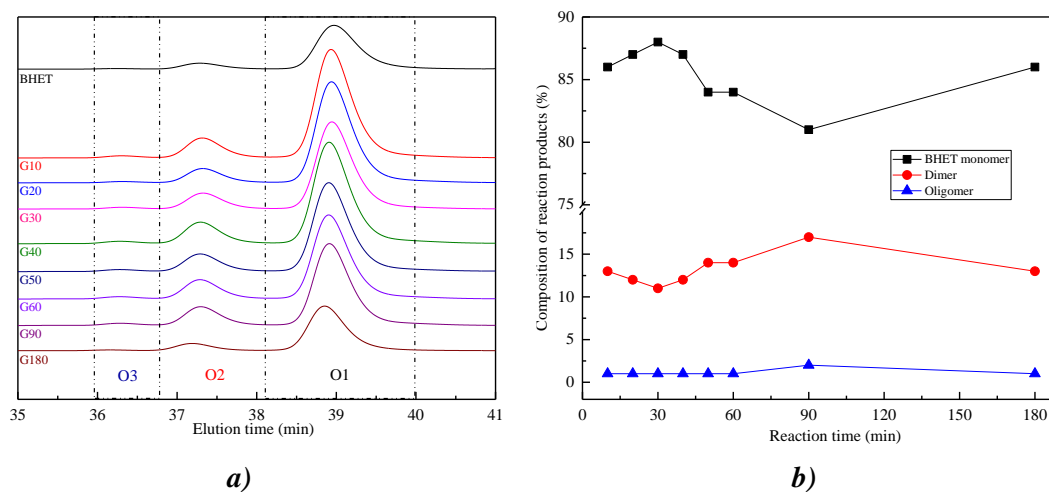


Figure 5.6. GPC results for products obtained at different reaction times: **a)** traces for G samples, together with that of BHET and **b)** evolution of BHET, dimer and oligomer fractions.

The peaks observed at elution times of around 39, 37 and 36 min, denoted as O1, O2 and O3, respectively, are attributed to BHET monomer, dimer and oligomer fractions, respectively [4].

The content of O1, O2 and O3 fractions, determined by integrating the area under the peak, and their corresponding M_w and M_n are summarized in Table 5.3.

Samples	O1	O2	O3
	$M_n = 155\text{--}167$ g/mol	$M_n = 358\text{--}379$ g/mol	$M_n = 556\text{--}595$ g/mol
	$M_w = 160\text{--}171$ g/mol	$M_w = 362\text{--}384$ g/mol	$M_w = 559\text{--}600$ g/mol
	(%)	(%)	(%)
G10	86 ± 3	13 ± 2	1 ± 0
G20	87 ± 0	12 ± 0	1 ± 0
G30	88 ± 6	11 ± 6	1 ± 1
G40	87 ± 5	12 ± 4	1 ± 1
G50	84 ± 3	14 ± 2	1 ± 0
G60	84 ± 7	14 ± 8	1 ± 1
G90	81 ± 1	17 ± 1	2 ± 0
G180	86 ± 2	13 ± 2	1 ± 0

Table 5.3. BHET, dimer and oligomer content (%), together with M_w and M_n values, as obtained by GPC.

For all G samples analyzed, the band corresponding to BHET monomer presents the biggest area, while area of peaks for dimer and oligomer fractions change depending on the samples. However, when the fractions obtained for each reaction time are plotted (Figure 5.6b), it can be seen that the dimer content seems to be quite constant between 10 and 20 % while oligomer fraction is residual. From Table 5.3 can be seen, that the highest amount of BHET monomer is obtained at 30 min of reaction, even though the error is within the values obtained for other reaction times.

The fractions obtained for BHET monomers and dimers do not follow a regular trend. As mentioned before, this is probably related to the fact that PET glycolysis is a reversible reaction, as shown in Figure 5.7 [4]. It seems that PET depolymerization into dimer occurs in a relatively short time interval, depolymerization rate of dimer into BHET constituting an important parameter [4].



Figure 5.7. Reversible PET glycolysis reaction.

Regarding the thermogravimetric analysis of the different glycolyzed fractions, Figure 5.8 shows weight evolution and DTG curves for samples analyzed, while the main parameters are summarized in Table 5.4.

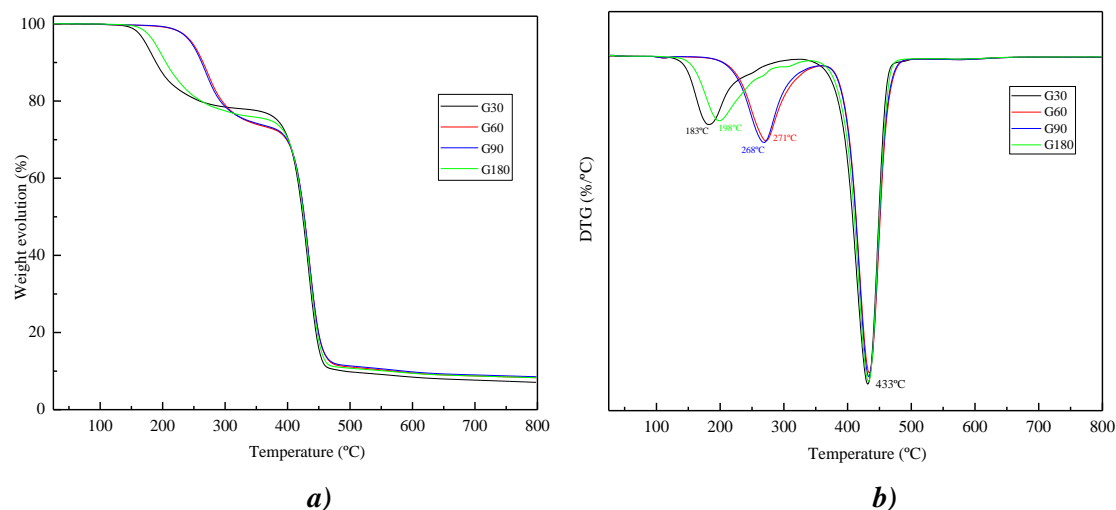


Figure 5.8. Weight evolution **a)** and DTG **b)** curves for samples obtained at different reaction times.

Two main weight losses are observed for all samples (Figure 5.8a). The most important weight loss occurs around 430 °C, constituting about the 65 % of weight loss. This is related to the thermal degradation of PET produced during the thermogravimetric analysis, due to thermal polymerization of BHET [8]. The first weight loss, which constitutes around the 21–27 %, is related to the thermal degradation of monomer and oligomer fractions [8]. As can be observed in Figure 5.8b, G30 and G180 start to degrade at lower temperature than G60 and G90. This fact could be attributed to the evolution of low molar mass dimers or oligomers, as G60 and G90 presented higher dimer fractions as observed in GPC results. Therefore, thermal degradation above 200 °C could be attributed to dimers and low molar mass oligomers, while that at lower temperatures it is related to the monomer [5,6,9].

Samples	1. Step		2. Step	
	T _{d1} (°C)	Weight loss (%)	T _{d2} (°C)	Weight loss (%)
G30	183	23	432	70
G60	271	27	434	64
G90	267	27	433	65
G180	198	24	433	67

Table 5.4. Main parameters obtained by thermogravimetric analysis.

Therefore, from samples characterization it can be concluded that for all the reaction times analyzed between 10 and 180 min, obtained glycolyzed product is mostly BHET monomer. It is also confirmed that the fraction of dimers obtained in the glycolyzed product depends on the reaction conditions, since it is a fast and reversible reaction.

5.3.2. Effect of temperature on the glycolysis reaction

The effect of temperature on glycolysis reaction was also analyzed. Depolymerization reactions were carried out at 180, 200 and 220 °C for 30, 60, 90 and 180 min. Reaction conditions were the same as those explained above. Yields and insoluble fractions for glycolyzed products at different temperatures and reaction times are shown in Figure 5.9.

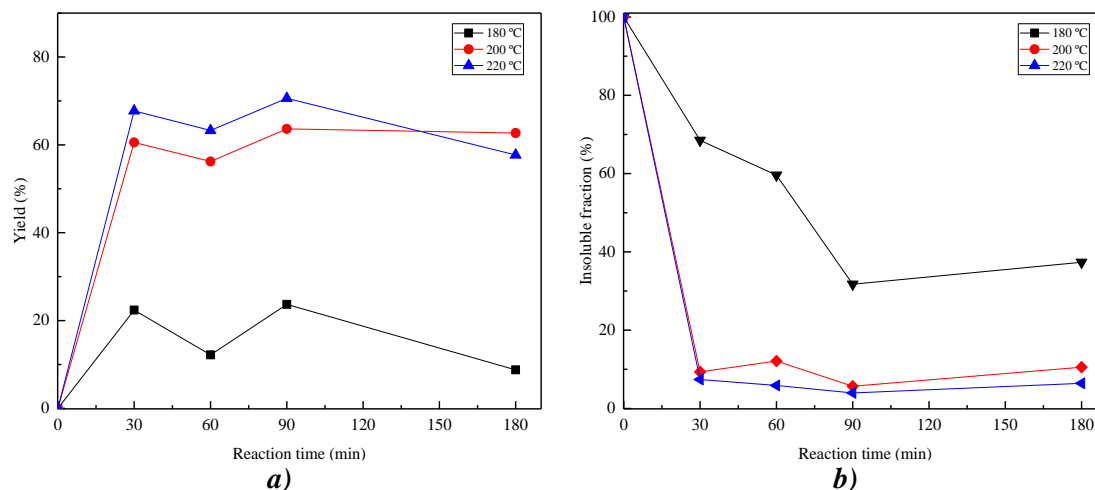


Figure 5.9. **a)** Reaction yield and **b)** insoluble fraction values vs. reaction time at 180, 200 and 220 °C.

A low yield of around 10-25 % was obtained at 180 °C (Figure 5.9a), while for higher temperatures yield increases up to range of 55-70 %. Furthermore, the insoluble fraction is found to be higher than 30 % for all reaction times at low temperatures, while at 200 and 220 °C it does not exceed the 10 % (Figure 5.9b).

As pointed by several authors, at 220 °C the diffusion of glycol through PET is favored, increasing the reaction rate when compared to reactions at lower temperatures [10,11]. Above 30 min BHET yield do not follow a clear trend, as polycondensation reactions are reversible [4]. In fact, the concentrations of monomers, oligomers and polymers reach equilibrium values.

The distribution of reaction products was analyzed by GPC (Figure 5.10). After 60 min at 180 and 200 °C, the dimer fraction, O₂, increases while the monomer content, O₁, decreases. On the other hand, after 90 min, it decreases up to 10 % at 200 °C and increases smoothly at 180 °C.

The behavior is different at 220 °C, in which the maximum value of the O₂ (around 17 %) is obtained after 60 min and the minimum (12 %) at 180 min. Therefore, it can be stated that during glycolysis reaction, polymerization reaction also takes place [4]. It can be also confirmed that for samples at 180 °C, almost pure BHET is obtained, with a negligible dimer fraction at 30 and 60 min.

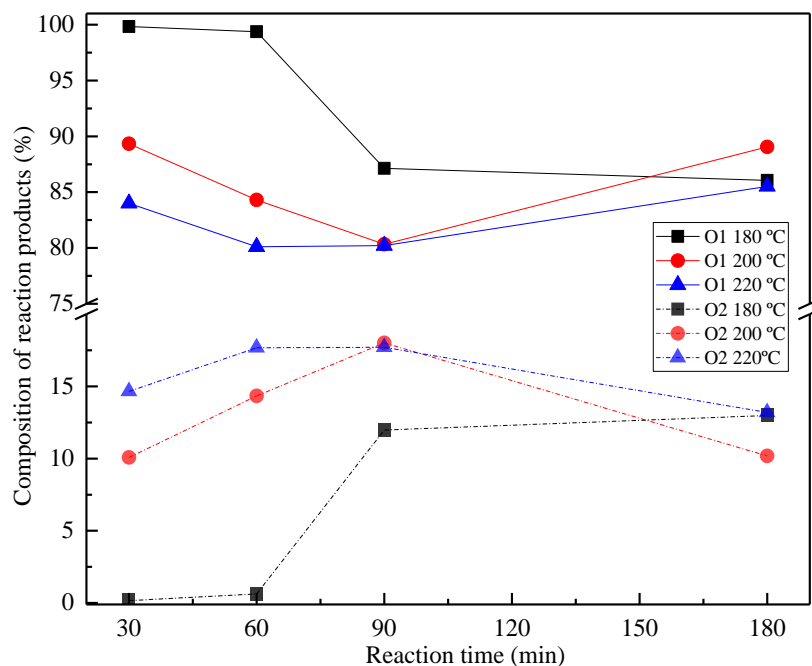


Figure 5.10. BHET monomer (—) and dimer (-----) fraction values of reaction products at different reaction temperatures and times, as obtained by GPC.

From GPC analysis, it can be also concluded that at 180 °C, for lower reaction times, a single peak is observed at 39 min (Figure 5.11), related with the monomer of BHET sample. As reaction progresses, the dimer fraction (at 37.5 min in chromatogram) is higher, confirming that polymerization reactions take place as discussed above.

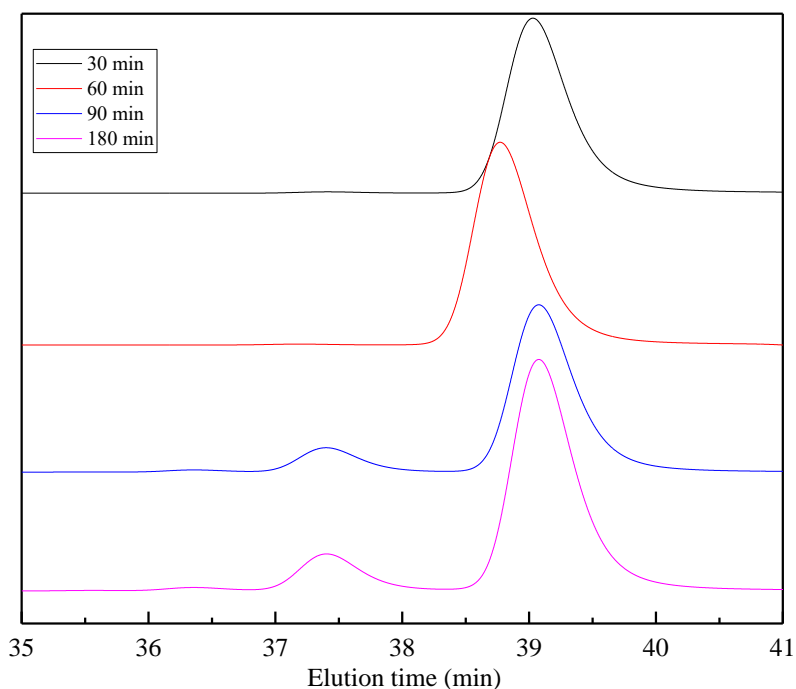


Figure 5.11. GPC results of depolymerization at 180 °C for different reaction times.

5.4. Influence of PET sample degradation on glycolysis

Once the influence of time and temperature variables was studied, the effect of PET raw material degradation on glycolysis kinetics was evaluated. For that purpose, PET depolymerization was carried out for 4 PET samples: two commercial samples (PET-v and PET-ssp) and two wastes, PET-u and PET-m. Those materials were already characterized in Chapter 3.

The glycolysis reaction was carried out in a closed reactor at 220 °C for 30 min, according to results previously obtained. The same amount of sample and the same weight ratio employed in section 5.2 (PET:EG 1:3 and 1 wt.% zinc acetate) were used. After placing all the reagents into the reactor, the 30 min start once the reactor reaches the 220 °C.

Figure 5.12 shows the appearance of glycolysis products after reaction. It can be seen that the most degraded PET-u and PET-m samples presented a darker color, attributed to the coloration observed in PET flakes.



Figure 5.12. Digital image of the glycolysis products obtained from the depolymerization reactions of PET-v, PET-ssp, PET-u and PET-m (from the left to the right).

5.4.1. Characterization of the glycolyzed product obtained from different PET samples

The final glycolyzed product (G) was obtained after purification, following the same procedure described in section 5.2. Reactions were carried out in duplicate, analyzing three samples for each reaction product. The mean value of yield and standard deviation were obtained for each reaction. The product G-m obtained from the depolymerization of PET-m is shown in Figure 5.13. In the purification step by filtration, most of the fractions responsible of the dark color (Figure 5.12) were washed out with the water and removed together with the EG.

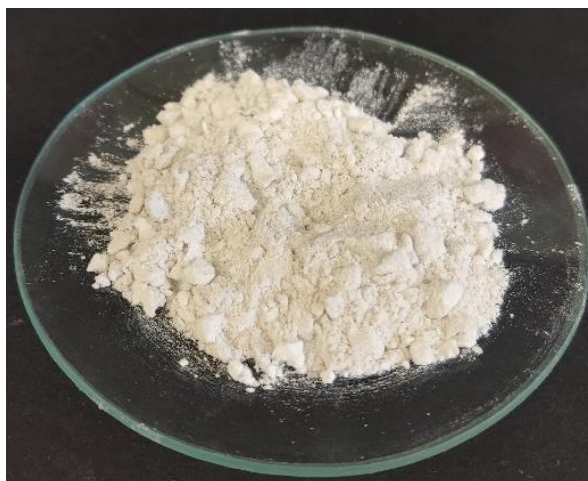


Figure 5.13. Glycolyzed G-m fraction after purification step.

Yield and insoluble fraction values obtained for different reactions are summarized in Table 5.5. The yield values are similar for all cases. This could indicate that degradation of raw material is not affecting the production of monomers and low molar mass oligomers. However, a higher content of insoluble fraction was determined PET-m sample (G-m).

Samples	IF (%)	η (%)
G-v	3.2	68 ± 9
G-ssp	3.6	65 ± 11
G-u	2.9	55 ± 13
G-m	4.2	63 ± 10

Table 5.5. Insoluble fraction in THF and yield value of glycolysis products obtained from different PET samples.

Purified glycolysis products obtained after the filtration and drying processes were characterized by FTIR, DSC and GPC. The FTIR spectra of G samples, with those of PET-v and BHET as reference, are shown in Figure 5.14. As can be seen, the spectrum of BHET monomer shows an absorption band around 3442 cm^{-1} , related to the -OH group stretching vibration. This band is also observed for glycolyzed products, while it is not appreciated for PET-v sample [6].

Moreover, a double band related to the carbonyl stretching vibration of the ester group at 1712 cm^{-1} is observed in the spectra of reference BHET and glycolyzed products, while PET sample shows a single peak [7]. From Figure 5.14, it can be stated that after 30 min of glycolysis all glycolyzed fractions are constituted by BHET.

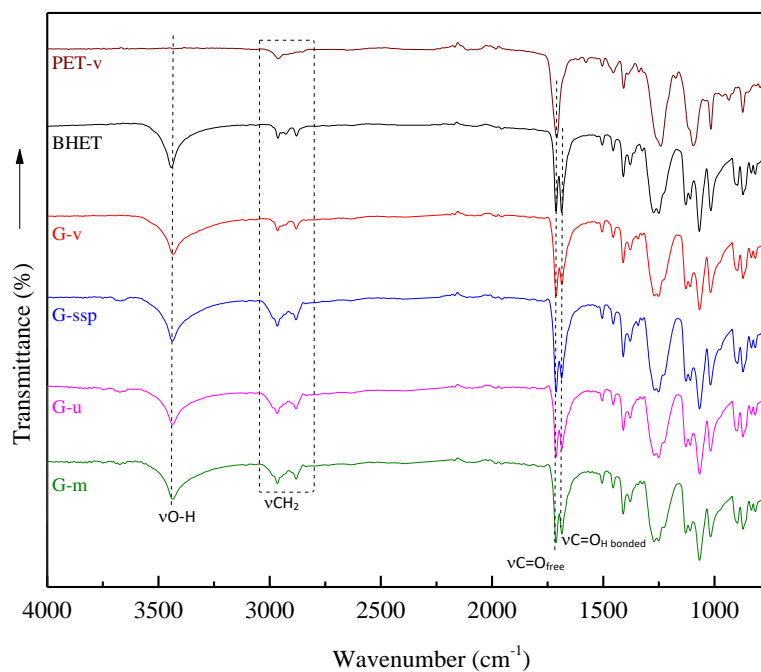


Figure 5.14. FTIR spectra of the glycolyzed products obtained from the depolymerization reaction of different PET samples, together with those corresponding to PET-v and commercial BHET.

DSC thermograms for glycolyzed products (G) obtained from different PET samples are shown in Figure 5.15.

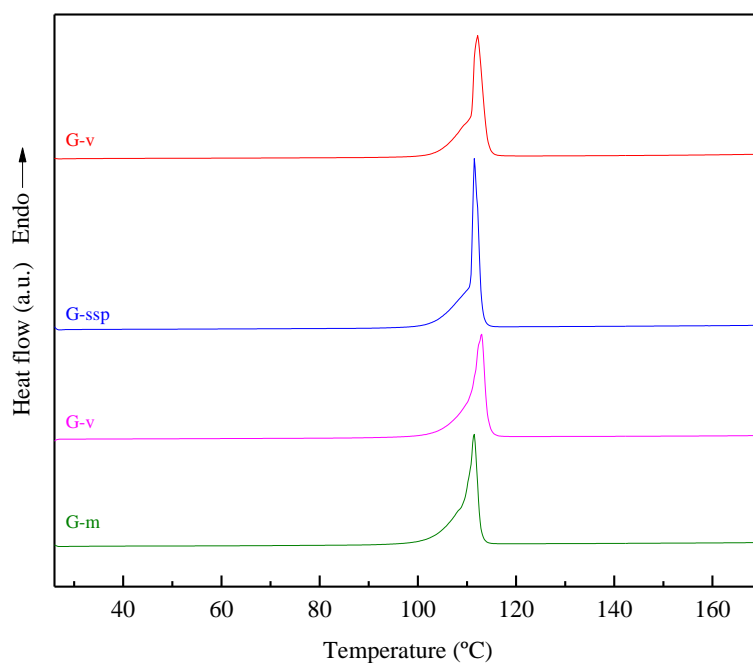


Figure 5.15. DSC thermograms corresponding to first heating scan of glycolyzed products obtained from different PET samples.

All samples present a single melting peak at around 100-110 °C, related with the T_m of BHET monomer [5]. Melting temperatures and enthalpies obtained from DSC study are summarized in Table 5.6. As can be seen, all samples show very similar values, suggesting that glycolyzed products obtained from all glycolysis reactions are practically BHET monomer.

	G-v	G-ssp	G-u	G-m
T_m (°C)	111	110	112	111
ΔH_m (J/g)	111	110	105	106

Table 5.6. Melting temperature and enthalpies obtained from DSC for glycolyzed from different PET samples.

The molar mass distribution of glycolysis products was analyzed by GPC. Figure 5.16a shows the GPC traces of glycolysis products as well as those for BHET monomer. Three different peaks can be seen, denoted as O1, O2 and O3, corresponding to the monomer, dimer and oligomer fractions of BHET, respectively, with elution times of 38, 37 and 36 min, respectively [5,12].

Figure 5.16b represents the composition of glycolyzed products. As it can be seen, the O1 component, with a M_w of 160- 171 g/mol referred to polystyrene standards, is the most significant one, attributed to BHET monomer [12]. Peaks of lower intensity appear at around 36-38 min, related to BHET oligomers of 2-3 repeating units: O2 with a M_w of 358-379 g/mol, and O3 with a M_w of 559-600 g/mol, both referred to polystyrene standards. Therefore, BHET is the main product obtained from glycolysis. Moreover, the most degraded PET-u and PET-m samples present a lower fraction of O2 dimer, which could be related to the fact that promotes chain scission into lower molar mass oligomers.

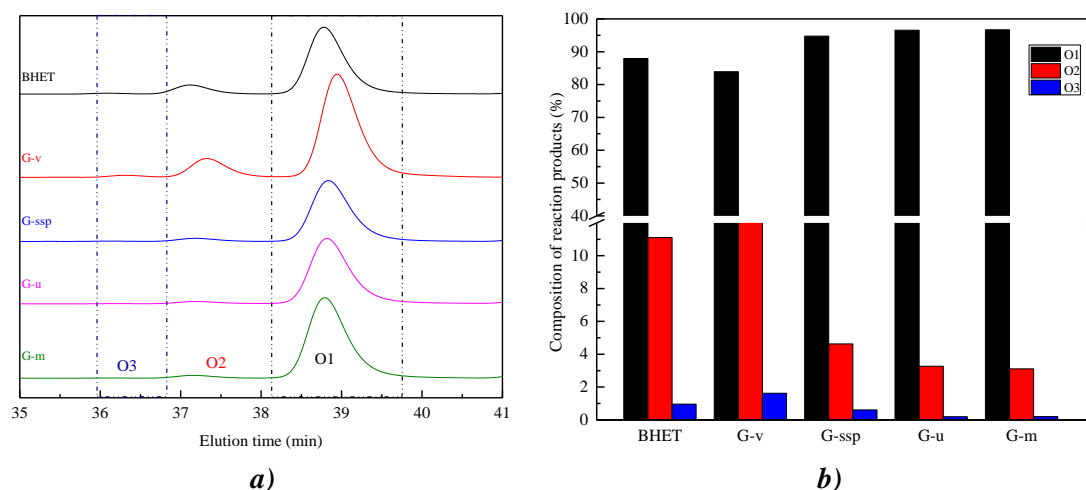


Figure 5.16. GPC results comparing reference BHET and fractions obtained from the depolymerization of different PET samples: a) GPC traces and b) BHET monomer, dimer and oligomer fraction values.

Table 5.7 summarizes the fractions corresponding to BHET monomer, dimer and oligomer, obtained from the glycolysis of different PET samples at 30 min of reaction. By analyzing the results, it can be concluded that G-ssp, G-u and G-m present higher BHET content in the glycolyzed product, comparing to G-v and commercial BHET. Similarly, G-ssp and their residues (G-u and G-m) show a similar composition, being the BHET content 2 % higher for the most degraded PET-m and PET-u samples. However, comparing G-u and G-m compositions with G-v, the BHET content is 13 % higher. Therefore, for undegraded PET samples, the percentage of BHET monomer in G-ssp is almost 11 % higher than in G-v, which could be related to the different structure of PET-v and PET-ssp. As analyzed in Chapter 3, PET-ssp sample presents two melting peaks due to the different crystalline structures generated by the post-condensation process [13]. The lower T_m may favor the depolymerization of PET to BHET, being able to start the reaction earlier, obtaining a higher BHET content after 30 min of reaction. However, it should be noted that the depolymerization reaction of PET to BHET monomer and dimer is reversible.

In addition, in the presence of EG, the amount of monomer and dimer changes in few minutes, as it was analyzed above. These results indicate that PET life cycle can be optimized by designing the glycolysis depolymerization reaction, not only by controlling the parameters but also the raw materials, in order to obtain tailor made molecules for next resin production.

Samples	O1	O2	O3
	$M_n = 155-167$ g/mol	$M_n = 358-379$ g/mol	$M_n = 556-595$ g/mol
	$M_w = 160-171$ g/mol	$M_w = 362-384$ g/mol	$M_w = 559-600$ g/mol
	(%)	(%)	(%)
BHET	88	11	1
G-v	84	14	2
G-ssp	95	5	1
G-u	97	3	0
G-m	97	3	0

Table 5.7. Oligomers content (%) and M_w and M_n values, as obtained by GPC.

5.5. Comparing commercial BHET and recycled BHET from marine PET litter

In this section, the product obtained from highly degraded marine PET litter, G-m sample, and the commercial BHET are compared. As already seen by FTIR, DSC and GPC, G-m shows similar characteristics to those of BHET. Figure 5.17 compares the FTIR spectra of G-m and commercial BHET-ref samples. The GPC result of G-m and BHET-ref are analyzed together with DSC, weight evolution and DTG results in Figure 5.18. As can be observed in Figure 5.17, both

show a similar FTIR spectra, denoting that both present the same characteristic functional groups, as it was previously studied.

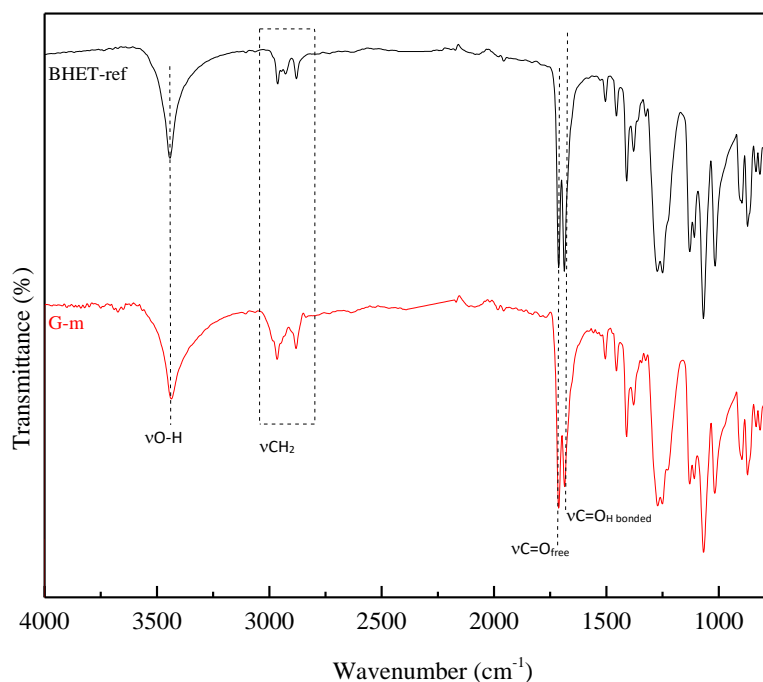


Figure 5.17. FTIR spectra of G-m and BHET-ref samples.

Regarding GPC (Figure 5.18a), both samples show only two peaks, O2 and O1, ascribed to BHET dimer and monomer respectively, whereas O3 ascribed to BHET oligomer is almost negligible. Both samples consist mainly on the monomer, even if for BHET-ref a higher amount of dimer is found (11 % and 3 % of O2 for BHET-ref and G-m, respectively). Regarding thermal properties (Figure 5.18b), both samples show a prominent melting peak around 100 °C, attributed to BHET monomer.

The main difference is that G-m presents a melting enthalpy centered at 213 °C, whereas in the case of BHET-ref the endothermic peak is centered at higher temperature (278 °C), suggesting the presence of crystalline structures formed by BHET oligomers with longer chain length. This fact can also be related to the higher thermal stability of BHET-ref observed in TGA (Figure 5.18c, d).

The first weight loss is related to the degradation of monomers and oligomers, while the second, centered at 433 °C, is related to the degradation of PET formed during thermogravimetric analysis [8]. Analyzing the thermal behavior of both samples, it can be concluded that, since the amount of dimer and oligomer is slightly higher for BHET-ref, it can form crystalline structures with higher T_m , close to that of PET, which delays the onset of degradation.

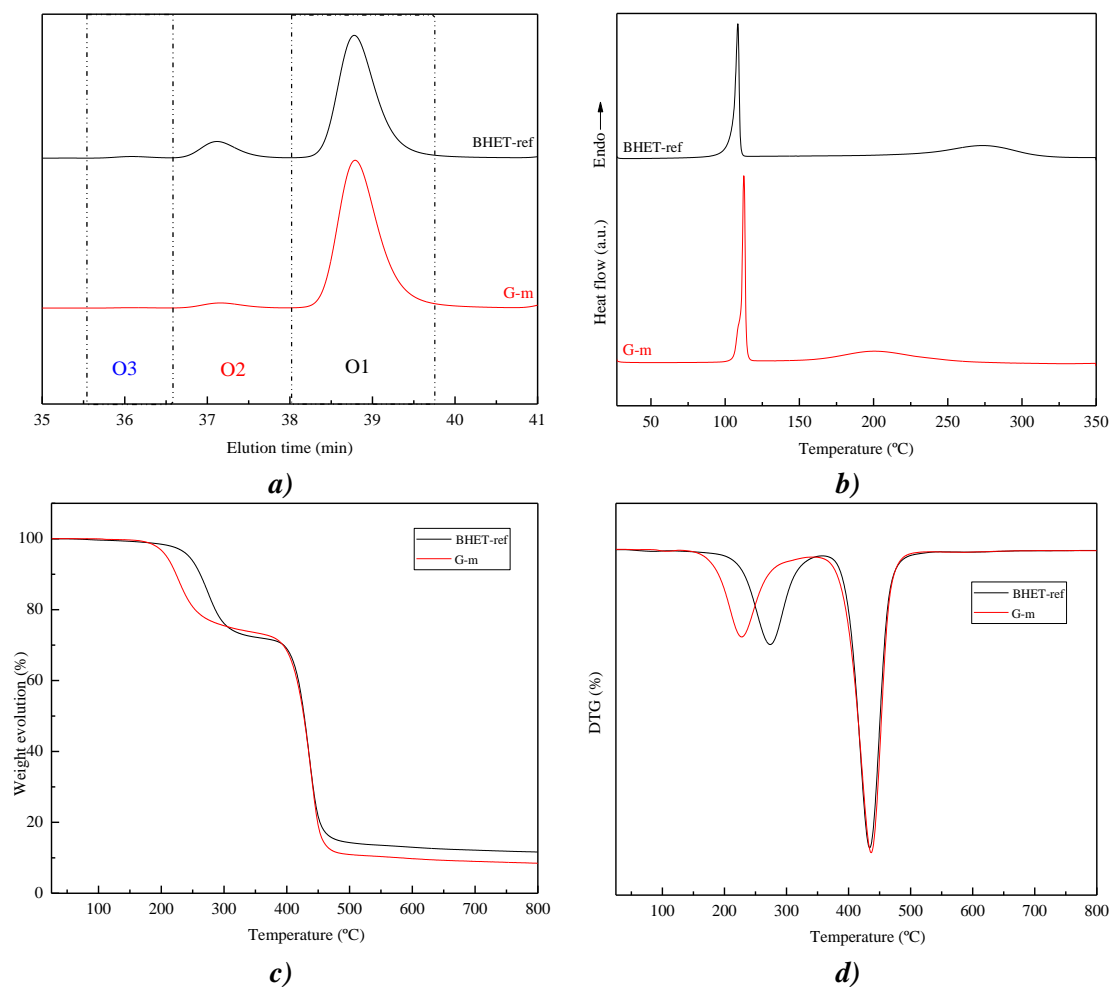


Figure 5.18. **a)** GPC traces, **b)** DSC thermograms, **c)** weight evolution and **d)** DTG plots for G-m and BHET-ref samples.

Their chemical structure was also analysed in terms of ^1H NMR, as shown in Figure 5.19.

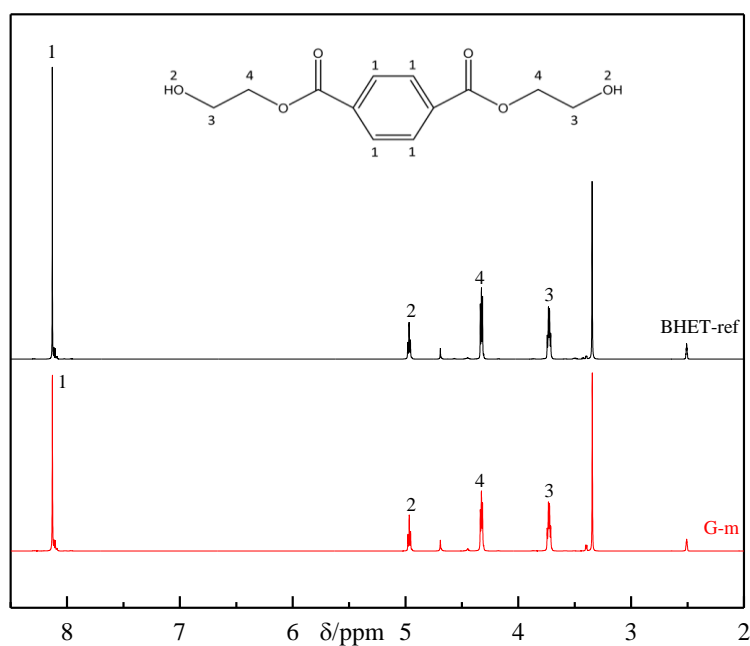


Figure 5.19. ^1H NMR spectra of BHET-ref and G-m samples.

Peaks labelled for BHET as 1, 2, 3 and 4, are assigned to protons of the aromatic ring ($\delta\text{H} = 8.1$ ppm, s, 4H), hydroxyl groups ($\delta\text{H} = 4.95$ ppm, t, 2H), methylene groups ($-\text{CH}_2-$) adjacent to the -OH groups ($\delta\text{H} = 3.73$ ppm, m, 4H), and methylene groups ($-\text{CH}_2-$) adjacent to the $-\text{COO}$ groups ($\delta\text{H} = 4.33$ ppm, t, 4H), respectively. The peak around 2.5 ppm belongs to DMSO- d_6 solvent and peak at 3.3 can be attributed to residual H_2O [14,15].

Therefore, after a deep analysis of G-m and BHET-ref samples, it can be confirmed that G-m sample corresponds to BHET, and will be referred to as BHET-m hereafter.

5.6. Conclusions

PET depolymerization process is temperature and time dependent, so these parameters must be adjusted to optimize the process. It was shown that after 10 min of reaction at 220 °C under pressure, the final product obtained was mostly BHET. However, as reaction time increased, dimers and low molar mass oligomers were also generated in the polymerization process, due to the reversibility of the depolymerization reaction of PET into BHET.

On the other hand, pure BHET was also obtained in a closed reactor at 180 °C and reaction times of 30 and 60 min, implying that depolymerization can also occur at lower temperatures. For longer reaction times, BHET yield increases but the purity is lower, as the fraction of dimers and oligomers also increases. It was found that there is a direct relationship between the BHET yield, the amount of dimers and monomers analyzed by GPC and degradation temperatures. A higher fraction of dimers in the final product translates into a higher degradation temperature.

Furthermore, glycolysis of marine PET litter was successfully carried out, obtaining very good results, demonstrating that chemical recycling is an option for degraded materials, obtaining BHET at very short reaction times. In addition, it was observed that the degradation of the materials can modify the properties of PET, increasing in this case in BHET monomer content at glycolyzed products, reducing of dimer and oligomer amount.

The variables for PET waste depolymerization reaction are of crucial importance, since products with different compositions and potential applications can be obtained. According to the literature, glycolysis of unpressurized PET can take long reaction times, between 3-8 h, as reported in Chapter 1. The use of a pressurized reactor allows working at lower temperatures and shorter reaction times, reducing the energy consumed during the process and consequently, the environmental impacts of chemical recycling. Regarding PET origin, results obtained suggest that the BHET monomer content is highly dependent on the selected raw materials. Furthermore, it was confirmed that the glycolyzed product obtained after the reaction is BHET, as it was also

proved by comparing the ^1H NMR spectrum with that of reference BHET. Therefore, the final product obtained from the chemical recycling of marine PET litter will be named as BHET-m from now on.

5.7. References

- [1] R. López-Fonseca, I. Duque-Ingunza, B. de Rivas, S. Arnaiz, J.I. Gutiérrez-Ortiz, Chemical recycling of post-consumer PET wastes by glycolysis in the presence of metal salts, *Polym Degrad Stab.* 95 (2010) 1022–1028. <https://doi.org/10.1016/j.polymdegradstab.2010.03.007>.
- [2] A. Aguado, L. Martínez, L. Becerra, M. Arieta-araunabeña, S. Arnaiz, A. Asueta, I. Robertson, Chemical depolymerisation of PET complex waste: hydrolysis vs. glycolysis, *J Mater Cycles Waste Manag.* 16 (2014) 201–210. <https://doi.org/10.1007/s10163-013-0177-y>.
- [3] S. Chaudhary, P. Surekha, D. Kumar, C. Rajagopal, P.K. Roy, Microwave assisted glycolysis of poly(ethylene terephthalate) for preparation of polyester polyols, *J Appl Polym Sci.* 129 (2013) 2779–2788. <https://doi.org/10.1002/app.38970>.
- [4] R. López-Fonseca, I. Duque-Ingunza, B. de Rivas, L. Flores-Giraldo, J.I. Gutiérrez-Ortiz, Kinetics of catalytic glycolysis of PET wastes with sodium carbonate, *Chemical Engineering Journal.* 168 (2011) 312–320. <https://doi.org/10.1016/J.CEJ.2011.01.031>.
- [5] P. Fang, B. Liu, J. Xu, Q. Zhou, S. Zhang, J. Ma, X. lu, High-efficiency glycolysis of poly(ethylene terephthalate) by sandwich-structure polyoxometalate catalyst with two active sites, *Polym Degrad Stab.* 156 (2018) 22–31. <https://doi.org/10.1016/J.POLYMDEGRADSTAB.2018.07.004>.
- [6] A.P. Siroèiae, A. Fijaèko, Z. Hrnjak-Murgiae, Chemical recycling of postconsumer poly(ethylene-terephthalate) bottles-depolymerization study, *Chem Biochem Eng Q.* 27 (2013) 65–71.
- [7] T. Amari, Y. Ozaki, Generalized two-dimensional attenuated total reflection/infrared and near-infrared correlation spectroscopy studies of real-time monitoring of the initial oligomerization of bis(hydroxyethyl terephthalate), *Macromolecules.* 35 (2002) 8020–8028. <https://doi.org/10.1021/ma020723y>.
- [8] C.-H. Chen, Study of glycolysis of poly(ethylene terephthalate) recycled from postconsumer soft-drink bottles. Further investigation, *J Appl Polym Sci.* 87 (2003) 2004–2010. <https://doi.org/10.1002/app.11694>.

- [9] Y. Geng, T. Dong, P. Fang, Q. Zhou, X. Lu, S. Zhang, Fast and effective glycolysis of poly(ethylene terephthalate) catalyzed by polyoxometalate, *Polym Degrad Stab.* 117 (2015) 30–36. <https://doi.org/10.1016/j.polymdegradstab.2015.03.019>.
- [10] M.E. Viana, A. Riul, G.M. Carvalho, A.F. Rubira, E.C. Muniz, Chemical recycling of PET by catalyzed glycolysis: Kinetics of the heterogeneous reaction, *Chem Eng J.* 173 (2011) 210–219. <https://doi.org/10.1016/j.cej.2011.07.031>.
- [11] F. Pardal, G. Tersac, Kinetics of poly(ethylene terephthalate) glycolysis by diethylene glycol. Evolution of liquid and solid phases, *Polym Degrad Stab.* 91 (2006) 2840–2847. <https://doi.org/10.1016/j.polymdegradstab.2006.09.009>.
- [12] R. López-Fonseca, I. Duque-Ingunza, B. de Rivas, L. Flores-Giraldo, J.I. Gutiérrez-Ortiz, Kinetics of catalytic glycolysis of PET wastes with sodium carbonate, *Chem Eng J.* 168 (2011) 312–320. <https://doi.org/10.1016/J.CEJ.2011.01.031>.
- [13] S. Tan, A. Su, W. Li, E. Zhou, New insight into melting and crystallization behavior in semicrystalline poly(ethylene terephthalate), *J Polym Sci B Polym Phys.* 38 (2000) 53–60. [https://doi.org/10.1002/\(SICI\)1099-0488\(20000101\)38:1<53::AID-POLB6>3.0.CO;2-G](https://doi.org/10.1002/(SICI)1099-0488(20000101)38:1<53::AID-POLB6>3.0.CO;2-G).
- [14] M. Imran, B.K. Kim, M. Han, B.G. Cho, D.H. Kim, Sub- and supercritical glycolysis of polyethylene terephthalate (PET) into the monomer bis(2-hydroxyethyl) terephthalate (BHET), *Polym Degrad Stab.* 95 (2010) 1686–1693. <https://doi.org/10.1016/J.POLYMDEGRADSTAB.2010.05.026>.
- [15] G.R. Lima, W.F. Monteiro, R. Ligabue, R.M.C. Santana, Titanate nanotubes as new nanostructured catalyst for depolymerization of PET by glycolysis reaction, *Mater Res.* 20 (2017) 588–595. <https://doi.org/10.1590/1980-5373-mr-2017-0645>.

Chapter 6

SYNTHESIS OF NEW THERMOPLASTIC
POLYURETHANES BASED ON RECYCLED BHET

6. SYNTHESIS OF NEW THERMOPLASTIC POLYURETHANES BASED ON RECYCLED BHET

6.1. Aim of the chapter

The aim of this chapter was to produce new materials based on the recycled BHET obtained from marine PET litter. Thermoplastic polyurethanes (TPU) were synthesized using BHET-m as a chain extender, thus reducing the consumption of commercial chain extenders from petrochemical origin. Furthermore, in order to produce more environmentally friendly materials, the new PUs were synthesized using a biobased macrodiol.

In this work, five different TPU compositions were synthesized by increasing the content of the segment formed by isocyanate and BHET-m, i.e. the content of the HS. Thus, TPUs were synthesized with more than 40 % of their components coming from renewable and recycled materials, reaching up to a 30 % of recycled marine BHET. In this way, PUs with a lower carbon footprint were synthesized, promoting their circular economy. For comparative purposes, PUs were also synthesized with commercial BHET (BHET-ref).

The synthesis was performed following a two-step synthesis procedure. In the first step, the prepolymer was formed, while in the second one the chain extension was carried out in a compression press, once the reaction mixture was casted into a rectangular mold to obtain TPU plaques, which were subsequently employed in the TPU characterization. The chemical structure of TPUs was studied by FTIR, while color differences were analyzed by spectrophotometry. Thermal transitions and stability, as well as thermo-mechanical and mechanical properties, were analyzed by DSC, TGA, DMA and mechanical tensile testing, respectively. The surface hydrophilicity of plaques was studied by WCA.

Finally, the recyclability study of new TPUs was carried out through thermo-mechanical recycling by injection molding and chemical recycling by glycolysis. Recycled products were also characterized.

6.2. Reactants and synthesis of TPUs

TPUs were synthesized using a macrodiol derived from vegetable oil (Priplast 3192®) as the SS. HDI (Desmodur H) was used as isocyanate component in HS. The PUs were synthesized in bulk without organic solvents or catalysts, in order to follow an environmentally friendly procedure. The synthesis was carried out by a two-step procedure in a 250 mL five-necked round bottom

flask equipped with a mechanical stirrer and a dry nitrogen inlet. In the first step, macrodiol and HDI were reacted at 110 °C for 2 h. In the second step, BHET was added to the mixture and stirred vigorously until a homogeneous mixture was obtained, which was poured between two Teflon-coated metal plates with a separation of 1.5 mm and pressed in a hot plate press at 100 °C and 50 bar for 10 h, and finally allowed to cool to room temperature in the press. The molar ratio between the NCO and OH groups was kept constant and equal to 1.0. Different polyurethanes were synthesized by varying the molar ratio of macrodiol:HDI:BHET-m, as well as pure HS, HDI:BHET-m. For reference, PUs were also synthesized with BHET-ref (with the minimum and maximum molar ratios employed for BHET-m) and pure HS, HDI:BHET-ref, as well. Synthesized TPU compositions together with BHET percentage employed are summarized in Table 6.1. Samples are designated by the type of BHET (BHET-m or BHET-ref) and the molar ratio of components.

Sample code	Molar ratio Macrodiol:HDI:BHET	HS (%)	BHET (%)
HDI:BHET-m	0:1:1	100	60
BHET-m 1:2:1	1:2:1	23	10
BHET-m 1:3:2	1:3:2	33	17
BHET-m 1:4:3	1:4:3	42	22
BHET-m 1:5:4	1:5:4	48	26
BHET-m 1:6:5	1:6:5	53	30
HDI:BHET-ref	0:1:1	100	60
BHET-ref 1:2:1	1:2:1	23	10
BHET-ref 1:6:5	1:6:5	53	30

Table 6.1. Designation, composition and HS and BHET content of different TPU samples synthesized.

6.3. Characterization of synthesized TPUs

6.3.1. Spectrophotometry

Firstly, the effect chain extender nature, BHET-m or BHET-ref, and reactants ratio on the appearance of obtained TPU samples was analyzed. As can be seen in Figure 6.1, in which a digital image of prepared TPUs is shown, regardless the nature of BHET, the opacity of TPU increases as the HS content increases. On the other hand, the color of TPUs with BHET derived from recycled PET is more brownish, more intense as the BHET-m content in the TPU formulation increases. The effect of increasing HS content on the opacity and color of the samples was further studied by analyzing the color parameters by spectrophotometry (Table 6.2). As for

the L^* values related to lightness-darkness, a decrease was observed as the HS content increased, which corroborated the trend observed BY naked eye. Regarding a^* and b^* values, no clear tendency is observed, whereas WI value decreases as BHET-m content increases, AS samples deviate from the standard white sample. As for the ΔE^* values related to color changes, a gradual increase was observed with increasing HS content. However, these variations were more pronounced in the case of the PUs synthesized with BHET-m chain extender, probably due to the darker color of this recycled BHET.



Figure 6.1. Digital image PUs synthesized using BHET-m (top) and BHET-ref (down) as chain extender.

Sample	L^*	a^*	b^*	ΔE^*	WI
BHET-m 1:2:1	78.4	1.2	20.8	23.9	70.0
BHET-m 1:3:2	58.9	3.4	22.2	41.3	53.1
BHET-m 1:4:3	53.9	4.3	18.3	44.6	50.2
BHET-m 1:5:4	52.0	4.6	16.0	45.8	49.2
BHET-m 1:6:5	48.3	4.2	13.1	48.8	46.5
BHET-ref 1:2:1	85.1	0.1	10.4	12.3	81.8
BHET-ref 1:6:5	80.5	-2.4	1.7	15.5	80.3

Table 6.2. L^ , a^* , b^* , and ΔE^* color values, together with WI ones, for TPU samples.*

6.3.2. FTIR

The influence of increasing HS content on the chemical structure of PUs synthesized with BHET from marine litter was analyzed by FTIR. In Figure 6.2a, the FTIR spectra of synthesized PUs together with those biobased macrodiol and BHET-m are shown.

As it can be seen, synthesized PUs does not show the characteristic band of NCO groups centered at 2270 cm^{-1} , nor the -OH stretching band observed for BHET-m at 3342 cm^{-1} , denoting that polymerization reaction was finished [1–3]. All of them show a band centered at 3317 cm^{-1} ascribed to N-H bond of urethane group [1,4], which increases with HS content increases, and thus, with the amount of urethane groups.

As it can be seen in the amide I region ($1750\text{-}1600\text{ cm}^{-1}$) (Figure 6.2b), while the macrodiol shows a single band at 1727 cm^{-1} attributed to carbonyl (C=O) groups, PUs present two bands. It is well known that for TPUs C=O groups of the urethane can be free or hydrogen bonded. The non-

hydrogen-bonded (free) C=O groups can be observed around 1730-1718 cm^{-1} , while the hydrogen-bonded ones appear around 1700-1680 cm^{-1} [5,6]. In the case of synthesized PUs, the band at higher wavenumber encompasses the C=O of the macrodiol as well as the free urethane C=O group. This band shifts slightly to a lower wavenumber as HS content increases, displacing from 1727 to 1721 cm^{-1} , in agreement with the higher content of urethane group in the polymer, whose intensity prevails over that of the C=O groups of the macrodiol. In addition, a band attributed to the hydrogen bonded C=O in the urethane group can be observed at 1689 cm^{-1} , which also increases with HS content.

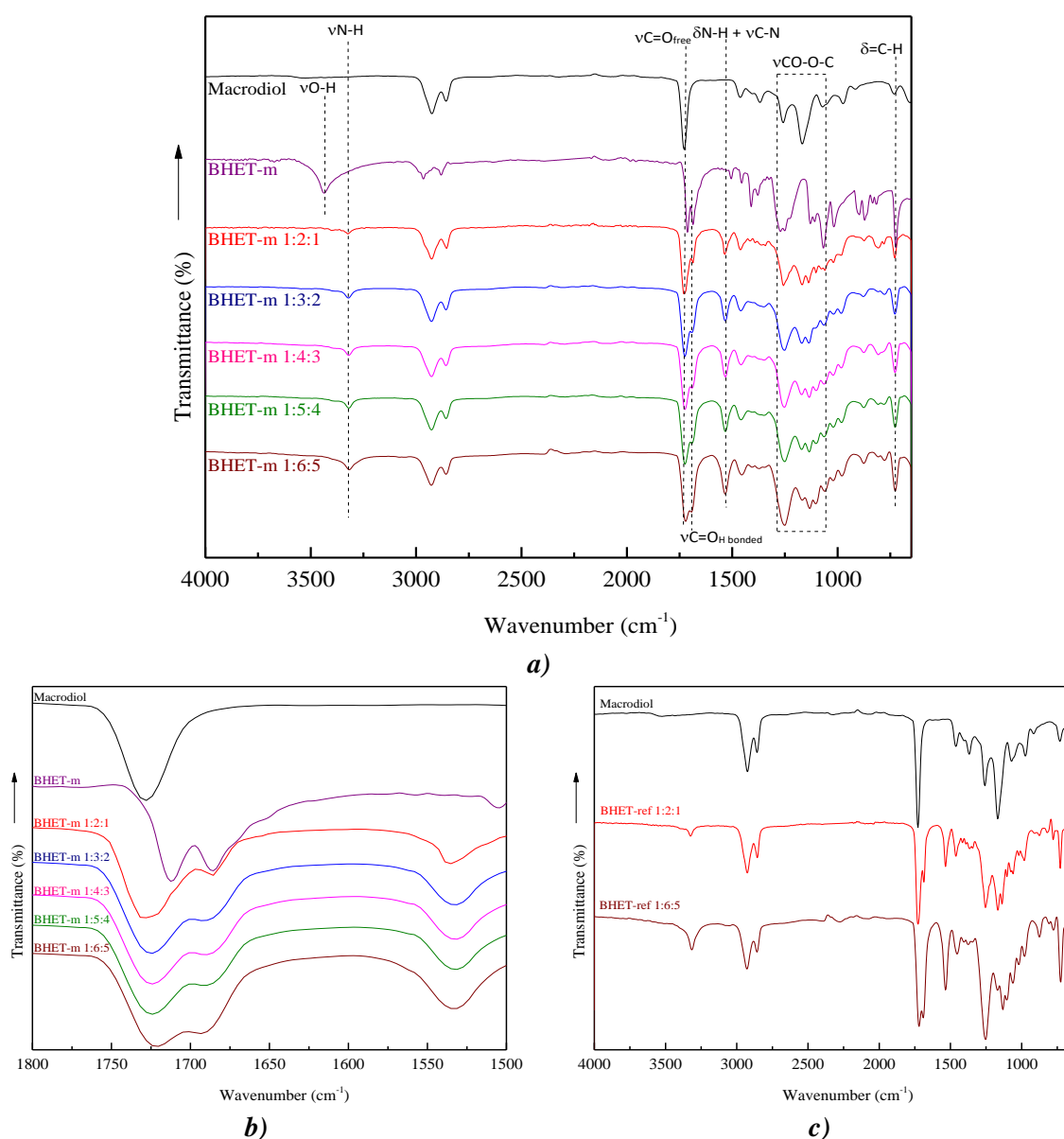


Figure 6.2. **a)** FTIR spectra of PUs synthesized with BHET-m. **b)** Amide I + amide II region from 1800-1500 cm^{-1} . **c)** FTIR spectra PUs synthesized with BHET-ref.

Furthermore, all TPUs show a band in amide II region ($1600\text{--}1500\text{ cm}^{-1}$) at 1535 cm^{-1} , related to the bending vibration of N-H combined with stretching vibration of C-N [6,7]. This band becomes more intense with increasing HS, due to the increased contribution of urethane groups. The bands between 1250 and 1110 cm^{-1} are related to the CO-O-C asymmetric and symmetric stretching vibration [8,9]. Moreover, at 728 cm^{-1} the characteristic band related to C-H linkages in the aromatic groups can be observed [10]. The intensity of this band increases with HS content, due to the increased presence of BHET, which presents an aromatic ring in the structure. Figure 6.2c shows the spectra of the TPUs synthesized with BHET-ref. Comparing both TPU systems, the lower and the higher molar ratio, it can be concluded that there is no relevant difference between the spectra of the both TPUs derived from BHET-m and the commercial one.

6.3.3. DSC

Thermal properties of synthesized TPUs were analyzed in terms of DSC. The thermograms of TPUs from BHET-m and, as reference, the employed biobased macrodiol and pure HS (HDI:BHET-m) are depicted in Figure 6.3a. In addition, thermal transitions are listed in Table 6.3.

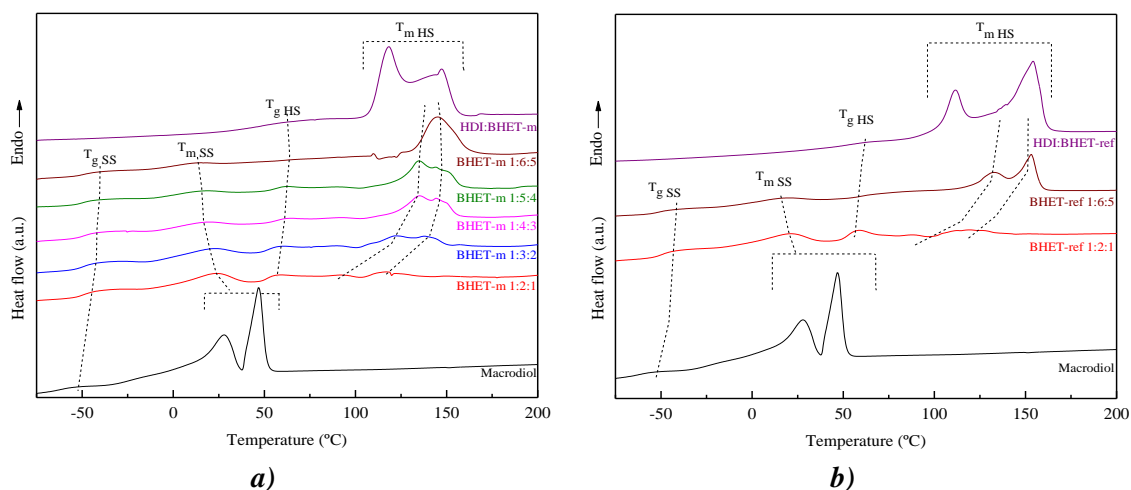


Figure 6.3. **a)** DSC thermograms of TPUs synthesized with BHET-m, together with those of neat macrodiol and HDI:BHET-m segment. **b)** DSC thermograms of TPUs synthesized with BHET-ref, together with those of neat macrodiol and HDI:BHET-ref segment.

On one side, T_g is observed around $-50\text{ }^\circ\text{C}$, also present for the macrodiol, which corresponds to the SS-rich domain ($T_{g,SS}$) and an endothermic peak, also detected in the macrodiol, associated with the melting enthalpy of the SS-rich domain ($\Delta H_{m,SS}$), centered in temperatures ranging from 12 to $23\text{ }^\circ\text{C}$.

Despite HS content increases $T_{g,SS}$ value remains almost constant, whereas $T_{m,SS}$ and $\Delta H_{m,SS}$ decrease according to the lower amount of crystallizable macrodiol. On the other hand, at higher

temperatures, the T_g observed in the neat HDI:BHET-m ascribed to HS-rich domain ($T_{g\text{ HS}}$), and a second endothermic peak also observed in neat HDI:BHET-m, related to the melting enthalpy of the HS-rich domain ($\Delta H_{m\text{ HS}}$), can be seen. In opposition to the abovementioned thermal behavior of the SS rich domain, the $T_{g\text{ HS}}$ and the $T_{m\text{ HS}}$ and melting enthalpy of the HS-rich domain increase with HS content. This fact is related, as already mentioned, to the amount of crystallizable segment in the TPU formulation. That is, the greater the amount of crystallizable SS or HS in the TPU, the higher the probability for SS or HS chains to pack together to form crystals. This is due to the formation of longer chains and, therefore, the greater capacity to associate through interurethane interactions [11].

Thus, as the HS content increases, the amount of macrodiol is lower, whereas the amount of diisocyanate and BHET is higher, hence, $T_{m\text{ HS}}$ and $\Delta H_{m\text{ HS}}$ increase, while $T_{m\text{ SS}}$ and $\Delta H_{m\text{ SS}}$ decrease. These results are in accordance with the increase of hydrogen bonded C=O band observed in FTIR spectra. Finally, the presence of differentiated transitions ascribed to HS and SS in the TPUs suggests a microphase separated morphology.

Comparing the thermograms of TPUs obtained from BHET-m with those using commercial BHET (Figure 6.3b), no significant differences are observed, denoting that the thermal properties of the material are not compromised when recycled BHET from marine PET litter is used in the formulation of TPUs.

Sample	$T_{g\text{ SS}}$ (°C)	$T_{m\text{ SS}}$ (°C)	$\Delta H_{m\text{ SS}}$ (J/g)	$T_{g\text{ HS}}$ (°C)	$T_{m\text{ HS}}$ (°C)	$\Delta H_{m\text{ HS}}$ (J/g)
Macrodiol	-62, -24	28, 46	40	-	-	-
HDI:BHET-m	-	-	-	50	118, 147	68
BHET-m 1:2:1	-49	23	10	52	116	3
BHET-m 1:3:2	-50	21	7	52	122, 138	18
BHET-m 1:4:3	-49	17	5	57	135, 144	20
BHET-m 1:5:4	-50	16	4	56	134, 144	23
BHET-m 1:6:5	-50	12	2	62	145	30
HDI:BHET-ref	-	-	-	52	111, 154	70
BHET-ref 1:2:1	-49	21	8	53	118	5
BHET-ref 1:6:5	-51	16	5	60	132, 153	24

Table 6.3. Thermal properties measured by DSC for all the samples.

6.3.4. AFM

The morphology of the TPUs synthesized with BHET-m was analyzed by AFM (Figure 6.4). As it can be seen, different domains can be distinguished, denoting that the synthesized TPUs present a microphase separated microstructure.

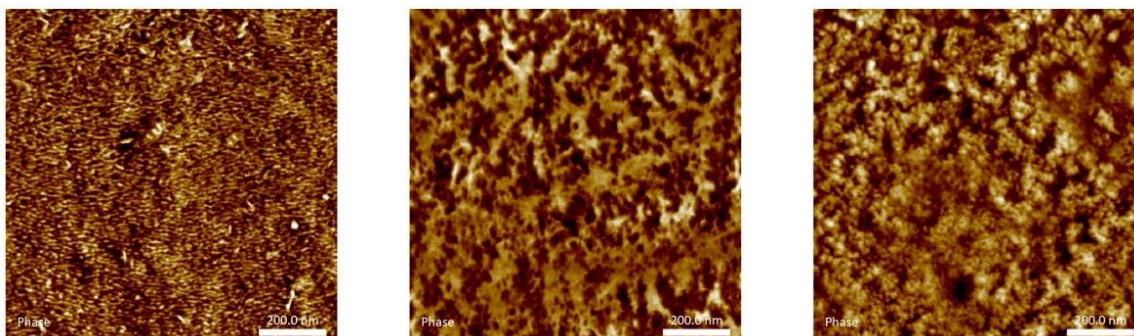


Figure 6.4. AFM phase images of TPUs synthesized from BHET-m with 1:2:1, 1:4:3 and 1:6:5 molar ratios, from left to right (scale bar 200 nm).

The darker regions are attributed to amorphous domains, while the lighter ones are related to crystalline domains. The frequency and size of the lighter regions increase with HS content, corroborating that the addition of BHET increases the ability of the chains to pack together forming interurethane interactions, in agreement with the DSC results, leading to larger crystalline domains.

6.3.5. TGA

The thermal stability of synthesized TPUs, as well as that of pure components, was analyzed by TGA. The weight evolution and their corresponding derivative curves are plotted in Figure 6.5.

As it can be seen, the degradation profiles change as HS content increases, being more appreciable in the derivative curve (Figure 6.5b). All TPU samples show a degradation step centered at 420 °C (T_{d1}), also observed in the macrodiol, related to the breaking of ester bonds in the SS macrodiol [12,13]. For TPUs with a high HS content (i.e., 1:6:5 and 1:5:4), the degradation peak observed at 316 °C in pure HS (T_{d2}), related to the degradation of the urethane group, is clearly observed. As the HS content decreases, the intensity of this peak decreases and shifts to higher temperatures, becoming a shoulder for TPUs with lower HS content. This shift to higher temperatures, which results in an overlap with the macrodiol degradation peak, is attributed to a greater dispersion of the small-sized hard segments in the macrodiol-rich phase, as has already been observed by AFM.

In addition, a third degradation step (T_{d3}) related to the degradation of the residue formed at higher temperature is observed [14], which is more noticeable as HS content increases agreeing with the trend observed for neat HS. Comparing the thermal degradation behavior of synthesized from BHET-m and BHET-ref in Figure 6.5c and d, a similar behavior is observed, denoting that the origin of employed BHET is not interfering in the degradation profile of the TPU.

TGA results of all TPUs synthesized with BHET-m and BHET-ref samples are summarized in Table 6.4. In the same way, the results of HS pure segment and macrodiol are also represented.

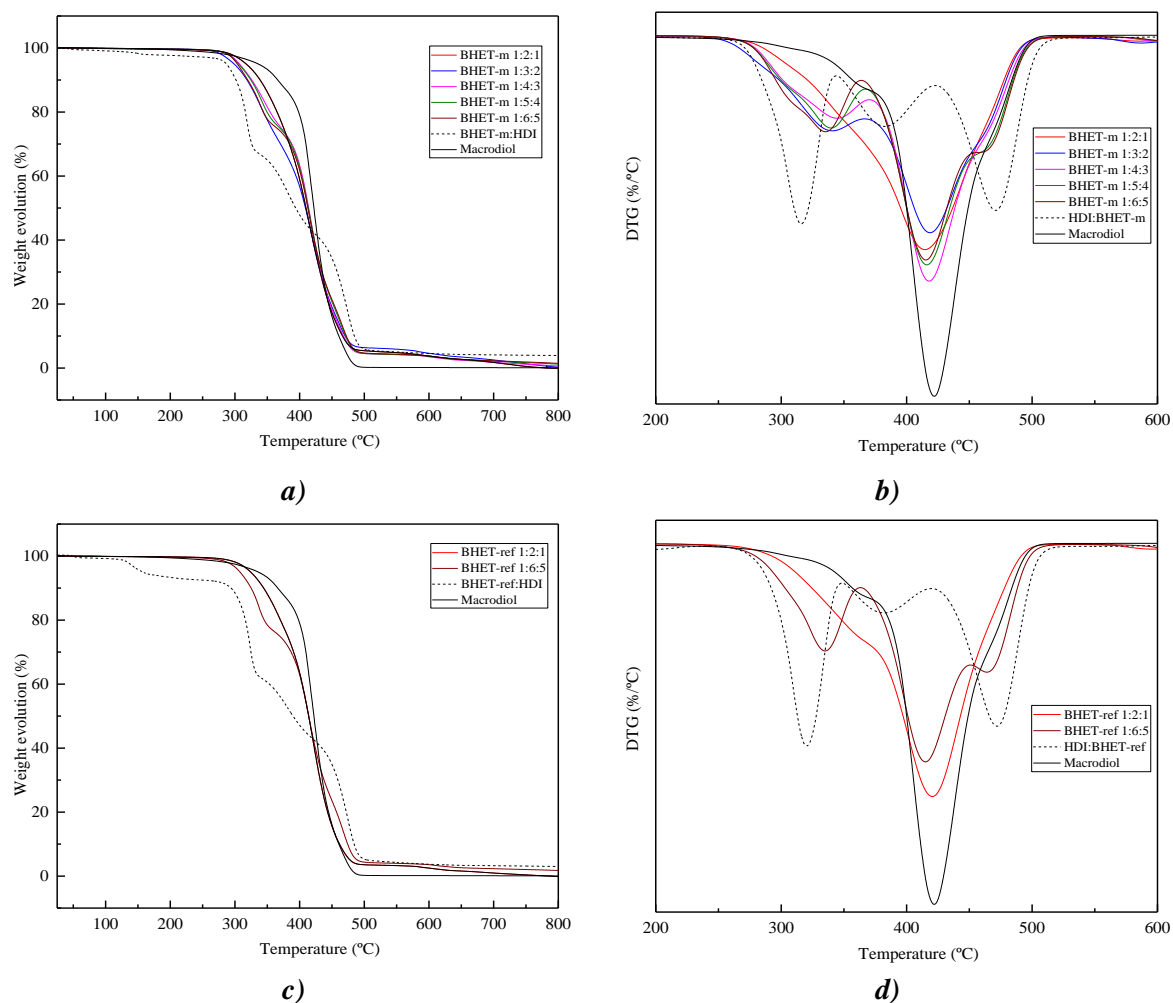


Figure 6.5. **a)** Weight evolution and **b)** DTG curves of TPUs synthesized from BHET-m and neat HDI:BHET-m and macrodiol. **c)** Weight evolution and **d)** DTG curves of TPUs synthesized with BHET-ref and neat HDI:BHET-ref and macrodiol.

Sample	T _{d1} (°C)	T _{d2} (°C)	T _{d3} (°C)	Residue (%)
HDI:BHET-m	313, 380	-	469	8
BHET-m 1:2:1	-	413	-	5
BHET-m 1:3:2	340	416	-	6
BHET-m 1:4:3	345	415	-	5
BHET-m 1:5:4	341	413	460	5
BHET-m 1:6:5	335	413	461	7
Macrodiol	-	420	-	0
HDI:BHET-ref	318, 379	-	469	8
BHET-ref 1:2:1	-	418	-	4
BHET-ref 1:6:5	333	412	463	5

Table 6.4. TGA results of synthesized thermoplastic TPUs.

6.3.6. DMA

The dynamic mechanical behavior of TPU samples synthesized with recycled BHET-m has been analyzed by DMA. The temperature dependence of the storage modulus (E') and loss factor ($\tan \delta$) is plotted in Figure 6.6. At low temperatures, all synthesized TPUs show a similar storage modulus and, for all cases, a drop is observed around $-52\text{ }^\circ\text{C}$, being more pronounced for samples with higher SS content.

Moreover, the $\tan \delta$ peak shows a maximum in the same temperature interval, corresponding to α relaxation from SS that can be related to the T_g of the SS domain ($T_{g\text{SS}}$) [1,6,7]. The magnitude of this peak decreases with HS content, since the height of the $\tan \delta$ peak is related to the amount of amorphous material, which is higher for the samples with higher SS content [15].

In addition, for samples with higher HS content, $\tan \delta$ shows a second transition around $25\text{ }^\circ\text{C}$ corresponding to the α relaxation of HS, which can be associated with the $T_{g\text{HS}}$. At higher temperatures, the storage modulus curve reaches a quasi-plateau for all samples, related with the interconnectivity of HS domains. Higher storage modulus values are observed in this interval as the HS content of the TPU increases, due to crystallizable and microphase separated HS domains, in agreement with the DSC results.

Moreover, this plateau extends to higher temperatures with HS content, providing higher thermo-mechanical stability to the TPU samples, and starting to decrease with the onset of the melting of previously observed crystals. Thus, this terminal temperature (T_t) is close to the HS melting temperature measured by DSC. The same behavior is observed for the samples synthesized from BHET-ref in Figure 6.6b.

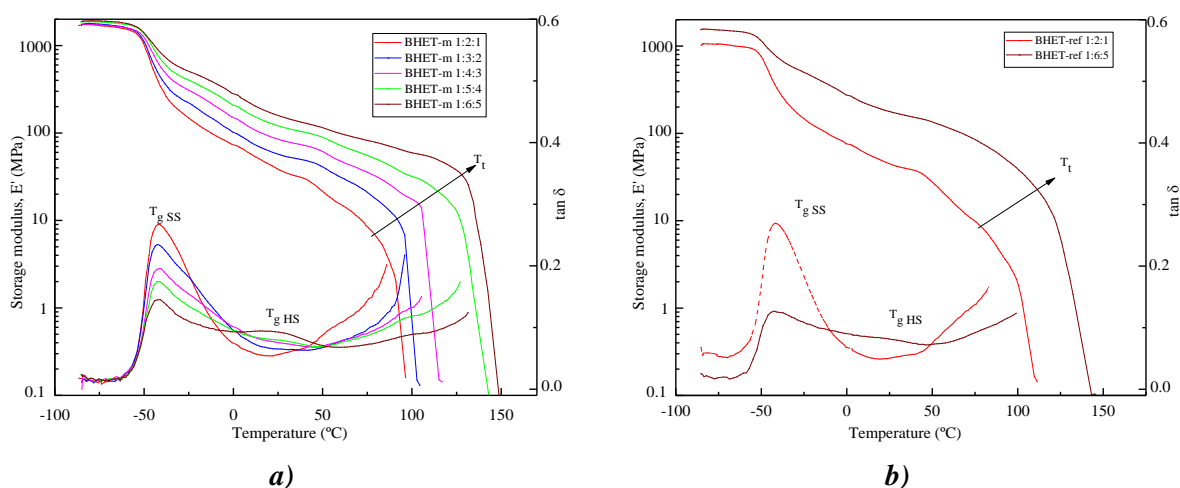


Figure 6.6. Storage modulus (E') and loss factor ($\tan \delta$) for TPUs synthesized with: **a)** BHET-m and **b)** BHET-ref.

6.3.7. Mechanical properties

The mechanical behavior of synthesized TPUs was also analyzed by tensile tests. The average values of tensile modulus, yield stress, stress at break and elongation at break for BHET-m and BHET-ref systems are summarized in Table 6.5, while the stress-strain curves of BHET-m systems are shown in Figure 6.7.

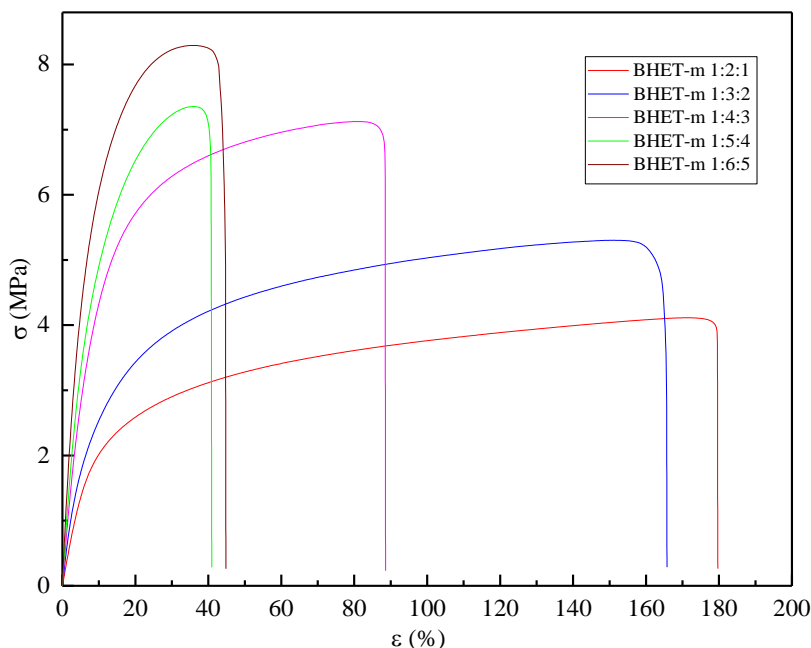


Figure 6.7. Stress-strain curves of TPUs synthesized with BHET-m as chain extender.

As HS content increases, higher values of tensile modulus, yield stress and stress at break are obtained, because, as mentioned above, the crystallizable HS domains act as reinforcement in the TPU [16]. However, the HS content decreases the strain at break, in accordance with the higher crystallinity of the material, which could act as breaking stress concentration points. It can be deduced that the increasing of HS content makes the material stiffer, due to the higher crystallinity observed by DSC and due to the present of the aromatic ring at BHET monomer. TPUs synthesized with BHET from the chemical recycling of marine PET bottles show similar properties than those synthesized with commercial BHET used as reference, thus corroborating that they can be a suitable alternative to raw materials from fossil sources. Moreover, the synthesized TPUs present properties in the range of those obtained for TPUs synthesized using polycaprolactone diol as SS and commercial BHET and HDI as HS [2,17]. However, by comparing them with TPUs synthesized with aliphatic chain extenders like 1,4-butanediol or 1,3-propanediol, and both aliphatic or aromatic diisocyanates, in general stiffer polyurethanes with higher modulus are obtained due to the aromatic structure of BHET [18,19].

Sample	E (MPa)	ϵ_b (%)	σ_y (MPa)	σ_b (MPa)
BHET-m 1:2:1	28 ± 3	176 ± 29	0.7 ± 0.2	4.1 ± 0.2
BHET-m 1:3:2	39 ± 2	191 ± 19	1.3 ± 0.3	5.6 ± 0.3
BHET-m 1:4:3	66 ± 3	89 ± 5	1.5 ± 0.0	7.0 ± 0.2
BHET-m 1:5:4	82 ± 3	40 ± 3	1.6 ± 0.2	7.0 ± 0.4
BHET-m 1:6:5	107 ± 1	45 ± 1	1.6 ± 0.3	8.4 ± 0.1
BHET-ref 1:2:1	29 ± 3	182 ± 22	0.9 ± 0.1	4.2 ± 0.2
BHET-ref 1:6:5	143 ± 11	16 ± 3	2.4 ± 0.2	7.8 ± 0.4

Table 6.5. Mechanical properties of synthesized thermoplastic polyurethanes.

6.3.8. WCA

Finally, the WCA of the synthesized TPU plaques was measured. The results are summarized in Table 6.6.

	Water contact angle (°)				
	1:2:1	1:3:2	1:4:3	1:5:4	1:6:5
BHET-m	79 ± 4	75 ± 4	75 ± 1	79 ± 1	79 ± 3
BHET-ref	79 ± 1	-	-	-	80 ± 1

Table 6.6. WCA results of the synthesized TPU plaques.

There is no a significant trend or change when HS content is increased. With HS content the urethane and BHET content increases. This leads to an increase in dipole-forming urethane groups, which should lead to a decrease in WCA [20,21], but in the same way, to an increase of the aromatic hydrophobic content present at BHET-m [22]. It seems that, both effects are compensated and no variation in WCA is observed.

6.4. Recycling of synthesized TPUs

TPUs are characterized by their versatility, being one of the most produced polymers in the world. Moreover, it was reported that TPUs can be mechanically and chemically recycled [23–26], becoming these materials interesting from the point of view of circular economy. In this section, thermo-mechanical recycling by injection molding and chemical recycling by glycolysis of previous synthesized and characterized TPU samples were performed.

6.4.1. Thermo-mechanical recycling of synthesized TPUs

Different samples of previously synthesized and characterized TPU (in particular BHET-m 1:4:5, BHET-m 1:5:4 and BHET-m 1:6:5) were cut in small pieces, and obtained mixture was used for

performing injection tests in order to evaluate the feasibility of thermo-mechanical recyclability. The dog bone shape samples shown in Figure 6.8 were prepared by injection (RTPU). This recycled samples were compared to the previously synthesized TPUs with higher BHET-m content, BHET-m 1:6:5.



Figure 6.8. Injected RTPU sample obtained by thermo-mechanical recycling.

Firstly, FTIR and DSC characterization of RTPU sample was performed to ensure that no reactions that generating new functional groups take place during the thermo-mechanical recycling.

Figure 6.9 shows the FTIR spectra of RTPU sample together with that of BHET-m 1:6:5 sample. Both samples present the same spectra, with no changes in bands wavenumbers or new bands observed after the thermo-mechanical recycling. The characteristic absorption bands of urethane group are detected in both spectra. However, a slight decrease of the intensity of urethane characteristic bands, ν N-H, ν C=O, δ N-H+C-N and ν CO-O-C, is observed for RTPU sample comparing with BHET-m 1:6:5 one. This can be due to the lower urethane content that can be expected for BHET-m 1:4:5, BHET-m 1:5:4 and BHET-m 1:6:5 mixtures, comparing with BHET-m 1:6:5 one.

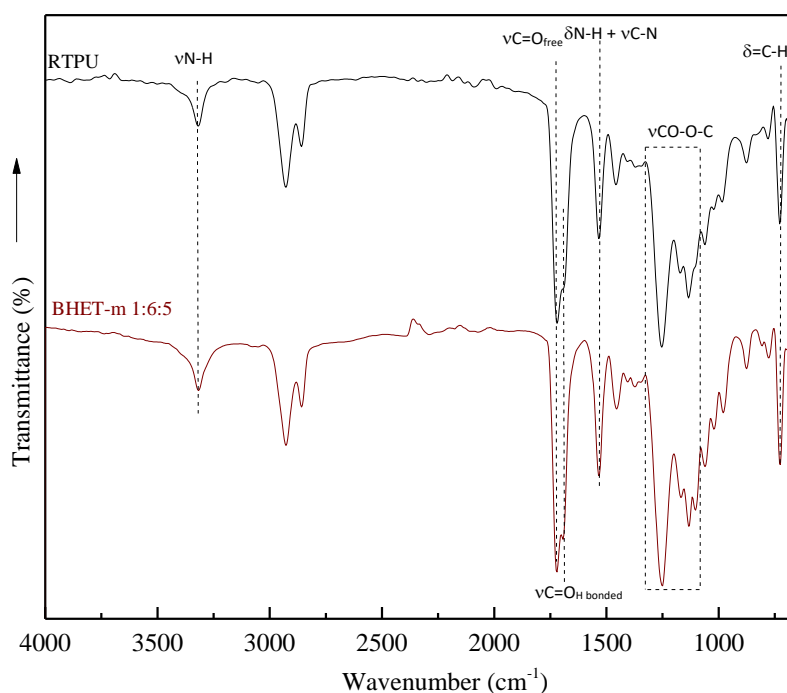


Figure 6.9. FTIR spectra of RTPU and previously synthesized BHET-m 1:6:5 TPUs.

On the other hand, the DSC thermograms shown in Figure 6.10 confirm the same thermal behavior. Thermal properties are summarized in Table 6.7.

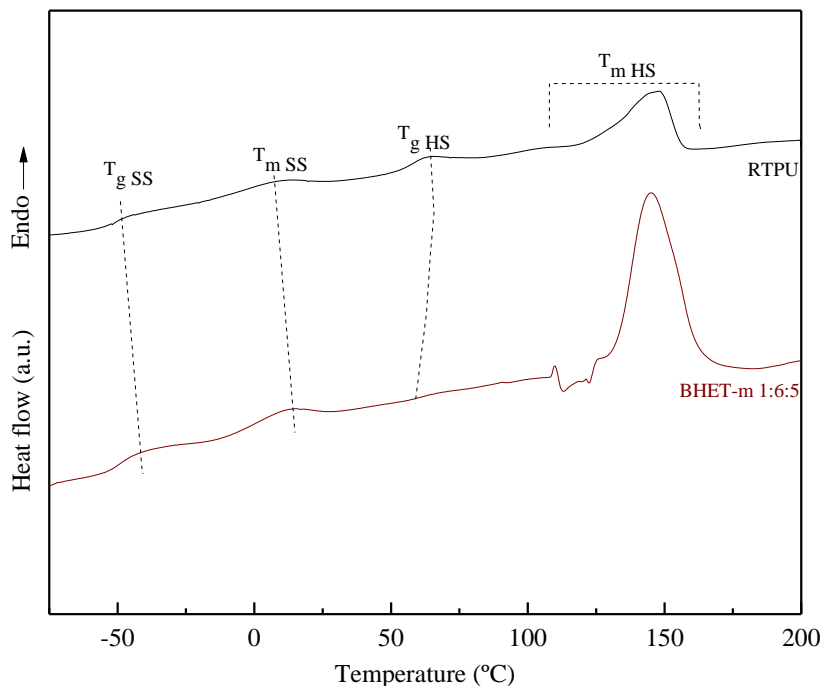


Figure 6.10. DSC thermograms of RTPU and BHET-m 1:6:5 TPUs.

Sample	T_g SS (°C)	T_m SS (°C)	ΔH_m SS (J/g)	T_g HS (°C)	T_m HS (°C)	ΔH_m HS (J/g)
RTPU	-51	10	2	59	148	17
BHET-m 1:6:5	-50	12	2	62	145	30

Table 6.7. DSC results of RTPU and BHET-m 1:6:5 polyurethanes.

Both PUs shows the same thermal transitions, those related with SS- and HS-rich domains. In the same way, $\Delta H_{m HS}$ value also decreases, attributed to the HS domain content present in RTPU, as already observed by FTIR.

Finally, RTPU samples were mechanically characterized. The stress-strain curves for RTPU and BHET-m 1:6:5 samples are represented in Figure 6.11. Moreover, the obtained mechanical properties, together with those obtained for BHET-m 1:6:5, are summarized in Table 6.8.

Tensile modulus, yield stress, stress at break and strain at break values for RTPU decrease compared to TPU sample. However, in addition to the lower urethane content of the RTPU sample, it is worth noting that the injected samples are air-cooled while synthesized TPU plaques are slowly cooled in the press, the thermal history of samples could be affecting the mechanical results. The BHET-m 1:6:5 polymer chains were able to pack into a more ordered structure, resulting in a stiffer and stronger material [25] compared to the reprocessed and air-cooled samples. Moreover, as it is well known, the thermo-mechanical recycling of polymers could lead

to thermo-oxidative degradation due the high injection temperature. This could promote chain excision during the, resulting in a more brittle material.

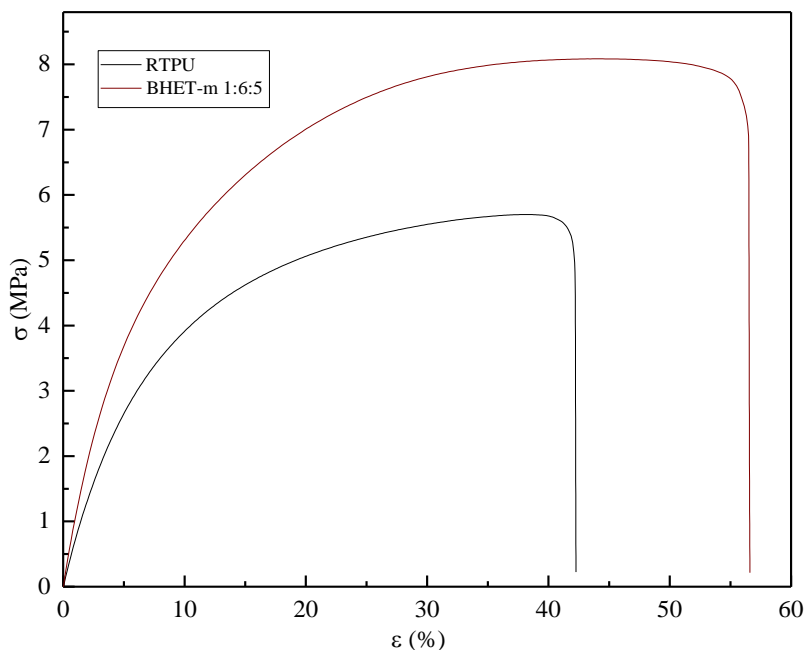


Figure 6.11. Stress-strain curves of RTPU and BHET-m 1:6:5 polyurethane.

Sample	E (MPa)	ϵ_b (%)	σ_y (MPa)	σ_b (MPa)
RTPU	63 ± 6	36 ± 2	1.1 ± 0.1	5.4 ± 0.4
BHET-m 1:6:5	102 ± 6	61 ± 13	1.6 ± 0.3	8.5 ± 0.3

Table 6.8. Mechanical properties of RTPU and BHET-m 1:6:5 polyurethane.

Therefore, it can be deduced that thermo-mechanical recycling is a valid option for the recycling of synthesized TPUs containing BHET, since no significant changes on physicochemical, mechanical and thermal properties were observed between the RTPU and TPU samples. However, comparisons should be made with caution, since in addition to the ratio of segments, both soft and hard, the final properties are also affected by the thermal history.

6.4.2. Chemical recycling of synthesized low molar mass TPUs by glycolysis

Chemical recycling processes allow to obtain basic hydrocarbon, monomers, dimers or oligomers, products with high added value. The two most successful methods of chemical recycling are glycolysis and hydrolysis, where exchange reactions are used to recover hydroxylated compounds [27].

Regarding PUs, glycolysis has been reported to be the most widely employed chemical recycling process [28]. Glycolysis involves a urethane exchange reaction, in which the C-O attached to the

carbonyl of urethane group is exchanged by the hydroxyl group of a glycol, as shown in Figure 6.12.

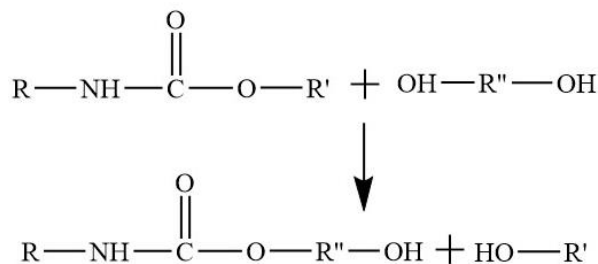


Figure 6.12. Main glycolysis reaction of polyurethanes.

In the case of the synthesized TPUs samples, as shown in Figure 6.13, the urethane group connected to with both the macrodiol and BHET. Therefore, exchange may result in the attachment of hydroxyl groups to BHET- or macrodiol-rich components, as shown in Figures 6.13a and 6.13b.

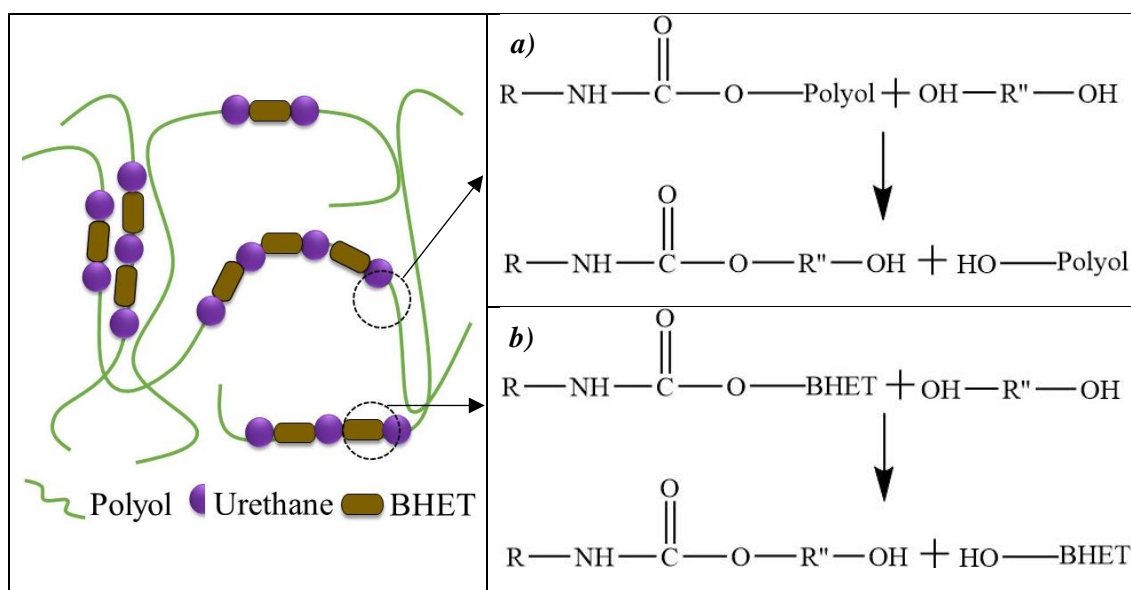


Figure 6.13. Graphical scheme and reactions that can take place in the glycolysis of synthesized TPUs.

The chemical recycling of a mixture of composed by all synthesized TPUs (BHET-m 1:2:1, BHET-m 1:3:2, BHET-m 1:4:3, BHET-m 1:5:4 and BHET-m 1:6:5) was performed by a glycolysis reaction. The reaction was carried out in a closed reactor placing 30 g of the mixture and EG in a weight ratio of 4:1 (TPU:EG). The glycolysis reaction was carried out at 180 °C for 2 h, using potassium acetate as a catalyst in a 0.4 wt%. After reaction, obtained mixture (TPU-Gly) was collected and cooled to room temperature. The next day, a few drops of phosphoric acid were added after heating the TPU-Gly to 80 °C, in order to prevent side reactions occurring when

the glycolyzed polyol is reused for other syntheses, obtaining a pH of 5.82. Figure 6.14 shows a digital image of obtained TPU-Gly.



Figure 6.14. TPU-Gly obtained from the glycolysis reaction of TPUs.

6.4.2.1. GPC

The weight distribution and molar mass of TPU-Gly were analyzed by GPC. Obtained chromatogram is represented in Figure 6.15 together with those of the macrodiol and BHET employed. Different peaks are observed for the glycolyzed sample, while only one significant peak is observed for the macrodiol. For this reason, two intervals have been differentiated in the chromatogram of the glycolyzed product, named as A and B.

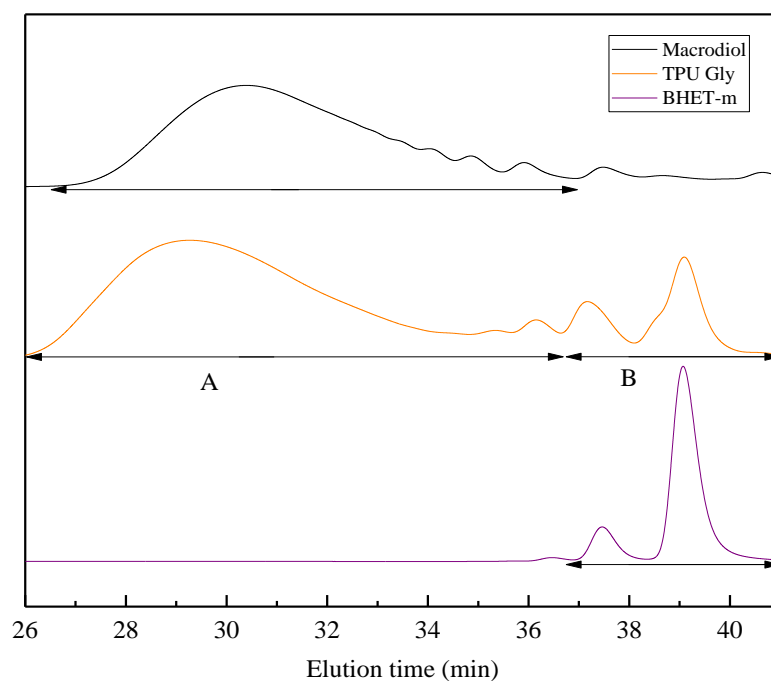


Figure 6.15. GPC chromatogram of the glycolyzed polyol, BHET-m and commercial macrodiol.

As seen in Figure 6.13, the zone A can be related with the macrodiol-based hydroxylated component, as the TPU-Gly shows a main peak with a elution time of 29 min ($M_n = 3316$ g/mol and $M_w = 10394$ g/mol, referred to PS standards) quite similar to that observed for the macrodiol at 30 min ($M_n = 2626$ g/mol and $M_w = 6306$ g/mol, referred to PS). The slightly higher molar mass measured for TPU-Gly could be attributed to the presence of slightly longer polymer chain after depolymerization reaction.

On the other hand, the B interval showed two peaks at 37 min ($M_n = 430$ g/mol and $M_w = 442$ g/mol) and 39 min ($M_n = 178$ g/mol and $M_w = 187$ g/mol) that seem to match quite well with the peaks observed for BHET-m at 37.5 min ($M_n = 393$ g/mol and $M_w = 398$ g/mol) and 39.1 min ($M_n = 168$ g/mol and $M_w = 174$ g/mol). Therefore, component B of the TPU-Gly sample can be attributed to BHET-based hydroxylated components [29,30]. Therefore, the area between 26 and 37 min (contribution A) is attributed to macrodiol-rich fraction, while that between 37 and 40 min (contribution B), is attributed to BHET-based products. Moreover, macrodiol and BHET fractions of 81 % and 19 %, respectively, were calculated integrating the area under the peak. The BHET fraction obtained was in the order of the average BHET content for all samples used in glycolysis, agreeing the scheme proposed in Figure 6.13.

6.4.2.2. FTIR

The FTIR spectrum of the TPU-Gly is represented in Figure 6.15a together with those of macrodiol and TPU synthesized with the highest BHET content (BHET-m 1:6:5).

Comparing TPU-Gly with the TPU, the former presents a wider band at around 3350-330 cm^{-1} , as shown in Figure 6.16b. This band encompasses the band corresponding to the stretching vibration of the -OH group characteristic of the glycolized product and the stretching vibration of N-H bond of urethane groups still present in the glycolized product (Figure 6.16b) [26]. Furthermore, the presence of -OH group in the TPU-Gly sample is also confirmed by the bands around 1100-1000 cm^{-1} , corresponding to primary alcohols [31].

At amide I and amide II region (1750-1500 cm^{-1}) shown in Figure 6.16c, is observed that BHET-m 1:6:5 TPU sample and the glycolized product present two bands related to the non-hydrogen bonded and hydrogen bonded C=O of the urethane group at 1730-1718 cm^{-1} and 1700-1680 cm^{-1} intervals, respectively [5,6]. The intensity of these bands decreases slightly for TPU-Gly compared to BHET-m 1:6:5 TPU, probably due to the lower overall urethane content in the glycolized TPU mixture compared to BHET-m 1:6:5 TPU.

Furthermore, at the amide II band interval, the spectrum of TPU-Gly also shows a lower intensity for the band located at 1535 cm^{-1} , related to the N-H bending vibration combined with C-N stretching vibration [6,7], probably due to the lower urethane content.

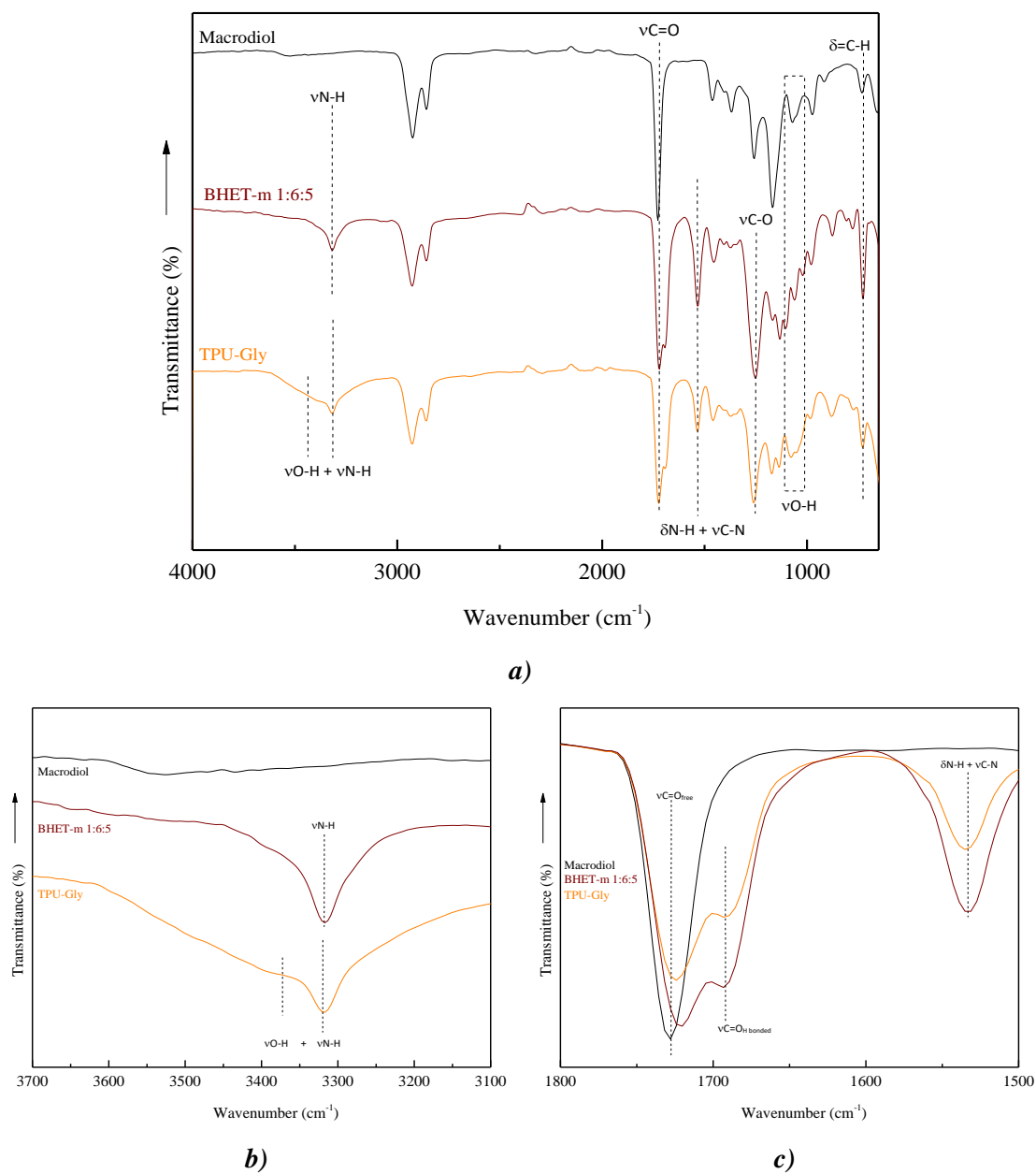


Figure 6.16. FTIR of TPU-Gly, macrodiol, and synthesized BHET-m 1:6:5 **a)** at 4000-700 cm^{-1} , **b)** at 3700-3100 cm^{-1} and **c)** at amide I and amide II region from 1800-1500 cm^{-1} .

6.4.2.3. DSC

Thermal properties of the glycolized product were analyzed by DSC. Figure 6.17 shows the thermograms of TPU-Gly, macrodiol and the BHET-m 1:6:5. The DSC results are summarized in Table 6.9.

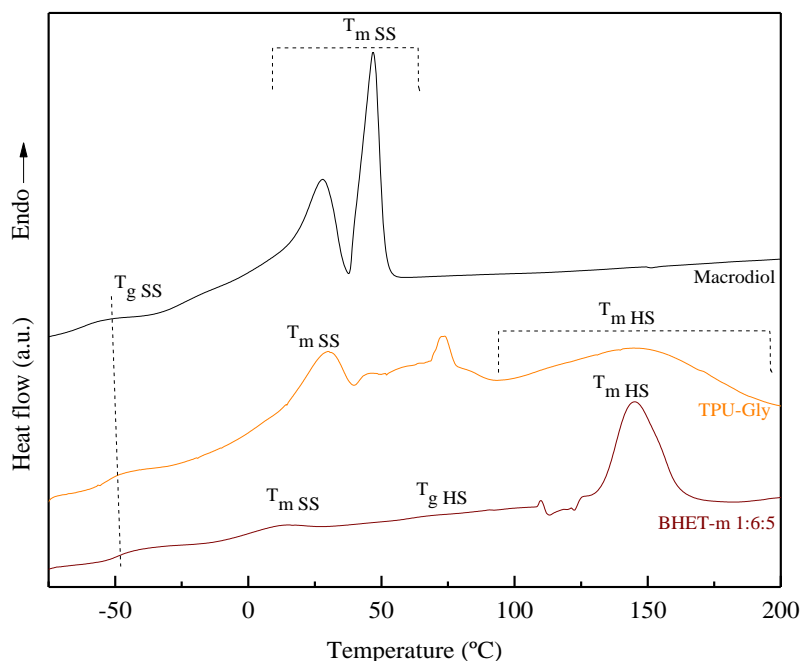


Figure 6.17. DSC thermograms for TPU-Gly, macrodiol and TPU BHET-m 1:6:5.

TPU-Gly shows several thermal transitions also observed for BHET-m 1:6:5 TPU, that would be related to SS and HS domains of synthesized TPUs. The observed transitions are the T_g at -53°C and the ΔH_m at $30\text{--}45^\circ\text{C}$, related to the macrodiol rich domain and the melting enthalpies at 73 and 150°C related to the HDI-BHET-rich domain. These transitions suggest that TPU-Gly is composed of low molar mass fractions, as already seen by GPC, consisting of either macrodiol or HDI:BHET-m rich segments, or even both.

Samples	$T_{g\text{ SS}}$ ($^\circ\text{C}$)	$T_{m\text{ SS}}$ ($^\circ\text{C}$)	$\Delta H_{m\text{ SS}}$ (J/g)	$T_{g\text{ HS}}$ ($^\circ\text{C}$)	$T_{m\text{ HS}}$ ($^\circ\text{C}$)	$\Delta H_{m\text{ HS}}$ (J/g)
Macrodiol	-62	28, 46	40	-	-	-
TPU-Gly	-53	30	10	-	73, 150	33
BHET-m 1:6:5	-50	1	2	62	145	30

Table 6.9. DSC results of TPU-Gly, macrodiol and TPU BHET-m 1:6:5.

6.4.2.4. TGA

The thermal stability of glycolyzed product was analyzed by TGA and compared with that of pure macrodiol and BHET-m 1:6:5 TPU. The thermograms and their corresponding derivative curves are plotted in Figure 6.18. As it can be seen, the TPU-Gly present three weight loss steps and lower thermal stability, as it starts to lose weight earlier.

The first weight loss at around $100\text{--}180^\circ\text{C}$ (corresponding to around 8 %) may be associated with the EG not consumed in the glycolysis [32], recovered in the glycolyzed product since glycolysis

was carried out in a single phase. The other two peaks at 320 and 420 °C, also observed in the BHET-m 1:6:5, are attributed to the degradation of BHET and urethane groups, and macrodiol, respectively. The degradation peak observed around 320-340 °C is broader in the TPU-Gly sample comparing with that of BHET-m 1:6:5. This fact may be related to the degradation of BHET, residual urethane and by-products presented in the TPU-Gly [26].

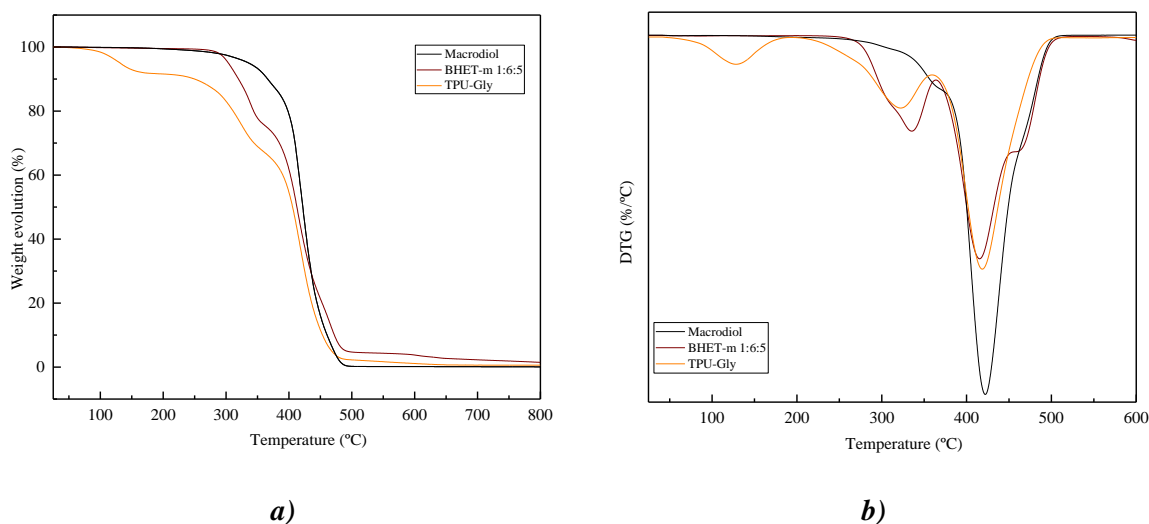


Figure 6.18. a) Weight evolution and b) DTG curves of TPU-Gly, macrodiol and BHET-m 1:6:5.

6.5. Conclusions

In this chapter, sustainable TPUs were successfully synthesized using chemically recycled BHET from marine PET litter and a macrodiol derived from renewable sources. In this way, TPU formulations containing up to 30 % recycled BHET were obtained. In all cases, the renewable and/or recycled content is higher than 40 %.

It was observed that the increase of recycled BHET leads to materials with high thermo-mechanical stability, since the segments formed by aromatic BHET and HDI isocyanate were able to form interurethane interactions between adjacent chain segments, giving rise to crystalline structures with high melting temperature. Moreover, these structures, dispersed in the macrodiol matrix as observed by AFM, act as reinforcement and provide stiffness to the material. Increasing the content of HS results in stiffer and more brittle materials. Furthermore, the physicochemical, thermal and mechanical properties of TPUs synthesized from recycled BHET were comparable to those of polyurethanes synthesized from commercial fossil-derived BHET, as both BHETs showed similar characteristics.

Therefore, it can be concluded that the use of recycled BHET from marine PET litter as a chain extender for the production of segmented TPUs is a suitable alternative to valorize highly

degraded PET waste. In addition, using biobased components, such as macrodiols derived from renewable vegetable oils, TPUs with a high content of recycled and/or renewable components can be synthesized. Environmentally friendly synthesis strategies can also be followed, without solvents or organic catalysts. All this contributes to the development of sustainable TPUs in line with the circular economy model.

On the other hand, to demonstrate the recyclability of synthesized TPUs, their thermo-mechanical and chemical recycling were performed. It was observed that thermo-mechanical recycling has no significant effect on the RTPUs chemical structure. However, regarding thermal and mechanical properties, it must be taken into account that properties may vary due to slight changes in composition, as is the case of HS and SS content, but also due to thermal history. It should also be taken into account that during thermo-mechanical recycling, chain cleavage may occur, which may affect the final properties.

Finally, chemical recycling by glycolysis with EG was performed. Obtained product showed a wide size distribution pattern with two main contributions, one representing the 81%, related with macrodiol-rich components and, second, representing the 19%, related with BHET-rich components. Moreover, TGA results suggested that unreacted EG could remain in the glycolyzed mixture, as glycolysis was performed in a single step.

6.6. References

- [1] T. Calvo-Correas, A. Santamaria-Echart, A. Saralegi, L. Martin, Á. Valea, M.A. Corcuera, A. Eceiza, Thermally-responsive biopolyurethanes from a biobased diisocyanate, *Eur Polym J.* 70 (2015) 173–185. <https://doi.org/10.1016/J.EURPOLYMJ.2015.07.022>.
- [2] E.M. Maafi, F. Malek, L. Tighzert, Synthesis and characterization of new polyurethane based on polycaprolactone, *J Appl Polym Sci.* 115 (2010) 3651–3658. <https://doi.org/10.1002/app.31448>.
- [3] C.-C. Hsieh, Y.-C. Chen, Synthesis of bio-based polyurethane foam modified with rosin using an environmentally-friendly process, *J Clean Prod.* 276 (2020) 124203–1242037. <https://doi.org/10.1016/j.jclepro.2020.124203>.
- [4] Y.-M. Tsai, T.-L. Yu, Y.-H. Tseng, Physical properties of crosslinked polyurethane, *Polym Int.* 47 (1998) 445–450. [https://doi.org/10.1002/\(SICI\)1097-0126\(199812\)47:4<445::AID-PI82>3.0.CO;2-B](https://doi.org/10.1002/(SICI)1097-0126(199812)47:4<445::AID-PI82>3.0.CO;2-B).
- [5] J.L. Ryszkowska, M. Auguścik, A. Sheikh, A.R. Boccaccini, Biodegradable polyurethane composite scaffolds containing Bioglass® for bone tissue engineering, *Compos Sci Technol.* 70 (2010) 1894–1908. <https://doi.org/10.1016/J.COMPSCITECH.2010.05.011>.

- [6] T. Calvo-Correas, L. Ugarte, P.J. Trzebiatowska, R. Sanzberro, J. Datta, M.Á. Corcuera, A. Eceiza, Thermoplastic polyurethanes with glycolysate intermediates from polyurethane waste recycling, *Polym Degrad Stab.* 144 (2017) 411–419. <https://doi.org/10.1016/J.POLYMDEGRADSTAB.2017.09.001>.
- [7] J. Datta, E. Głowińska, Effect of hydroxylated soybean oil and bio-based propanediol on the structure and thermal properties of synthesized bio-polyurethanes, *Ind Crops Prod.* 61 (2014) 84–91. <https://doi.org/10.1016/J.INDCROP.2014.06.050>.
- [8] Q. Tang, K. Gao, Structure analysis of polyether-based thermoplastic polyurethane elastomers by FTIR, 1H NMR and 13C NMR, *Int J Polym Anal.* 22 (2017) 569–574. <https://doi.org/10.1080/1023666X.2017.1312754>.
- [9] M.A. Pérez-Limiñana, F. Arán-Aís, A.M. Torró-Palau, A.C. Orgilés-Barceló, J.M. Martín-Martínez, Characterization of waterborne polyurethane adhesives containing different amounts of ionic groups, *Int J Adhes Adhes.* 25 (2005) 507–517. <https://doi.org/10.1016/j.ijadhadh.2005.02.002>.
- [10] A. Bhattacharyya, D. Mukherjee, R. Mishra, P.P. Kundu, Preparation of polyurethane–alginate/chitosan core shell nanoparticles for the purpose of oral insulin delivery, *Eur Polym J.* 92 (2017) 294–313. <https://doi.org/10.1016/j.eurpolymj.2017.05.015>.
- [11] M.A. Corcuera, L. Rueda, B. Fernandez d’Arlas, A. Arbelaz, C. Marieta, I. Mondragon, A. Eceiza, Microstructure and properties of polyurethanes derived from castor oil, *Polym Degrad Stab.* 95 (2010) 2175–2184. <https://doi.org/10.1016/j.polymdegradstab.2010.03.001>.
- [12] M.A. Corcuera, L. Rueda, A. Saralegui, Ma.D. Martín, B. Fernández-d’Arlas, I. Mondragon, A. Eceiza, Effect of diisocyanate structure on the properties and microstructure of polyurethanes based on polyols derived from renewable resources, *J Appl Polym Sci.* 122 (2011) 3677–3685. <https://doi.org/10.1002/app.34781>.
- [13] C. Bueno-Ferrer, E. Hablot, M. del C. Garrigós, S. Bocchini, L. Averous, A. Jiménez, Relationship between morphology, properties and degradation parameters of novative biobased thermoplastic polyurethanes obtained from dimer fatty acids, *Polym Degrad Stab.* 97 (2012) 1964–1969. <https://doi.org/10.1016/j.polymdegradstab.2012.03.002>.
- [14] S. Mondal, J.L. Hu, Influence of hard segment on thermal degradation of thermoplastic segmented polyurethane for textile coating application, *Polym Plast Technol Eng.* 46 (2007) 37–41. <https://doi.org/10.1080/03602550600948715>.

- [15] D.M. Crawford, R.G. Bass, T.W. Haas, Strain effects on thermal transitions and mechanical properties of thermoplastic polyurethane elastomers, *Thermochim Acta.* 323 (1998) 53–63. [https://doi.org/10.1016/S0040-6031\(98\)00541-3](https://doi.org/10.1016/S0040-6031(98)00541-3).
- [16] M.L. Auad, M.A. Mosiewicki, T. Richardson, M.I. Aranguren, N.E. Marcovich, Nanocomposites made from cellulose nanocrystals and tailored segmented polyurethanes, *J Appl Polym Sci.* 115 (2010) 1215–1225. <https://doi.org/10.1002/app.31218>.
- [17] E.M. Maafi, L. Tighzert, F. Malek, Synthesis and characterization of new polyurethanes: influence of monomer composition, *Polymer Bulletin.* 66 (2011) 391–406. <https://doi.org/10.1007/s00289-010-0347-1>.
- [18] L. Ugarte, B. Fernández-d'Arlas, A. Valea, M.L. González, M.A. Corcuera, A. Eceiza, Morphology-properties relationship in high-renewable content polyurethanes, *Polym Eng Sci.* 54 (2014) 2282–2291. <https://doi.org/10.1002/pen.23777>.
- [19] B. Fernández-d'Arlas, L. Rueda, R. Fernández, U. Khan, J.N. Coleman, I. Mondragon, A. Eceiza, Inverting polyurethanes synthesis: effects on nano/micro-structure and mechanical properties, *Soft Mater.* 9 (2010) 79–93. <https://doi.org/10.1080/1539445X.2010.525173>.
- [20] B. Fernández-D'Arlas, A. Alonso-Varona, T. Palomares, M.A. Corcuera, A. Eceiza, Studies on the morphology, properties and biocompatibility of aliphatic diisocyanate-polycarbonate polyurethanes, *Polym Degrad Stab.* 122 (2015) 153–160. <https://doi.org/10.1016/j.polymdegradstab.2015.10.023>.
- [21] B. Fernández-D'Arlas, L. Rueda, K. de La Caba, I. Mondragon, A. Eceiza, Microdomain composition and properties differences of biodegradable polyurethanes based on MDI and HDI, *Polym Eng Sci.* 48 (2008) 519–529. <https://doi.org/10.1002/pen.20983>.
- [22] K. Sarkar, S. Rama, K. Meka, A. Bagchi, N.S. Krishna, S.G. Ramachandra, G. Madras, K. Chatterjee, Polyester derived from recycled poly(ethylene terephthalate) waste for regenerative medicine, *RSC Adv.* (2014) 58805–58815. <https://doi.org/10.1039/c4ra09560j>.
- [23] G. Kiss, G. Rusu, F. Peter, I. Tănase, G. Bandur, Recovery of flexible polyurethane foam waste for efficient reuse in industrial formulations, *Polymers (Basel).* 12 (2020) 1533–1547. <https://doi.org/10.3390/polym12071533>.
- [24] L. Gausas, S.K. Kristensen, H. Sun, A. Ahrens, B.S. Donslund, A.T. Lindhardt, T. Skrydstrup, Catalytic hydrogenation of polyurethanes to base chemicals: from model systems to commercial and end-of-life polyurethane materials, *JACS Au.* 1 (2021) 517–524. <https://doi.org/10.1021/jacsau.1c00050>.

- [25] T. Calvo-Correas, M. Benitez, I. Larraza, L. Ugarte, C. Peña-Rodríguez, A. Eceiza, Advanced and traditional processing of thermoplastic polyurethane waste, *Polym Degrad Stab.* 198 (2022) 109880–109889. <https://doi.org/10.1016/j.polymdegradstab.2022.109880>.
- [26] T. Calvo-Correas, L. Ugarte, P.J. Trzebiatowska, R. Sanzberro, J. Datta, M.Á. Corcuera, A. Eceiza, Thermoplastic polyurethanes with glycolysate intermediates from polyurethane waste recycling, *Polym Degrad Stab.* 144 (2017) 411–419. <https://doi.org/10.1016/j.polymdegradstab.2017.09.001>.
- [27] D.K. Schneiderman, M.E. Vanderlaan, A.M. Mannion, T.R. Panthani, D.C. Batiste, J.Z. Wang, F.S. Bates, C.W. Macosko, M.A. Hillmyer, Chemically recyclable biobased polyurethanes, *ACS Macro Lett.* 5 (2016) 515–518. <https://doi.org/10.1021/acsmacrolett.6b00193>.
- [28] C.-H. Wu, C.-Y. Chang, J.-K. Li, Glycolysis of rigid polyurethane from waste refrigerators, *Polym Degrad Stab.* 75 (2002) 413–421. [https://doi.org/10.1016/S0141-3910\(01\)00237-3](https://doi.org/10.1016/S0141-3910(01)00237-3).
- [29] R. López-Fonseca, I. Duque-Ingunza, B. de Rivas, L. Flores-Giraldo, J.I. Gutiérrez-Ortiz, Kinetics of catalytic glycolysis of PET wastes with sodium carbonate, *Chem Eng J.* 168 (2011) 312–320. <https://doi.org/10.1016/J.CEJ.2011.01.031>.
- [30] P. Fang, B. Liu, J. Xu, Q. Zhou, S. Zhang, J. Ma, X. lu, High-efficiency glycolysis of poly(ethylene terephthalate) by sandwich-structure polyoxometalate catalyst with two active sites, *Polym Degrad Stab.* 156 (2018) 22–31. <https://doi.org/10.1016/J.POLYMDEGRADSTAB.2018.07.004>.
- [31] M. Ștefănescu, M. Stoia, O. Ștefănescu, C. Davidescu, G. Vlase, P. Sfirloagă, Synthesis and characterization of poly (vinyl alcohol)/ethylene glycol/silica hybrids. Thermal analysis and FT-IR study, *Rev Roum Chim.* 55 (2010) 17–23. <http://web.icf.ro/rrech/>.
- [32] A. Pasha, S. Khasim, O.A. Al-Hartomy, M. Lakshmi, K.G. Manjunatha, Highly sensitive ethylene glycol-doped PEDOT-PSS organic thin films for LPG sensing, *RSC Adv.* 8 (2018) 18074–18083. <https://doi.org/10.1039/c8ra01061g>.

Chapter 7

SYNTHESIS OF NEW THERMOSET POLYURETHANES

BASED ON RECYCLED BHET

7. SYNTHESIS OF NEW THERMOSET POLYURETHANES BASED ON RECYCLED BHET

7.1. Aim of the chapter

In this chapter, BHET-m recycled from marine PET litter was used for the synthesis of new thermoset PUs. Thermoset polymers present higher thermal and thermo-mechanical stability and mechanical properties, being more suitable for structural applications than thermoplastic ones. The objective of this chapter was to incorporate recycled monomers in the formulation of thermoset PUs characterizing their final properties and evaluate their suitability as high performance polyurethanes, thus evaluating another alternative to the BHET-m already used in the synthesis of thermoplastic polyurethanes. To carry out the synthesis of thermoset PUs, a biobased polyol derived from castor oil and a polymeric methylene diphenyl diisocyanate (pMDI) were used together with BHET-m obtained and characterized in Chapter 5.

In this work, five different thermoset PU compositions were synthesized varying the proportion of biobased polyol and BHET-m. More than 40 % of the components used in the synthesis were from renewable/recycled origin, with a recycled BHET-m content being up to 20 %. In this way, PUs were synthesized with a lower carbon footprint promoting the circular economy of these materials.

The different thermoset PUs resins were processed by compression molding to obtain compact plaques. The transparency and color parameters of plaques were analyzed by spectrophotometry and the presence of characteristic functional groups by FTIR. The thermal, thermo-mechanical and mechanical properties were analyzed by DSC, TGA, DMA and mechanical flexural tests. Finally, the surface hydrophilicity of the plaques was studied using the WCA.

In addition, the recyclability of synthesized thermoset PUs was evaluated by chemical recycling through glycolysis reaction. The glycolyzed product was characterized and compared with the polyol and BHET used for the synthesis of thermoset PUs.

7.2. Reactants and synthesis of thermoset PUs

A commercial biobased polyol derived from castor oil (Polycin 12, Vertellus, Denham Springs, USA), BHET-m monomer obtained from the glycolysis reaction of marine PET litter in Chapter 5 and a commercial pMDI (Desmodur 44 V, Covestro, Germany) were used for the synthesis of the thermoset PUs. PUs with different Polyol:BHET ratios were synthesized and characterized in order to analyze the effect of BHET-m on the final properties. PUs with a BHET-m content up

to 20 wt% were synthesized. In all cases, an isocyanate index of 1.1 was used. Designation, components molar ratio and content of components (%) employed in the synthesis together with the biobased content, are summarized in Table 7.1. Samples were named as PU and the Polyol:BHET molar ratio, since the ratio of pMDI remains constant for all samples.

Sample code	Molar ratio Polyol:BHET:pMDI	Polyol (%)	BHET-m (%)	pMDI (%)	Biobased content (%)
PU 1:0	1-0-1.1	54	0	46	43
PU 0.8:0.2	0.8-0.2-1.1	45	8	47	36
PU 0.7:0.3	0.7-0.3-1.1	40	12	48	32
PU 0.6:0.4	0.6-0.4-1.1	34	17	49	27
PU 0.5:0.5	0.5-0.5-1.1	29	21	50	23

Table 7.1. Designation, components molar ratio, percentage of components and biobased content of the different thermoset polyurethanes.

Thermoset PUs were synthesized by an one-step bulk polymerization process. First, pMDI and BHET-m were mixed at room temperature in a 250 mL round-bottom flask equipped with a mechanical stirrer for around 15-20 min, until a homogeneous mixture was observed. Then, the previously dried polyol was added to the mixture and stirred vigorously for 5-10 min until a homogeneous mixture was obtained. It is worth noting that longer mixing times were required for systems containing the highest BHET-m. Subsequently, the reaction mixture was casted between two Teflon coated metal plates separated by 1.5 mm and pressed under 50 bar, first at 120 °C for 2 h, and then at 140 °C for 2 h. A fraction of the mixture was separated to analyze the curing reaction by DSC. Figure 7.1 shows a digital image of the synthesized thermoset PUs.



Figure 7.1. Thermoset PUs with increasing BHET-m content, from left to right.

7.3. Characterization of synthesized thermoset PUs

7.3.1. DSC

The curing reaction of the PU mixture was analyzed by dynamic DSC (Figure 7.2). A clear T_g is observed for all mixtures around -40 °C, associated with the neat polyol, which increases with BHET-m content, probably due to some reaction occurring during mixing. In addition, an exothermic peak is observed around 100 °C, attributed to the curing reaction between pMDI

and polyol, and a second peak around 110 °C, attributed to the curing reaction of the remaining isocyanate groups with BHET-m, which becomes clearer as BHET-m content increases.

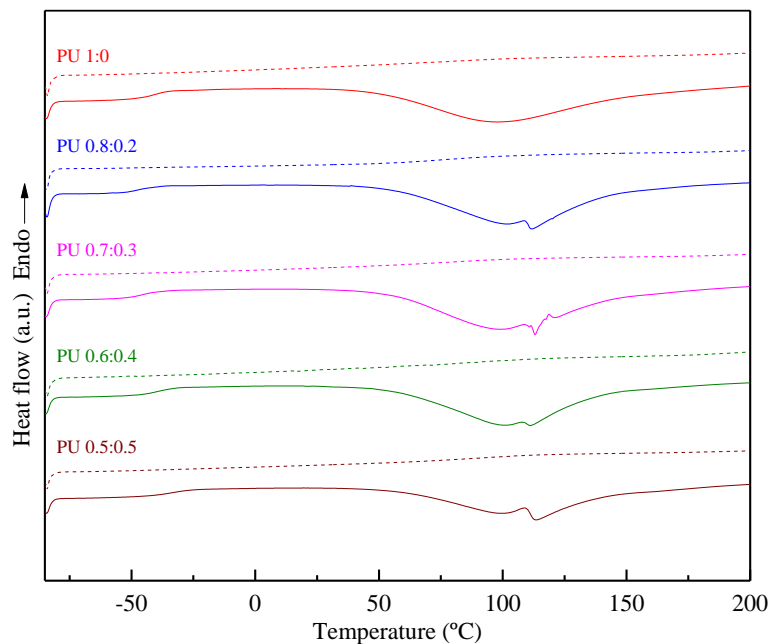


Figure 7.2. Dynamic DSC first (—) and second scan (-----) thermograms for the different PU systems.

The total enthalpy of curing reaction and the T_g , those before and after curing, are summarized in Table 7.2. It can be seen that the enthalpy of cure remains almost constant for the systems containing low BHET-m contents. However, although the isocyanate content was similar for all systems and a similar enthalpy of cure could be expected, a lower enthalpy of cure was measured for system containing the highest BHET-m content. The higher T_g measured for systems with the higher BHET-m content and the lower enthalpy shown by the PU 0.5:0:5 could be attributed to part of the curing reaction taking place during the mixing of the components, prior to the DSC test, being this effect more pronounced for higher BHET-m contents. In addition, all samples were subjected to a subsequent dynamic DSC scan to confirm the reaction completion (Figure 7.2), finding that none of the systems showed any trace of residual exothermic heat. Similar T_g values were obtained for all cured systems.

		PU 1:0	PU 0.8:0.2	PU 0.7:0.3	PU 0.6:0.4	PU 0.5:0.5
1 st scan	T_g (°C)	-41	-48	-46	-41	-34
	ΔH_{cur} (J/g)	116	118	127	118	90
2 nd scan	T_g (°C)	80	85	85	89	83

Table 7.2. DSC results obtained in the 1st and 2nd dynamic scans for different PUs.

7.3.2. Spectrophotometry

The color parameters of synthesized thermoset PUs were analyzed by spectrophotometry. As it can be seen in Figure 7.1, the samples became browner in color as BHET-m content increased. The changes in color were further studied by analyzing the color parameters by spectrophotometry (Table 7.3) taking as a white sample a Whatman® filter paper ($L^*=93.03$ $a^*=-0.34$ and $b^*=2.53$). Regarding the L^* values related to light-darkness, a decrease is observed with BHET-m content, corroborating the browning trend observed. Analyzing the a^* parameter related to red-green, an increasing trend is observed, indicating a shift of the red-green coordinates towards green. Similarly, with increasing of BHET-m content, an increase in ΔE^* is also observed, moving away from the parameters of the white sample. Regarding the WI values related to the whiteness index, a gradual decrease is observed with BHET-m content, due to the fact that these samples move away from the white color and are less reflective.

Samples	L^*	a^*	b^*	ΔE^*	WI
PU 1:0	69.8	1.5	63.4	65.2	29.8
PU 0.8:0:2	64.3	2.7	56.4	61.1	33.2
PU 0.7:0:3	62.8	4.9	58.2	63.6	30.8
PU 0.6:0:4	62.0	7.0	62.6	68.0	26.4
PU 0.5:0:5	60.9	7.1	61.0	67.2	27.1

Table 7.3. L^* , a^* , b^* , and ΔE^* color values and whiteness index of the thermoset PU samples.

7.3.3. FTIR

FTIR spectra of synthesized thermoset PUs, together with those of the polyol and BHET-m are presented in Figure 7.3.

A residual band characteristic of the isocyanate stretching vibration is observed around 2270 cm^{-1} , which can be attributed to the excess of isocyanate ($\text{NCO:OH} = 1.1$) employed in the synthesis [1,2]. However, none of the synthesized PUs showed the characteristic -OH stretching vibration band observed for BHET-m and polyol at 3342 cm^{-1} [3], denoting that the polymerization was completed, in agreement with DSC results. In addition, all PU samples showed characteristic bands of urethane group, as the band centered at 3317 cm^{-1} , ascribed to the stretching vibration of N-H bond [4], that remained constant for all samples due to the similar isocyanate content (Table 7.1). The bands in the 2930 and 2850 cm^{-1} range are related with the absorption band of -CH- and -CH₂- groups [5]. The band at 1712 cm^{-1} , attributed to the stretching vibration of carbonyl group, encompassed the stretching vibration of carbonyl group in urethane, and also the carbonyl of ester observed in the polyol at 1724 cm^{-1} and in BHET-m at 1708 cm^{-1} [6]. Furthermore, a new

absorption band is observed for all PUs in the amide II region ($1600\text{-}1500\text{ cm}^{-1}$) at 1523 cm^{-1} related to the bending vibration of N-H combined with the stretching vibration of C-N, characteristics of the urethane group [7,8].

Bands appearing between 1250 and 1050 cm^{-1} are related to the CO-O-C asymmetric and symmetric stretching vibrations [9,10] and remain constant for the synthesized PUs. Finally, the characteristic band at 725 cm^{-1} attributed to the C-H bond in the aromatic group of BHET-m is also observed [11]. The band intensity increases with the increase of BHET-m content in the thermoset PU.

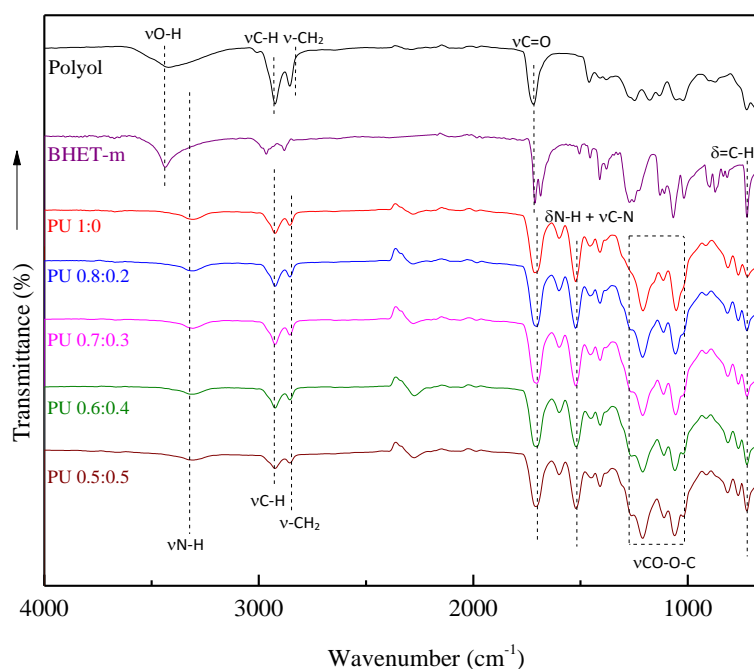


Figure 7.3. FTIR spectra of the synthesized thermoset polyurethane samples, polyol and BHET-m.

7.3.4. TGA

The thermal stability of synthesized PUs was analyzed in terms of TGA. The thermograms and the corresponding derivative curves are represented in Figure 7.4, while thermal degradation temperatures are summarized in Table 7.4. For comparative purposes, the thermogram of polyol and its derivative are also represented in Figure 7.4.

The thermal degradation of the polyol was observed between $250\text{-}474\text{ }^{\circ}\text{C}$, with a two-step weight loss, specifically at 393 and $470\text{ }^{\circ}\text{C}$. It has been reported in the literature that vegetable castor oil-based polyols usually show a double weight loss [12,13]. Thermal degradation of PU 1:0, without BHET-m, showed two weight losses, one between 300 and $330\text{ }^{\circ}\text{C}$, related to the degradation of urethane groups, T_{d1} , and the second around $470\text{ }^{\circ}\text{C}$, related to polyol degradation, T_{d2} [14–16]. Concerning the PUs containing BHET-m, it was observed that as the BHET-m content increased,

the first degradation temperature shifted to lower temperatures, which could be attributed to the lower thermal stability of BHET-m, which depending on the monomer, dimer and oligomer percentages shows a degradation temperature at the 180-280 °C interval.

Similarly, as summarized in Table 7.4, the thermoset PU samples containing BHET-m presented a higher residue with BHET-m content. This fact could be due to the incorporation of an aromatic component such as BHET-m, which generates char during combustion [17].

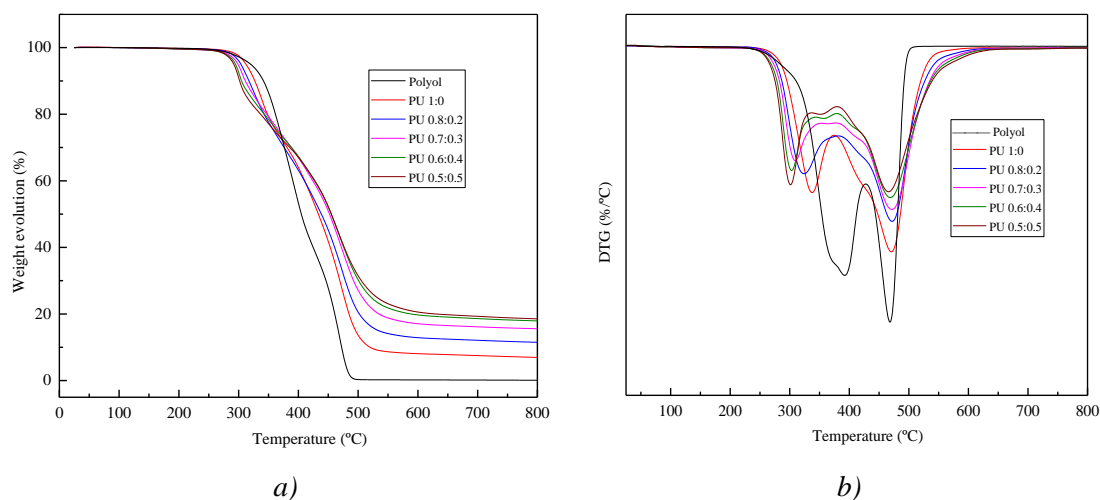


Figure 7.4. a) Weight evolution and b) DTG curves of synthesized thermoset PUs.

Sample	T _{d1} (°C)	T _{d2} (°C)	Residue (%)
PU 1:0	333	470	9
PU 0.8:0.2	317	471	13
PU 0.7:0.3	305	472	18
PU 0.6:0.4	300	468	20
PU 0.5:0.5	298	465	21

Table 7.4. Thermal degradation temperatures and residue content of for synthesized thermoset PUs.

7.3.5. DMA

The dynamic mechanical behavior of synthesized thermoset PUs was analyzed in flexural mode. Figure 7.5 shows the temperature dependence of the storage modulus (E') and loss factor ($\tan \delta$). The peak of $\tan \delta$ corresponds to the α relaxation and is related with the T_g of thermoset PUs [18]. The T_g values obtained by DMA, together with the values of E' at room temperature and in the rubbery plateau region (at T_g+50 °C), are summarized in Table 7.5, together with the cross-linking density values calculated with the Equation 2.4.

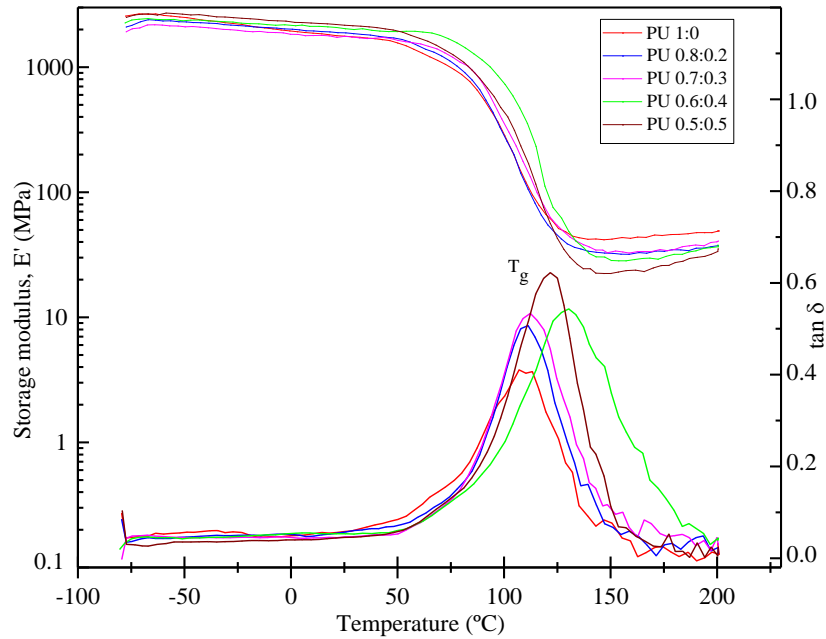


Figure 7.5. DMA results of synthesized thermoset PUs.

Samples	T_g °C ($\tan\delta$ max)	E' (MPa) (25 °C)	E' (MPa) (T_g+50)	ν (mol /m ³)
PU 1:0	107	1773	43	4036
PU 0.8:0.2	111	1882	32	2982
PU 0.7:0.3	112	1760	34	3085
PU 0.6:0.4	131	2041	32	2820
PU 0.5:0.5	122	2166	25	2272

 Table 7.5. T_g , storage modulus at 25 °C and in the rubbery region and cross-linking density for different PUs.

At temperatures below T_g , all systems showed a similar storage modulus, presenting at 25 °C, a value around 1.8 GPa for the PU 1:0 and, values between 1.8-2.2 GPa for systems containing BHET-m. However, above T_g , in the rubbery plateau region, lower storage modulus values were measured as BHET-m content increased. Regarding cross-linking density, a decrease was observed with the addition of BHET-m, due to replacement of a polyol with functionality higher than 2 by BHET-m with a functionality of 2. In general, although the cross-linking density decreased with BHET-m content, an increase of the T_g values was observed, with the exception of PU 0.5:0.5 sample, for which a lower value was observed. Therefore, it seems that with increasing BHET-m content, there was higher restriction to chain mobility and, consequently, T_g increased. The observed trend agrees with the T_g values previously obtained by DSC. Regarding the difference in T_g values obtained by both techniques, lower T_g values by DSC have been reported in the literature [19]. The mechanical test is much more sensitive than DSC to the

changes occurring at T_g , that is the reason for employing the maximum of $\tan \delta$ peak to determine the T_g [20,21].

7.3.6. Mechanical properties

The mechanical properties of synthesized thermoset PUs were measured by flexural tests. A representative stress-strain curve of each PU is shown in Figure 7.6. Table 7.6 summarizes the average value of flexural modulus (E), flexural strength (σ) and flexural strain (ϵ) obtained.

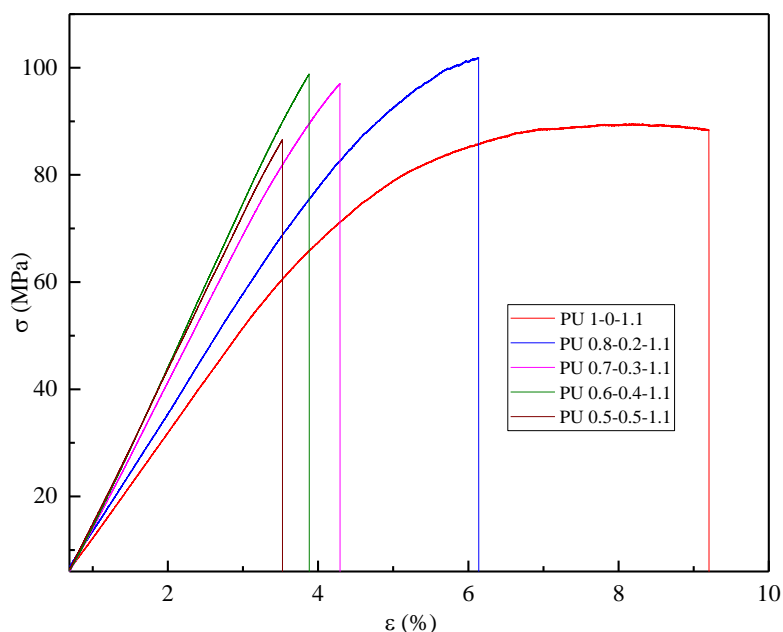


Figure 7.6. Mechanical properties of synthesized thermoset PUs.

It was clearly observed BHET-m addition increased flexural modulus, even if lower flexural strain was obtained. The aromatic structure of BHET-m provided stiffness to the system [21], but the incorporation of a difunctional monomer like BHET-m instead of polyol ($f = 4$) resulted in a lower cross-linking density as already observed in DMA, resulting in lower strength and faster breakage of the material, hence lower flexural strain.

Samples	E (MPa)	σ (MPa)	ϵ (%)
PU 1:0	1942 ± 25	89 ± 1	8.2 ± 0.0
PU 0.8:0.2	2323 ± 64	103 ± 2	5.9 ± 0.3
PU 0.7:0.3	2769 ± 28	94 ± 3	4.1 ± 0.2
PU 0.6:0.4	3103 ± 41	101 ± 3	3.5 ± 0.5
PU 0.5:0.5	2945 ± 18	88 ± 3	3.6 ± 0.2

Table 7.6. Mechanical properties of synthesized thermoset PUs.

7.3.7. WCA

Finally, the effect of the incorporation of BHET-m on the hydrophilicity of synthesized PUs was also analyzed. In the synthesized thermoset PU, the density of hydrophilic dipole-forming urethane groups [22,23] remains almost constant (Table 7.1), and therefore the only effect would come from the increase in BHET-m content.

In this context, as shown in Table 7.7, an increase in the WCA values was observed with BHET-m content, which can be attributed to the increase in the hydrophobic aromatic content present at BHET [24]. Hydrophobic surfaces with WCA values of almost 90° were obtained at high BHET contents.

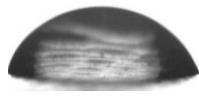
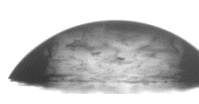
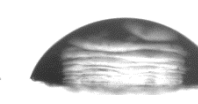
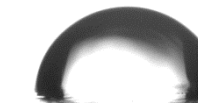
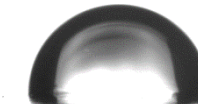
PU 1:0	PU 0.8:0.2	PU 0.7:0.3	PU 0.6:0.4	PU 0.5:0.5
Water contact angle (°)				
63 ± 3	60 ± 3	68 ± 5	84 ± 6	86 ± 4
				

Table 7.7. WCA results of synthesized thermoset PUs.

7.4. Chemical recycling of synthesized thermoset PUs

TPUs can be mechanically and chemically recycled, but thermoset PUs cannot be reprocessed again because they cannot be melted, the chemical recycling being the only possible way [25,26]. As already discussed in Chapter 6, glycolysis is the most commonly used chemical recycling process for PU wastes. Glycolysis of synthesized thermoset PUs could result in the obtention of both polyol-based hydroxylated component and BHET-based hydroxylated component, Figure 7.7.

The glycolysis reaction was carried out in a closed reactor by placing 30 g pellets of all synthesized thermoset PUs containing BHET-m (milled samples from PU 0.8:0.2 to PU 0.5:0.5) and EG in a weight ratio of 4:1 (PU:EG). Potassium acetate was used as a catalyst (0.4 wt.%) and the reactor was heated at 180 °C for 2 h. It should be noted that a single-phase was observed after the glycolysis process, which mainly consist on a mixture of the polyol-based and BHET-based hydroxylated components and the unreacted diol used in the glycolysis.

After reaction, the single-phase glycolyzed mixture product was collected and cooled down to room temperature. Then, phosphoric acid was added at 80 °C until the pH was in the range between 5 and 6.5 to avoid side reactions taking place when the glycolyzed product is reused in

further synthesis. The glycolyzed mixture product (PU-Gly) with a pH of 5.76 was then characterized.

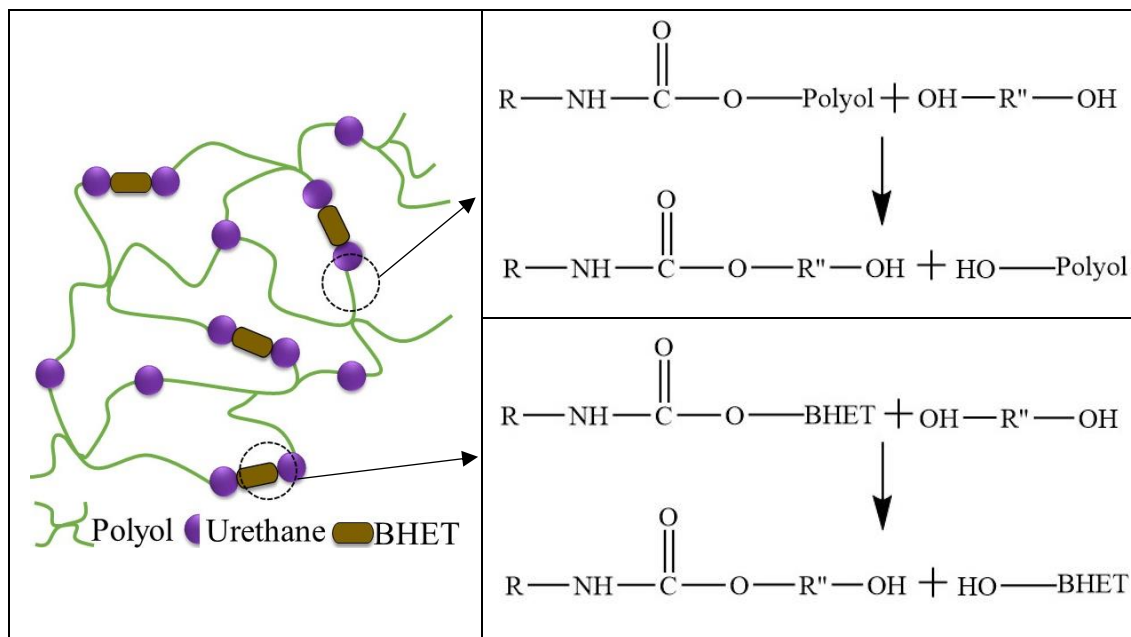


Figure 7.7. Graphical scheme and reactions that can take place in the glycolysis of synthesized thermoset PUs.

A digital image of the obtained PU-Gly is shown in Figure 7.8. As it could be observed the product obtained was a dark brown viscous liquid.



Figure 7.8. Glycolyzed mixture product obtained after the glycolysis of the synthesized thermoset PUs.

7.4.1. GPC

Firstly, the molar mass values and the polydispersity were measured by GPC. Figure 7.9 shows GPC chromatograms obtained for PU-Gly and for the commercial polyol and the BHET-m used in the synthesis of the thermoset PUs. The glycolyzed mixture product shows several peaks

between 30 and 41 min suggesting a broad size distribution, which encompass the distribution observed for polyol and BHET-m. That is why two intervals A and B, have been differentiated in the glycolyzed product.

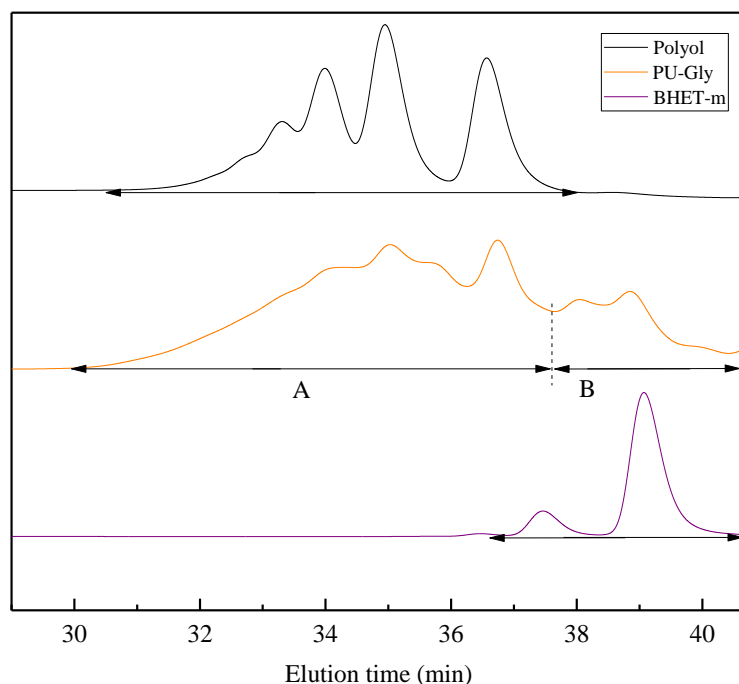


Figure 7.9. GPC traces of PU-Gly, and polyol and BHET-m employed in the synthesized thermoset PUs.

As seen in Figure 7.7, B interval could be attributed to the glycolysis fraction containing BHET-rich monomers, dimers or other alcohols, since the peak observed at 39 min is related to BHET-m and the polyol does not present peaks at longer elution times.

On the other hand, A interval could be mainly attributed to the polyol-rich hydroxylated components. Therefore, the weight and number average molar mass (based on calibration curve with monodisperse PS standards) between 30.0 and 37.6 min attributed to polyol-rich fraction would be $M_w= 1475$ g/mol and $M_n= 936$ g/mol respectively, while between 37.6 and 40.5, min attributed to BHET-rich fraction, would be $M_w= 196$ g/mol and $M_n= 167$ g/mol, respectively. These values are in the range of those measured in Figure 9a for polyol ($M_w= 1379$ g/mol and $M_n= 1054$ g/mol) and for BHET-m (at 37.5 min, $M_n= 393$ g/mol and $M_w= 398$ g/mol and at 39.1 min $M_n= 168$ g/mol and $M_w= 174$ g/mol). It should be remarked that values measured for BHET-m agree with those previously reported [27,28]. However, it is important to note that the contribution of both polyol-rich and BHET-rich fractions could overlap in the interval between 36.8 and 37.9 min. Therefore, the polyol-rich and BHET-rich fractions, calculated by integrating the area under the peak in each interval, were of 72 and 28 %, respectively. The BHET-m fraction

obtained was close to the BHET-m content average used in the thermoset PU samples, corroborating the scheme proposed in Figure 7.7.

7.4.2. FTIR

The evolution of functional groups in PU-Gly with respect to the thermoset PUs synthesized was analyzed by FTIR. Figure 7.10 shows the spectra of one of the synthesized PUs, the polyol used in the synthesis and the glycolyzed product. PU-Gly showed a band at 3342 cm^{-1} , which appeared between the absorption band observed for the polyol at 3429 cm^{-1} , characteristic of the -OH stretching vibration, and the absorption band observed in the PU at 3317 cm^{-1} , characteristic of the N-H stretching vibration of the urethane group. Therefore, the absorption band observed for the glycolyzed product suggests that, in addition to the newly formed hydroxyl groups, urethane groups remained in the mixture after the glycolysis [29]. The formation of -OH groups during glycolysis was also confirmed by the new absorption bands around $1100\text{-}1000\text{ cm}^{-1}$, not present in the PU, characteristic of the absorption of C-OH stretching vibration of primary alcohols [30]. On the other hand, the rest of the bands such as that related to the stretching vibration of carbonyl groups of esters and urethanes at around $1720\text{-}1710\text{ cm}^{-1}$, combined with the C-N stretching and the N-H bending bands at 1523 cm^{-1} , the C-O stretching vibration at 1220 cm^{-1} and band related to aromatic C-H bonds at 725 cm^{-1} , were also observed in the PU. All spectra showed bands related to $-\text{CH}_2-$ groups around $2950\text{-}2850\text{ cm}^{-1}$ [30].

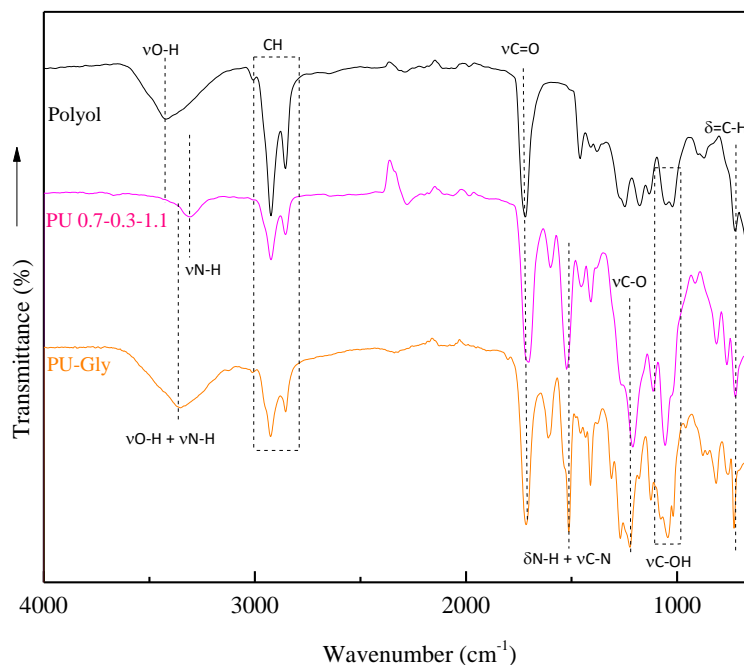


Figure 7.10. FTIR spectra of glycolyzed product, polyol employed in the synthesis of PU and thermoset PU.

7.4.3. DSC

Thermal properties of glycolyzed product were analyzed in terms of DSC. The thermograms of PU-Gly, polyol and synthesized PU 0.7:0.3 samples are shown in Figure 7.11.

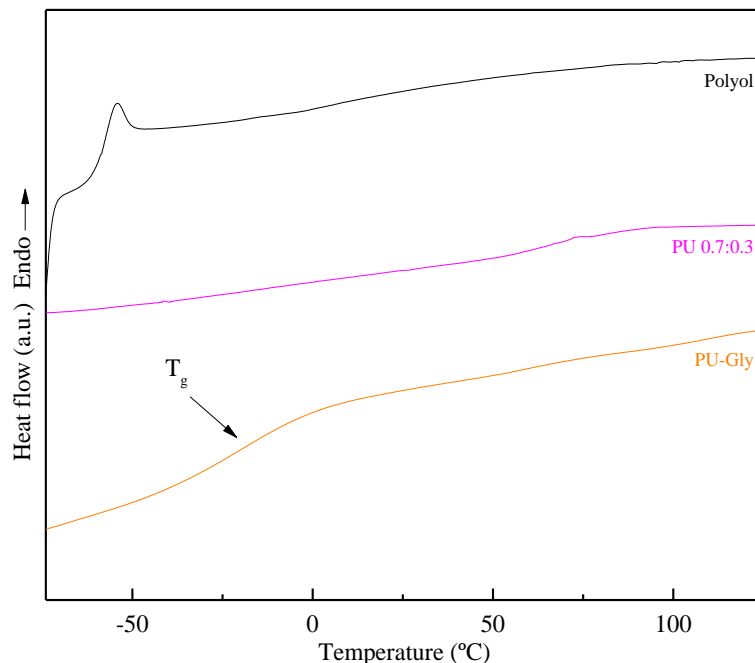


Figure 7.11. DSC thermograms of PU-Gly, polyol and synthesized thermoset PU.

As it can be observed, PU-Gly sample showed a T_g higher than that of the original polyol, but lower than that of the synthesized PU (Table 7.8). This is attributed to the fact that in the depolymerization process the breakage of the three-dimensional structure occurs randomly, resulting in shorter chains and lower molar mass, which due to the higher mobility of chains compared to those of the thermoset PU, leads to a lower T_g . However, the T_g is higher than that of the starting polyol because the network breakage is not complete, and the chains have higher mobility restriction when compared to the polyol.

	Polyol	PU 0.7:0.3	PU-Gly
T_g (°C)	-58	85	-19

Table 7.8. DSC results of PU-Gly, polyol and PU 0.7:0.3.

7.4.4. TGA

The PU-Gly obtained in the glycolysis of the thermoset PU was also analyzed by TGA. Figure 7.12 shows the TG and DTG curves of glycolyzed product, polyol used in the synthesis of thermoset PU and the PU. Different weight loss steps were observed in the glycolyzed product. The first one, around 140-180 °C, with a loss of around 4 %, could be associated with the EG used in the glycolysis process [31], probably due to the unreacted residual EG remaining in the single-

phase PU-Gly. The second significant weight loss occurs at around 300 °C and it was also observed in the thermoset PU sample. This step could be related to the degradation of urethane groups [14,15], as they were previously observed by FTIR.

Moreover, a shoulder is observed at lower temperature, around 250 °C, which may be related to the degradation of BHET-rich components obtained in the glycolyzed product, according to previous TGA results reported in Chapter 5. At higher temperatures, two weight losses were observed, also observed for the polyol at around 350 and 470 °C. It could be concluded that the glycolyzed product is a mixture of different components, some of which are constituted by several functional groups with different thermal stability such as the urethane group or chains derived from vegetable oils, and BHET-m as well.

Furthermore, it was observed that the PU-Gly had a significantly high residue of around 22 %. This value is higher than that of PU 0.7:0.3 sample, and may be due to the fact that all synthesized PU samples were used in the glycolysis, including those with higher BHET-m content, such as PU 0.6:0.4 and PU 0.5:0.5. These samples present higher BHET-m content comparing with PU 0.7:0.3, which can generate more char by combustion [17].

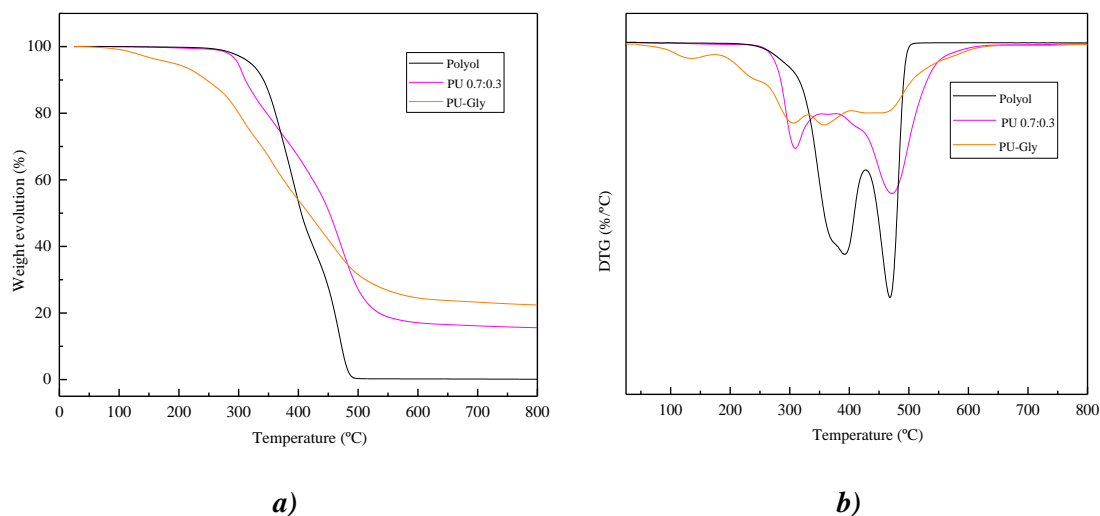


Figure 7.12. **a)** Weight evolution and **b)** DTG curves of polyol, synthesized thermoset PU and glycolyzed product.

7.5. Conclusions

In this chapter, biobased and recycled thermoset PUs were synthesized using a castor oil derived polyol and BHET-m recycled from marine PET litter, producing more environmentally friendly materials. Five different thermoset PUs were synthesized by varying the ratio of polyol and BHET-m, and deeply characterized to understand their influence on the final properties.

Results showed that marine BHET-m could be a good alternative for the synthesis of high performance thermoset PUs. DSC results indicated a higher T_g as the amount of BHET increased. DMA results confirmed that the crosslinking density decreased with the addition of difunctional BHET-m, but T_g increased due to the aromatic structure of BHET-m, that restricts the chain mobility. Furthermore, flexural test results demonstrated that BHET-m increases the flexural modulus, resulting in a stiffer material, due to the aromatic structure of BHET-m.

On the other hand, in order to demonstrate the recyclability of synthesized thermoset PUs, glycolysis was carried out, obtaining a single-phase viscous liquid. Obtained PU-Gly was characterized with several techniques, finding that glycolysis resulted in depolymerization, obtaining fractions with similar molar mass than raw components.

7.6. References

- [1] E.M. Maafi, F. Malek, L. Tighzert, Synthesis and characterization of new polyurethane based on polycaprolactone, *J Appl Polym Sci.* 115 (2010) 3651–3658. <https://doi.org/10.1002/app.31448>.
- [2] X. Pan, D.C. Webster, New biobased high functionality polyols and their use in polyurethane coatings, *ChemSusChem.* 5 (2012) 419–429. <https://doi.org/10.1002/cssc.201100415>.
- [3] A.P. Siroèiae, A. Fijaèko, Z. Hrnjak-Murgiae, Chemical recycling of postconsumer poly(ethylene-terephthalate) bottles-depolymerization study, *Chem Biochem Eng Q.* 27 (2013) 65–71.
- [4] T. Calvo-Correas, A. Santamaria-Echart, A. Saralegi, L. Martin, Á. Valea, M.A. Corcuera, A. Eceiza, Thermally-responsive biopolyurethanes from a biobased diisocyanate, *Eur Polym J.* 70 (2015) 173–185. <https://doi.org/10.1016/J.EURPOLYMJ.2015.07.022>.
- [5] X. Da, C. Liu, Y. Long, X. Xie, Polyurethane foaming with CO₂ adducts from C8 alkyl grafted polyethyleneimines: Optimization of the grafting rate and application of the blowing agents, *J Appl Polym Sci.* 137 (2020) 48752–48761. <https://doi.org/10.1002/app.48752>.
- [6] J.L. Ryszkowska, M. Auguścik, A. Sheikh, A.R. Boccaccini, Biodegradable polyurethane composite scaffolds containing Bioglass® for bone tissue engineering, *Compos Sci Technol.* 70 (2010) 1894–1908. <https://doi.org/10.1016/J.COMPSCITECH.2010.05.011>.
- [7] T. Calvo-Correas, L. Ugarte, P.J. Trzebiatowska, R. Sanzberro, J. Datta, M.Á. Corcuera, A. Eceiza, Thermoplastic polyurethanes with glycolysate intermediates from polyurethane

- waste recycling, *Polym Degrad Stab.* 144 (2017) 411–419. <https://doi.org/10.1016/J.POLYMDEGRADSTAB.2017.09.001>.
- [8] J. Datta, E. Głowińska, Effect of hydroxylated soybean oil and bio-based propanediol on the structure and thermal properties of synthesized bio-polyurethanes, *Ind Crops Prod.* 61 (2014) 84–91. <https://doi.org/10.1016/J.INDCROP.2014.06.050>.
- [9] Q. Tang, K. Gao, Structure analysis of polyether-based thermoplastic polyurethane elastomers by FTIR, ¹H NMR and ¹³C NMR, *Int J Polym Anal.* 22 (2017) 569–574. <https://doi.org/10.1080/1023666X.2017.1312754>.
- [10] M.A. Pérez-Limiñana, F. Arán-Aís, A.M. Torró-Palau, A.C. Orgilés-Barceló, J.M. Martín-Martínez, Characterization of waterborne polyurethane adhesives containing different amounts of ionic groups, *Int J Adhes Adhes.* 25 (2005) 507–517. <https://doi.org/10.1016/j.ijadhadh.2005.02.002>.
- [11] A. Bhattacharyya, D. Mukherjee, R. Mishra, P.P. Kundu, Preparation of polyurethane–alginate/chitosan core shell nanoparticles for the purpose of oral insulin delivery, *Eur Polym J.* 92 (2017) 294–313. <https://doi.org/10.1016/j.eurpolymj.2017.05.015>.
- [12] S. Jayavani, S. Sunanda, T.O. Varghese, S.K. Nayak, Synthesis and characterizations of sustainable polyester polyols from non-edible vegetable oils: Thermal and structural evaluation, *J Clean Prod.* 162 (2017) 795–805. <https://doi.org/10.1016/j.jclepro.2017.06.040>.
- [13] M. Zhang, H. Pan, L. Zhang, L. Hu, Y. Zhou, Study of the mechanical, thermal properties and flame retardancy of rigid polyurethane foams prepared from modified castor-oil-based polyols, *Ind Crops Prod.* 59 (2014) 135–143. <https://doi.org/10.1016/j.indcrop.2014.05.016>.
- [14] M.A. Corcuera, L. Rueda, A. Saralegui, Ma.D. Martín, B. Fernández-d’Arlas, I. Mondragon, A. Eceiza, Effect of diisocyanate structure on the properties and microstructure of polyurethanes based on polyols derived from renewable resources, *J Appl Polym Sci.* 122 (2011) 3677–3685. <https://doi.org/10.1002/app.34781>.
- [15] C. Bueno-Ferrer, E. Hablot, M. del C. Garrigós, S. Bocchini, L. Averous, A. Jiménez, Relationship between morphology, properties and degradation parameters of novative biobased thermoplastic polyurethanes obtained from dimer fatty acids, *Polym Degrad Stab.* 97 (2012) 1964–1969. <https://doi.org/10.1016/j.polymdegradstab.2012.03.002>.
- [16] L.B. Gonella, A.J. Zattera, M. Zeni, R.V.B. Oliveira, L.B. Canto, New reclaiming process of thermoset polyurethane foam and blending with polyamide-12 and thermoplastic

- polyurethane, *J Elastomers Plast.* 41 (2009) 303–322. <https://doi.org/10.1177/0095244309099413>.
- [17] P.S. Lee, S.M.G. Jung, Flame retardancy of polyurethane foams prepared from green polyols with flame retardants, *J Appl Polym Sci.* 139 (2022) 52010–52021. <https://doi.org/10.1002/app.52010>.
- [18] P.J. Achorn, R.C. Ferrillot, Comparison of thermal techniques for glass transition measurements of polystyrene and cross-linked acrylic polyurethane films *J Appl Polym Sci*, 54 (1994) 2033–2044. <https://doi.org/10.1002/app.1994.070541305>
- [19] J. Zhang, C. Zhang, S.A. Madbouly, In situ polymerization of bio-based thermosetting polyurethane/graphene oxide nanocomposites, *J Appl Polym Sci.* 132 (2015) 41751–41759. <https://doi.org/10.1002/app.41751>.
- [20] J.C. Domínguez, Rheology and curing process of thermosets, in: *Thermosets: Structure, Properties, and Applications: Second Edition*, Elsevier, 2018: pp. 115–146. <https://doi.org/10.1016/B978-0-08-101021-1.00004-6>.
- [21] K.P. Menard, N.R. Menard, *Dynamic mechanical analysis*, CRC Press, 2020. <https://doi.org/10.1201/9780429190308>.
- [22] B. Fernández-D’Arlas, A. Alonso-Varona, T. Palomares, M.A. Corcuera, A. Eceiza, Studies on the morphology, properties and biocompatibility of aliphatic diisocyanate-polycarbonate polyurethanes, *Polym Degrad Stab.* 122 (2015) 153–160. <https://doi.org/10.1016/j.polymdegradstab.2015.10.023>.
- [23] B. Fernández-D’Arlas, L. Rueda, K. de La Caba, I. Mondragon, A. Eceiza, Microdomain composition and properties differences of biodegradable polyurethanes based on MDI and HDI, *Polym Eng Sci.* 48 (2008) 519–529. <https://doi.org/10.1002/pen.20983>.
- [24] K. Sarkar, S. Rama, K. Meka, A. Bagchi, N.S. Krishna, S.G. Ramachandra, G. Madras, K. Chatterjee, Polyester derived from recycled poly(ethylene terephthalate) waste for regenerative medicine, *RSC Adv.* (2014) 58805–58815. <https://doi.org/10.1039/c4ra09560j>.
- [25] L. Gausas, S.K. Kristensen, H. Sun, A. Ahrens, B.S. Donslund, A.T. Lindhardt, T. Skrydstrup, Catalytic hydrogenation of polyurethanes to base chemicals: from model systems to commercial and end-of-life polyurethane materials, *JACS Au.* 1 (2021) 517–524. <https://doi.org/10.1021/jacsau.1c00050>.
- [26] T. Calvo-Correas, L. Ugarte, P.J. Trzebiatowska, R. Sanzberro, J. Datta, M.Á. Corcuera, A. Eceiza, Thermoplastic polyurethanes with glycolysate intermediates from polyurethane

- waste recycling, *Polym Degrad Stab.* 144 (2017) 411–419. <https://doi.org/10.1016/j.polymdegradstab.2017.09.001>.
- [27] R. López-Fonseca, I. Duque-Ingunza, B. de Rivas, L. Flores-Giraldo, J.I. Gutiérrez-Ortiz, Kinetics of catalytic glycolysis of PET wastes with sodium carbonate, *Chem Eng J.* 168 (2011) 312–320. <https://doi.org/10.1016/J.CEJ.2011.01.031>.
- [28] P. Fang, B. Liu, J. Xu, Q. Zhou, S. Zhang, J. Ma, X. lu, High-efficiency glycolysis of poly(ethylene terephthalate) by sandwich-structure polyoxometalate catalyst with two active sites, *Polym Degrad Stab.* 156 (2018) 22–31. <https://doi.org/10.1016/J.POLYMDEGRADSTAB.2018.07.004>.
- [29] T. Calvo-Correas, L. Ugarte, P.J. Trzebiatowska, R. Sanzberro, J. Datta, M.Á. Corcuera, A. Eceiza, Thermoplastic polyurethanes with glycolysate intermediates from polyurethane waste recycling, *Polym Degrad Stab.* 144 (2017) 411–419. <https://doi.org/10.1016/j.polymdegradstab.2017.09.001>.
- [30] M. Ștefănescu, M. Stoia, O. Ștefănescu, C. Davidescu, G. Vlase, P. Sfirloagă, Synthesis and characterization of poly (vinyl alcohol)/ethylene glycol/silica hybrids. Thermal analysis and FT-IR study., *Rev Roum Chim.* 55 (2010) 17–23. <http://web.icf.ro/rrch/>.
- [31] A. Pasha, S. Khasim, O.A. Al-Hartomy, M. Lakshmi, K.G. Manjunatha, Highly sensitive ethylene glycol-doped PEDOT-PSS organic thin films for LPG sensing, *RSC Adv.* 8 (2018) 18074–18083. <https://doi.org/10.1039/c8ra01061g>

Chapter 8

LIFE CYCLE ASSESSMENT OF THE DIFFERENT
PROCESSES AND MATERIALS DEVELOPED

8. LIFE CYCLE ASSESSMENT OF THE DIFFERENT PROCESSES AND MATERIALS DEVELOPED

8.1. Aim of the chapter

In previous chapters, the optimization of PET glycolysis obtaining high purity BHET-m from marine PET litter, employed in the synthesis of PUs was performed. This chapter focuses on the evaluation of the environmental impacts for all those processes. With this aim, a quantitative analysis by the Life Cycle Assessment (LCA) of environmental impacts is developed in the present chapter.

With this objective, three LCA groups were evaluated. Firstly, the LCA corresponding to the glycolysis reaction of PET litter, defined in Chapter 5, is presented, from the collection of marine PET litter to the final purification of BHET monomer, taking into account all steps, materials and energy consumption of the process.

Secondly, the LCA of the TPU synthesis process, developed in Chapter 6, was performed. In order to analyze the effect of recycled BHET-m addition on the synthesis of TPUs, a LCA study of TPUs synthesized with a commercial BHET-m was also carried out. Finally, the LCA corresponding to a TPUs obtained from petrochemical polyol was analyzed. Thus, the environmental impacts of the synthesis of biobased and BHET-m containing TPUs were analyzed and compared with those of a fossil-based one.

8.2. Life Cycle Assessment for the chemical recycling of marine PET litter

The environmental impacts of chemical recycling of PET are lower than those resulting for incineration and landfilling [1]. However, thermo-mechanical recycling, compared to chemical one, shows the best results for all plastics in terms of impact on global warming [2]. Thermo-mechanical recycling is therefore preferred from an environmental point of view, if the chemical and physical characteristics of wastes allow it. In contrast, chemical recycling for monomer production also offers a positive environmental impact for residues not suitable for thermo-mechanical recycling.

The LCA of the chemical recycling of marine PET litter was carried out from the collection of wastes at the sea, to the final purification of BHET-m, including the transport to the laboratory, the cleaning and preparation of materials and the recycling reaction. In addition, all necessary reagents and energy consumption for the process of obtaining the final BHET-m product, were taken into account. PET recycling scheme, with all the inputs and outputs of the process, is presented in Figure 8.1.

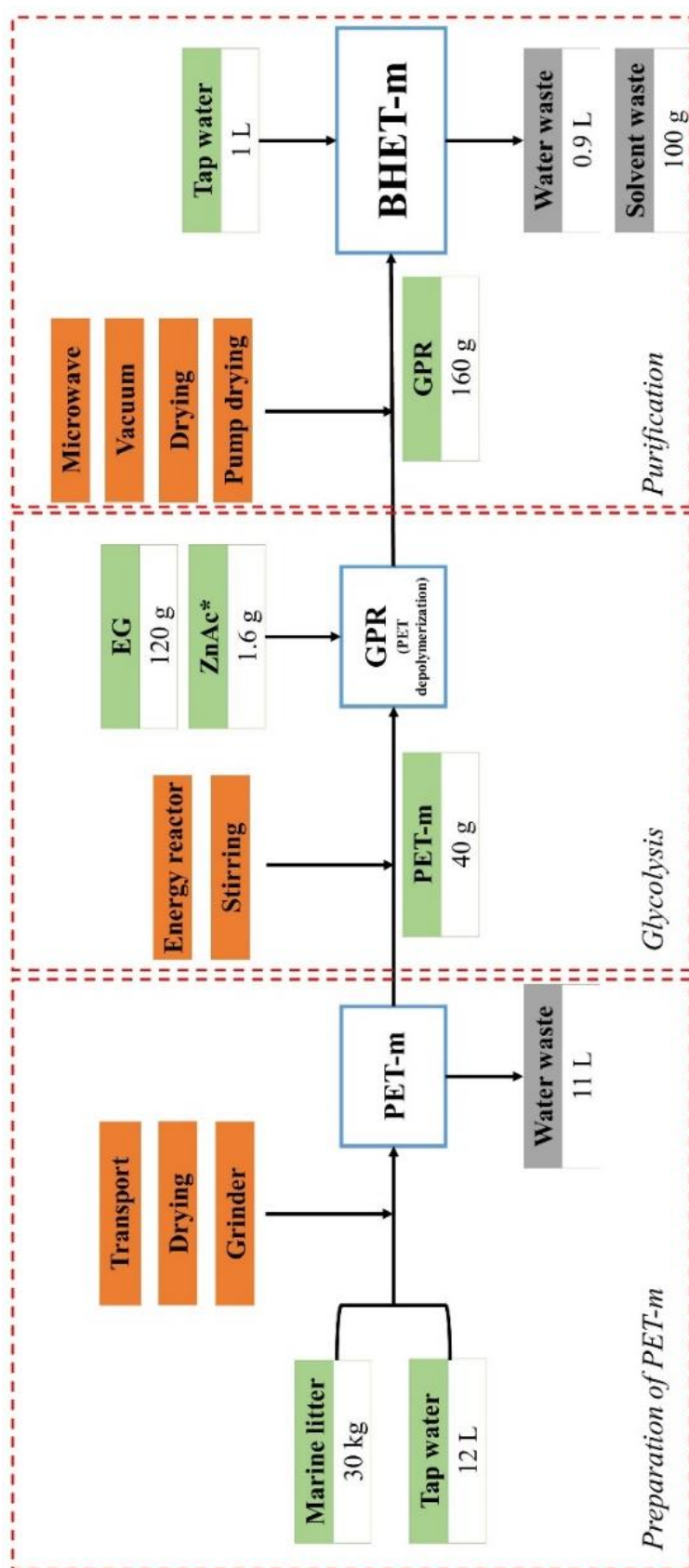


Figure 8.1. Recycling scheme of marine PET litter to produce BHET-m. Color legend: green refers to raw material inputs; orange to energy inputs; grey to waste outputs; and blue to outputs obtained after each step. Asterisk (*) refers previously modeled to parameters.

It is important to note that the input marine PET litter was created excluding its previous production impacts as it refers to a waste. For the recycling of marine PET, three different steps were distinguished: the first one, the collection, transport and preparation of PET-m waste; the second one, the glycolysis of PET-m; and, the last one the purification of the BHET-m from glycolyzed product (GPR). Quantification was performed with the values corresponding to the process carried out in the laboratory, described in Chapter 5.

Inputs for the modelling of LCA study were taken from Ecoinvent v3.5 database. However, as the zinc acetate catalyst was not included in this database, it was modelled separately. Table 8.1 shows the inventory with all the inputs and outputs of each unit of PET-m. Inputs marked with an asterisk (*) indicate that they have been previously modelled, in Chapter 2. It is important to note that the column labeled *Remarks* refers to the input used in SimaPro, as it is named in the program.

Preparation of PET-m: collection, transport and conditioning			
Inputs	Amount	Unit	Remarks
Marine PET litter	30	kg	
Transport lorry	939	kgkm	Transport, lorry {RER} transport all sizes EURO6 to generic market for APOS, U
Water for cleaning	12	kg	Tap water {RER} market for APOS, U
Drying system (oven 24 h, 50 °C)	2.4	kWh	Electricity, low voltage {ES} market for APOS, U
Grinder energy (3 h)	0.225	kWh	Electricity, low voltage {ES} market for APOS, U
Outputs	Amount	Unit	Remarks
PET-m	30	kg	
Wastewater for treatment	11	L	Wastewater, average {Europe without Switzerland} market for wastewater, average APOS, U

Table 8.1. Inventory of marine PET litter collection and preparation. Main outputs are identified in bold.

Similarly, Table 8.2. shows the inventory with all the inputs and outputs of each unit of the system for the chemical recycling of PET-m and the purification process of BHET monomer.

The total global warming impact of the process for obtaining 34 g BHET-m through chemical recycling of PET-m was of about 0.713 kg CO₂ eq. This impact was selected as an environmental indicator as it is the most reliable data available [3]. However, more impacts were analyzed in LCA studies. The main contributors and environmental impacts during BHET-m monomer production (above 10 % contribution) are presented in the tree diagram Figure 8.2.

Glycolysis: obtaining GPR			
Inputs	Amount	Unit	Remarks
PET-m	40	g	
Ethylene glycol	120	g	Ethylene glycol {GLO} market for APOS, U
Zinc acetate*	1.6	g	Modeled* in Chapter 2
Energy reactor	0.173	kWh	Electricity, low voltage {ES} market for APOS, U
Stirring (1000 rpm, 30 min)	0.00156	kWh	Electricity, low voltage {ES} market for APOS, U
Outputs	Amount	Unit	Remarks
Glycolyzed product (GPR)	160	g	
Purification: obtaining BHET-m			
Inputs	Amount	Unit	Remarks
Glycolyzed product (GPR)	160	g	
Water	1	kg	Tap water {RER} market for APOS, U
Microwave (warm up water 4 min)	0.00267	kWh	Electricity, low voltage {ES} market for APOS, U
Vacuum pump filtrate (2 h, 3 bar)	0.058	kWh	Electricity, low voltage {ES} market for APOS, U
Drying in vacuum oven (24 h, 50 °C)	0.648	kWh	Electricity, low voltage {ES} market for APOS, U
Pump of vacuum drying	0.0001	kWh	Electricity, low voltage {ES} market for APOS, U
Outputs	Amount	Unit	Remarks
BHET-m	34	g	
Wastewater	900	cm ³	Wastewater, average {Europe without Switzerland} market for wastewater, average APOS, U
Ethylene glycol waste	100	g	Spent solvent mixture {Europe without Switzerland} market for spent solvent mixture APOS, U

Table 8.2. Inventory for the chemical recycling of PET-m for obtaining BHET-m, considering three different steps. Outputs are identified in bold.

As it can be seen in Figure 8.2, the main environmental impact was attributed to the energy consumption (electricity) for the depolymerization reaction, followed by the production of the EG required for the reaction. Energy consumption was the dominant factor in the LCA, so it must be calculated with high accuracy [4]. However, the treatment of EG waste also present a high impact, of around 21 %. This contribution could be reduced by designing a system for separation and reuse of this glycol. Some models assume full recovery of EG in the chemical recycling of PET

[5], but in this work EG was not recovered. The energy consumption and therefore the impact of EG could be reduced transferring this process to an optimized industrial scale, due to the larger amounts obtained. This would require suitable management of marine litter. Management constitutes the first step towards recycling.

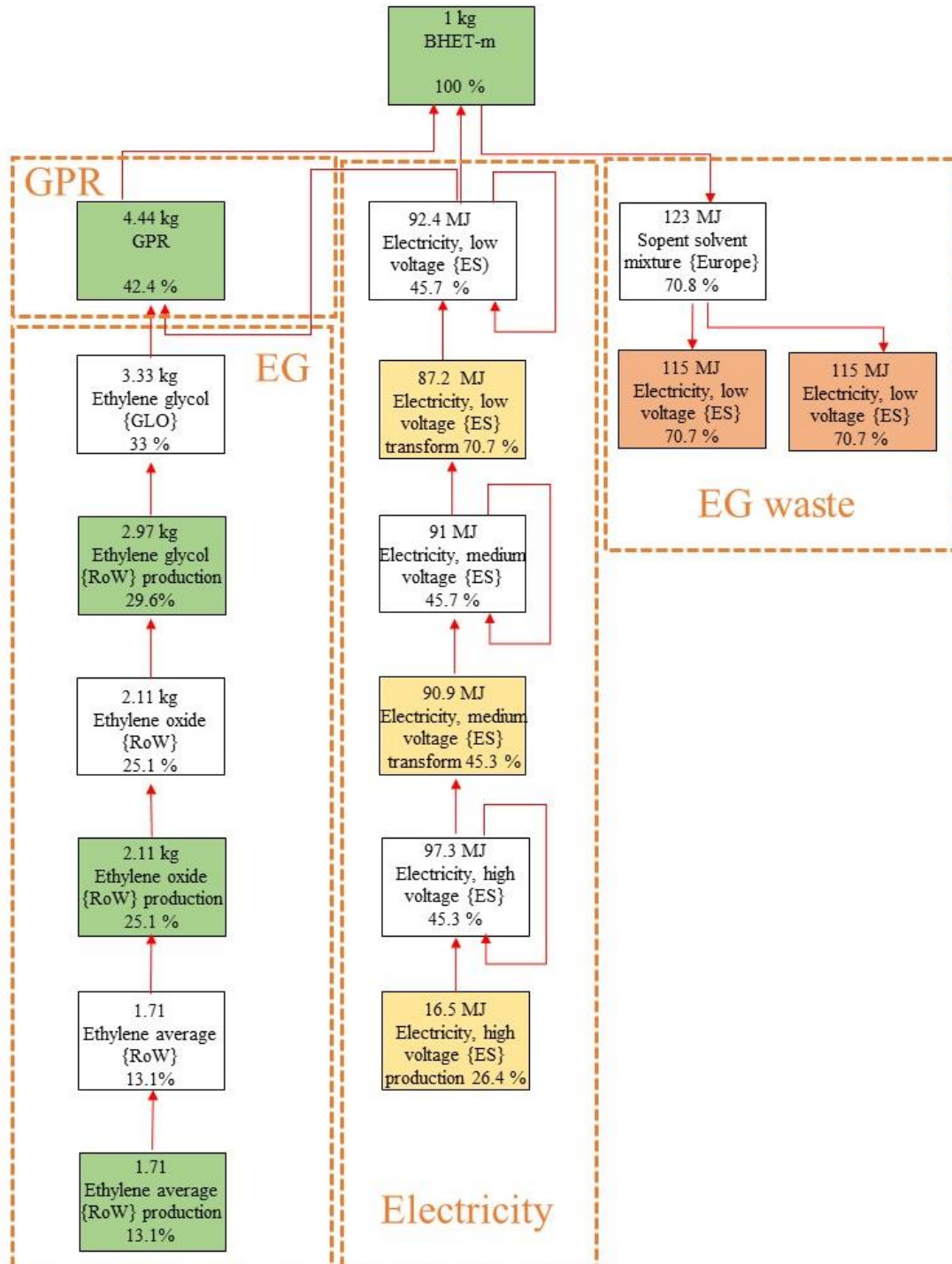


Figure 8.2. Tree diagram of the main contributions (above 10%) to environmental impacts in BHET-m production.

The production of BHET-m by the depolymerization reaction of PET-m was compared with the production of commercial BHET (BHET-ref) obtained by the glycolysis reaction of PET [4,5]. BHET-ref production was modelled in Chapter 2 and the impacts contributions are shown in the Figure 8.3.

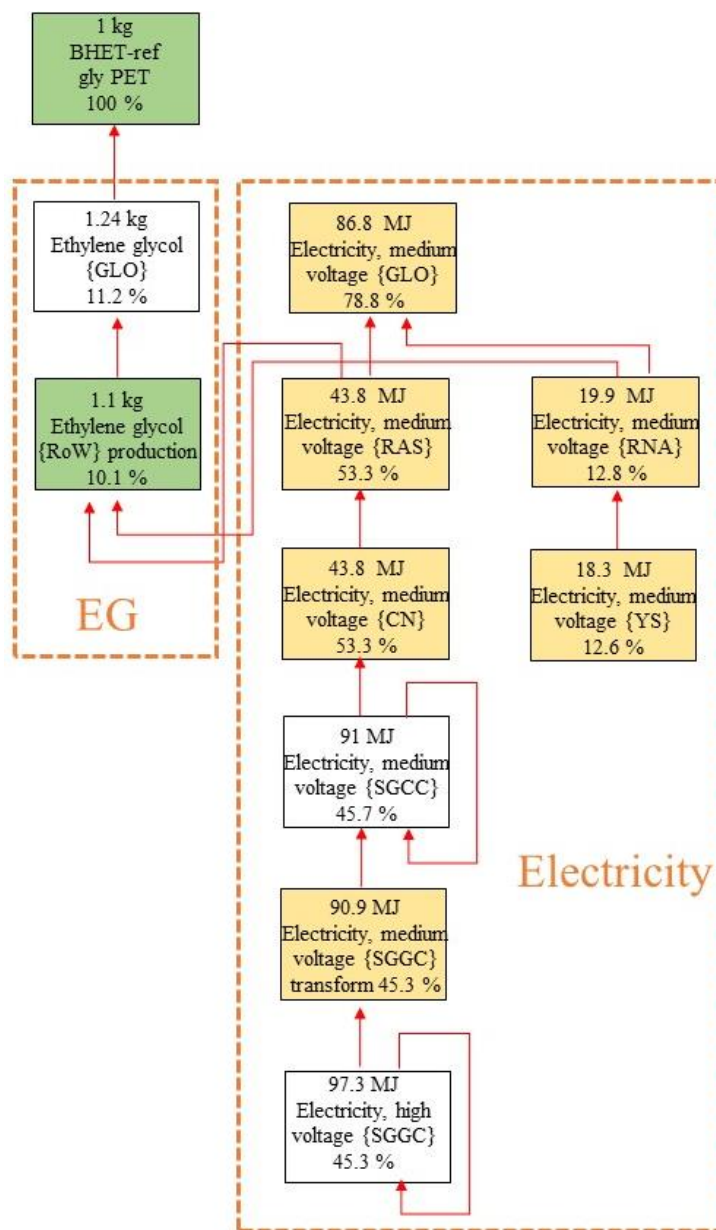


Figure 8.3. Tree diagram of the main environmental contributions for BHET-ref.

As it can be observed, the main contribution was the electricity needed, being the most denominated input, followed by the impact of EG, with a contribution of 11 %.

The different environmental impacts for the production of 1 kg of BHET-m and BHET-ref are compared in Table 8.3. Ten different normalized impacts were analyzed by ReCiPe 2016 Midpoint (H) methodology. The impacts are listed in the table in order of importance. It can be

stated that the effect on global warming was higher for BHET-ref samples, due to both the high energy consumption required for glycolysis and the consumption of EG [6].

Impact	No. impact category	BHET-m	BHET-ref	Unit
Global warming	1	19.82	21.64	kg CO ₂ eq
Stratospheric ozone depletion	2	$6.49 \cdot 10^{-6}$	$7.87 \cdot 10^{-6}$	kg CFC11 eq
Ionizing radiation	3	0.41	0.20	kBq Co-60 eq
Ozone formation	4	$8.9 \cdot 10^{-2}$	$8.5 \cdot 10^{-2}$	kg NO _x eq
Terrestrial acidification	5	$7.3 \cdot 10^{-2}$	$6.4 \cdot 10^{-2}$	kg SO ₂ eq
Terrestrial ecotoxicity	6	10.6	11.0	kg 1,4-DCB
Freshwater ecotoxicity	7	$5.9 \cdot 10^{-3}$	$7.3 \cdot 10^{-3}$	kg 1,4-DCB
Land use	8	0.90	0.50	m ² crop eq
Human toxicity	9	3.15	3.25	kg 1,4-DCB
Water consumption	10	$5.4 \cdot 10^{-3}$	$2.0 \cdot 10^{-3}$	m ³

Table 8.3. LCA results of impact categories for the production of 1kg of BHET-m and BHET-ref.

Figure 8.4 represents the ten impacts analyzed after normalization. According to ISO 14044 standard on Life Cycle Assessment (LCA), normalization relates the results of category indicators of the product under study to those of a reference system [7,8]. In this case, it was normalized respect to ReCiPe 2016 Midpoint (H) method with the SimaPro software.

It could be observed that the highest contribution to the impact was human toxicity, being higher for BHET-ref process, probably due to the chemicals released into the environment in the manufacturing process [9]. Furthermore, it has been reported that PET production is the plastic production with the highest impact on human toxicity [10], so human toxicity could be attributed to the production of BHET-ref in which PET was used. Similarly, the impacts of BHET-ref were also higher when analyzing the categories of global warming, stratospheric ozone depletion, terrestrial ecotoxicity, freshwater ecotoxicity and water consumption. However, impacts were higher for BHET-m in the cases of ionizing radiation, ozone formation, land acidification and land use. In 6 of the 10 impact categories studied, the performance of BHET-m was better than that of BHET-ref, with lower human toxicity and global warming. In addition, it should be noted that the BHET-m process could be optimized by recovering EG as in the production of commercial BHET.

Comparing the results of the glycolysis for BHET-m production with those reported in the literature, it can be concluded that the model followed in this work presents a greater impact

associated with higher energy consumption. Specifically, the study of Shen et al. [5] indicated that the production of 1 kg of BHET by glycolysis has an impact of 2.6 kg CO₂ eq, based on data received from Far Eastern New Century (FENC) in a small-scale production. In contrast, in the model employed in this work, the impact was of 19.8 kg CO₂ eq. As shown in Figure 8.2, the energy required is 92.4 MJ/kg, in contrast to the 39 MJ/kg reported by Shen et al.

This difference could be attributed to the higher energy consumption of the laboratory equipment compared to data obtained from FENC. On the other hand, if the full recovery of EG was included in the model, as reported in the literature [5], the overall warming impact obtained for the model followed in this work would be of 3.6 kg CO₂ eq, which is similar to that reported in the literature.

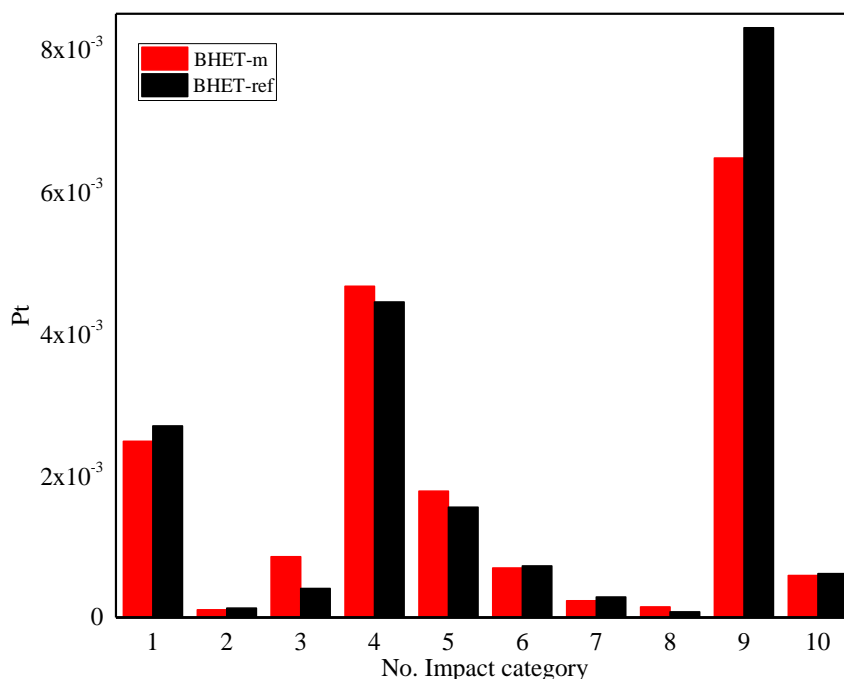


Figure 8.4. Normalized representation of different impacts for BHET-m and BHET-ref production.

8.3. LCA of synthesized TPUs

Once BHET-m was produced from the chemical recycling of PET-m, thermoplastic TPUs were synthesized with the incorporation of BHET-m as chain extender (Chapter 6). The LCA of the whole process up to the final production of the TPU samples was developed.

As described in Chapter 6, five different TPU compositions were synthesized by varying the macrodiol:isocyanate:BHET-m ratio. TPU samples shown in Table 8.4 were analyzed in the LCA in order to evaluate the effect of using different amounts of BHET-m. TPU samples have been denoted as TPU-m 1:x:y, being x and y the molar ratio of isocyanate (HDI) and BHET-m.

Sample code	Molar ratio	BHET-m
	Macrodiol:HDI:BHET	(%)
TPU-m 1:2:1	1:2:1	10
TPU-m 1:3:2	1:3:2	17
TPU-m 1:4:3	1:4:3	22
TPU-m 1:5:4	1:5:4	26
TPU-m 1:6:5	1:6:5	30

Table 8.4. TPUs studied by LCA.

The overall process for the synthesis of TPUs containing BHET-m is summarized in Figure 8.5. Two different steps were defined: the first one, related to the preparation of the waste to obtain PET-m for the subsequent production of BHET-m suitable for the second step, constituted by the synthesis of biobased PUs using castor oil derived macrodiol, and BHET-m as chain extender.

As for PET-m recycling and BHET-m production, LCA inputs were taken from the Ecoinvent v3.5 database. However, inputs not included in the database were modelled separately, such as macrodiol and HDI (Chapter 2). The macrodiol used for the synthesis, Priplast 3192, was a castor oil derived biobased polyol with a 38 % of renewable content and a footprint of 3.5 kg CO₂. In order to model it, the work of Fridrihsone et al., in which bio-polyols were modelled [11], was taken as reference. Therefore, in this LCA study, the name of macrodiol was replaced by bio-polyol, as it would not be accurate to name it as macrodiol, the information not corresponding to the production of Priplast 3192.

The inventory of the TPU-m 1:2:1 synthesis process is detailed in Table 8.5 from the BHET-m obtained above. The modelling of inputs marked with * were presented in Chapter 2.

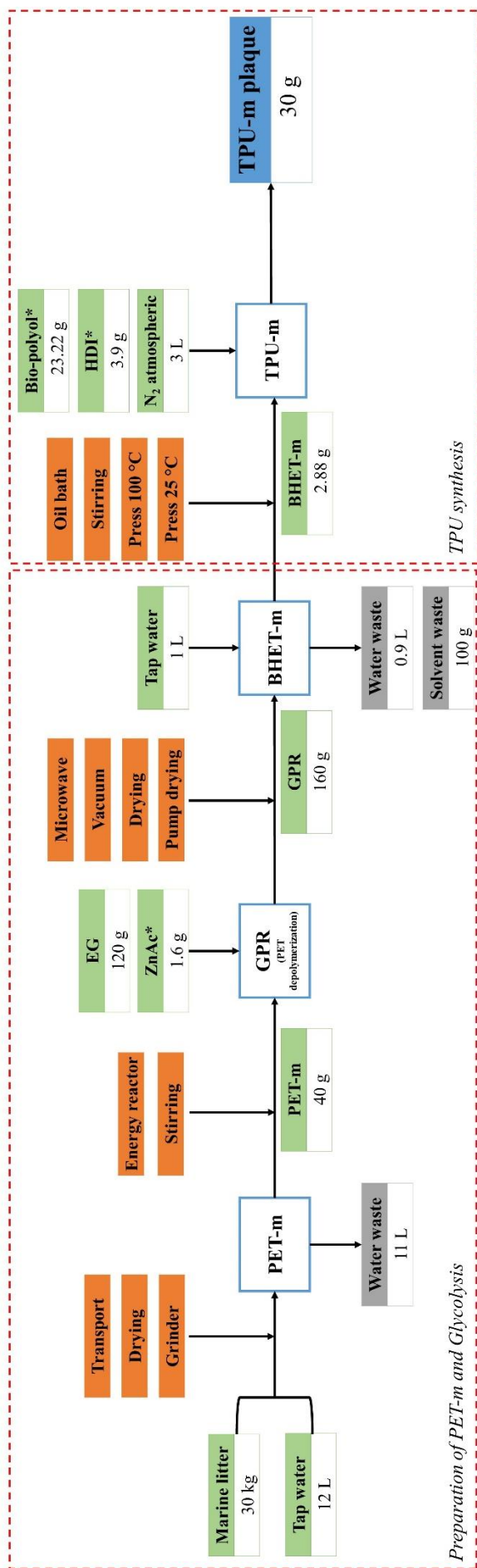


Figure 8.5. Scheme of the complete process for the synthesis of thermoplastic TPU-m 1:2:1 sample. Asterisk (*) refer to previously modeled parameters.

TPU synthesis			
Inputs	Amount	Unit	Remarks
BHET-m*	2.88	g	Modeled* in the previous step
Bio-polyol*	23.22	g	Modeled* in Chapter 2
HDI*	3.90	g	Modeled* in Chapter 2
Atmospheric nitrogen	3.0	L	Nitrogen, liquid {RER} market for APOS, U
Energy oil bath 110 °C 3 h	0.1	kWh	Electricity, low voltage {ES} market for APOS, U
Stirring reactor 300 rpm 2 h	0.005	kWh	Electricity, low voltage {ES} market for APOS, U
Press 100 °C, 50 bar, 10 h	0.625	kWh	Electricity, low voltage {ES} market for APOS, U
Press 25 °C, 50 bar, 3 h	0.2	kWh	Electricity, low voltage {ES} market for APOS, U
Outputs	Amount	Unit	Remarks
TPU-m	30	g	

Table 8.5. Inventory for TPU-m 1:2:1 sample.

Concerning the synthesis of TPU-m 1:3:2, TPU-m 1:4:3, TPU-m 1:5:4 and TPU-m 1:6:5, the only variation is the amount of BHET-m, bio-polyol and HDI. Table 8.6 shows the amount used for each reaction and also the global warming impact (GWP) for the laboratory scale synthesis of 30 g of each TPU.

Sample code	Bio-polyol (g)	HDI (g)	BHET-m (g)	GWP (kg CO ₂ eq)
TPU-m 1:2:1	23.22	3.90	2.88	0.511
TPU-m 1:3:2	20.00	5.04	4.96	0.552
TPU-m 1:4:3	17.56	5.90	6.53	0.583
TPU-m 1:5:4	15.66	6.58	7.77	0.607
TPU-m 1:6:5	14.12	7.12	8.76	0.626

Table 8.6. Bio-polyol, HDI and BHET-m amounts for the synthesis of each TPU together with the GWP impact.

The tree diagram shown in Figure 8.6 summarizes the main contributions for TPU-m 1:2:1 sample. As it can be seen, the largest contribution is from energy consumption, followed by bio-polyol production. Table 8.7 shows the contributions to the environmental impacts for each TPU synthesized.

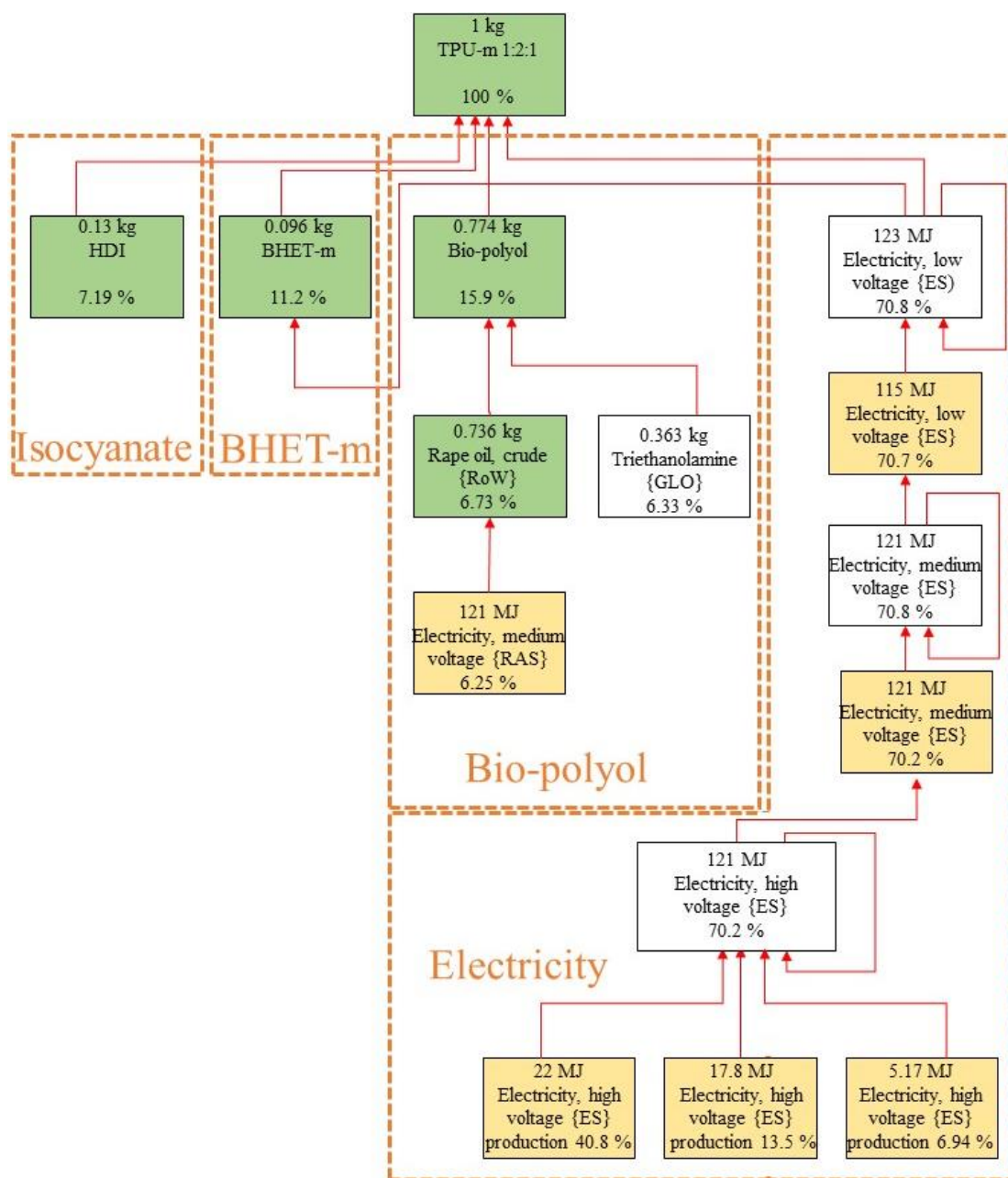


Figure 8.6. Tree diagram of the main environmental contributions TPU-m 1:2:1 sample.

Sample code	Energy (%)	Bio-polyol (%)	BHET-m (%)	HDI (%)
TPU-m 1:2:1	70.8	15.9	11.2	7.2
TPU-m 1:3:2	69.0	12.6	17.8	8.6
TPU-m 1:4:3	67.8	10.5	22.2	9.5
TPU-m 1:5:4	66.9	9.0	25.4	10.2
TPU-m 1:6:5	66.3	7.9	27.7	10.7

Table 8.7. Main contributions to environmental impacts for synthesized TPUs.

As it can be seen, the energy contribution was the largest impact in all cases. This result may be related to the fact that the LCA was carried out at laboratory scale, in which the energy consumption is overestimated being its contribution to the impacts higher [4]. However, it can be observed that as BHET-m content increases, the second largest contribution was for BHET-m, due to the greater impact of BHET-m production. It should be noted that the LCA performed with BHET-m included all impacts. In contrast, in the case of isocyanate and bio-polymer, modelling was performed despising several factors comparing with BHET-m, which could lead to lower environmental impacts.

The results for the production of 1 kg of the five synthesized TPUs, are summarized in Table 8.8. Ten impact categories were analyzed in Table 8.3.

No. impact category	TPU-m 1:2:1	TPU-m 1:3:2	TPU-m 1:4:3	TPU-m 1:5:4	TPU-m 1:6:5	Unit
1	17.04	18.39	19.42	20.23	20.87	kg CO ₂ eq
2	2.85·10 ⁻⁵	2.59·10 ⁻⁵	2.40·10 ⁻⁵	2.26·10 ⁻⁵	2.14·10 ⁻⁵	kg CFC11 eq
3	0.54	0.57	0.59	0.61	0.62	kBq Co-60 eq
4	9.97·10 ⁻²	1.05·10 ⁻¹	1.10·10 ⁻¹	1.13·10 ⁻¹	1.16·10 ⁻¹	kg NO _x eq
5	1.02·10 ⁻¹	1.05·10 ⁻¹	1.07·10 ⁻¹	1.08·10 ⁻¹	1.10·10 ⁻¹	kg SO ₂ eq
6	11.91	12.71	13.31	13.79	14.16	kg 1,4-DCB
7	1.14·10 ⁻²	1.10·10 ⁻²	1.07·10 ⁻²	1.04·10 ⁻²	1.02·10 ⁻²	kg 1,4-DCB
8	5.82	5.26	4.84	4.52	4.25	m ² crop eq
9	7.81	7.44	7.16	6.94	6.76	kg 1,4-DCB
10	0.25	0.27	0.29	0.30	0.31	m ³

Table 8.8. LCA results of impact categories for 1 kg of synthesized TPU samples.

As it can be seen from the impacts analysis, the production of BHET-m was one of the main contributors. As BHET-m content increased, the impacts of global warming, ionizing radiation, ozone formation, terrestrial acidification, terrestrial ecotoxicity, human toxicity and water consumption were higher, as can be observed in Figure 8.7.

This is because increasing the HS content decreases that of SS (bio-polyol), an input that presents a lower environmental impact than BHET-m. However, the impacts of stratospheric ozone depletion, freshwater ecotoxicity and land use decreased for samples with higher BHET-m content. These impacts are related to bio-polyol production including those related to the cultivation of vegetable oil needed for bio-polyol synthesis [11,12]. Therefore, as bio-polyol content increased, impacts related to land use, ozone depletion and ecotoxicity impacts on

freshwater increased. It should be noted that the synthesis of PU was carried out employing a bio-polyol with a relatively low food footprint, this input not having high impact.

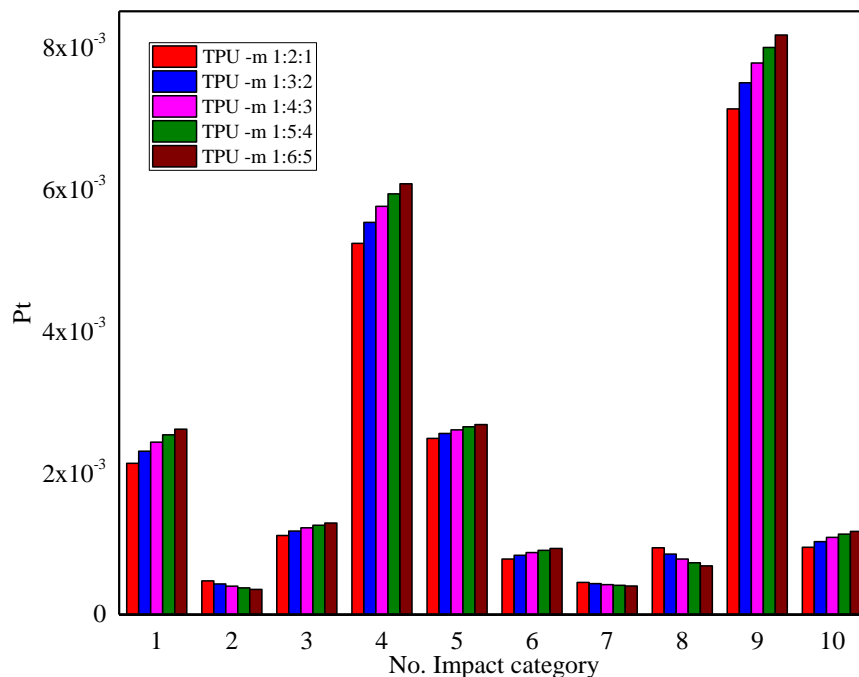


Figure 8.7. Impact categories of TPU-m samples.

8.3.1. Comparative of LCA between TPU-m and TPU-ref

In the LCA performed up to this point, the synthesis of TPUs with recycled BHET-m as chain extender was analyzed. To compare the impacts of BHET-m with those of BHET-ref, the LCA study of TPU synthesis using commercial BHET-ref as chain extender was performed. The scheme of synthesis is shown in Figure 8.8. The inventory table for TPU-ref synthesis was the same as for TPU-m one (Table 8.3).

Figure 8.9 shows the contribution of impacts of each process for TPU-ref 1:2:1 sample, energy consumption being the largest, as explained above. In addition, the impacts of bio-polyol and commercial BHET-ref were also relevant. As can be seen, the production of bio-polyol has a greater impact on the synthesis of TPU-ref 1:2:1 than the production of commercial BHET-ref.

However, as the content of BHET-ref increased in the synthesized TPUs, the impact of BHET-ref increased, decreasing the contribution of bio-polyols to the impacts, as shown in Table 8.9. The contribution of BHET-ref production in the TPU-ref 1:6:5 to the impacts is significant, which was close to 30 %, while the impact of bio-polyol is of 7.6 % and that of HDI production of 10.3 %.

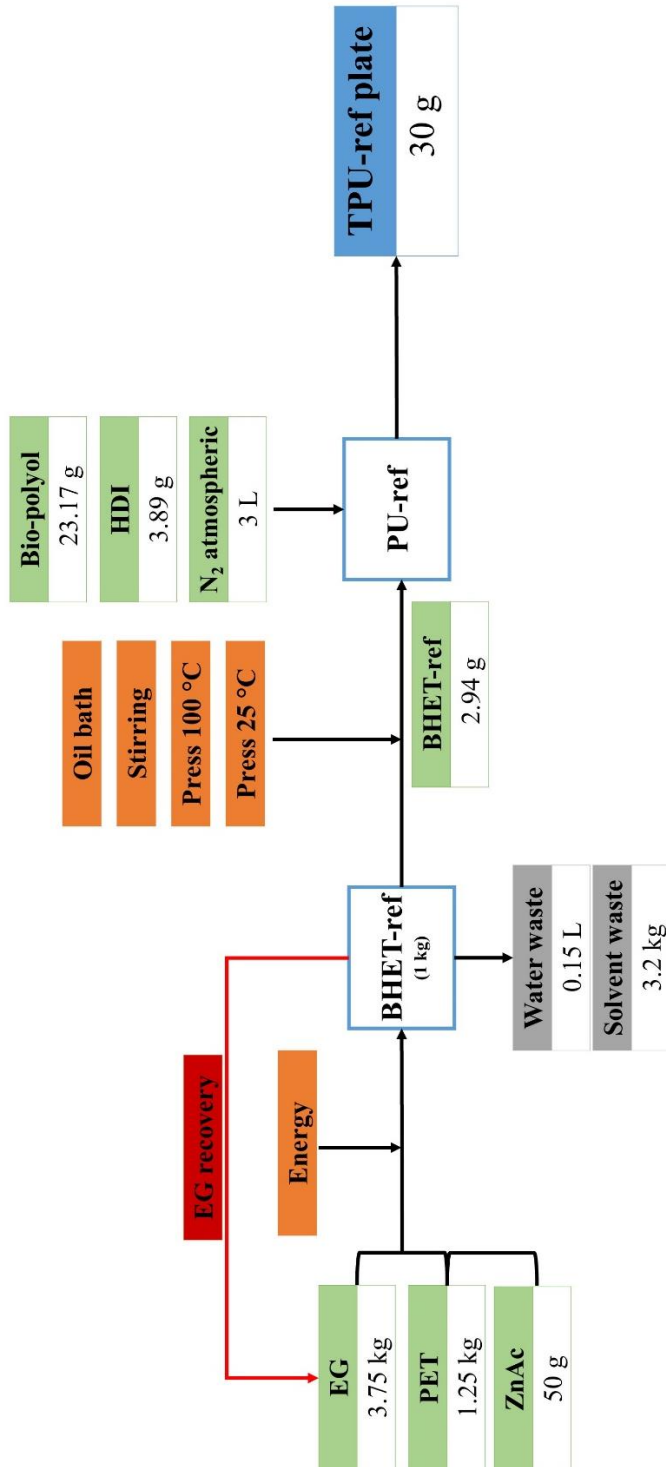


Figure 8.8. Scheme for the process followed in the synthesis of TPU-ref 1:2:1 sample.

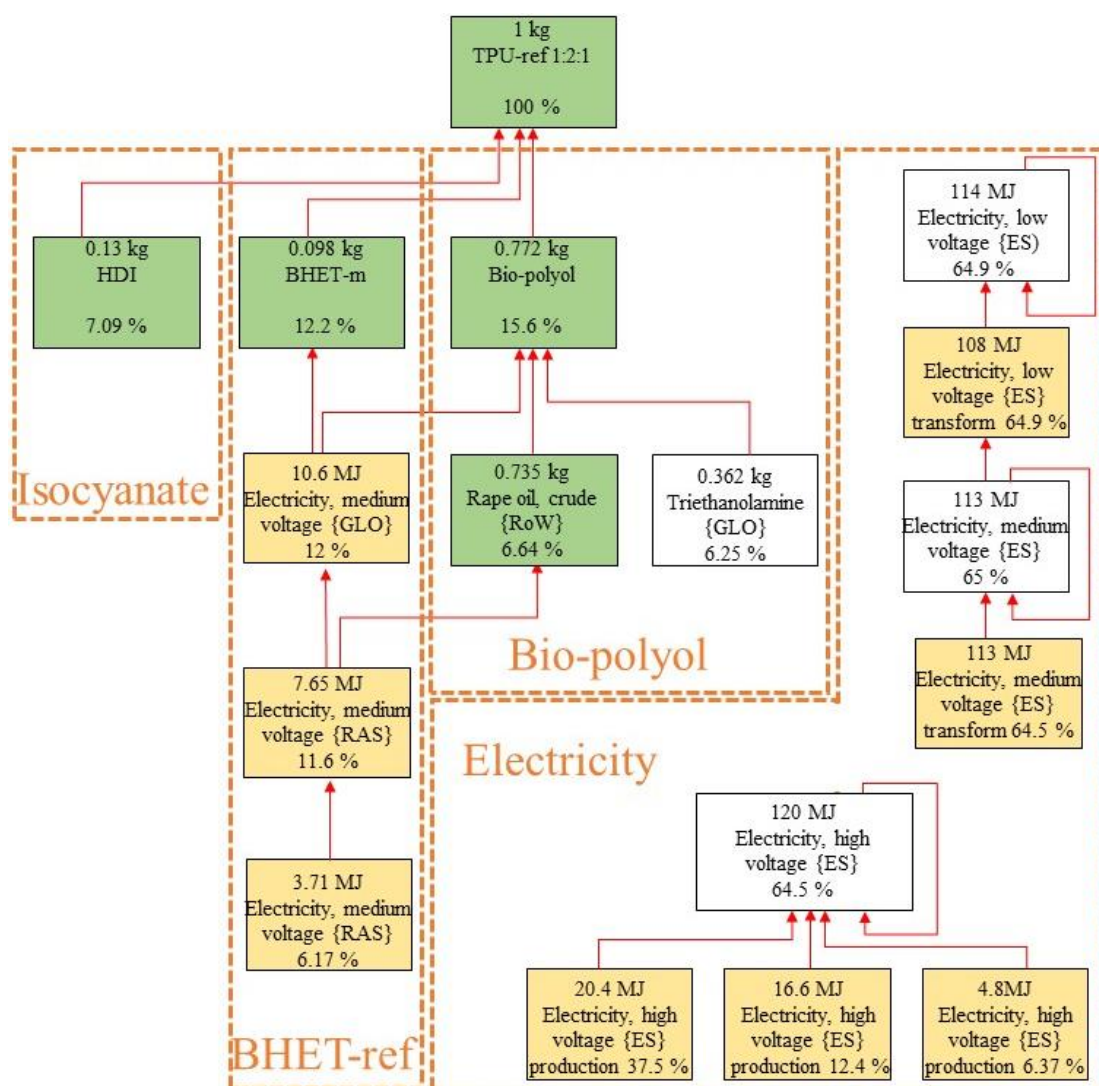


Figure 8.9. Network tree for the environmental contributions of TPU-ref 1:2:1 sample.

Sample code	Energy (%)	Bio-polyol (%)	BHET-ref (%)	HDI (%)
TPU-ref 1:2:1	64.9	15.6	12.2	4.2
TPU-ref 1:3:2	59.7	12.4	19.4	8.4
TPU-ref 1:4:3	56.3	10.2	24.1	9.3
TPU-ref 1:5:4	53.9	8.7	27.3	9.9
TPU-ref 1:6:5	52.1	7.6	28.9	10.3

Table 8.9. Main contributions to environmental impacts for synthesized TPU-ref samples.

Results obtained for the different TPUs synthesized with BHET-ref and BHET-m are summarized in Table 8.10.

No. impact category	TPU-m				TPU-ref				Unit		
	1:2:1	1:3:2	1:4:3	1:5:4	1:6:5	1:2:1	1:3:2	1:4:3		1:5:4	1:6:5
1	17.04	18.39	19.42	20.23	20.87	17.24	18.74	19.87	20.75	21.46	kg CO ₂ eq
2	2.85	2.59	2.40	2.26	2.14	2.86	2.61	2.43	2.29	2.17	kg CFC11 · 10 ⁻⁵ eq
3	0.54	0.57	0.59	0.61	0.62	0.52	0.53	0.54	0.55	0.56	kBq Co-60 eq
4	1.00	1.05	1.10	1.13	1.16	0.99	1.05	1.09	1.12	1.15	kg NO _x · 10 ⁻² eq
5	1.02	1.05	1.07	1.08	1.10	1.01	1.03	1.05	1.06	1.07	kg SO ₂ · 10 ⁻¹ eq
6	11.91	12.71	13.31	13.79	14.16	11.97	12.80	13.43	13.92	14.32	kg 1,4-DCB
7	1.14	1.10	1.07	1.04	1.02	1.16	1.12	1.1	1.08	1.06	kg 1,4-DCB · 10 ⁻²
8	5.82	5.26	4.84	4.52	4.25	5.77	5.18	4.73	4.39	4.11	m ² crop eq
9	7.81	7.44	7.16	6.94	6.76	7.81	7.44	7.17	6.95	6.78	kg 1,4-DCB
10	0.25	0.27	0.29	0.30	0.31	0.25	0.28	0.29	0.30	0.31	m ³

Table 8.10. LCA results of impact categories for synthesized TPU-m and TPU-ref samples.

As it can be seen, the synthesis of TPU-ref samples results in a higher GWP impact than for those synthesized with recycled BHET-m. Comparing both syntheses, it can be concluded that no important changes were observed for the impact categories studied. Categories No. 2, 5, 6, 7, 8 and 10 have been assumed to be the same for both systems, since the same bio-polyol was used, leading in the same impacts in several categories such as land use or acidification, which are closely related to bio-polyol production [11]. However, according to GWP, stratospheric ozone depletion and freshwater ecotoxicity show greater impact for TPU-m samples. These categories are related with the use of fossil combustible or chemical manufacturing that give rise to greenhouse gas emissions of and ozone-depleting substances such as CFC (chlorofluorocarbon) and other halocarbon emissions [13]. The normalized graph of the most significant impacts is represented in Figure 8.10, where the trend of each impact is observed to increase with BHET content for all of the samples.

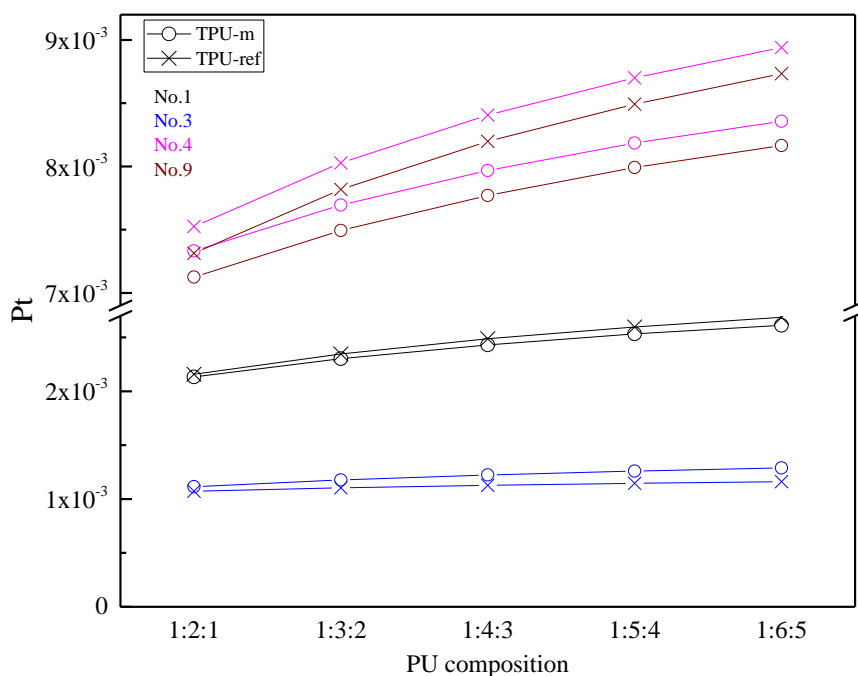


Figure 8.10. Normalized graph of relevant impact categories on TPU-m and TPU-ref samples.

As it can be seen, as the BHET content increased, the ozone formation (No. 4) and human toxicity (No. 9) impacts increased in both TPU systems (Figure 8.10). This could be related to the process of BHET production, whose feedstocks may contribute to the emission of greenhouse and harmful gases. Furthermore, these impacts were higher for the TPU-ref system, in agreement with the previous LCA study, in which higher impacts were obtained for commercial BHET-ref. The global warming impact (No. 1) also increased with BHET content and was higher for the TPU-ref samples as well. On the other hand, the ionization impact (No. 3) slightly increased with BHET, presenting lower impact on samples synthesized with commercial BHET.

8.3.2. Comparative analysis between TPU-m and a TPU synthesized with a commercial polyol

The study of BHET-m containing TPU synthesis was completed with the study of the influence of the polyol origin on the impacts evaluated by LCA. Therefore, the impacts of the synthesis of a TPU based on a bio-polyol, synthesized in Chapter 6, and another TPU prepared with a polyol of fossil origin were determined. In this context, the LCA study for TPU-m sample was compared with that of a PU synthesized with a commercial polyol (TPU-petropolyol) from the Ecoinvent v3.5 database and BHET-ref as chain extender. In both cases, the same synthesis conditions and molar ratios were considered. The modeling of petropolyol was made taking into account a CO₂ footprint value between 4-6 kg CO₂ eq, as reported in the literature [14].

Therefore, the polyol used in the SimaPro model as petropolyol has an impact of around 4.8 kg CO₂ eq. The TPU-petropolyol was compared to TPU-m 1:4:3 sample. In addition to the ten impact categories discussed above, the midpoint impact of fossil resource scarcity was studied, as it is relevant when comparing a bio-polyol with a petrochemical polyol [11,12]. In the same way, the human carcinogenic toxicity was analyzed. The twelve midpoint impacts are summarized in Table 8.11 and represented in a normalized graph in Figure 8.11, for comparison.

Impact	No. impact category	TPU-m	TPU-petropolyol	Unit
Global warming	1	19.42	20.60	kg CO ₂ eq
Ozone depletion	2	$2.40 \cdot 10^{-5}$	$7.87 \cdot 10^{-6}$	kg CFC11 eq
Ionizing radiation	3	0.59	0.532	kBq Co-60 eq
Ozone formation	4	$1.10 \cdot 10^{-1}$	$1.09 \cdot 10^{-1}$	kg NO _x eq
Terrestrial acidification	5	$1.07 \cdot 10^{-1}$	$9.48 \cdot 10^{-2}$	kg SO ₂ eq
Terrestrial ecotoxicity	6	13.31	12.10	kg 1,4-DCB
Freshwater ecotoxicity	7	$1.07 \cdot 10^{-2}$	$8.38 \cdot 10^{-3}$	kg 1,4-DCB
Land use	8	4.84	1.26	m ² crop eq
Human non-carcinogenic	9	7.16	3.85	kg 1,4-DCB
Water consumption	10	0.29	0.32	m ³
Fossil resource scarcity	11	5.69	6.16	kg oil eq
Human carcinogenic	12	0.08	0.10	kg 1,4-DCB

Table 8.11. LCA results of impact categories for synthesized TPU-m and TPU-petropolyol samples.

As it can be seen, the impact category with the highest contribution is the human carcinogenic toxicity (No. 12), being considerably higher for the TPU-petropolyol sample. This impact

reflected the potential damage in one unit of chemical discharged into the environment, usually evaluated in terms of benzene equivalence (carcinogenic) [9]. Therefore, in general terms it can be said that the impact of human toxicity increases with fuel or energy use, as for TPU-petropolyol sample. However, the impact of biobased TPU is also considerable, as it is related to pesticides, fertilizers and water employed in the agricultural sector [15]. Therefore, a reduction in the impact of fossil resources was observed for the TPU-m sample (No. 11), despite the fact that the consumption of EG in this sample was linear because its recovery was not taken into account.

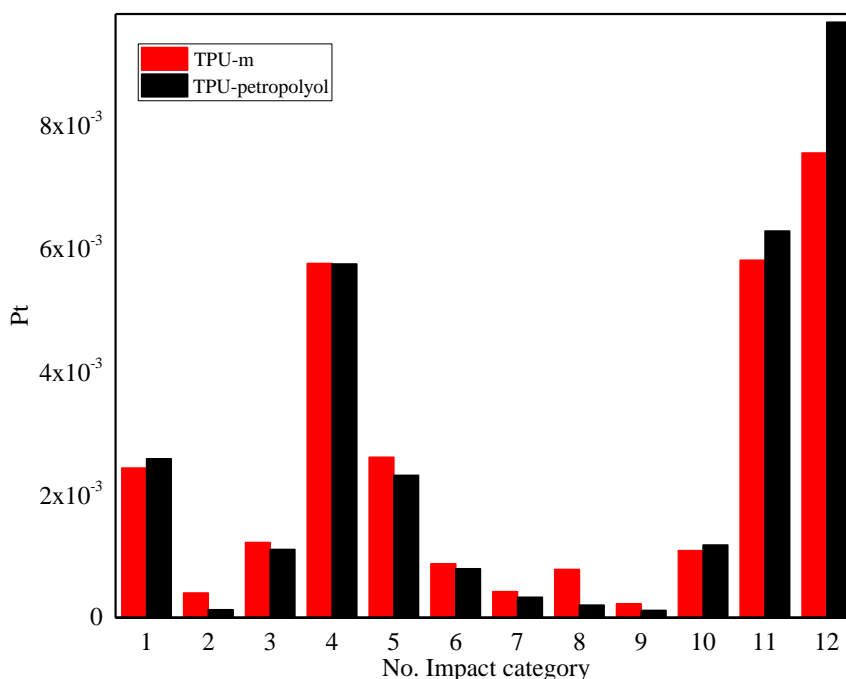


Figure 8.11. Normalized graph of different impact categories for TPU-m and TPU-petropolyol samples.

In general, the use of a biobased polyol results in significant savings of fossil resources [11]. Patel et al. have reported [16] that a good practice goal for biobased polymers to be environmentally friendly is to avoid at least 1 kg of CO₂ per kg of polymer obtained. As shown in Table 8.10, more than 1 kg CO₂ eq was saved in the case of TPU-m, confirming that it is a propped biobased PU from an environmental point of view. Moreover, the water consumption impact was similar for both polyols, the biobased and the petrochemical [11,17].

In contrast, some important midpoint impacts, such as ionizing radiation (No. 3), terrestrial acidification (No. 5), terrestrial ecotoxicity (No. 6) and land use (No. 8) performed worse for the biobased TPU sample, being in agreement with the literature [11,17]. Acidification, ecotoxicity and land use are impact categories directly related to agricultural production. The biggest

difference was observed in land use, which increases considerably in the case of biobased polyol employed in TPU-m, due to cultivated land [12,17].

8.4. Conclusions

In this chapter, the environmental impact of BHET-m, BHET-ref, TPU-m, TPU-ref, and TPU-petropolyol were evaluated using a LCA model. From the analysis of 10 impact categories, it could be concluded that the recycling of PET-m for the production of BHET-m monomer is more environmentally friendly than commercial BHET. In addition, the overall warming impact for BHET-m sample was lower than that modeled for the commercial BHET. Besides, the human toxicity is relatively higher for BHET-ref than for BHET-m. This was because for the production of BHET-ref, PET, which is the plastic with the highest impact of human toxicity in production, was used as an input [10], while for the BHET-m sample, an input of marine litter with no previous impacts was created.

From the LCA study of TPU-m and TPU-ref samples, no relevant differences were obtained since the only variation was the BHET used. Even so, for the different samples synthesized, higher environmental impacts were observed with increasing BHET content (or with decreasing bio-polyol), due to the higher impacts of BHET compared to bio-polyol. In addition, TPU-ref samples present in all cases higher impacts than TPU-m samples, due to the fact that BHET-m is more environmentally friendly than BHET-ref.

Furthermore, it is confirmed that the use of a biobased polyol for the synthesis of TPUs is generally advantageous according to the LCA study. Although impacts related to the agricultural sector, are higher for the biobased PU, these impacts are less negative than the others [11,12]. Moreover, synthesized TPUs are environmentally friendly biobased materials, as they avoid at least 1 kg of CO₂ per kg of polymer obtained [16].

Therefore, the LCA studies confirm that all the processes developed in this research present lower environmental impact than conventional processes. The use of a biobased polyol and recycled BHET-m from PET-m for the synthesis of PUs has been shown to be an environmentally friendly alternative. Compared to TPU-petropolyol, a greater decrease in the impact categories of human carcinogenesis and fossil resource scarcity was obtained, along with a lower carbon footprint. However, although the modeled bio-polyol is better than petropolyol from an environmental point of view, their footprint impact is not that different, 3.5 and 4.8 kg CO₂ eq, respectively. In the supplier's data other Pripast-type polyols with lower footprint can be found [14], of around 0 and 1 kg CO₂, so if a biobased polyol with higher renewable content was used, the environmental impacts would be lower and the results compared to TPU-petropolyol much more significant.

The highest impact in all cases is attributed to energy consumption. However, it is important to mention that the modeled processes are oversized in terms of energy consumption, since they have been performed at a laboratory scale. In order to obtain better results, an exhaustive study of the net energy consumption of the processes should be carried out, using energy meters on all the machinery used. Furthermore, it should be noted that an EG recovery system in the depolymerization stage would improve already obtained positive results. These facts will be taken into account in future works.

8.5. References

- [1] S. Cornago, D. Rovelli, C. Brondi, M. Crippa, B. Morico, A. Ballarino, G. Dotelli, Stochastic consequential Life Cycle Assessment of technology substitution in the case of a novel PET chemical recycling technology, *J Clean Prod.* 311 (2021) 127406–127420. <https://doi.org/10.1016/J.JCLEPRO.2021.127406>.
- [2] R. Meys, F. Frick, S. Westhues, A. Sternberg, J. Klankermayer, A. Bardow, Towards a circular economy for plastic packaging wastes – the environmental potential of chemical recycling, *Resour Conserv Recycl.* 162 (2020) 105010–105020. <https://doi.org/10.1016/j.resconrec.2020.105010>.
- [3] I. Deviatkin, M. Khan, E. Ernst, M. Horttanainen, Wooden and plastic pallets: A review of life cycle assessment (LCA) studies, *Sustainability.* 11 (2019) 5750–5767. <https://doi.org/10.3390/su11205750>.
- [4] H. Sugiyama, M. Hirao, R. Mendivil, U. Fischer, K. Hungerbühler, A hierarchical Activity model of chemical process design based on Life cycle Assessment, *Process Saf Environ Prot.* 84 (2006) 63–74. <https://doi.org/10.1205/PSEP.04142>.
- [5] L. Shen, E. Worrell, M.K. Patel, Open-loop recycling: A LCA case study of PET bottle-to-fibre recycling, *Resour Conserv Recycl.* 55 (2010) 34–52. <https://doi.org/10.1016/j.resconrec.2010.06.014>.
- [6] E.S. Barboza, D.R. Lopez, S.C. Amico, C.A. Ferreira, Determination of a recyclability index for the PET glycolysis, *Resour Conserv Recycl.* 53 (2009) 122–128. <https://doi.org/10.1016/j.resconrec.2008.10.002>.
- [7] J. Kim, Y. Yang, J. Bae, S. Suh, The importance of normalization references in interpreting Life Cycle Assessment results, *J Ind Ecol.* 17 (2013) 385–395. <https://doi.org/10.1111/j.1530-9290.2012.00535.x>.

- [8] M. Pizzol, A. Laurent, S. Sala, B. Weidema, F. Verones, C. Koffler, Normalisation and weighting in life cycle assessment: quo vadis?, *Int J Life Cycle Assess.* 22 (2017) 853–866. <https://doi.org/10.1007/s11367-016-1199-1>.
- [9] E.G. Hertwich, S.F. Mateles, W.S. Pease, T.E. Mckone, Human toxicity potentials for life-cycle assessment and toxics release inventory risk screening, *Environ Toxicol Chem.* 20 (2001) 928–939. <https://doi.org/https://doi.org/10.1002/etc.5620200431>.
- [10] P. Fantke, A. Ernstoff, LCA of chemicals and chemical products, in: *Life Cycle Assessment: Theory and Practice*, Springer International Publishing, 2017: pp. 783–815. https://doi.org/10.1007/978-3-319-56475-3_31.
- [11] A. Fridrihsone, F. Romagnoli, V. Kirsanovs, U. Cabulis, Life Cycle Assessment of vegetable oil based polyols for polyurethane production, *J Clean Prod.* 266 (2020) 121403–121431. <https://doi.org/10.1016/j.jclepro.2020.121403>.
- [12] S. Tortoioli, L. Paolotti, F. Romagnoli, A. Boggia, L. Rocchi, Environmental assessment of bio-oil transformation from thistle in the Italian context: an LCA study, *Environ Clim Technol.* 24 (2020) 430–446. <https://doi.org/10.2478/rtulect-2020-0114>.
- [13] J.L. Lane, Stratospheric ozone depletion, in *Life Cycle Impact Assessment: 2015*: pp. 51–73. https://doi.org/10.1007/978-94-017-9744-3_4.
- [14] Croda, Product carbon footprint of Priplast™ grades, 2011.
- [15] S.V. Hjulær, S.B. Hansen, LCA of biofuels and biomaterials, in: *Life Cycle Assessment: Theory and Practice*, Springer International Publishing, 2017: pp. 755–782. https://doi.org/10.1007/978-3-319-56475-3_30.
- [16] M. Patel, C. Bastioli, L. Marini, E. Würdinger, Environmental assessment of bio-based polymers and natural fibres, in: A. Steinbüchel (Ed.), *Biopolymers Online*, Wiley, 2002 1-59. <https://doi.org/10.1002/3527600035.bpola014>.
- [17] P. Pawelzik, M. Carus, J. Hotchkiss, R. Narayan, S. Selke, M. Wellisch, M. Weiss, B. Wicke, M.K. Patel, Critical aspects in the life cycle assessment (LCA) of bio-based materials - Reviewing methodologies and deriving recommendations, *Resour Conserv Recycl.* 73 (2013) 211–228. <https://doi.org/10.1016/j.resconrec.2013.02.006>.

Chapter 9

GENERAL CONCLUSIONS, FUTURE WORKS AND
PUBLICATIONS

9. GENERAL CONCLUSIONS, FUTURE WORKS AND PUBLICATIONS

9.1. General conclusions

The aim of this work was to analyze the valorization opportunities of highly degraded PET residues as marine PET litter, that nowadays are not systematically recycled in the industry. For this purpose, different PET samples were characterized, raw PET (PET-v and PET-ssp) and wastes (PET-u and PET-m), in order to study the effect of degradation on their physicochemical properties. The main degradation process undergone by the samples appeared to be photodegradation and hydrolysis, resulting in the formation of -COOH and -OH end groups due to chain scission. This fact was corroborated by FTIR and also by WCA, and it was seen that the cleavage of the ester group in the polymer chain results in the formation of carboxyl and hydroxyl groups, increasing the hydrophilicity of the PET-u and PET-m samples and reducing the contact angle considerably. Moreover, the degradation of PET-u and PET-m was also confirmed by MFI and IV results, with an important decrease in molar mass. In addition, it was confirmed that as consequence of UV radiation and seawater, PET from the marine environment suffered higher degradation than of urban PET waste.

For this reason, several methods for the valorization of PET-m were studied in order to produce new, more environmentally friendly materials, and thus reduce the impacts and consumption of raw materials, towards circular economy. Regarding thermo-mechanical recycling, it was confirmed that it was not a suitable alternative for previously degraded samples, such as PET-m, since the samples, due to the high temperature, degrade fastly under extrusion conditions. Several evidences, such as the noticeably brown color related to thermo-oxidative degradation or the decrease of molar mass and viscosity values in the recycled PET-m samples, corroborated the degradation. Moreover, the chain scission and the formation of -COOH and -OH groups in the recycling process were also confirmed by TGA, FTIR and WCA, increasing hydrophilicity of samples. Similarly, the formation of -COOH groups in the RPET samples confirmed the autocatalytic degradation experienced by RPET samples. That is the reason for the thermo-mechanical recycling of these highly degraded materials to be discarded and the second conventional method, energy recovery, was studied. In this case, even if for degraded samples the energy values were lower, results obtained are in the range found in the literature.

Even so, as the combustion of PET was not the best option from the environmental and ecological point of view, the chemical recycling of PET samples was analyzed as alternative. The

depolymerization reaction depends on reaction time and temperature. Very good results were obtained for short reaction times. In the same way, pure BHET was also obtained at 180 °C for 30 min. For PET-m glycolysis reaction in a close reactor, yield values of 63 ± 10 % for 30 min of reaction were obtained, demonstrating that chemical recycling was a valid option for degraded materials. It was confirmed that physical and chemical properties of raw material are an important factor to be taking into account in depolymerisation, since degradation can help the depolymerization of the material, increasing the monomer content in the glycolyzed product. Thus, chemical recycling is confirmed as a good alternative for PET-m and highly degraded PET samples.

Moreover, different composition of thermoplastic and thermoset PUs were synthesized with obtained BHET-m. The thermoplastic samples obtained were compared with PUs synthesized with commercial BHET, obtaining very close properties. Therefore, it can be concluded that BHET-m recycled from PET-m could be a suitable alternative to fossil derived BHET for the production of TPUs. Similarly, it was confirmed that marine BHET was a good alternative for the synthesis of high-performance thermoset PUs. Stiff materials were obtained due to the aromatic structure of BHET. Moreover, the recyclability of both polyurethanes, reprocessing and chemical recycling for TPUs and chemical recycling for thermoset PUs, were confirmed, involving these products in the circular economy.

Finally, the Life Cycle Assessment (LCA) studies performed for the chemical recycling PET-m and for the synthesis of TPU-m showed favorable results compared to the production of commercial BHET-ref and synthesis of PUs with commercial BHET. Furthermore, greater differences were observed when comparing TPU-m with a PU synthesized with a polyol derived from fossil sources, obtaining lower environmental impacts for TPU-m samples. Therefore, it can be concluded that recycled BHET-m from PET-m is a suitable alternative for the synthesis of biobased and recycled PUs, considerably decreasing environmental impacts. In this way, emphasis has been placed on the circular economy and sustainability, very necessary nowadays.

9.2. Future works

From the results obtained in this thesis and following research line, different proposals for future work are shown, with the aim completing this work as well as for being able to give rise to new research lines.

- To further optimize the chemical recycling of PET, by varying the PET:EG ratio. In this way, we intend study the glycolysis and BHET conversion by consuming the lowest amount of EG as possible.

- To further optimize PU synthesis, eco-isocyanates and biopolyols with a lower footprint of kg CO₂ eq could be used. In this way, the footprint of the synthesis could decrease considerably.
- Recover the EG used in the chemical recycling to further reduce LCA impacts.
- Finally, in order to carry out a more accurate Life Cycle Assessment study, it is proposed to place energy meters on the equipment used in order to know the exact consumption and avoid energy oversize

9.3. List of publications and communications

9.3.1. List of publications

- Authors:** Eider Mendiburu-Valor, Gurutz Mondragon, Nekane González, Galder Kortaberria, Arantxa Eceiza, Cristina Peña-Rodríguez
- Title:** Improving the efficiency for the production of bis-(2-hydroxyethyl) terephthalate (BHET) from the glycolysis reaction of poly (ethylene terephthalate) (PET) in a pressure reactor
- Journal:** Polymers **Volume:** 13
- Article number:** 1461
- Year:** 2021
- DOI:** <https://doi.org/10.3390/polym13091461>
- Impact factor:** 4.967 (JCR 2021)
- Rank:** POLYMER SCIENCE 16/90 (Q1)
-
- Authors:** Eider Mendiburu-Valor, Gurutz Mondragon, Nekane González, Galder Kortaberria, Loli Martin, Arantxa Eceiza, Cristina Peña-Rodríguez
- Title:** Valorization of urban and marine PET waste by optimized chemical recycling
- Journal:** Resources, Conservation and Recycling **Volume:** 184
- Article number:** 106413
- Year:** 2022
- DOI:** <https://doi.org/10.1016/j.resconrec.2022.106413>
- Impact factor:** 13.716 (JCR 2022)
- Rank:** ENGINEERING, ENVIRONMENTAL 4/54 (Q1, D1)
ENVIROMENTAL SCIENCES 12/279 (Q1, D1)

Authors: Eider Mendiburu-Valor, Tamara Calvo-Correas, Loli Martin, Isabel Harismendy, Cristina Peña-Rodríguez, Arantxa Eceiza
Title: Synthesis and characterization of sustainable polyurethanes from renewable and recycled feedstocks
Journal: Journal of Cleaner Production **Volume:** 400
Article number: 136749
Year: 2023
DOI: <https://doi.org/10.1016/j.jclepro.2023.136749>
Impact factor: 11.072 (JCR 2023)
Rank: ENGINEERING, ENVIRONMENTAL 9/54 (Q1)
ENVIRONMENTAL SCIENCES 24/279 (Q1, D1)

Authors: Eider Mendiburu-Valor, Izaskun Larraza, Oihane Echeverria-Altuna, Isabel Harismendy, Cristina Peña-Rodríguez, Arantxa Eceiza
Title: Thermoset polyurethanes from biobased and recycled components
Journal: Journal of Polymers and the Environment
Year: 2023
DOI: <https://doi.org/10.1007/s10924-023-02891-1>
Impact factor: 4.705 (JCR 2023)
Rank: ENGINEERING, ENVIRONMENTAL 25/54 (Q2)
POLYMER SCIENCE 20/90 (Q1)

Autoreak: Eider Mendiburu-Valor, Florencio Fernandez Marzo, Giovanni Dotelli, Cristina Peña-Rodríguez, Arantxa Eceiza
Title: Life Cycle Assessment of polyurethane synthesis from biobased and recycled components
Year: Developing

Collaborations

Authors: Gurutz Mondragon, Galder Kortaberria, Eider Mendiburu-Valor, Nekane González, Aitor Arbelaiz, Cristina Peña-Rodríguez
Title: Thermomechanical recycling of polyamide 6 from fishing nets waste
Journal: Journal of Cleaner Applied Polymer Science **Volume:** 137
Article number: 48442
Year: 2020

DOI: <https://doi.org/10.1002/app.48442>
Impact factor: 3.057 (JCR 2020)
Rank: POLYMER SCIENCE 43/90 (Q2)

Authors: Cristina Peña-Rodríguez, Gurutz Mondragon, Eider Mendiburu-Valor, Amaia Mendoza, Galder Kortaberria, Arantxa Eceiza
Title book: Recent Developments in Plastic Recycling
Title Chapter: Recycling of Marine Plastic Debris pp 121-141
Editors: Jyotishkumar Parameswaranpillai, Sanjay Mavinkere Rangappa, Arpitha Gulihonnehalli Rajkumar, Suchart Siengchin
Editorial: Springer Nature Singapore
Book series: Composites Science and Technology (CST)
Year: 2021
ISBN 978-981-16-3626-4
DOI: <https://doi.org/10.1007/978-981-16-3627-1>

9.3.2. Conferences

Authors: Eider Mendiburu-Valor, Gurutz Mondragon, Iker González, Nekane González, Arantxa Eceiza, Cristina Peña-Rodríguez
Title: Itsas-hondakinak: PET-aren birziklapena eta balorizazioa
Conference: Materialen Zientzia eta Teknologiaren IV. kongresua
Contribution: Oral Communication
Year: 2018
Place: Donostia- San Sebastián (Spain)

Authors: Eider Mendiburu-Valor, Gurutz Mondragon, Nekane González Arantxa Eceiza, Cristina Peña-Rodríguez
Title: Physico-Chemical Characterization and Mechanical Process of Poly (Ethylene Terephthalate) Recovered from the Basque Coast
Conference: World Congress on Recycling
Contribution: Oral Communication
Year: 2019
Place: Valencia (Spain)

Authors: Eider Mendiburu-Valor, Arantxa Eceiza, Cristina Peña-Rodríguez

Title: PET-aren birziklapena: prozesaketa termo-mekanikoaren optimizazioa eta kimikoan oinarritutako material berrien garapena
Conference: II Jornadas Doctorales de la UPV/EHU
Contribution: Poster Communication
Year: 2019
Place: Bilbao (Spain)

Authors: Eider Mendiburu-Valor, Arantxa Eceiza, Cristina Peña-Rodríguez
Title: Study of Degradation and Chemical Recycling by Glycolysis of Urban and Marine PET litter
Conference: New Trends in Polymer Science: Health of Planet, Health of the People- Polymers
Contribution: Poster Communication
Year: 2022
Place: Turin (Italy)

Collaborations

Authors: **Gurutz Mondragon**, Eider Mendiburu-Valor, Alex Garcia, Aitor Arbelaz, Nekane González, Cristina Peña-Rodríguez
Title: Arrantza-sareen birziklapen termo-mekanikoa
Conference: Materialen Zientzia eta Teknologiaren IV. kongresua
Contribution: Oral Communication
Year: 2018
Place: Donostia- San Sebastián (Spain)

Authors: A. Saralegi, T. Calvo-Correa, L. Ugarte, J. Vadillo, I. Larraza, O. Echevarria, R. Olmos, S. Torresi, E. Mendiburu, **A. Eceiza**
Title: New biobased polyurethane materials
Conference: GEP-SLAP 2022
Contribution: Oral Communication
Year: 2022
Place: Donostia- San Sebastián (Spain)

Authors: E. Mendiburu-Valor, I. Larraza, O. Echevarria-Altuna, I. Harismendy, C. Peña-Rodriguez, **A. Eceiza**

Title: Poliuretanos termoestables en base constituyentes reciclados y biobasados

Conference: MATCOMP 2023

Contribution: Poster Communication

Year: 2023

Place: Gijón, Asturias (Spainia)

9.3.3. Diffusion

- E. Mendiburu-Valor, A. Mendoza, A. Elejoste, G. Mondragon, C. Peña-Rodriguez. ¿Y qué hacemos con los residuos del mar? Zientzia astea, UPV/EHU Science, Technology and Innovation Week. Donostia- San Sebastián (Spain), 8-10/11/2018.
- E. Mendiburu-Valor. Jornadas de Ecología- Campo creativo cero. Oral communication: Proyecto Reciclado y Valorización de Residuos Marinos PET. 16/04/2018 [Web link](#).
- E. Mendiburu-Valor, A. Mendoza, G. Mondragon, A. Eceiza, C. Peña-Rodriguez. Visit of GMT installations in the International Meeting of Circular Economy, promoted by the Department of Environment of the Provincial Council of Gipuzkoa. Donostia- San Sebastián (Spain) 31/01/2019.
- E. Mendiburu-Valor, A. Mendoza, A. Elejoste, G. Mondragon, C. Peña-Rodriguez. Zientzia astea, UPV/EHU Science, Technology and Innovation Week. Donostia-San Sebastián (Spain), 10/11/2019.
- E. Mendiburu-Valor. GK Recycling Alderdi Eder. Oral communication and stand: GMT research group Engineering School of Gipuzkoa UPV/EHU. Donostia-San Sebastián (Spain), 20/11/2019. [Web link](#).
- E. Mendiburu-Valor and G. Mondragon. Radio interview. Naiz Irratia – Gelditu makinak. Urak eta plastikoak maite al dute elkar? 12/05/2020. [Web link](#).
- E. Mendiburu Valor and G. Mondragon. News paper interview. Plastikoak eta Irratia, GAUR8. Donostia-San Sebastián (Spain), 27/02/2021. [Web link](#).
- E. Mendiburu-Valor et al. ¿Dónde empieza el mar? Difussion video 06/05/2021. [Web link](#).

- E. Mendiburu-Valor, A. Mendoza, A. Elejoste, C. Peña-Rodríguez. Materials and circular economy. European Research Night. Bilbao (Spain) 29/09/2021. [Web link](#).

9.3.4. Predoctoral Stay

- Politecnico di Milano, “Materials for Energy and Environment Mat4En2”, from March 20, 2022 till June 19, 2022.

Annexes

ANNEXE I- List of tables

Chapter 1. Introduction

Table 1.1. Intrinsic viscosity range depending on PET type and application.	10
Table 1.2. Glycolysis procedures reported in the literature.	16

Chapter 2. Materials and Methods

Table 2.1. Inventory of modeled zinc acetate.	56
Table 2.2. Inventory of modeled commercial BHET.	57
Table 2.3. Inventory of modeled bio-polyol.	58
Table 2.4. Inventory of modeled HMDA.	59
Table 2.5. Inventory of modeled HDI.	59

Chapter 3. Characterization of poly(ethylene terephthalate) samples of different sources

Table 3.1. Measured MFI values, together with the corresponding IV and M_n and M_w values for different PET samples.	66
Table 3.2. Ash content values of the different PET samples.	66
Table 3.3. EA results of PET samples from different sources.	70
Table 3.4. Main thermal parameters obtained from DSC thermograms of PET-v, PET-ssp, PET-u, PET-m, and PET-bottle during the 1 st heating scan, cooling and 2 nd heating scan.	71
Table 3.5. TGA results of the different PET samples.	73
Table 3.6. Contact angle values for different PET samples, together with the corresponding image of water drop over each sample.	74

Chapter 4. Study of the valorization of marine PET litter by conventional methods

Table 4.1. Values of different color parameters for RPET samples.	83
Table 4.2. MFI, IV, M_n and M_w values of raw PET and recycled RPET samples.	84
Table 4.3. DSC results of RPET samples.	87
Table 4.4. Water contact angle values for the different RPET samples, together with the corresponding images of water drop over the samples.	90
Table 4.5. MFI, IV and M_n and M_w values of RPET samples processed at a constant temperature of 255 °C.	91

Table 4.6. Color parameter values of RPET blends with different compositions.	92
Table 4.7. MFI, IV, Mn and Mw values of RPET blends with different compositions.	93
Table 4.8. WCA results of RPET blends with different compositions.	94
Table 4.9. Values of heat combustion of PET samples.	95

Chapter 5. Chemical recycling

Table 5.1. GPC results of commercial BHET and G180.	106
Table 5.2. Insoluble fraction and yield values obtained at 220 °C for different reaction times.	107
Table 5.3. BHET, dimer and oligomer content (%), together with Mw and Mn values, as obtained by GPC.	110
Table 5.4. Main parameters obtained by thermogravimetric analysis.	111
Table 5.5. Insoluble fraction in THF and yield value of glycolysis products obtained from different PET samples.	115
Table 5.6. Melting temperature and enthalpies obtained from DSC for glycolyzed from different PET samples.	117
Table 5.7. Oligomers content (%) and Mw and Mn values, as obtained by GPC.	118

Chapter 6. Synthesis of new thermoplastic polyurethanes based on recycled BHET

Table 6.1. Designation, composition and HS and BHET content of different TPU samples synthesized.	128
Table 6.2. L*, a*, b*, and ΔE^* color values, together with WI ones, for TPU samples.	129
Table 6.3. Thermal properties measured by DSC for all the samples.	132
Table 6.4. TGA results of synthesized thermoplastic TPUs.	134
Table 6.5. Mechanical properties of synthesized thermoplastic polyurethanes.	137
Table 6.6. WCA results of the synthesized TPU plaques.	137
Table 6.7. DSC results of RTPU and BHET-m 1:6:5 polyurethanes.	139
Table 6.8. Mechanical properties of RTPU and BHET-m 1:6:5 polyurethane.	140
Table 6.9. DSC results of TPU-Gly, macrodiol and TPU BHET-m 1:6:5.	145

Chapter 7. Synthesis of new thermoset polyurethanes based on recycled BHET

Table 7.1. Designation, components molar ratio, percentage of components and biobased content of the different thermoset polyurethanes.	154
Table 7.2. DSC results obtained in the 1 st and 2 nd dynamic scans for different PUs.	155

Table 7.3. L^* , a^* , b^* , and ΔE^* color values and whiteness index of the thermoset PU samples.	156
Table 7.4. Thermal degradation temperatures and residue content of for synthesized thermoset PUs.	158
Table 7.5. T_g , storage modulus at 25 °C and in the rubbery region and cross-linking density for different PUs.	159
Table 7.6. Mechanical properties of synthesized thermoset PUs.	160
Table 7.7. WCA results of synthesized thermoset PUs.	161
Table 7.8. DSC results of PU-Gly, polyol and PU 0.7:0.3.	165

Chapter 8. Life Cycle Assessment of different processes and material developed

Table 8.1. Inventory of marine PET litter collection and preparation. Main outputs are identified in bold.	175
Table 8.2. Inventory for the chemical recycling of PET-m for obtaining BHET-m, considering three different steps. Outputs are identified in bold.	176
Table 8.3. LCA results of impact categories for the production of 1kg of BHET-m and BHET-ref.	179
Table 8.4. TPUs studied by LCA.	181
Table 8.5. Inventory for TPU-m 1:2:1 sample.	183
Table 8.6. Bio-polyol, HDI and BHET-m amounts for the synthesis of each TPU together with the GWP impact.	183
Table 8.7. Main contributions to environmental impacts for synthesized TPUs.	184
Table 8.8. LCA results of impact categories for 1 kg of synthesized TPU samples.	185
Table 8.9. Main contributions to environmental impacts for synthesized TPU-ref samples. ...	188
Table 8.10. LCA results of impact categories for synthesized TPU-m and TPU-ref samples. ..	189
Table 8.11. LCA results of impact categories for synthesized TPU-m and TPU-petropolyol samples.	191

ANNEXE II- List of figures

Chapter 1. Introduction

Figure 1.1. Global plastic demand.	4
Figure 1.2. PET hydrolytic degradation.	6
Figure 1.3. Formation of hydroperoxide groups.	6
Figure 1.4. PET photodegradation scheme.	7
Figure 1.5. Thermal degradation of PET.....	8
Figure 1.6. Linear economy flow diagram.	9
Figure 1.7. Circular economy strategies.....	9
Figure 1.8. Chemical structure of PET.....	10
Figure 1.9. Direct esterification between TA and EG for the synthesis of PET.	11
Figure 1.10. Transesterification reaction between DMT and EG for the synthesis of PET.	11
Figure 1.11. Scheme of the thermo-mechanical recycling process.	13
Figure 1.12. Methanolysis of PET.	14
Figure 1.13. Glycolysis of PET [101].	15
Figure 1.14. PET hydrolysis processes.	17
Figure. 1.15. PET ammonolysis scheme.	18
Figure 1.16. PET aminolysis scheme.	19
Figure 1.17. Chemical structure of BHET.	20
Figure 1.18. Addition reaction for a) urethane and b) urea groups formation.	22
Figure 1.19. Molecular structure of thermoplastic, elastomer and thermoset PUs [158].	23
Figure 1.20. Hard segment and hydrogen bonding interactions between urethane groups in a PU.	24
Figure 1.21. General scheme of two-step TPU synthesis reaction.	25
Figure 1.22. Schematic representation of HS and SS domains in TPU.	25
Figure 1.23. Overall molecular structure of thermoset PU.	26

Chapter 2. Materials and Methods

Figure 2.1. PET bottles recovered from the sea.	48
Figure 2.2. Digital images of different PET materials analyzed.	48
Figure 2.3. Structure of reagents used in the chemical recycling reactions.	48
Figure 2.4. Structure of reagents used in the synthesis of TPUs.	49
Figure 2.5. Structure of isocyanate used in the synthesis of thermoset PUs.	49
Figure 2.6. Zinc acetate synthesis reaction.	56

Figure 2.7. Scheme of the modeled zinc acetate.	56
Figure 2.8. Scheme of the modeled bio-polyol.	57
Figure 2.9. HDI synthesis reaction.	58
Figure 2.10. Scheme of the modeled HDI.	60

Chapter 3. Characterization of poly(ethylene terephthalate) samples of different sources

Figure 3.1. Ashes for PET-v, PET-ssp, PET-bottle, PET-m and PET-u from left to right.	66
Figure 3.2. FTIR spectra of: a) PET-v, PET-ssp, PET-u and PET-m samples and b) PET-v and PET-ssp at the 1450-1300 cm^{-1} interval.	67
Figure 3.3. FTIR spectra of PET-ssp, PET-u and PET-m at different intervals: a) 3500-2700 cm^{-1} , b) 1800-1600 cm^{-1} , c) 1600-1000 cm^{-1} , and d) spectra of PET-ssp, PET-u and PET-m samples and PET-bottle for comparison, at the interval corresponding to the $-\text{CH}_2-$ wagging region (1450-1300 cm^{-1}).	69
Figure 3.4. DSC thermograms of the different PET samples. First heating scan (—), cooling scan (-----) and second heating scan (----).	70
Figure 3.5. Weight evolution curves of PET-ssp, PET-v, PET-u and PET-m samples.	73
Figure 3.6. Images of PET samples obtained by compression molding. From left to right: PET-ssp, PET-v, PET-u and PET-m.	74

Chapter 4. Study of the valorization of marine PET litter by conventional methods

Figure 4.1. Digital images of conditioned samples before the thermo-mechanical recycling, a) PET-ssp, b) PET-u and c) PET-m samples.	82
Figure 4.2. Samples shredded after thermo-mechanical recycling from left to right: RPET-ssp, RPET-u and RPET-m.	82
Figure 4.3. FTIR spectra of RPET samples at different intervals: a) 4000-700 cm^{-1} , b) 3500-2700 cm^{-1} , c) 1800-1600 cm^{-1} and d) 1600-1000 cm^{-1}	85
Figure 4.4. Comparative FTIR spectra of original samples before (PET) and after thermo-mechanical recycling (RPET) at: a) 4000-700 cm^{-1} and b) 3500-2700 cm^{-1} intervals.	86
Figure 4.5. DSC thermograms of RPET-ssp, RPET-u and RPET-m samples. First heating scan (—), cooling scan (-----) and second heating scan (----).	87
Figure 4.6. Weight evolution a) and DTG b) curves for RPET samples.	88
Figure 4.7. From left to right digital images of the compressed (at the top) and thermo-mechanically processed RPET-ssp, RPET-u and RPET-m samples.	89
Figure 4.8. Viscosity evolution for PET-ssp, PET-u and PET-m samples with temperature after maintaining 10 (-----) and 20 (—) minutes at each ones.	91

Figure 4.9. RPET blends with different compositions, from left to right 90u/10m, 80u/20m and 70u/30m.....	92
Figure 4.10. FTIR spectra for different formulations of RPET blends with different intervals: a) 3500-270 cm^{-1} and b) 1600-1000 cm^{-1}	93

Chapter 5. Chemical recycling

Figure 5.1. Closed mini reactor used for the glycolysis.....	104
Figure 5.2. PET glycolysis reaction and products purification before characterization.....	104
Figure 5.3. a) FTIR spectra of G180, commercial BHET and PET and b) GPC traces of G180 and commercial BHET.....	105
Figure 5.4. FTIR spectra of PET and glycolysis reaction products: a) FTIR spectra of products obtained at different reaction times together with that of the reference BHET; b) PET, BHET and G products spectra at 3100-2800 cm^{-1} ; c) PET, BHET and G products spectra at 1800-1600 cm^{-1}	108
Figure 5.5. DSC thermograms corresponding to the products obtained at different reaction times, together with that of BHET-ref.	109
Figure 5.6. GPC results for products obtained at different reaction times: a) traces for G samples, together with that of BHET and b) evolution of BHET, dimer and oligomer fractions.	109
Figure 5.7. Reversible PET glycolysis reaction.	110
Figure 5.8. Weight evolution a) and DTG b) curves for samples obtained at different reaction times.	111
Figure 5.9. a) Reaction yield and b) insoluble fraction values vs. reaction time at 180, 200 and 220 $^{\circ}\text{C}$	112
Figure 5.10. BHET monomer (—) and dimer (-----) fraction values of reaction products at different reaction temperatures and times, as obtained by GPC.	113
Figure 5.11. GPC results of depolymerization at 180 $^{\circ}\text{C}$ for different reaction times.	113
Figure 5.12. Digital image of the glycolysis products obtained from the depolymerization reactions of PET-v, PET-ssp, PET-u and PET-m (from the left to the right).	114
Figure 5.13. Glycolyzed G-m fraction after purification step.....	115
Figure 5.14. FTIR spectra of the glycolyzed products obtained from the depolymerization reaction of different PET samples, together with those corresponding to PET-v and commercial BHET.	116
Figure 5.15. DSC thermograms corresponding to first heating scan of glycolyzed products obtained from different PET samples.....	116

Figure 5.16. GPC results comparing reference BHET and fractions obtained from the depolymerization of different PET samples: a) GPC traces and b) BHET monomer, dimer and oligomer fraction values.....	117
Figure 5.17. FTIR spectra of G-m and BHET-ref samples.	119
Figure 5.18. a) GPC traces, b) DSC thermograms, c) weight evolution and d) DTG plots for G-m and BHET-ref samples.....	120
Figure 5.19. ¹ H NMR spectra of BHET-ref and G-m samples.....	121

Chapter 6. Synthesis of new thermoplastic polyurethanes based on recycled BHET

Figure 6.1. Digital image PUs synthesized using BHET-m (top) and BHET-ref (down) as chain extender.	129
Figure 6.2. a) FTIR spectra of PUs synthesized with BHET-m. b) Amide I + amide II region from 1800-1500 cm ⁻¹ . c) FTIR spectra PUs synthesized with BHET-ref.....	130
Figure 6.3. a) DSC thermograms of TPUs synthesized with BHET-m, together with those of neat macrodiol and HDI:BHET-m segment. b) DSC thermograms of TPUs synthesized with BHET-ref, together with those of neat macrodiol and HDI:BHET-ref segment.....	131
Figure 6.4. AFM phase images of TPUs synthesized from BHET-m with 1:2:1, 1:4:3 and 1:6:5 molar ratios, from left to right (scale bar 200 nm).	133
Figure 6.5. a) Weight evolution and b) DTG curves of TPUs synthesized from BHET-m and neat HDI:BHET-m and macrodiol. c) Weight evolution and d) DTG curves of TPUs synthesized with BHET-ref and neat HDI:BHET-ref and macrodiol.	134
Figure 6.6. Storage modulus (E') and loss factor (tan δ) for TPUs synthesized with: a) BHET-m and b) BHET-ref.	135
Figure 6.7. Stress-strain curves of TPUs synthesized with BHET-m as chain extender.	136
Figure 6.8. Injected RTPU sample obtained by thermo-mechanical recycling.....	138
Figure 6.9. FTIR spectra of RTPU and previously synthesized BHET-m 1:6:5 TPUs.	138
Figure 6.10. DSC thermograms of RTPU and BHET-m 1:6:5 TPUs.	139
Figure 6.11. Stress-strain curves of RTPU and BHET-m 1:6:5 polyurethane.	140
Figure 6.12. Main glycolysis reaction of polyurethanes.	141
Figure 6.13. Graphical scheme and reactions that can take place in the glycolysis of synthesized TPUs.....	141
Figure 6.14. TPU-Gly obtained from the glycolysis reaction of TPUs.....	142
Figure 6.15. GPC chromatogram of the glycolyzed polyol, BHET-m and commercial macrodiol.	142
Figure 6.16. FTIR of TPU-Gly, macrodiol, and synthesized BHET-m 1:6:5 a) at 4000-700 cm ⁻¹ , b) at 3700-3100 cm ⁻¹ and c) at amide I and amide II region from 1800-1500 cm ⁻¹	144

Figure 6.17. DSC thermograms for TPU-Gly, macrodiol and TPU BHET-m 1.6:5.....	145
Figure 6.18. a) Weight evolution and b) DTG curves of TPU-Gly, macrodiol and BHET-m 1:6:5.....	146

Chapter 7. Synthesis of new thermoset polyurethanes based on recycled BHET

Figure 7.1. Thermoset PUs with increasing BHET-m content, from left to right.	154
Figure 7.2. Dynamic DSC first (—) and second scan (-----) thermograms for the different PU systems.	155
Figure 7.3. FTIR spectra of the synthesized thermoset polyurethane samples, polyol and BHET-m.....	157
Figure 7.4. a) Weight evolution and b) DTG curves of synthesized thermoset PUs.....	158
Figure 7.5. DMA results of synthesized thermoset PUs.	159
Figure 7.6. Mechanical properties of synthesized thermoset PUs.....	160
Figure 7.7. Graphical scheme and reactions that can take place in the glycolysis of synthesized thermoset PUs.	162
Figure 7.8. Glycolyzed mixture product obtained after the glycolysis of the synthesized thermoset PUs.	162
Figure 7.9. GPC traces of PU-Gly, and polyol and BHET-m employed in the synthesized thermoset PUs.	163
Figure 7.10. FTIR spectra of glycolyzed product, polyol employed in the synthesis of PU and thermoset PU.....	164
Figure 7.11. DSC thermograms of PU-Gly, polyol and synthesized thermoset PU.....	165
Figure 7.12. a) Weight evolution and b) DTG curves of polyol, synthesized thermoset PU and glycolyzed product.	166

Chapter 8. Life Cycle Assessment of different processes and material developed

Figure 8.1. Recycling scheme of marine PET litter to produce BHET-m. Color legend: green refers to raw material inputs; orange to energy inputs; grey to waste outputs; and blue to outputs obtained after each step. Asterisk (*) refers previously modeled to parameters.....	174
Figure 8.2. Tree diagram of the main contributions (above 10 %) to environmental impacts in BHET-m production.....	177
Figure 8.3. Tree diagram of the main environmental contributions for BHET-ref.....	178
Figure 8.4. Normalized representation of different impacts for BHET-m and BHET-ref production.	180
Figure 8.5. Scheme of the complete process for the synthesis of thermoplastic TPU-m 1:2:1 sample. Asterisk (*) refer to previously modeled parameters.....	182

Figure 8.6. Tree diagram of the main environmental contributions TPU-m 1:2:1 sample. 184

Figure 8.7. Impact categories of TPU-m samples..... 186

Figure 8.8. Scheme for the process followed in the synthesis of TPU-ref 1:2:1 sample. 187

Figure 8.9. Network tree for the environmental contributions of TPU-ref 1:2:1 sample..... 188

Figure 8.10. Normalized graph of relevant impact categories on TPU-m and TPU-ref samples.
..... 190

Figure 8.11. Normalized graph of different impact categories for TPU-m and TPU-petropolyol
samples..... 192

ANNEXE III- List of abbreviations

^1H NMR	Proton nuclear magnetic resonance
ADN	Adiponitrile
AFM	Atomic force microscopy
BHET	Bis(2-hydroxyethyl) terephthalate
DEG	Diethylene glycol
DMA	Dynamic mechanical analysis
DMSO	Dimethyl sulfoxide
DMT	Dimethyl terephthalate
DSC	Differential scanning calorimetry
EG	Ethylene glycol
FTIR	Fourier transform infrared spectroscopy
G	Glycolized fraction
GPC	Gel permeation chromatography
GPR	Glycolized reaction product
HDI	Hexamethylene diisocyanate
HDPE	High density polyethylene
HHV	Higher heating value
HMDA	Hexamethylenediamine
HS	Hard segment
IF	Insoluble fraction
IV	Intrinsic viscosity
LCA	Life Cycle Assessment
LDPE	Low density polyethylene
LHV	Lower heating value
MA	Maleic anhydride
MDA	Methylenedianiline
MDI	Methylene diphenyl diisocyanate
MFI	Melt flow index
PCL	Polycaprolactone
PET	Poly(ethylene terephthalate)
pMDI	Polymeric methylene diphenyl diisocyanate
PG	Propylene glycol
PS	Polystyrene

PU	Polyurethane
PU-Gly	Glycolized thermoset polyurethane
PVC	Polyvinyl chloride
RPET	Recycled poly(ethylene terephthalate)
rpm	Revolutions per minute
RTPU	Recycled thermoplastic polyurethane
SS	Soft segment
TA	Terephthalic acid
TDI	Toluene diisocyanate
TEG	Triethylene glycol
TGA	Thermogravimetry analysis
THF	Tetrahydrofuran
TPU	Thermoplastic polyurethane
TPU-Gly	Glycolized thermoplastic polyurethane
UP	Unsaturated polyester
UV	Ultraviolet
UNEP	United Nations environment programme
VOC	Volatile organic compound
WCA	Water contact angle

ANNEXE IV- List of symbols

a^*	Red-green spectrophotometry parameter
b^*	Yellow-blue spectrophotometry parameter
E	Tensile/Flexural modulus
E'	Storage modulus
$E'_{T\alpha+50}$	Storage modulus in the rubbery region
H	Hydrogen weight
I_{OH}	Hydroxyl index
L^*	Lightness-darkness spectrophotometry parameter
M^{eq}	Equivalent weight
M_n	Number molar mass
M_w	Weight molar mass
P	Potency
Pt	Point
Q	Energy consumption
T	Temperature
t	Time
$\tan \delta$	Tangent of phase angle
T_d	Maximum degradation temperature
T_g	Glass transition temperature
tkm	Weight per distance unit (tone per kilometers)
T_m	Melting temperature
T_t	Terminal temperature
W	Moisture weight
WI	Whiteness index
X_c	Degree of crystallinity
α	Relaxation of DMA
ΔE^*	Color differences between samples and white standard in spectrophotometry
ΔH_0	Melting enthalpy of a 100 % crystalline polymer
ΔH_m	Melting enthalpy
ε	Strain
ε_b	Elongation at break
η	Yield
σ	Flexural strength
σ_b	Stress at break

σ_y	Stress at yield
ν	Cross-linking density

